A Comparison of Melt Depletion, Thermal Structure and Metasomatism of Proterozoic Mantle Lithosphere in the Namaqua-Natal and Rehoboth Provinces of Southern Africa

Ellwin Taleni Shiimi

Thesis presented for the degree of Master of Science

Geological Sciences Department

University of Cape Town

March 2017

Supervisor: Dr Philip Janney

I know the meaning of plagiarism and declare that all of the work in the thesis, except for that which is properly acknowledged, is my own

Ellwin Taleni Shiimi

March 2017

ABSTRACT

Major and trace element mineral data are presented for garnet and spinel bearing peridotite xenolith suites from four Late Cretaceous kimberlites to the west of the Kaapvaal craton in two Proterozoic terranes: Hoedkop and Pofadder in the north-western Namaqua-Natal Province and Rietfontein and Louwrensia (Gibeon) in the Rehoboth Province. These are used to constrain and compare the thermal structure, the extents of melt extraction and metasomatism of the two mantle terranes with each other and with the Archaean Kaapvaal craton. Xenoliths from the Rietfontein and Pofadder localities have never previously been studied in detail. The information from this study is crucial for understanding the thermal and chemical evolution of Southern Africa's off-craton lithospheric mantle and the various processes (e.g., kimberlite and other magmatism, continental breakup) that have affected it.

Mineral thermobarometry from a variety of independent thermobarometers indicates that, at pressures less than about 4 GPa, xenoliths from the Rehoboth Province (Louwrensia and Rietfontein) lie on or very near the Kaapvaal geotherm and between the 40mWm^{-2} and 45mWm^{-2} conductive geotherms, demonstrating that the lithospheric mantle in the Rehoboth Province was thermally similar to that of the Kaapvaal craton during the Late Cretaceous. In contrast, peridotites from the Namaqua-Natal Province (Hoedkop and Pofadder) in this pressure range fall at temperatures approximately 100°C - 200°C warmer than the Kaapvaal geotherm at any given depth and lie between the 45mWm^{-2} and 50 mWm^{-2} conduction geotherms, suggesting a Phanerozoic thermal disturbance in these regions. At higher pressures, samples from both terranes (represented only by Louwrensia and Hoedkop) fall above the Kaapvaal geotherm. However, these deeper, higher temperature peridotites are mostly sheared and indicate localised melt-rock interaction, therefore are not likely representative of the general thermal state of the lithosphere.

Peridotites from the four suites have similar mineral major element compositions and their compositional variations fall well within the range of other southern Africa off-craton xenolith localities. Most garnets have smooth REE patterns with LREE depletions and relatively enriched, flat MREE - HREE abundances and patterns, while most clinopyroxenes have negatively sloping REE patterns with maximum enrichments in Nd and Sm. The average extents of melting beneath both Proterozoic provinces are moderate, and the samples are more fertile, on average, than cratonic lithospheric mantle. Peridotites from Louwrensia (Gibeon) appear to have experienced the greatest extents of melt extraction, as garnets from this locality extend to the lowest Y contents and some display strongly sinusoidal REE patterns similar to cratonic subcalcic garnets, suggesting that all of the REE were initially strongly depleted prior to metasomatism. A notable difference between the two terranes is that peridotites from Gibeon and Rietfontein (Rehoboth Province) show well developed trace element equilibrium between clinopyroxene and garnet, whereas those from Hoedkop and Pofadder (NW Namaqua-Natal Province) display significant disequilibrium.

Although all peridotites show evidence for metasomatic incompatible element enrichments, some peridotites from Hoedkop show strong disequilibrium in Rb, Ba, Th and Nb (with clinopyroxene being overly enriched in these elements) and all Pofadder peridotites show major disequilibrium, with clinopyroxene being overly enriched in Ba and Nb and overly depleted in the middle and heavy REE relative to garnet. Further, clinopyroxenes from Pofadder peridotites are unique in that they have linear REE patterns, with maximum enrichment in La, in contrast to clinopyroxenes from all other localities in this study, which show concave-down patterns in the light to middle REE. Differences in the likely nature of the metasomatising agents affecting the lithosphere of the two off-craton terranes are discussed, as well as implications for the region's geological evolution.

ACKNOWLEDGEMENTS

I would like to thank everyone who contributed in some way to the work described in this thesis. First and foremost, I thank my academic supervisor, Dr Philip Janney for all the support and time invested in discussions and reading drafts. Thank you for teaching me how to conduct science and simply for being an awesome mentor. I am grateful and privileged to be your protégé. Much appreciation to the staff at the University of Cape Town and the Mantle Room, in particular Dave Wilson and Christel Tinguely for all the assistance with preparing and analysing samples. I wish to acknowledge the generous financial support from the National Research Foundation (NRF) toward this thesis. And finally to my family and friends, thank you for being the biggest supporters in everything I do, for all the encouragement and love.

TABLE OF CONTENTS

1. INTRODUCTION

1.1. THE UPPER MANTLE – AN OVERVIEW

The mantle has only been recognised as a major division of the earth's interior for perhaps 120 years, and has only been the focus of scientific study for perhaps 80 years. But since then, both geophysical and geochemical instruments, resolution and techniques have drastically improved and have greatly increased our understanding of the mantle's structure and the various events and processes affecting its evolution. Seismic techniques have proven very useful in studying the large-scale properties and structural heterogeneities within the mantle, and have facilitated the subdivision and classification of the mantle into various layers based on fundamental differences in thermal, rheology and mineral phase changes; for instance, the upper mantle, transition zone and lower mantle (Ringwood, 1975; Anderson, 1989). On continents, it was largely on the basis of seismic velocity structure that a distinction was made between Archaean mantle lithosphere characterised by high seismic velocities, great thickness, and low density underlying Archaean cratons; and off-craton (i.e., post-Archaean) lithosphere, which is generally characterised by lower seismic velocities, lesser thickness, and higher density and underlies Proterozoic and Phanerozoic continental crust (Jordan, 1975; Jordan, 1978; Anderson, 1987; Duffy and Anderson, 1989; O'Reilly et al., 2001). The drawback of geophysical tools is their inability to provide chemical, compositional and direct thermal information on the upper mantle. Geochemical analysis of mantle xenoliths that are transported to the surface via volcanism as well as orogenic peridotites and ophiolites that are brought up to the surface through tectonic means at plate boundaries have both proven useful in providing this data.

Mantle xenoliths (also called "mantle nodules") occur in deep-seated volcanic rocks on the continents and oceans and vary in size from a few millimetres up to about 1 m in size. These include garnet peridotites, spinel peridotites, eclogites, pyroxenites and metasomatic xenolith types (for example, MARID, composed of mica, amphibole, rutile, ilmenite and diopside, and possibly other minerals), as well as xenocryst minerals such as olivine, garnet, pyroxene and ilmenite (Williams, 1932; Ringwood, 1969; Harte, 1978; Boyd and Meyer, 1979). The varying nature of mantle-derived xenoliths attests to the heterogeneous and complex nature of the lithospheric mantle. Those from Archaean cratons are transported to the surface via kimberlites while those from post-Archaean, off-craton regions are more commonly conveyed by alkalic and potassic mafic magmas, with kimberlites being a more minor mechanism.

Mantle xenoliths, particularly peridotites, provide a depiction of the lithospheric mantle during xenolith entrainment and for that reason, provide crucial direct evidence of the composition, temperature and pressure of the lithospheric mantle, which is particularly significant in continental interiors far from tectonic mantle exposures. Xenoliths, as well as tectonically exposed orogenic peridotites and ophiolites provide important information on the lithospheric mantle although xenoliths provide no geological context. Other challenges in xenolith studies include the small size of many xenoliths (especially from post-Archaean terranes) that makes estimating accurate bulk compositions difficult and may be biased by modal heterogeneities, and infiltration of xenoliths by their host magma, which complicates the chemical analysis of xenoliths and (to a much lesser extent) their constituent minerals (Pearson et al., 2014). Although the study of mantle xenoliths is limited by these complications, they are however very important, and often the only source of information that is available beneath many areas. As mantle xenoliths are often quickly exhumed, they are able to retain the mineralogical and chemical equilibria of the level in the mantle from which they originated. In contrast, large blocks of the mantle tectonically exhumed in massifs often re-equilibrate to surrounding conditions during emplacement into the crust. Peridotite xenolith suits exhumed by kimberlites are

also derived from a larger variety of depths in comparison to orogenic peridotites (Pearson et al., 2014).

A vast number of mantle xenoliths have been subjected to petrographic analysis, with some xenoliths showing evidence of textural equilibrium, while others show evidence of recrystallization and disequilibrium features such as exsolution that are understood to be transient (Boullier and Nicolas, 1973; Field and Haggerty, 1994; Xu et al., 1998). Textural relationships between minerals are also widely utilised in detecting the growth of new minerals after earlier melt depletion. Such minerals may include clinopyroxene, phlogopite, amphibole, ilmenite and others, and their presence and texture can reflect the occurrence and nature of modal metasomatism (i.e., the chemical alteration of solid rock that involves the formation of new minerals) and provide information on heterogeneities in the lithospheric mantle (Carswell, 1975; Erlank et al., 1987).

The major element concentrations in mantle xenoliths, as well as their minerals are controlled by a variety of processes. Major element mineral chemistry has proven to be an especially useful indicator of the processes that have affected xenoliths throughout their history, such as partial melt extraction and metasomatism. With regards to whole-rock composition, the extent of depletion of Fe relative to Mg and also elements that are concentrated in minerals with low melting temperatures such as Na and Ca (in clinopyroxene) and Al (in garnet) is related to the degree of melt depletion (Nixon and Davies, 1987). In contrast, xenoliths enriched in these elements may result from refertilisation (e.g., van Acken et al., 2008) or metasomatism.

The partitioning of major elements (and some trace elements) between coexisting minerals in mantle xenoliths can be useful in calculating pressures and temperatures of equilibration using thermobarometers that are calibrated from experimental phase equilibria data (e.g. Brey and Köhler, 1990; Ryan et al., 1996; Glebovitsky et al., 2004). The resulting information can be employed to construct paleogeotherms of the continental lithospheric mantle existing during

kimberlite emplacement (Dawson et al., 1975; MacGregor, 1975; Rudnick and Nyblade, 1999).

Studying the composition of trace elements in minerals of mantle xenoliths is also useful to constrain dynamic processes occurring within the mantle. The relative depletion or enrichment of the rare earth elements (REE), large ion lithophile elements (LILE), high field strength elements (HFSE), 1st series transition metals and other compatible and incompatible elements such as Th and U are useful for inferring the degrees of melt extraction and extents of metasomatic enrichment that mantle samples have experienced, which may be cryptic and thus not involve the precipitation of new, obviously metasomatic minerals (e.g., Griffin and Ryan, 1995; Gregoire et al., 2003).

The cratonic mantle in southern Africa has received a lot of attention from the scientific community due to the presence of many diamond-bearing kimberlites on the craton. Exploration as well as the diamond mining industry has facilitated the discovery of numerous kimberlite pipes and have similarly provided access to a large number of mantle xenoliths originating from a wide depth range. In contrast, fewer mantle xenoliths have been studied from off-craton localities due to the smaller numbers of kimberlites discovered, their non-diamondiferous nature as well as the smaller number and generally more altered state of the peridotite xenoliths. Further, there are far fewer garnet bearing peridotites as xenoliths in off-craton settings, because xenolith-carrying magmas are dominantly alkaline basalts that exhume shallower spinel-facies peridotites (O'Reilly et al., 2001). As a result of these limiting factors, geochemical data on garnet peridotites from off-craton lithospheric mantle remain scarce and fragmentary (Ionov et al., 2005). The new geochemical and thermobarometry data from garnet and spinel bearing peridotite xenoliths in this study will help to fill gaps in our understanding of the off-craton lithospheric evolution of the Rehoboth and Namaqua-Natal lithospheric provinces of southern Africa.

1.2. EVOLUTION OF SOUTHERN AFRICA'S LITHOSPHERIC MANTLE

The evolution of southern Africa's lithosphere spans a period from the Archaean at approximately 3.8 Ga (Tankard et al., 1982) to the Mesozoic at about 70-100 Ma (Begg et al., 2009), although the youngest crustal basement is only of Pan African age (≈700-500 Ma). The core of the southern African continent is made up of the Kaapvaal craton, the Zimbabwe craton, and the Limpopo Mobile Belt that connects them. The cratons are the Archaean nuclei, and oldest portions, of the continents, dominated by granite-greenstone belts and with unusually thick lithospheric mantle roots. The Limpopo Belt also formed during the Archaean as a result of cratonic collision. This Archaean region is bordered by Proterozoic terranes, namely the Rehoboth Province to the west and the Namaqua-Natal Province from the south-west to the south, as well as the Pan-African age Mozambique belt to the east. Proterozoic lithospheric evolution in southern Africa involves the oldest portions of the Rehoboth and Namaqua-Natal provinces forming as discrete lithospheric terranes in the Early Proterozoic (Jacobs et al., 1993; Jacobs et al., 2008), although there is a (speculative) indication of an Archaean age for the Rehoboth Province (Cornell et al., 2011). At around 1.7 Ga, the Rehoboth Province accreted onto the western Kaapvaal craton and at about 1.2 Ga the Namaqua-Natal Province accreted onto the "Kalahari craton" (which includes the Kaapvaal-Zimbabwe craton and neighbouring stable Early to mid-Proterozoic terranes) consisting of the now-joined Rehoboth and Kaapvaal terranes. The collision of the Namaqua-Natal Province with the Kaapvaal craton caused a major orogenic event (the Namaquan Orogeny) and is associated with magmatism and granulite formation over the whole length of the Namaqua-Natal Province from 1.2 to 1.1 Ga (e.g., Jacobs et al., 2008). This was then followed by regional metamorphism from 1.1 to 1.0 Ga, (e.g., Eglington, 2006; McCourt et al., 2006). The amalgamation doubled the area of the Kalahari craton and was the final stage in its formation at the end of the Mesoproterozoic (≈1.0 Ga) (Jacobs et al., 2008). Evidence from xenolith geochemistry has indicated that these major lithospheric forming and

modifying events are associated with variable degrees of melt extraction from the off-craton mantle lithosphere (Janney et al., 2010).

The Kalahari craton most likely collided with southern Laurentia at around 1.05 Ga (Jacobs et al., 2008; Li et al., 2008) to form part of the supercontinent Rodinia that existed during the Mesoproterozoic from about 1.3 Ga to 600 Ma (Li et al., 2008). The exact paleo-geographical position of Rodinia is poorly known due to the paucity of geochronological and paleomagnetic evidence, but the centre is presumed to have been situated close to the equator and most likely included all major crust on Earth at the time, with the Kalahari located south of the equator (Jacobs et al., 2008). Following the breakup of Rodinia, the Kalahari craton was amalgamated into the super-continent Gondwana, together with the rest of Africa, Antarctica, Australia, India and South America. This super-continent was mainly assembled in the southern hemisphere (with Africa at its centre) by approximately 530 Ma with a series of orogenic belts forming between older lithosphere during the Pan-African orogeny.

Gondwana began to break up at about 170 Ma (Wilson et al., 1997; Trompette, 2000; Li et al., 2008), with the Karoo flood basalt province emplaced just before Gondwana breakup, at ≈180 Ma. Subsequent to the separation, a small number of kimberlite pipes erupted in the eastern and western parts of the Namaqua-Natal Province resulting in the ≈150 Ma East Griqualand and Melton Wold kimberlites respectively (Smith et al., 1985; 1994; Figure 1). Geochemical and thermobarometry data for xenoliths from East Griqualand show evidence of intense metasomatism accompanied by a thermal disturbance in the eastern part of the province, while xenoliths from Melton World show evidence of mild metasomatism in the west, prior to 140 Ma (Bell et al., 2003; Kobussen et al., 2008; Janney et al., 2010; le Roex and Class, 2016).

Kimberlite magmatism occurred again in the Late Cretaceous (100 to 70 Ma) in the western Namaqua-Natal Province resulting in kimberlites such as Pofadder, Uintjiesberg, Hebron, and Gansfontein in addition to the eruption of various ultrapotassic and ultramafic rocks, e.g. the Hoedkop lamprophyre (Smith et al.,

1994; Kiviets, unpublished data, 2000; Griffin et al., 2014). In the Rehoboth province, Late Cretaceous kimberlite magmatism led to the formation of the Rietfontein and Gibeon kimberlites (Figure 1). Geochemical and thermobarometric evidence from xenoliths from these localities show evidence of moderate metasomatism and significant thermal disturbance in the western part of the Namaqua-Natal lithosphere, but only mild metasomatism with little to no discernible evidence for thermal disturbance in the Rehoboth Province (Hoal et al., 1994; Franz et al., 1996a; Franz et al., 1996b; Boyd et al., 2004; Appleyard et al., 2007; Janney et al., 2010).

As a result of the multifarious geological history of southern Africa, the overprinting of the pan-African orogeny and the poor basement exposure due to Cenozoic sedimentary accumulation over the region, there are portions in the evolution of the lithospheric mantle in southern Africa that we do not yet fully understand. While there is good magnetotelluric coverage of the Rehoboth Province (Muller et al., 2009), only a minor part of the Namaqua-Natal Province has good seismic coverage, with none in north-western South Africa or Namibia. Previous xenolith studies in the two provinces (e.g., Bell et al., 2003; Boyd et al., 2004) hint at thermal and metasomatic differences between the Namaqua-Natal and Rehoboth provinces, but this is based on relatively limited numbers of localities and further study of samples from additional localities will help to confirmed or disprove this difference. Moreover, xenolith samples from localities in this study are all within 200 km or so of the terrane boundary between the Namaqua-Natal Province and the Rehoboth Province, and therefore are ideally located to test whether thermal and compositional variations are related to differences between the two terranes, rather than simply reflecting more general regional variations.

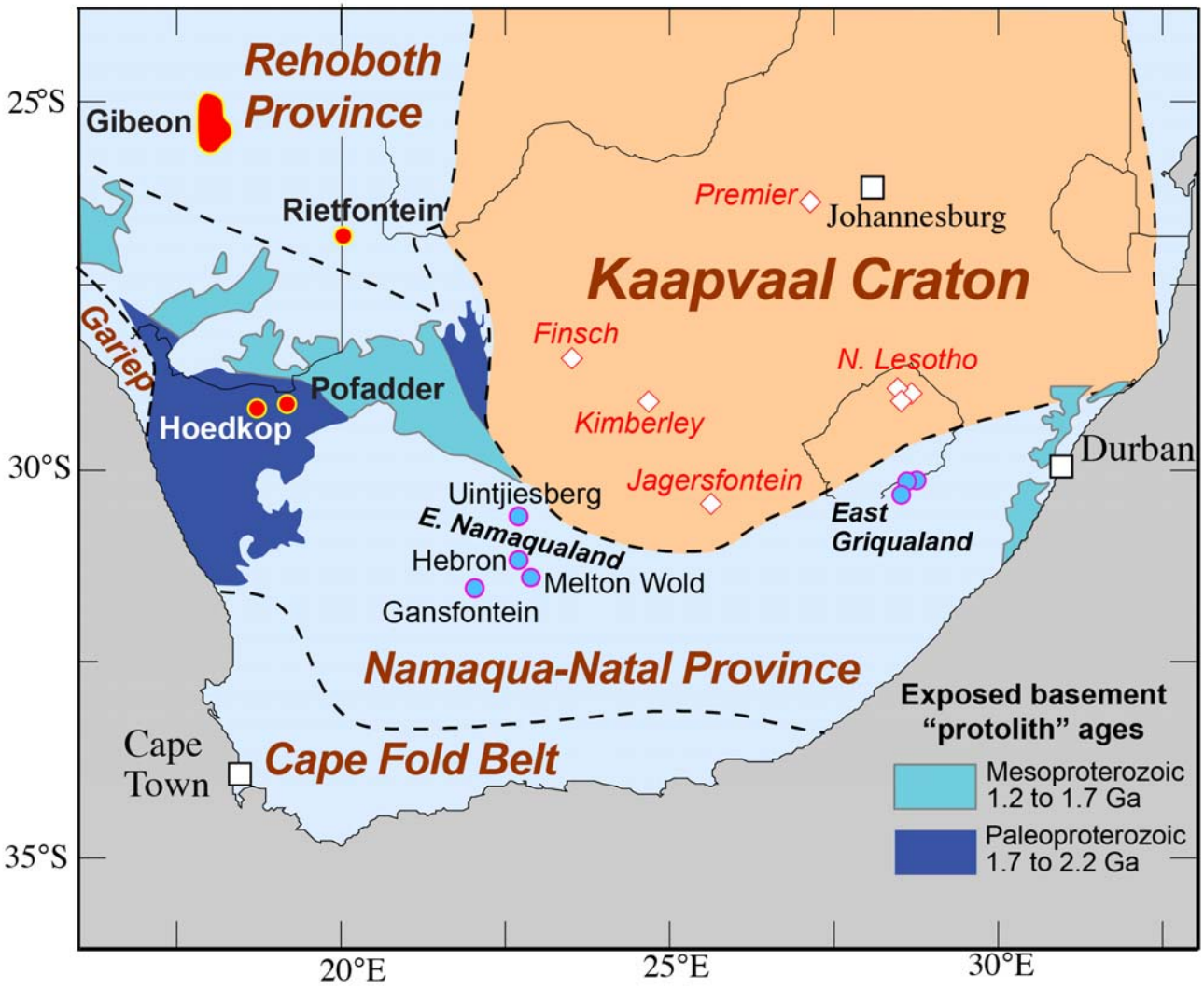

Figure 1. A schematic map of southern Africa showing location of xenolith localities investigated in this study (red and yellow circles & fields). Other studied off-craton xenolith localities are shown in the blue and red circles and well-studied on-craton xenolith localities are shown in the red and white diamonds. Also shown are regions of crustal basement exposure in the Namaqua-Natal Province, with shading to differentiate 'protolith' age (the maximum age of crustal rocks, or in the case of metamorphic or magmatic overprinting, the maximum age of zircon populations from a given area). Modified after Janney et al. (2010).

1.3. AIMS AND OBJECTIVES

In this study, the major element mineral chemistry of all major silicate phases (garnet, clinopyroxene, orthopyroxene and, where present, olivine) and trace element compositions of garnet and clinopyroxene are presented for peridotite xenoliths from four localities: the Farm Louwrensia kimberlite pipe (part of the ≈72 Ma Gibeon Group 1 kimberlite province, hereafter termed "Louwrensia", Davies et al., 2001; Boyd et al., 2004) and Rietfontein (72 Ma Group 1 kimberlite, Davis, 1977) both in the Rehoboth Province; and Hoedkop (79 Ma ultramafic lamprophyre; Griffin et al., 2014) and the Nouzees 2 pipe of the Pofadder kimberlite field (83 Ma Group 1 kimberlites, hereafter termed "Pofadder"; Griffin et al., 2014), both located in the north-western Namaqua-Natal Province. These data are used to characterise the temperatures and pressures of equilibration as well as the melt extraction and metasomatic histories of the different suites. In turn, systematic compositional differences and/or similarities between the four suites will be evaluated to constrain:

- The overall extents of melt-depletion of the lithospheric mantle in the Namaqua-Natal Province and the Rehoboth Province

- The thermal state of the lithospheric mantle of the Rehoboth and Namaqua-Natal Provinces so as to compare these two off-craton lithospheric terranes and constrain their possible thermal histories.

- The extent of mantle metasomatism that has affected the lithosphere of both the Namaqua-Natal and the Rehoboth Province and the nature of the metasomatic agent(s).

2. GEOLOGICAL BACKGROUND

2.1. THE REHOBOTH PROVINCE

The Rehoboth Province is roughly triangular in shape, with the 3 vertices located in central Namibia, north-western South Africa and northern Botswana, with each side of the triangle having a length of about 700 km (Van Schijndel et al., 2011) (Figure 2.1). The shape of the province is defined by long-wavelength anomalies on total magnetic intensity maps (Corner, 2008). Deep lithospheric electrical resistivity models provided by the 2-D magnetotellurics study of Muller et al. (2009) reveal that the present day lithospheric thickness of the province is about 180 km. The 1.8 to 1.1 Ga Kheis terrane of the Namaqua-Natal Province sits between the Rehoboth Province and Kaapvaal Craton along the eastern edge of the Rehoboth Province for about 100km along the Kalahari Lineament near its southern tip (Moen and Armstrong, 2008). The exact nature of the contact between the Rehoboth Province and the Kaapvaal Craton is poorly known due to thick Kalahari sand that extends from north-western South Africa to north-western Botswana. In addition, the magnetotelluric study of Muller et al., (2009) has also shown that the Kaapvaal craton has a greater thickness (≈220 km and 190 km in the Eastern and Western Kimberley Blocks of the Kaapvaal craton respectively) than the Rehoboth Province which has a thickness of 180 km. The Rehoboth Province borders the Namaqua-Natal Province on its south-western side along the Namaqua Front, a north-western trending fault zone in Namibia that is characterised by late-ductile shearing, granite intrusions and uplift (Stowe, 1983; Corner, 2008). Finally, to the northwest it is bordered by the Pan-African Damara Belt, which has a thinner lithosphere (of about 160 km) than the Rehoboth Province (Muller et al., 2009).

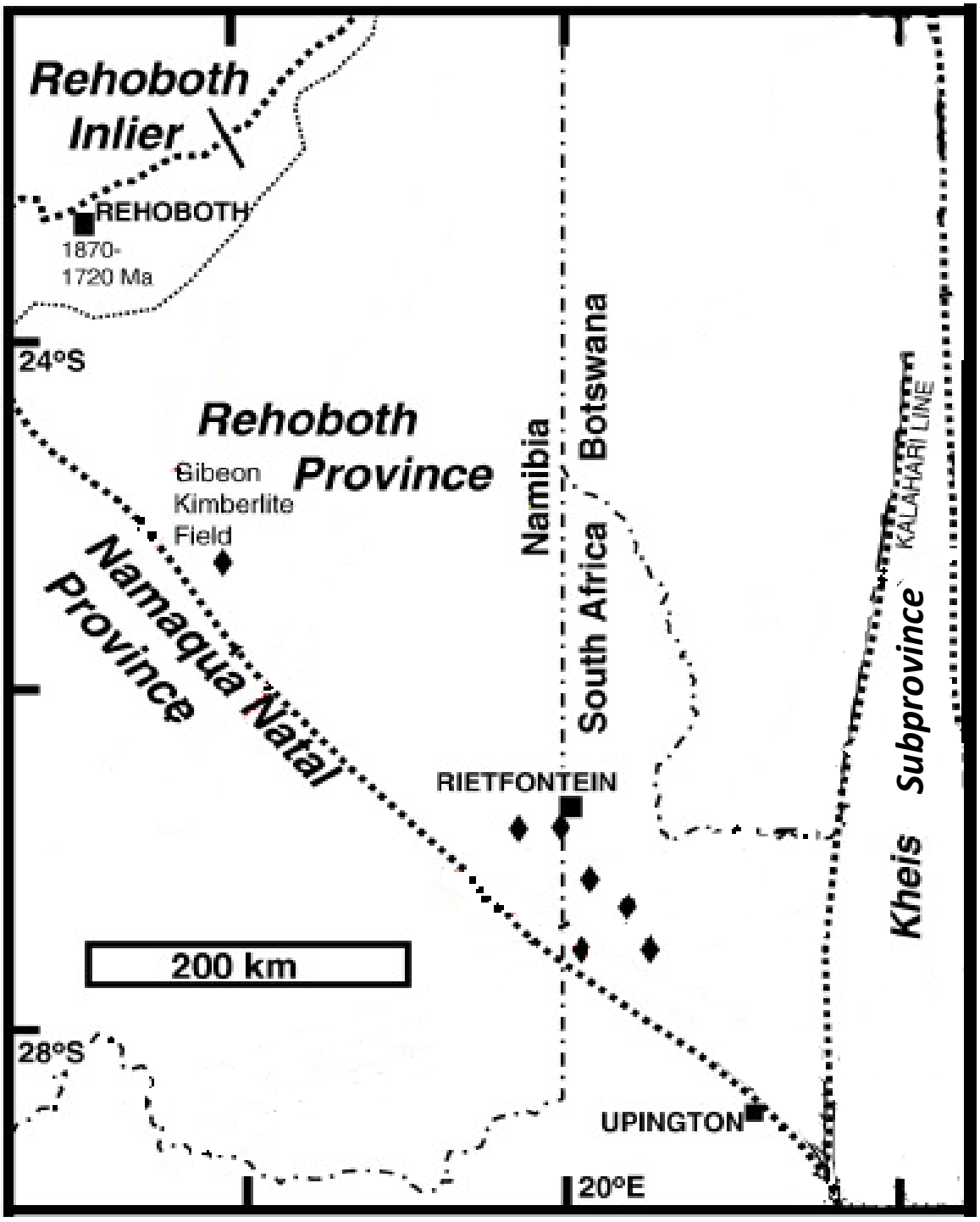

Figure 2.1. A schematic map of the Rehoboth Province showing the boundaries between the province and the adjacent terranes, as well as the position of kimberlites (indicated by diamond symbols) and the Rehoboth basement Inlier. Modified after (Cornell et al., 2011).

The Rehoboth Province has a smooth magnetic fabric with broad highs and lows, reflecting basement rocks located at depths of up to 10 km (Corner, 2008; van Schijndel et al., 2014). A difference in depth to crustal basement along the Kalahari Lineament from 8-10 km in the west to approximately 300 m in the east indicates a much deeper basement of the Rehoboth Province in comparison to that of the Kheis subprovince of the Namaqua-Natal Province (Corner, 2008). Similarly, an offset in depth to basement of up to 6 km in the Rehoboth Province along the Namaqua-Front illustrates a deeper basement in the Rehoboth province than in the Namaqua-Natal Province (Stowe, 1983; Corner, 2008).

The oldest rocks in the province are situated within the Rehoboth Basement Inlier, an area of rare exposed basement rocks along the north-western margin of the Province within the southern foreland of the Neoproterozoic Damara belt (Becker et al., 2006) (Figure 2.1). Most studies of crustal and mantle rocks from the region indicate that crust formation and modification (e.g., due to collision with the Kaapvaal craton) of the Rehoboth Province mainly occurred in the Early Proterozoic (Ziegler and Stoessel, 1993; Hoal et al., 1995; Pearson et al., 2004; Becker et al., 2006; Jacobs et al., 2008; Janney et al., 2010). Sm–Nd and U–Pb analyses of granitoids, amphibolites and basic dykes within the Rehoboth Basement Inlier suggest that the earliest crust formed between 2.37 and 1.8 Ga (Ziegler and Stoessel, 1993), while the analysis of the volcano-sedimentary sequence of the Rehoboth group and associated intrusions that are also exposed in the Rehoboth Inlier yield ages of 1.8 to 1.7 Ga. Generation of most of the crust of the Rehoboth Province during the Proterozoic is also supported by zircon age populations with peaks between 2.0 and 1.8 Ga (Van Schijndel et al., 2011). The most recent crust formation in the province is believed to have occurred during the Mesoproterozoic between 1.3 Ga-1.1 Ga (inferred from dating of zircon from the Langberg formation) concurrent with the collision of the Rehoboth with the Namaqua-Natal terranes (Van Schijndel et al., 2011).

Re-Os isotope model ages of peridotite xenoliths provide constraints on the time of melt extraction from the mantle, which is linked to lithosphere stabilisation and formation (Pearson et al., 1995; Carlson et al., 1999). An early study of

peridotites from the Gibeon kimberlite field, located near the south-western edge of the Rehoboth Province, span a rhenium depletion model age (T_{RD}) range of 2.3 to 0.8 Ga (Pearson et al. 2004), while the later study of Aulbach et al. (2014) obtained a slightly wider range of T_{RD} ages from 2.7 to 0.4 Ga for peridotites from different kimberlites in the Gibeon field. Two peridotites from the Rietfontein kimberlite, also located in the Rehoboth Province, yielded a narrower T_{RD} age range from 1.5 to 1.0 Ga (Janney et al., 2010), however it is important to note that T_{RD} values represent minimum age estimates only. These studies demonstrate that, by far, most of the lithospheric mantle in the Rehoboth province was generated during the Proterozoic.

Some workers have argued for the presence of Archaean lithosphere within the Rehoboth Province, on the basis of late Archaean T_{RD} ages for example the 2.7-2.5 Ga T_{RD} ages found by Aulbach and Brey (2014). An Archaean origin is also argued on the basis of Archaean crustal zircons (Van Schijndel et al., 2011) found in granite cobbles thought to originate from the Rehoboth Province and Kheis subprovince found in the Dwyka formation (Cornell et al., 2011) and because of textural and geochemical similarities between peridotites from the province and the Kaapvaal Craton (Franz et al., 1996a; Franz et al., 1996b; Griffin et al., 2003; Boyd et al., 2004; Kobussen et al., 2008). Griffin et al. (2003) also argued, on the basis of the "craton-like" compositions of garnets from some off-craton kimberlites, that most of the Proterozoic terranes surrounding the Kaapvaal craton are underlain by modified/metasomatised Archaean cratonic mantle. These pieces of evidence raise the possibility that the formation of the Rehoboth crust and lithospheric mantle began in the Archaean. The significance of such ages, however, is still controversial. Archaean T_{RD} ages, textural and geochemical similarities are contentious due to uncertainties related to the isotopic composition and possibly heterogeneity of the source from which the lithospheric mantle of the Rehoboth Province was formed (Janney et al., 2010; Aulbach et al., 2014) while the possibility that cobbles with Archaean age zircons found in the province could have been introduced from the Archaean cratonic crust to the east cannot be ignored.

The Lu-Hf and Sm-Nd isotope systems are subject to resetting by the passage of low degree partial melts or fluids through the lithospheric mantle and their isotopic data are useful in revealing the metasomatic history of xenoliths (Downes, 2001; Choi et al., 2005; Wittig et al., 2007; Luchs et al., 2013). Lu-Hf isotope data from the Gibeon peridotites indicate two events in which the Rehoboth Province mantle lithosphere was enriched by passage of partial melts at 1.8 - 1.9 Ga and 850 - 900 Ma while Sm-Nd isotope data record a last enrichment event at about 460 Ma (Luchs et al., 2013). The oldest event appears associated with cryptic metasomatism by a silicate melt, while the youngest appears to be associated with modal metasomatism through the addition of clinopyroxene possibly by a Ca-rich silicate (or hybrid silicate-carbonate) melt such as alkali basalt or kimberlite (Aulbach et al., 2014).

2.2 THE NAMAQUA-NATAL PROVINCE

The western part of the Namaqua-Natal Province (i.e., the "Namaqua sector") is divided up into several stable crustal blocks that are bound by tectonic discontinuities. These includes the Garies, Bushmanland, Richtersveld, Kakamas, Areachap, Kheis and the Kaaien subprovinces (Hartnady et al., 1985; Cornell et al., 2006; Eglington, 2006; Jacobs et al., 2008; Moen and Armstrong, 2008) (Figure 2.2). The exposed basement of the western part of the Namaqua-Natal Province predominantly consists of granulite and rocks of amphibolite facies as well as volcanic sequences that yielded U–Pb zircon ages of 2.1-1.7 Ga (Robb et al., 1999; Eglington, 2006) in addition to Sm-Nd isotope mantle model ages of 2.4-2.0 Ga (Cornell et al., 1986; Reid, 1997; Reid et al., 1997). This basement is intruded by younger gneissic granitoids with U–Pb zircon ages of 2.0-1.7 Ga and 1.3-1.1 Ga (Cornell et al., 1990; Robb et al., 1999; Pettersson et al., 2007).

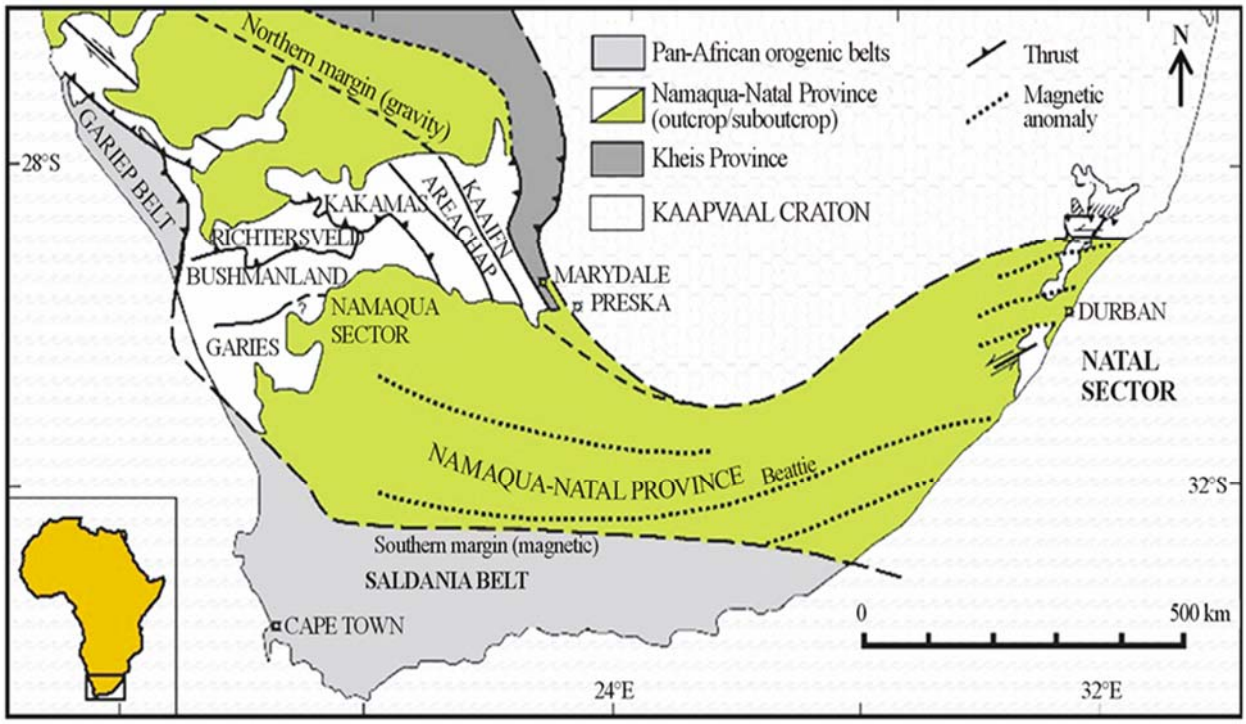

Figure 2.2. A schematic map of the Namaqua-Natal Province showing the subdivision of the Namaqua sector into varies terranes and its spatial relationship to the Kaapvaal Craton. Image from (Cornell et al., 2006)

Both the Hoedkop lamprophyre diatreme and the Pofadder kimberlites are located within the Bushmanland terrane, which is the largest in the western Namaqua-Natal Province. The Bushmanland terrane largely grew during the Paleoproterozoic, yielding Sm-Nd model ages with T_{DM} value of 2.5-1.6 Ga (Pettersson et al., 2009). The Mesoproterozoic collisional event of the Namaqua-Natal province with the "Kalahari craton" (i.e., Rehoboth Province + Kaapvaal Craton) at about 1.3 Ga was accompanied by a major crustal growth event in the region due to magmatic and volcanic activity and from the accumulation of sediments across the terrane (Pettersson et al., 2007; Pettersson et al., 2009). The voluminous granitoids that formed during this period also indicate that rifting was followed by subduction at a volcanic arc (e.g., the Areachap group rift sequence) led to the thickening of the crust, suggesting large scale reworking of the crust as the Namaqua-Natal Province entered the final stage of the Wilson cycle (Eglington, 2006; Pettersson et al., 2007). The terrane experienced high temperature metamorphism at 1.05-1.01 Ga which was followed by cooling of the

rocks from this period to about 965-950 Ma (Eglington and Armstrong, 2003; Eglington, 2006; Pettersson et al., 2007). Re-Os isotope data for peridotite xenoliths from the Namaqua-Natal Province provide rhenium depletion model ages (T_{RD}) ranging from 2.75 to 0.5 Ga, but with a large data population (≈50%) in the range from 1.25 to 1.75 Ga, which could be the result of major melt extraction during the ≈1.1 Ga Namaquan orogeny following initial formation in the Early Proterozoic (Janney et al., 2010).

2.3 XENOLITH LOCALITIES

Peridotite samples used in this study were collected from four localities, two each located in the Rehoboth and Namaqua-Natal Provinces, respectively. In the Rehoboth Province, the xenoliths studied come from a kimberlite pipe on Farm Louwrensia, located in the Gibeon kimberlite field, as well as the Rietfontein kimberlite situated in the town of Rietfontein along the N-S border between South Africa and Namibia. In the Namaqua-Natal Province, samples come from the Farm Nouzees #2 pipe of the Pofadder kimberlite field (Frick, 1974), south of the town of Pofadder and from the Hoedkop ultramafic lamprophyre, with both localities situated in the Bushmanland Subprovince of the Namaqua-Natal Province (Figure 2.3). Table 2.1 summarises information on xenolith localities.

Table 2.1 *Xenolith locality information for samples investigated in this study*

Locality	Latitude (°S)	Longitude (°E)	Distance from craton (km)	Host rock type	Age (Ma)	Technique (reference)
Louwrensia	25.31	17.82	365	Group 1 Kimberlite	71.5	Rb-Sr mica (1)
Rietfontein	26.75	20.04	140	Group 1 Kimberlite	71	U-Pb zircon (2)
Hoedkop	29.29	18.71	310	Ultram. Lamprophyre	80±2, 79±3	Ar-Ar (3), U-Pb perovskite (4)
Pofadder	29.23	19.48	280	Group 1 Kimberlite	83	U-Pb perovskite (4)

(1) Davies et al. (2001)
(2) Davis (1977)
(3) Kiviets (unpublished data, 2000)
(4) Griffin et al. (2014)

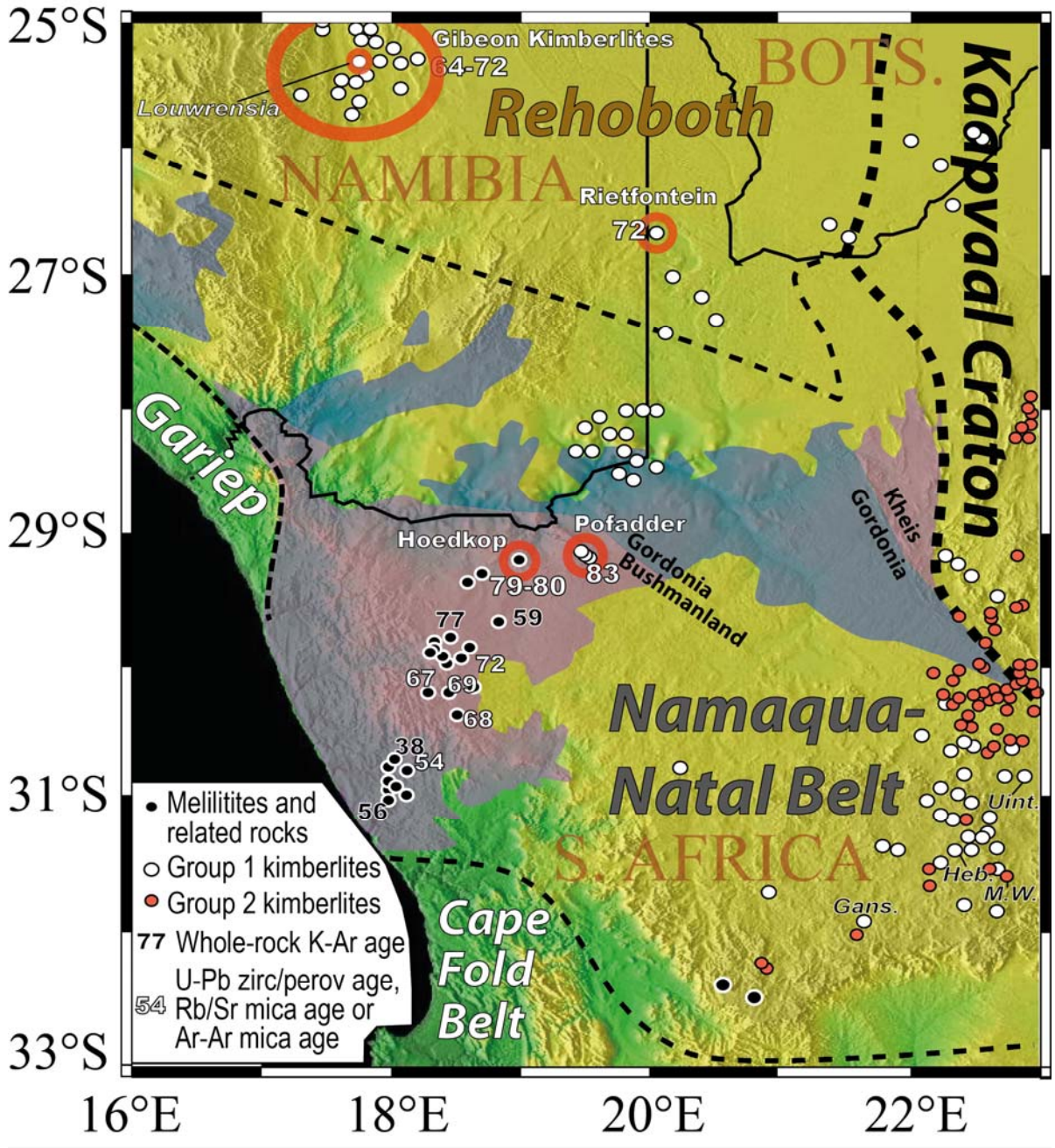

Figure 2.3. Map of kimberlites and related diatremes in western South Africa, southern Namibia and southernmost Botswana. The four xenolith localities studied are circled in red. Numbers are the ages in millions of years. Only ages for the Namaqualand-Bushmanland-Warmbad kimberlitic lineament and the Gibeon kimberlite province are given. Relatively low-precision whole-rock K-Ar ages, and higher-precision mineral ages (from U-Pb in zircon or perovskite, or Rb-Sr or $^{40}Ar/^{39}Ar$ in mica) are shown in black and white, respectively. Sources for age data are: Davis et al. (1977), Moore & Verwoerd (1985), Davies et al. (2001), Griffin et al. (2014) and G.B. Kiviets, unpublished data (2000). Purple-coloured region show the basement exposure of the Namaqua-Natal Province, specifically the Paleoproterozoic to Mesoproterozoic Bushmanland, Richtersveld and Kheis subprovinces (purple) and the Mesoproterozoic Gordonia Subprovince (blue). Ages and basement exposure regions, as well as terrane boundaries, are summarised from Eglington & Armstrong (2004) and Eglington (2006). Finally, the locations of the Eastern Namaqualand xenolith-bearing kimberlites Melton Wold ("M.W."; ≈150 Ma), Uintjiesberg ("Uint."; 100 Ma); Hebron ("Heb.", 74 Ma) and Gansfontein ("Gans."; undated) are shown for reference. Ages for these kimberlites are from Smith et al. (1994).

2.3.1. Louwrensia and the Gibeon Kimberlite Field

The Gibeon kimberlite field is located in southern Namibia between the towns of Mariental and Keetmanshoop (Mitchell, 1984). The field covers an area of approximately 70 km east to west and 110 km north to south, and consists of about 42 Group 1 kimberlite diatremes and many associated dykes (Kurszlaukis et al., 1998). The diatremes mostly occur in clusters and are either circular or elongated and tend to be oriented in a NNE-SSW direction, as are their associated dykes. Diatreme diameters of about 100 m are typical, although some pipes are elongated or irregular, reaching 400 m in maximum length, and the original upper levels of the diatremes have been removed by erosion (Kurszlaukis et al., 1998). The peridotite xenoliths used for this study were collected from the Louwrensia kimberlite diatreme (25.31 °S, 017. 82 °E) and are from the same suite of samples previously studied by Pearson et al. (2004) and Boyd et al. (2004).

The Gibeon kimberlites are all of the Group 1 classification (Davies et al., 2001) and, consistent with their off-craton location, are non-diamondiferous. Overall, the mantle xenolith suite from the Gibeon kimberlites is dominated by garnet lherzolites, with harzburgites and garnet-free peridotites being rare (Mitchell, 1986). Eclogites, pyroxenites and crustal xenoliths are extremely rare (Spriggs, 1988). Louwrensia is notable for producing the largest xenoliths from the Gibeon field and they range in size up to 10 cm in maximum dimension (Boyd et al., 2004). The Gibeon kimberlites have been dated as Late Cretaceous, about 71.5 Ma according to Davies et al. (2001) by the Rb/Sr phlogopite technique. However, unpublished Rb-Sr ages between 72 and 77 Ma have been reported by Spriggs (1988).

2.3.2. The Rietfontein Kimberlite

The Rietfontein kimberlite pipe is located near the town of Rietfontein (26.75°S, 20.04°E) in the Northern Cape Province of South Africa. The diatreme is in the immediate vicinity of the north-south oriented border between South Africa and Namibia (Appleyard et al., 2007) and is the most northerly kimberlite pipe of the of the Warmbad kimberlite cluster (Skinner et al., 1992). The diatreme has a diameter of about 137 m, covers a surface area of about 15 000 m^2 and has an accompanying dyke that extends roughly 150m from the diatreme in a NE direction (Gurney et al., 1971; Appleyard et al., 2007).

The kimberlite is classified as a Group 1 kimberlite (after Smith, 1983) and is non-diamondiferous. It is characterised by rounded macrocrystic olivine, chrome diopside, enstatite, phlogopite and garnet that are less than 3 mm in size in addition to country rock xenoliths, set in a fine grained matrix bearing a trace amount of phlogopite (Gurney et al., 1971; Appleyard et al., 2007). The kimberlite has yielded a large variety of mantle xenoliths, including bimineralic as well as orthopyroxene- and kyanite-bearing eclogites, peridotites and websterites. Aside from a few specimens as large as 5 cm, the vast majority of peridotite xenoliths from Rietfontein are small (1-2 cm) with all olivine replaced by secondary minerals. Even the larger xenoliths tend to show moderate (≈10-20%) replacement by serpentine. Early mining activity has also left behind an abundance of heavy mineral concentrate including minerals such as garnet, pyroxene, ilmenite, rutile, olivine and zircon have also been observed in the diatreme (Gurney et al., 1971; Appleyard et al., 2007). Zircon grains from this kimberlite have been dated at 71 Ma by the U-Pb technique (Davis, 1977).

2.3.3. The Hoedkop Ultramafic Lamprophyre

The Hoedkop pipe is located in the Northern Cape province of South Africa (29.29°S, 18.71°E), roughly 10 km SW of the mining town of Aggeneys, and 310 km from the western boundary of the Kaapvaal craton (Janney et al., 2010). It forms part of the Bushmanland olivine melilitite cluster (Bell et al., 2003). The diatreme is slightly elongated, approximately 200 m in diameter and penetrates through the side of a hill composed of supracrustal gneisses (Moore, 1979).

Hoedkop is classified as an ultramafic lamprophyre by the criteria of Tappe et al. (2005) on the basis that it contains more than 90% modal mafic minerals and on the absence of significant carbonate, melilite, feldspars or feldspathoids. The rock is dominated by olivine as the major phenocryst phase and by phlogopite, clinopyroxene and oxides as the main groundmass phases. In terms of bulk rock major and trace element composition, it closely resembles the Bushmanland olivine melilitites (Moore, 1979; Moore and Verwoerd, 1985). Mantle xenoliths from the diatreme include garnet and spinel lherzolite and abundant olivine megacrysts. Xenoliths from both the lower crust and from the surrounding upper crustal gneiss country rocks are also found in the diatreme (Moore, 1979). The peridotite xenoliths from Hoedkop tend to be small (typically ≤4 cm in maximum dimension) but relatively fresh, with minimal replacement by secondary minerals. The pipe has been dated at 80 ± 2 Ma by the $^{40}Ar/^{39}Ar$ technique on phlogopite separates, to have intruded at 80 Ma (G. Kiviets personal communication, 2000 as reported in Janney et al., 2010), and at 79 ± 3 Ma by the laser ablation U-Pb perovskite method (Griffin et al., 2014).

2.3.4. The Pofadder Kimberlites

The Pofadder kimberlites form a group of about 10 pipes mainly situated on the farm Nouzees (29.23°S, 19.48°E) which is located in the Northern Cape approximately 10 km south of the town of Pofadder, roughly 50 km south of the Orange River (Frick, 1974) and less than 100 km east of the Hoedkop diatreme. The Pofadder kimberlites are located between the Bushmanland melilitite cluster and the Warmbad kimberlite cluster, which is centred just north of the Orange River. Exposure of the pipes at the surface is very poor, with most of the diatremes buried under recent sediment cover.

The kimberlites are highly weathered, and most of the pipes are partly sediment-filled and calcretised. The kimberlites have been partly excavated during diamond exploration, with spoil piles revealing large quantities of garnet, pyroxene and ilmenite macrocrysts as discrete grains and Nouzees pipe 2 has yielded rare peridotite xenoliths. The peridotites are small (typically <2 cm in maximum dimension) and in all cases olivine has been replaced, leaving fresh garnet and variably altered clinopyroxene and orthopyroxene. No information has been published thus far on xenoliths from Pofadder. One of these kimberlites (Nouzees pipe 1) has been dated by the U-Pb perovskite technique and a date of 83 ± 4 Ma was obtained (Griffin et al., 2014), which is identical within uncertainties to the age of the nearby Hoedkop xenolith locality.

3. A SUMMARY OF PREVIOUS WORK ON THE XENOLITH LOCALITIES STUDIED

The purpose of this thesis is to assemble and interpret a complete major and trace element data set for four peridotite xenolith suites from four localities situated in the Rehoboth Province and the western Namaqua-Natal Province. Some of these suites have either never been previously investigated (Pofadder) or only a very small number of samples have been studied (Rietfontein). In contrast, the Louwrensia locality is notable for providing the largest xenolith suite and by far the largest xenolith specimens of any locality investigated in this thesis or indeed of virtually any off-craton mantle xenolith localities in southern Africa, and it has been the focus of significant whole rock geochemical (including isotopic) and mineral chemical characterisation (e.g., Boyd et al., 2004; Pearson et al., 2004). Peridotite xenolith suites from several off-craton kimberlites in the western Namaqua-Natal belt have also been described (including one suite investigated here, from Hoedkop). The previous petrographic, mineral chemistry (major and, where available, trace elements) and thermobarometry results published for the Rehoboth Province and western Namaqua-Natal Belt, including (where appropriate) those suites investigated here, are discussed below to provide geological context.

3.1. PETROGRAPHY

3.1.1. The Rehoboth Province

Gibeon - A number of peridotites in this study come from the Louwrensia locality in the Gibeon kimberlite field, studied by Mitchell (1984) and Boyd et al. (2004). Additionally, MacGregor (1975), Mitchell (1984) and Franz et al. (1996a; 1996b) conducted detailed petrographic descriptions of the xenolith suite from the Hanaus, Anis Kubub and Gibeon Townlands kimberlites of the Gibeon cluster. A large majority of the samples from Gibeon kimberlites are classified as garnet lherzolites (mostly coarse, but a substantial minority are deformed) with the remainder classified as garnet harzburgites.

The coarse garnet lherzolites from Gibeon mostly comprise large interlocking grains of olivine and orthopyroxene that are characterised by smoothly curving edges. Relatively sparse, pale green, granular to interstitial clinopyroxene grains are found in isolation between the olivine and orthopyroxene grains, while fractured pale pink to purple garnet forms large, rounded to irregular grains, usually with a kelyphitic rim (Mitchell, 1984; Boyd et al., 2004). In many cases, garnet grains are surrounded by a band of very fine grained interlocking clinopyroxene, phlogopite and euhedral orange-brown spinel surrounding the kelyphite, termed "collars" by Mitchell (1984). Louwrensia peridotites show a moderate amount of serpentinisation (typically 5-10 vol.% replacement) of the silicate minerals and, in some places contain patches of interlocking, anhedral grains of pyroxene and phlogopite, which are referred to as "pools" by Mitchell (1984) that appear to be a replacement texture after garnet and are occasionally connected to vein-like structures containing clinopyroxene and phlogopite.

Coarse garnet harzburgites from Gibeon also tend to have a coarse equant texture, characterised by large grains of olivine and very large grains of orthopyroxene that occasionally have thin exsolution lamellae of clinopyroxene, with the clinopyroxenes also found in veins and "pools", but not as discrete grains in textural equilibrium. Garnet is found to be a minor phase in most

garnet harzburgites from Gibeon localities and occurs as rounded to elongated crystals that are anhedral and have poorly developed kelyphite rims (Mitchell, 1984).

Deformed peridotites from Gibeon kimberlites have either porphyroclastic or mosaic porphyroclastic textures with small recrystallized neoblasts of olivine and porphyroclasts of orthopyroxene commonly surrounded by smaller neoblasts. The deformed lherzolites contain clinopyroxene crystals are irregular to rounded in shape and have not recrystallized, while garnet grains are rounded with kelyphite rims and "collars" forming around a few of the grains. In addition, anhedral chromite grains are also randomly distributed throughout the olivine neoblasts mosaic (Mitchell, 1984). Porphyroclastic garnet lherzolites from the neighbouring Hanaus kimberlite have a laminated and disrupted mosaic porphyroclastic texture with most of the olivine and orthopyroxene occurring as bands of neoblasts while clinopyroxenes and garnets form elongated crystals (Mitchell, 1984). Franz et al. (1996a) also noted that the coarse equant xenoliths were more affected by secondary alteration, such as serpentinisation and carbonatization, than the deformed peridotites.

Rietfontein - Most xenoliths from the Rietfontein kimberlite belong to the eclogite - websterite suite, with peridotites being a relatively minor component of the xenolith suite (Gurney et al., 1971; Appleyard et al., 2007). Some of these eclogites are orthopyroxene-bearing and so provide thermobarometric constraints (Appleyard et al., 2007). One garnet and one spinel lherzolite xenolith were described by Janney et al (2010), both of which are classified as "coarse granular", denoting that the sample showed no evidence of any significant deformation. The garnet lherzolite is reported to have uncommonly large clinopyroxenes and garnets occur as small crystals, in clusters or as inclusions present along the cleavage planes of clinopyroxene. The spinel lherzolite is characterized by large olivines, small pyroxenes and large symplectic spinel intergrowths.

3.1.2. The Western Namaqua-Natal Province

In general, most western NNP localities have yielded coarse granular peridotites, with the exception of Hoedkop, as it is the only western NNP locality containing deformed as well as coarse granular peridotites. The proportion of garnet-bearing peridotites varies between localities e.g., rare at Uintjiesberg and Gansfontein, ubiquitous at Hebron and Melton Wold. Phlogopite is also relatively rare in peridotites from all western Namaqua-Natal localities except where phlogopite is a reaction product after garnet. In addition there is an absence of other metasomatic minerals, such as ilmenite. It is also vital to note that overall, deformed peridotites are absent in the western Namaqua-Natal Province localities other than Hoedkop.

Hoedkop - Moore (1973 & 1979) first noted that both garnet and spinel lherzolites are present in the Hoedkop ultramafic lamprophyre. Peridotites from Hoedkop have been described by Janney et al. (2010) as consisting of both coarse granular and deformed varieties. Coarse equant spinel lherzolites make up a slight majority of the samples and are predominantly characterized by commonly strained anhedral to polygonal-shaped olivine and pyroxene grains while spinel occurs as either small grains that cluster along grain boundaries or in symplectite intergrowths. With regard to the garnet lherzolites, slightly over half are deformed, have an incipient porphyroclastic texture and are composed of olivine (partly recrystallized) of a variety of sizes, rounded medium-grained orthopyroxenes (1mm-4mm), large garnet grains (3mm-6mm) and generally small (≤1mm), anhedral clinopyroxenes. Janney et al., (2010) also noted that all garnets present have experienced significant replacement by thick kelyphite rims, and some garnet-free xenoliths have equant-shaped patches of fine-grained phlogopite, spinel and clinopyroxene that appear to represent reaction products after garnet.

Pofadder - Peridotite xenoliths from Pofadder have not been previously described in the literature. Descriptions of samples investigated in this study are provided in Chapter 4.

3.2. MAJOR ELEMENTS

3.2.1. Introduction

The abundance and distribution of major elements in peridotites and their constituent minerals are useful tools in geochemistry, to understand processes such as partial melt extraction, which stabilised the lithospheric mantle, and metasomatism that has subsequently modified it, until fragments were rapidly exhumed by volcanic processes. The composition of peridotite xenolith minerals, therefore, represent their composition at the depth at which the peridotites last equilibrated, given that the entrainment and exhumation of the xenoliths by their host kimberlite is too rapid for them to re-equilibrate.

Coarse granular off-craton peridotite xenoliths are known to be compositionally distinct from coarse granular peridotites from the craton as they usually have higher concentrations of CaO and Al_2O_3 than cratonic peridotites, along with olivine Mg numbers (i.e., 100*[Mg/ (Mg+Fe)]) of typically less than 92 (Boyd, 1989). They are also reported to have higher average modal proportions of diopside and distinct mineral compositions (Boyd et al., 1994). For example, garnets from the off-craton lithospheric mantle show lower concentrations of Al_2O_3 and CaO than garnet from the asthenospheric mantle but, display higher concentrations of these two oxides than garnets from the cratonic mantle (Griffin et al., 2008). In southern Africa, peridotitic garnet, clinopyroxene and orthopyroxene display large compositional variations as result of varying extents of melt extraction and metasomatism (Boyd, 1989; Simon et al., 2003; Griffin et al., 2008). It is widely agreed by mantle workers that Proterozoic off-craton

lithospheric mantle is less fertile (i.e., contains smaller amounts of basaltic components) in comparison to the asthenospheric mantle, but is significantly more fertile than cratonic lithospheric mantle. These properties are understood to be a consequence of the lower degrees of partial melting in the Proterozoic relative to that experienced by the cratonic lithospheric mantle in the Archaean (Nixon et al., 1981; Griffin et al., 2008; Janney et al., 2010).

3.2.2. The Rehoboth Province

Coarse granular peridotites from the Louwrensia pipe in the Gibeon kimberlite cluster are reported to have an average olivine Mg number of 91.6 ± 0.5 (2σ; Boyd et al., 2004 and references therein) which is lower than the mean value for coarse granular peridotites from the Kaapvaal craton (with average Mg number of 92.5 ± 1.3 Pearson and Wittig, 2008 and references therein), suggesting a less melt-depleted sublithospheric mantle under the Rehoboth province in comparison to the adjacent cratonic lithospheric mantle. The vast majority of garnets from both lherzolite and harzburgite xenoliths from Louwrensia and other Gibeon localities are of the calcic-lherzolitic type (Mitchell., 1984; Franz et al., 1996a; Franz et al., 1996b). Garnets from the coarse grained lherzolites from Louwrensia are poor in TiO_2 with less than 0.1 wt. %, while those from deformed peridotites contain more TiO_2 (with an average of 0.55 wt. %). Clinopyroxenes have Na_2O contents ranging from 1.0 wt. % to 2.0 wt. % with the Al_2O_3 and Cr_2O_3 ranging from 1.1 wt. % to 3.1 wt. % and 0.8 wt. % to 2.1 wt. % respectively. The Louwrensia peridotites have an average orthopyroxene modal proportion of 24 wt. %, which is lower than the mean value for coarse peridotites from the Kaapvaal craton (31.5 wt. %) Due to the presence of a significant proportion of deformed, high temperature samples, the ranges and absolute values for CaO and Ca number (100*Ca/ [Ca+Mg] on an atomic basis) for clinopyroxene and orthopyroxene are fairly high. Workers such as Mitchell, (1984) and Franz et al. (1996a; 1996b) reported comparable mineral compositions for peridotites from other kimberlites within the Gibeon cluster.

3.2.3. The Western Namaqua-Natal Province

There is a smaller, but still significant amount of data for peridotites from off-craton kimberlites in the western Namaqua-Natal Province, including Hoedkop, although there is none for Pofadder peridotites. Kobussen et al. (2008) published a very large data set for peridotitic garnets, from a large number of kimberlite localities southwest of the craton, but these are all from heavy mineral concentrate rather than from xenoliths.

Peridotite xenoliths from several kimberlites in the western Namaqua-Natal Province (aside from Hoedkop, all located southwest of the Kaapvaal Craton within 150 km of the craton boundary) have been analysed by Janney et al., (2010). These have olivines with an average Mg number of 91.4 ± 1.8 (2σ), which is comparable to the average and standard deviation of Mg number for olivines from the Rehoboth province (Boyd et al., 2004 and references therein) but is significantly lower than the average olivine Mg number values reported from Kaapvaal and other cratonic peridotites (which have a mean value of 92.5 ± 1.3 2σ; Pearson and Wittig, 2008 and references therein). As is true of Kaapvaal and Rehoboth Province peridotites, the modal proportion of orthopyroxene is also unusually high in Namaqua-Natal peridotite xenoliths, compared to other off-craton peridotites worldwide, causing them to plot at low olivine modal abundance for a given mean olivine Mg number relative to the low-pressure "oceanic" melt extraction trend formed by abyssal and ophiolitic peridotites (e.g., Boyd, 1989). The composition of orthopyroxenes from western Namaqua-Natal varies widely, with CaO and Cr_2O_3 value that range between 0.2 wt. % and 1.6 wt. % and 0.01 wt. % and 0.6 wt. %. Namaqua-Natal clinopyroxenes have a significant compositional range of minor oxides, such as TiO_2 (ranging up to 0.7 wt. %) (Janney et al., 2010). All analysed garnets from xenoliths are of the calcic-lherzolite type (Janney et al., 2010) based on the criteria of Gurney (1985) but a small minority of subcalcic garnets do occur and can be seen in the garnet concentrate data set of Kobussen et al. (2008). Peridotitic garnets from group 1 kimberlites in eastern Namaqualand have TiO_2 contents comparable to those

from Gibeon and the Kaapvaal craton but those originating from pressures greater than about 3.5 GPa are more enriched e.g.,TiO_2> 0.125 wt. % (Janney et al., 2010). This correlates with the conclusion of Kobussen et al. (2008) who analysed a large set of peridotitic macrocrysts also from the Namaqua-Natal province and concluded that garnets from a depth greater than 140 km (≈ 4.6 Gpa) are enriched in TiO_2 (>0.5 wt. %). Furthermore, Namaqua-Natal garnets are more enriched in CaO than garnets from the Kaapvaal craton (Janney et al., 2010).

Overall, off-craton peridotites from the Rehoboth and Namaqua-Natal provinces have modal mineralogies and mineral compositions (and while rock major element compositions) that are very similar and, together, they are more similar to Kaapvaal cratonic peridotites than to peridotites from other Proterozoic terranes around the world (Figure 3.1) (Boyd et al., 2004; Janney et al., 2010).

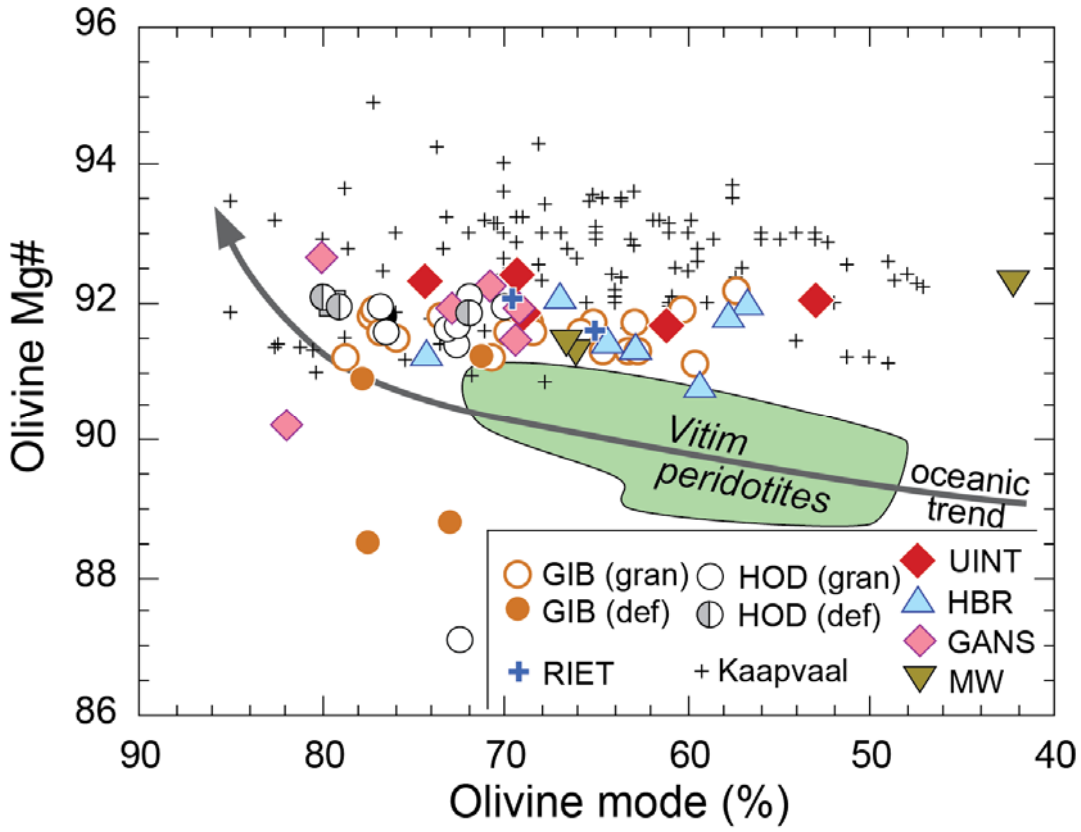

Figure 3.1. A plot of olivine modal % vs. olivine Mg#. GIB = Gibeon, RIET = Rietfontein, HOD = Hoedkop UINT = Uintjiesberg, HBR = Hebron, GANS = Gansfontein, MW = Melton World. Modified after (Janney et al., 2010).

3.3. TRACE ELEMENTS

3.3.1. The Rehoboth Province

Hoal et al. (1994) and Boyd et al. (2004) analysed trace elements in a small number of garnets from lherzolite xenoliths from Louwrensia within the Gibeon kimberlite field, southern Namibia by secondary ion mass spectrometry. These workers concluded that the grains have highly variable REE patterns, with several garnet grains displaying "sigmoidal" (i.e., sinusoidal) REE patterns that are frequently seen in subcalcic garnets from cratonic peridotites, although the Louwrensia garnets are all calcic. Overall, the garnet grains display depletions in the LREE and extremely variable HREE and MREE patterns. Luchs et al. (2013) also described two populations of peridotitic garnet from the Hanaus and Gibeon Townsland kimberlites on the basis of their REE patterns determined by laser ablation ICP-MS. Garnets with "normal" (defined as "N-type") chondrite-normalised REE patterns are characterised by high HREE contents and relatively flat chondrite-normalised patterns of the middle to heavy REE and a smooth decrease to low but variable LREE contents. They are therefore similar to the majority of Louwrensia garnets described by Hoal et al., (1994). The second population (described as "sigma" or "S-type") display sinusoidal REE patterns with relatively low HREE contents and fractionated HREE patterns (often with a strong positive slope in the HREE) and the MREE are elevated relative to some or all of the HREE and form a concave downward pattern. Hence, they display patterns that are equivalent to what Hoal et al. (1994) described as "sigmoidal".

Louwrensia clinopyroxene REE data reported by Boyd et al., (2004) are consistently enriched in the LREE, with La, Ce and Nd concentrations exceeding 10x chondrite. In addition, the clinopyroxenes studied by Luchs et al., (2013) have qualitatively similar REE patterns that are differ slightly depending on the composition of the garnet in the same sample. Clinopyroxenes from xenoliths

with garnets with "normal" REE patterns are enriched in LREE and characterised by strongly negatively sloping REE patterns from Nd to Lu, while clinopyroxenes from xenoliths with "sigma-type" garnets are often less LREE-enriched and have flatter MREE-HREE patterns and a wider range of (and most often lower) HREE contents than the clinopyroxene with "normal" patterns. The "normal" clinopyroxene grains are believed to have interacted with a melt of kimberlitic composition since the REE pattern of the melt that is in equilibrium with these clinopyroxenes is similar to kimberlite (Boyd et al., 2004).

An investigation of the partitioning of trace elements between garnet and clinopyroxene for Louwrensia peridotites show that the partitioning of Sr between the two minerals is close to equilibrium, while the partitioning of some LREE, most HREE and particularly HFSE such as Hf diverge significantly from equilibrium values (Boyd et al., 2004). In general, Boyd et al. (2004) showed that garnet and clinopyroxene grains in the coarse peridotites from Louwrensia show similar trace element characteristics to those from Kaapvaal craton peridotites (e.g., Harte et al., 1993 and Grégoire et al., 2003).

3.3.1. The Western Namaqua-Natal Province

No previous trace element data have been reported for peridotite xenoliths from the Namaqua-Natal Province. However, Griffin et al. (2003) and Kobussen et al. (2008; 2009) presented major and trace element data for peridotitic (Cr-pyrope) garnets collected from heavy mineral concentrates from a variety of kimberlites located to the southwest of the Kaapvaal Craton in the Namaqua-Natal Province. Using the high field strength element concentrations of the peridotitic garnets to classify them, Griffin et al. (2003) concluded that the lithospheric mantle in the western Namaqua-Natal province, southwest of the Kaapvaal craton is relatively fertile in comparison to the Archaean lithospheric mantle in the Kaapvaal and Zimbabwe cratons. Kobussen et al. (2008), with a much larger data set, refined this further, noting that peridotitic garnet xenocrysts from the

younger (70-105 Ma) Group 1 kimberlites in this region (SW of the craton) display high concentrations of Ti and Fe which are not observed in garnet xenocrysts from the older (115-150 Ma) transitional and Group 2 kimberlites in this area. This led the Kobussen et al (2008; 2009) to argue that the difference in fertility observed in the region by previous workers (e.g. Griffin et al., 2003) is a result of metasomatic refertilisation by interaction of mafic silicate melts with the lithospheric mantle, in the 115-105 Ma interval between the emplacement of Group 2 and Group 1 kimberlites. They claimed that this change in the chemical composition of the mantle is further supported by higher concentration of Zr and lower Zr/Y values in garnets from younger Group 1 kimberlites compared to what is observed in garnets from older transitional and Group 2 kimberlites from the same area (Kobussen et al. 2009). However, it is also important to note that there are a few inconsistencies interpretations based on garnets alone and those based on xenolith whole-rock data. For example, in the western Namaqua-Natal region and the Rehoboth Province, the xenolith data actually show a decrease in peridotite fertility (i.e., whole rock Al_2O_3 content) with depth (Janney et al., 2010), whereas Kobussen et al. (2008) and Kobussen et al. (2009) infer an increase in fertility with depth based on garnet compositions, at least for samples younger than 105 Ma.

3.4. THERMOBAROMETRY AND THERMAL STRUCTURE

3.4.1. The Rehoboth Province

Several previous xenolith geothermobarometry studies from the Rehoboth Province are mainly based on xenoliths from the Gibeon kimberlites. A pioneering study by MacGregor (1975) was first to recognise that off-craton peridotites are derived from shallower depths, on average, than their cratonic counterparts. Mineral composition data from the Gibeon kimberlite field has

been used to generate the largest calculated thermobarometry data set in the Rehoboth Province. It consists of data for peridotites from Louwrensia (Mitchell, 1984; Boyd et al., 2004), Gibeon Townlands (Franz et al., 1996b), Anis Kubub and Hanaus kimberlites (Franz et al., 1996a).

The T_{BKN}-P_{BKN} thermometer-barometer pair of Brey and Köhler (1990) yields similar ranges of equilibration temperatures and pressures for coarse granular peridotites from the four Gibeon xenolith localities, ranging from 746^{o}C to 1349^{o}C at 2.2 Gpa to 5.3 Gpa (Figure 3.1), with a majority of peridotites falling on or close to the Kalahari geotherm. A few granular peridotites from Louwrensia (833 ^{o}C to 1260 ^{o}C at 2.8 to 5.1 Gpa) and Hanaus (spanning the entire pressure and temperature range) are distinct in that they yield much higher calculated equilibration temperatures at any given pressure than the rest of the Gibeon peridotites, and as a result lie above the Kalahari geotherm. The deformed peridotites generally yield higher equilibration temperatures and pressures than the granular peridotites falling within the range of 981 ^{o}C to 1333 ^{o}C at 3.5 Gpa to 5.0 Gpa, with a great majority of deformed peridotites lying 100 ^{o}C - 200 ^{o}C higher than the Kalahari geotherm.

The similarities between the thermobarometry data for Louwrensia granular and deformed peridotites and similar peridotites from other Gibeon kimberlites reveal that the data from Louwrensia is broadly representative of the Gibeon data set as a whole. An origin of the deformed, high temperature peridotites from the Gibeon kimberlite field was proposed by Mitchell (1984), who proposed that they were formed in a thermal aureole above a rising mantle diapir. The diapir would not only have provided heat and stress on the local mantle, but also melt, which would have interacted with the lithosphere and facilitated deformation and further heating. Franz et al. (1996b) reached similar conclusions that the pre-existing mantle must have experienced local heating coupled with deformation by intruding melt just prior to kimberlite eruption. Similarly, Bell et al. (2003), Boyd et al. (2004) and Janney et al. (2010) also inferred that the high thermal gradient recorded by the Gibeon deformed peridotites is a local feature most likely related to localised melt-wall rock interaction in the lower

lithospheric mantle beneath Gibeon, not likely related to any regional process, such as continental breakup. Moreover, they cite evidence from the P-T array and composition of xenoliths that the Kaapvaal craton and the adjacent Proterozoic Rehoboth Province had very similar thicknesses at the time of Gibeon xenolith entrainment. Mather et al. (2011), in a separate numerical analysis of xenolith thermobarometry data, agreed with this conclusion. Furthermore, Boyd et al. (2004) and Janney et al. (2010) strongly suggest that thinning of the lithosphere resulted from thermal erosion at the base of the lithosphere contemporaneously with, or subsequent to, kimberlite eruption.

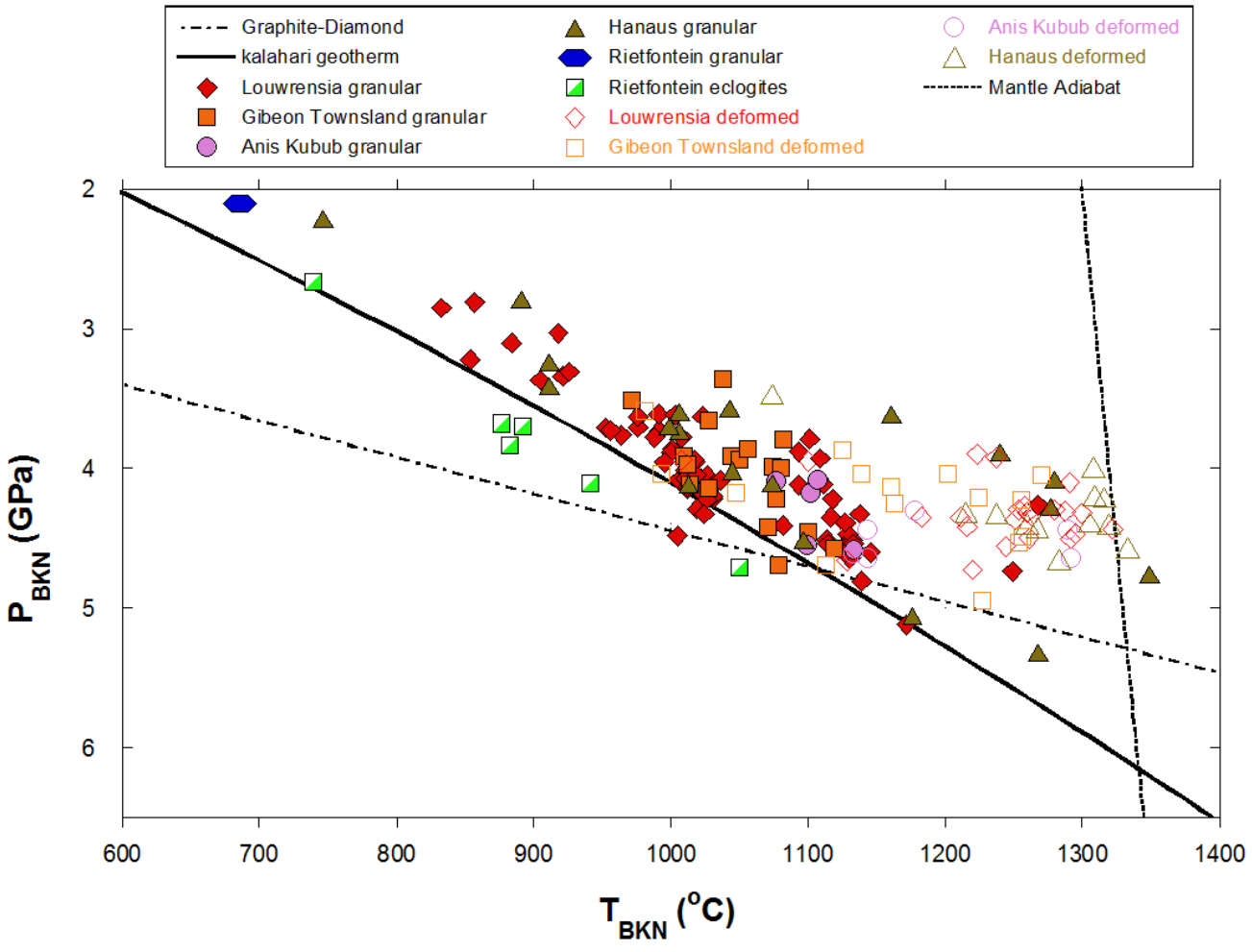

Figure 3.2 P-T arrays with estimates calculated with the T_{BKN} - P_{BKN} thermobarometer combination for Rehoboth Province xenolith localities. The diamond-graphite transition is after Kennedy and Kennedy (1976), while the mantle adiabat with potential temperature of ≈ 1300 °C is indicated by the bold dotted line. The bold continuous curve represents the 'Kalahari' geotherm of Rudnick and Nyblade, (1999). Data sources: Louwrensia (Mitchell, 1984; Boyd et al., 2004), Gibeon Townsland (Franz et al., 1996b), Hanaus (Franz et al., 1996a).

3.4.2. The Western Namaqua-Natal Province

Peridotite suites from the western Namaqua-Natal Province (west of the Kaapvaal province) exhibit a range of equilibration pressures and temperatures, ranging from 780 °C to 1250 °C at 2.0 GPa to 5.7 GPa. They also display a considerable range of temperatures at any given pressure, indicating significant thermal heterogeneity in the mantle in time and space (Figure 3.2).

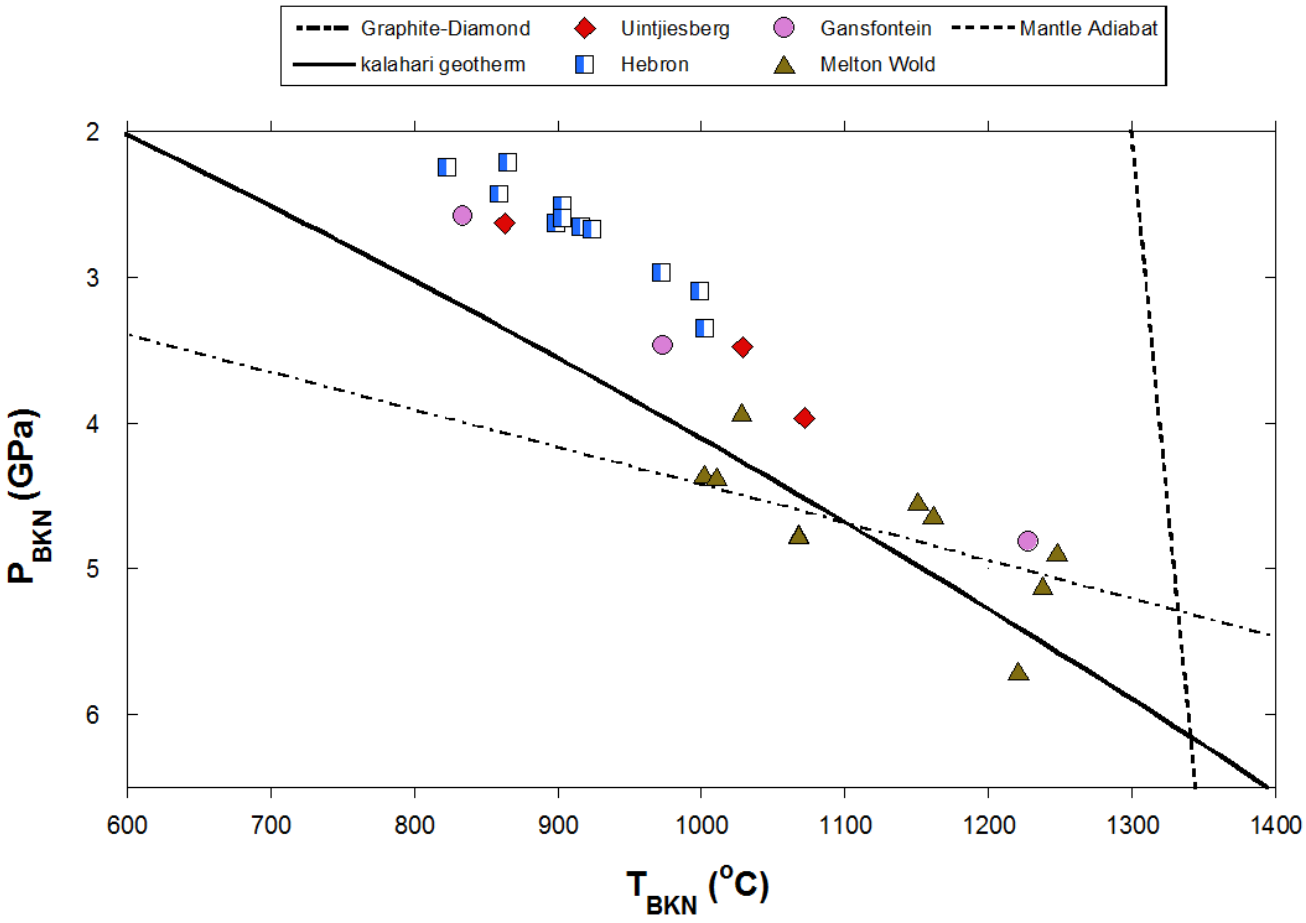

Figure 3.3 P-T arrays with estimates calculated with the TBKN - PBKN thermobarometer combination for western Namaqua-Natal Province off-craton localities. The diamond-graphite transition is after Kennedy and Kennedy (1976), while the mantle adiabat with potential temperature of ≈ 1300 oC is indicated by the bold dotted line. The bold continuous curve represents the 'Kalahari' geotherm of Rudnick and Nyblade, (1999). Data sourced from Janney et al. (2010).

The garnet peridotites from the ≈74 to 100 Ma Uintjiesberg, Hebron and Gansfontein kimberlites record pressure and temperature values that essentially form a single geotherm, which is displaced about 100°C above the Kalahari (Kaapvaal craton) geotherm at any given pressure, while those from the older, ≈150 Ma Melton Wold kimberlite define a P-T array that is approximately centred on the Kalahari geotherm at moderate pressures (Janney et al., 2010). It is proposed that the high regional thermal gradient recorded by granular peridotites from the younger kimberlites in the Namaqua-Natal Province is due to heating and thinning of the lithospheric mantle in the Namaqua-Natal province as a result of heating and possible thermal erosion during the Cretaceous prior to, or contemporaneously with, Group 1 kimberlite magmatism (Kobussen et al., 2008; Bell et al., 2003; Boyd et al., 2004; Janney et al., 2010). The change in the regional thermal gradient recorded by paleogeotherms from kimberlites of different ages in the NNP is consistent with the Cretaceous thermal disturbance being linked to continental breakup (e.g., Bell et al., 2003).

4. SAMPLES AND PETROGRAPHY

4.1. PERIDOTITE NOMENCLATURE AND CLASSIFICATION

Peridotites are classified according to the minerals present and their modal proportions, as well as the overall texture of the rock. According to the nomenclature of Streckeisen (1976), peridotites containing more than 90 modal % olivine are classified as dunite, harzburgite if containing olivine and orthopyroxene with less than 5% clinopyroxene, wherlite if comprised of olivine and clinopyroxene with less than 5% orthopyroxene, and lherzolite if composed of olivine, orthopyroxene and clinopyroxene (with each present at >5%). It was proposed by Dawson (1980) and agreed by most southern African mantle workers that the term lherzolite should not be restricted to peridotites that contain >5 vol.% clinopyroxene (diopside), but rather, the presence of any visible modal clinopyroxene should be sufficient to classify a peridotite as a lherzolite. Minor phases such as magnesian garnet and magnesian spinel are used as qualifiers (e.g. garnet lherzolite). Other primary minerals that are also commonly present include metasomatic minerals such as phlogopite, amphibole and ilmenite as well as secondary alteration minerals such as serpentine (Dawson, 1980).

Boyd and Nixon (1972) texturally classified kimberlite-borne peridotites into two categories, “granular” and “sheared”. “Granular” peridotites are characterized by coarse mineral grains with a unimodal grain size distribution, displaying a lack of deformation-related textural features (e.g., undulatory extinction) due to long equilibration at constant temperature and pressure conditions. “Sheared” peridotites display non-equilibrium textures with bimodal grain size distributions, consisting of porphyroclasts (large and strained mineral fragments surrounded by finer-grained groundmass) and fine neoblasts (recrystallized, fine

grained crystals), often with minerals arranged in distinct lens-shaped zones. Such textures are understood to be generated as a result of strong deformation. More recently, the term "deformed" has come to be preferred to "sheared" because not all peridotites appearing to have undergone stress-related recrystallization show evidence for shearing. The two peridotite types also tend to display compositional differences. In most cases deformed peridotites have higher equilibration pressures and especially temperatures and have lower Mg-number values of their minerals. This suggests that in most cases they represent samples of the deep lithospheric mantle which may have experienced heating by, and chemical exchange with, percolating melts and/or fluids. This textural classification, however, while useful, is too broad to provide much insight into the pressure, temperature and deformation conditions of individual samples.

Workers such as Boullier and Nicolas (1973) and Harte (1977) used grain size and size range in combination with evidence for deformation and recrystallization to texturally classify peridotites. A "coarse" peridotite is described as a rock that lacks porphyroclasts, has grains that are greater than 2 mm in average size, with predominantly straight or smoothly curved grain boundaries and the grains being either equant (roughly equidimensional) or tabular (one dimension smaller than the other two) in shape. A peridotite that has more than 10% of the olivine grains occurring as porphyroclasts is classified as "porphyroclastic", while that with more than 90% of the olivine occurring as neoblasts is classified as a "mosaic-porphyroclastic" (Harte, 1977). Distinctions are made if the rock appears to be disrupted (garnet or spinel occurs in discontinuous stringers or groups of relatively small grains) or laminated. "Laminated" is an umbrella term referring to a rock that has thin layers due to modal variation in olivine and orthopyroxene. Laminated peridotites predominantly show "fluidal" textures when porphyroclasts of a particular mineral have stripes or lenticles made up of finer grains (approximately 0.03mm) of the same mineral connected to them, that extend in areas dominated by another mineral mainly showing a mosaic texture. In the most highly deformed peridotites, minerals are predominantly or entirely fine-grained (typically much less than 2mm) with, at most, a small proportion (less than 5%) of porphyroclasts

larger than this size. This texture is referred to as "granuloblastic" (Harte, 1977). Furthermore, a wide range of textures occur in peridotites as a result of sub-solidus reactions between minerals, such as the kelyphite rims (composed of fine mineral intergrowth) that surround some garnet grains (Dawson, 1980). Peridotites in this study are classified according to the textures discussed above.

4.2. PHYSICAL AND PETROGRAPHIC FEATURES

A total of forty-four spinel and garnet bearing lherzolites were investigated in this study. Some of these samples come from the J.J. Gurney Upper Mantle Research Collection at the University of Cape Town (all Pofadder and most Rietfontein samples), with others sourced from the research collections of F.R. Boyd (now housed in the Smithsonian Institution, USA; Louwrensia samples) and P.E. Janney (Hoedkop and the remaining Rietfontein samples). From the north-western Namaqua-Natal Province, seven samples are from Pofadder and eleven are from Hoedkop, while from the Rehoboth Province fifteen samples are from Rietfontein and eleven are from Louwrensia (Gibeon kimberlite field). Polished thin sections were made for a total of twenty-three peridotite samples that were relatively large and fresh. Three of these samples are from Rietfontein, eleven are from Louwrensia and nine are from Hoedkop. The remaining samples, including all from Pofadder and most from Rietfontein were too small (and often too altered) to merit being sectioned. These samples were gently crushed and fresh mineral grains were selected and mounted in epoxy disks for analysis. Samples from the four localities are listed in Table 4.1, and display a range of deformation textures, reaction textures and extents of alteration.

Table 4.1 *List of peridotite samples from Louwrensia, Rietfontein, Hoedkop and Pofadder, with their mineralogical and textural classification types*

Sample Name	Location	Type	Texture
FRB-1180	Louwrensia	Garnet-spinel lherzolite	Coarse
FRB-1183	Louwrensia	Garnet lherzolite	Coarse
FRB-1652	Louwrensia	Garnet lherzolite	Coarse
FRB-1683	Louwrensia	Garnet-spinel lherzolite	porphyroclastic
FRB-1684	Louwrensia	Garnet lherzolite	Coarse
FRB-1686	Louwrensia	Garnet lherzolite	Coarse
JJG-2513	Louwrensia	Garnet lherzolite	Coarse
JJG-2514	Louwrensia	Spinel lherzolite	Coarse
PHN-5316	Louwrensia	Garnet lherzolite	Coarse
PHN-5364	Louwrensia	Garnet lherzolite	Coarse
PHN-5365	Louwrensia	Garnet-spinel lherzolite	Coarse
RIET-1	Rietfontein	Spinel lherzolite	Coarse
RIET-2	Rietfontein	Garnet lherzolite	Coarse
RIET-3	Rietfontein	Garnet-spinel lherzolite	Coarse
RIET-4	Rietfontein	Garnet lherzolite	Coarse
RIET-5	Rietfontein	Garnet lherzolite	Coarse
RIET-6	Rietfontein	Garnet-spinel lherzolite	Coarse
RTFN30-1	Rietfontein	Garnet lherzolite	Coarse
RTFN30-2	Rietfontein	Garnet lherzolite	Coarse
RTFN30-4	Rietfontein	Garnet lherzolite	Coarse
RTFN30-5	Rietfontein	Garnet lherzolite	Coarse
RTFN30-7	Rietfontein	Garnet lherzolite	Coarse
RTFN30-8	Rietfontein	Garnet lherzolite	Coarse
RTFN30-13	Rietfontein	Garnet-spinel lherzolite	Coarse
RTFN30-14	Rietfontein	Garnet-spinel lherzolite	Coarse
RTFN31-5	Rietfontein	Garnet-spinel lherzolite	Coarse
HOD-1	Hoedkop	Garnet lherzolite	Coarse
HOD-2	Hoedkop	Garnet lherzolite	porphyroclastic
HOD-3	Hoedkop	Garnet lherzolite	porphyroclastic
HOD-4	Hoedkop	Garnet lherzolite	porphyroclastic
HOD-5	Hoedkop	Garnet-spinel lherzolite	Coarse
HOD-6	Hoedkop	Spinel lherzolite	Coarse
HOD-7	Hoedkop	Spinel lherzolite	Coarse
HOD-8	Hoedkop	Spinel lherzolite	Coarse
HOD-9	Hoedkop	Spinel lherzolite	Coarse
HOD-10	Hoedkop	Spinel lherzolite	Coarse
HOD-11	Hoedkop	Garnet-spinel lherzolite	Coarse
JJG 2499-4	Pofadder	Garnet lherzolite	Coarse
JJG 2499-6	Pofadder	Garnet lherzolite	Coarse
JJG 2499-7	Pofadder	Garnet lherzolite	Coarse
JJG 2499-12	Pofadder	Garnet lherzolite	Coarse
JJG 2499-14	Pofadder	Garnet lherzolite	Coarse
JJG 2499-15	Pofadder	Garnet lherzolite	Coarse
JJG 2499-16	Pofadder	Garnet lherzolite	Coarse

4.2.1. Louwrensia

All eleven peridotites from Louwrensia (Gibeon) were large enough to be sectioned. Out of these eleven peridotites analysed, ten are granular lherzolites and one peridotite is deformed. The granular lherzolites display coarse, undeformed textures that are characterised by large interlocking grains of garnet, clinopyroxene, orthopyroxene and olivine. Garnet grains are purple to violet in colour, rounded to irregular in shape and occasionally fractured. The grains range between 1.5 to 3 mm in average size and are found in isolation throughout the samples. In sample PHN 5365 (Figure 4.1a) and FRB 1185, some garnet grains contain inclusions of clinopyroxene and olivine (roughly 0.2 mm), and symplectic spinel (up to 1 mm in size), while in sample PHN 1684 garnet grains are irregularly mantled by tabular phlogopite and fibrous spinel (Figure 4.1b). Furthermore, thin kelyphite rims (0.05 mm) are common. Clinopyroxene crystals are anhedral to ovoid in shape and are typically between 0.5 and 2mm in size, although some grains are as large as 4 mm in maximum dimension. In a few samples such as PHN 5365 and PHN 1652, the clinopyroxene mostly occurs in clusters, but can also be found in isolation or as inclusions in other minerals. In three of the granular peridotite samples (FRB 1185, FRB 1652 and FRB 1684), clinopyroxenes are largely replaced by fibrous phlogopite as seen in Figure 4.1c. Orthopyroxenes form large subhedral to anhedral crystals that are typically about 2.5 mm, but can be as large as 7 mm. In sample PHN 5365, some orthopyroxene grains display exsolution lamellae of clinopyroxene and spinel. Olivine grains occur as large anhedral crystals that are about 4 mm in average size, with a few grains reaching 12 mm. These grains are moderately fractured, with iron oxide staining on the fractures. Three granular lherzolites studied from Louwrensia contain primary spinel (i.e., not including that present in kelyphite rims) in addition to garnet. In sample FRB 1180, spinel occurs as isolated rounded to tabular grains that are about 0.5mm in size, while in sample FRB 1683 and PHN 5365 it occurs as symplectite intergrowths with garnet. Coarse granular lherzolites from Louwrensia show evidence of alteration, with

serpentine veins replacement ranging from 1 to 25% total volume of rock (mostly replacing olivine). In addition, minor calcite veins have been noted in two samples.

The deformed peridotite from Louwrensia investigated in the study (FRB 1683) shows mosaic-porphyroclastic textures. Garnet grains are rounded to anhedral in shape and are roughly 1 mm in average size. Most of the garnet grains are fully or partially replaced by fibrous spinel which is mantled by fine-grained tabular spinel grains about 0.1 mm in size, with a few garnet grains also containing tabular inclusions of spinel. Clinopyroxenes in this sample are anhedral and very fine grained (<0.2mm) and occasionally occur as inclusions in garnet. Orthopyroxenes have a subhedral to tabular shape, and are characterised by a mean grain size of 1.5 mm. The olivine porphyroclasts form subhedral to anhedral shaped crystals that range between 1 and 3 mm, while olivine neoblasts are rounded to tabular in shape, are predominantly less than 0.1mm in size and constitute the groundmass of the xenolith. About 35% total volume of the rock is replaced by serpentine veins.

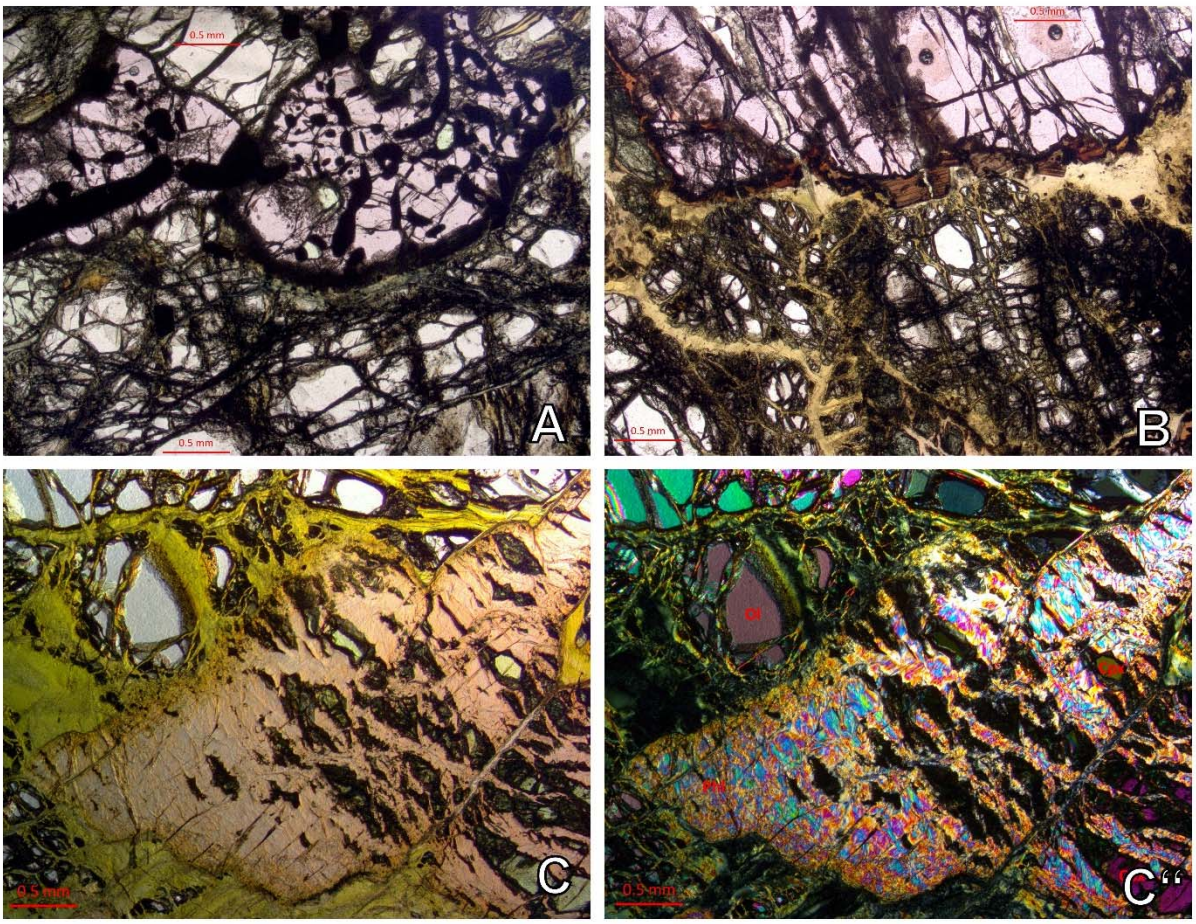

Figure 4.1. Photomicrographs of representative textures of Gibeon (Louwrensia) showing **A:** garnet grains containing inclusions of clinopyroxene and exsolved spinel in PHN 5365; **B**: a garnet grain irregularly mantled by tabular phlogopite and fibrous spinel on either rims of the grain in PHN 1684; **C:** clinopyroxene replaced by fibrous phlogopite in FRB 1185 while **C**" is the cross polarised image of the same clinopyroxene grain. Red scale bar = 0.5 mm.

4.2.2. Rietfontein

Peridotite xenoliths from Rietfontein used in the study are ovoid to rounded in shape, with pitted surfaces due to differential weathering, and, aside from three larger specimens (3 to 6 cm) they range between 1 and 2 cm in maximum dimension. The xenoliths are classified as coarse granular lherzolites (e.g., Figure 4.2) following the classification scheme of Harte (1977), bearing either garnet, spinel or both.

Garnets vary in shape and size between samples, for example in sample RIET-3, they are large, ranging between 3 to 4 mm in average size and occur as rounded to tabular isolated crystals, while in another sample RIET 2, they are fine grained ranging from 0.01 to 0.4 mm and occur as tabular or anhedral crystals, in intergranular clusters and chains, or as isolated grains between grain boundaries (Figure 4.2b).

In RIET-2, some clinopyroxene grains contains fine, tabular inclusions of garnet oriented along either one or both the cleavage planes which appear to have exsolved out of the clinopyroxene (Figure 4.2b). The clinopyroxenes are mostly anhedral in shape and about 3mm in average size. Some clinopyroxenes in RIET-2 also show simple twinning and have exsolution lamellae (Figure 4.2b).

Orthopyroxenes form large subhedral crystals with an average size of 4 mm and triple junction intersections are common. Olivines are anhedral and vary in size between samples, ranging between 2 mm and 8 mm, with an average size of 4.5 mm. In the spinel lherzolite RIET- 1, spinel occurs in large (≈ 6 mm) fingerprint-like symplectite intergrowths with the pyroxenes (Figure 4.2c), while in the garnet-spinel lherzolite RIET-3, it occurs as fine (0.2 - 0.7 mm) rounded crystals that are found in isolation. Rietfontein samples have been lightly affected by alteration, which has resulted in 20% and 40% serpentinisation of RIET-3 and RIET-1, respectively.

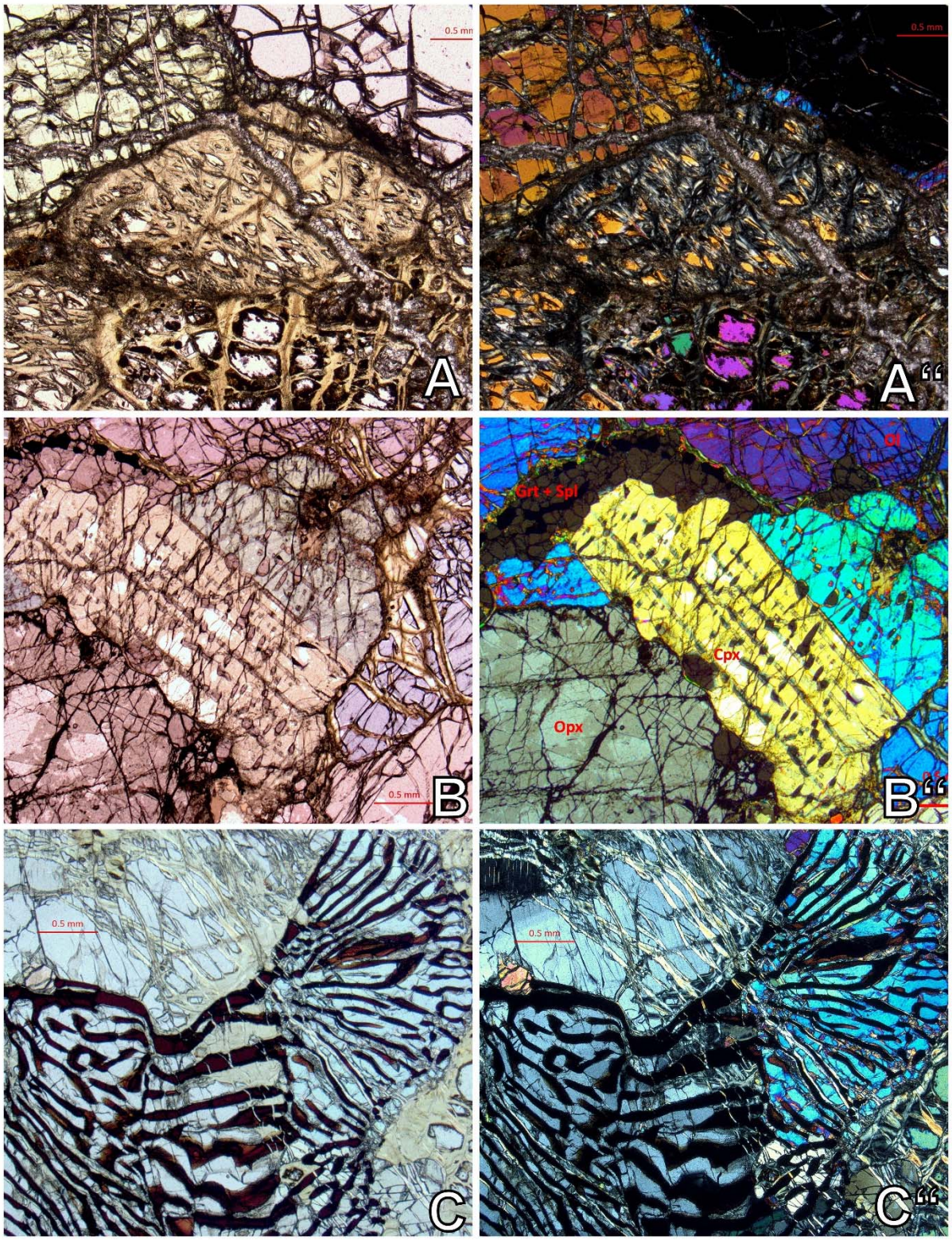

Figure 4.2. Plane polarised and cross polarised photomicrographs of representative textures in Rietfontein peridotites showing **A:** RIET 3 garnet lherzolite showing typical coarse granular texture in Rietfontein peridotites as well as serpentine alteration **B:** RIET 2 garnet lherzolite with a simply twinned clinopyroxene grain that contains fine inclusions of exsolved garnet and orthopyroxene along cleavage planes. There is also an Intergranular cluster and chain of garnet and spinel (Grt + Spl) can be seen in the top left corner **C:** RIET-1 spinel lherzolite displaying a large fingerprint-like symplectite intergrowth of spinel with orthopyroxene and clinopyroxene. Red scale bar = 0.5 mm

4.2.3. Hoedkop

In the peridotite suite from Hoedkop, the granular xenoliths display typical textural equilibrium features such as straight to curved grain boundaries and 120° grain intersections, and are classified as coarse lherzolites. In these peridotites, garnet crystals are mostly anhedral with an average size of 2 mm, but grains can be as large as 4 mm. The garnets in Hoedkop peridotites are frequently surrounded by a brown to opaque kelyphite rim, typically with thicknesses of approximately 0.4 mm, consisting of a brown, very fine-grained intergrowth of fibrous spinel and phlogopite, that is mantled by a fine grained opaque reaction zone and a corona of euhedral spinel along with fine pyroxene (

Figure 4.3a). A few garnet grains in HOD-11 also contain olivine inclusions. Clinopyroxenes are anhedral in shape and about 2 mm in average size. The clinopyroxene grains are occasionally surrounded by a thin layer (≈20 μm) of fine recrystallized clinopyroxene. Orthopyroxene forms anhedral crystals that range between 1 and 2 mm in average size. The grains are also surrounded by a layer of fine grained recrystallized orthopyroxene. Anhedral olivine grains are large, with an average length of 3 mm but can be up to 8 mm in size. Spinel grains are rounded to polygonal, and are typically found in isolation, located at grain boundaries of olivine and pyroxene or in symplectitic intergrowths with pyroxenes. Sample HOD-5 contains numerous clusters consisting of fine grained pyroxene, olivine and spinel

Figure 4.3b), while sample HOD-7 contains a polygonal-shaped aggregates of phlogopite, fine grained clinopyroxene and subhedral spinel grains found scattered within the cluster (Figure 4.3c), which appear to represent breakdown products after garnet.

The three deformed xenoliths from Hoedkop all display porphyroclastic textures (

Figure 4.3d). Pink to violet garnet grains are rounded to polygonal in shape, with an average size of 3 mm (excluding the kelyphite rims). The grains are partially or fully replaced by a brown to opaque kelyphite rim similar to that observed in

the coarse granular samples. Clinopyroxene grains are variable in shape but are mostly anhedral and typically range from 1.5 to 2 mm in size. Orthopyroxenes are anhedral and have an average size of 2 mm. They tend to be rimmed by a thin layer of fine recrystallized orthopyroxene. Olivine grains are tabular to irregular to rounded and form a continuous range of grain sizes, with a significant percentage in the size range of 0.1 to 3 mm. The larger olivine grains tend to display undulose extinction as a result of internal strain, while the finer grains have 120^{o} grain intersection and display a mosaic texture.

4.2.4.Pofadder

Peridotite xenoliths from Pofadder are small, varying from 2 to 3 cm in length, and tend to be rounded in shape with pitted surfaces due to weathering. All are garnet or garnet-spinel lherzolites characterised by red to violet garnet, bright green clinopyroxene, yellow to dull green orthopyroxene and black spinel crystals. All olivine and a significant amount of orthopyroxene has been replaced by serpentine and other secondary minerals, with cpx and garnet being almost entirely unaltered. The fresh mineral grains are all relatively fine grained, typically less than 2 mm in size. No thin-sections of Pofadder peridotite xenoliths were made due to their small size and friable nature as a result of alteration. Based on grain size, the Pofadder peridotite xenoliths can be generally classified as granular, although mild deformation cannot be ruled out.

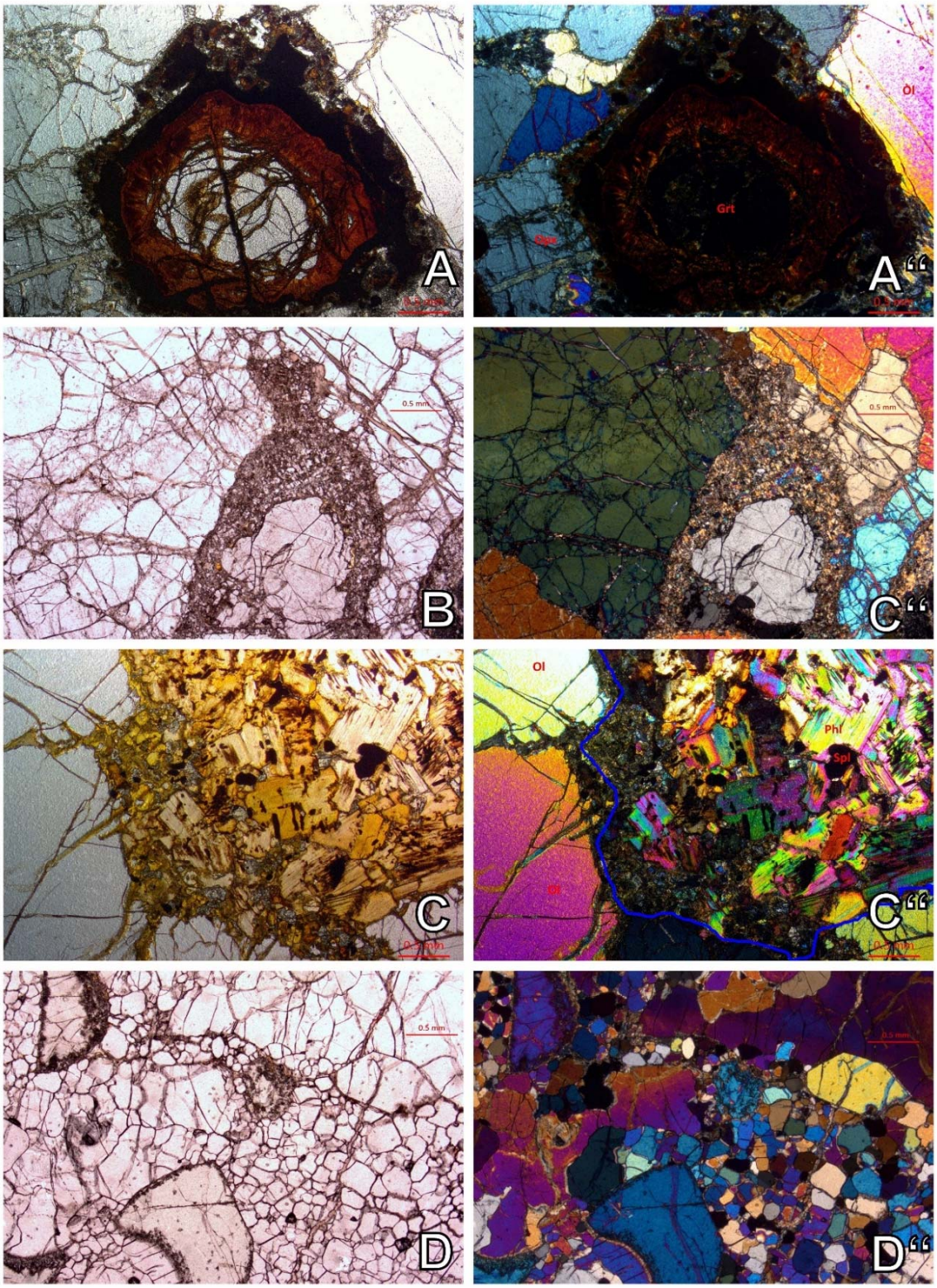

Figure 4.3. Plane polarised and cross polarised photomicrographs of representative textures of Hoedkop showing **A:** reaction kelyphite rim around a garnet grain at is mantled outwards by corona of pyroxene with fine euhedral intergrown spinel in HOD 5. **B:** orthopyroxene grain replaced by a cluster of fine grained pyroxene, olivine and spinel in HOD 5. **C:** a polygonal shaped aggregate of phlogopite, fine grained clinopyroxene and subhedral spinel grains in HOD 7. The contact zone between the aggregate and the surrounding olivine grains is inked in for clarity. **D:** sheared xenolith with a porphyroclastic texture defined by olivine (Ol) and clinopyroxene (Cpx) porphyroclast and olivine neoblasts. Red scale bar = 0.5 mm.

4.3. EVALUATION OF PETROGRAPHIC FEATURES

The peridotite suites from Louwrensia, Rietfontein, Hoedkop and Pofadder include both garnet- and spinel-bearing lherzolites and also several garnet-spinel lherzolites. In the Rehoboth Province, petrographic descriptions of samples from Louwrensia closely match those provided by Mitchell (1984) and Boyd et al. (2004) except for the new identification of fine clinopyroxene grains in textural equilibrium with surrounding grains, found within two samples, FRB 1180 and JJG2514, that were previously described as spinel harzburgite and garnet-spinel harzburgite by Boyd et al. (2004) and are now classified as spinel lherzolite and garnet-spinel lherzolite respectively. Compared to peridotites from the other Gibeon kimberlites, Louwrensia samples have an average olivine content of 68% (Boyd et al., 2004), which is identical to peridotites from Gibeon Townlands 1 kimberlite (average of 68%) (Franz et al., 1996b) although peridotites from Anis Kubub and Hanaus have considerably higher olivine contents of 80% and 75%, respectively (Franz et al., 1996a). The coarse granular peridotites from Louwrensia are slightly higher in orthopyroxene (11%-40%) (Boyd et al., 2004) than granular peridotites from the Gibeon Townlands 1 kimberlite (7%-35%) (Franz et al., 1996b), Hanaus (15%-32%) or Anis Kubub (15%-30%). However, they show similar orthopyroxene contents to granular lherzolites from the Kaapvaal craton (Boyd et al., 2004).

In the Namaqua-Natal Province, descriptions of the samples from Hoedkop that were investigated here match those described by Janney et al., (2010), with the only difference being that porphyroclastic textures are assigned to samples that they simply described as deformed peridotites. It is also notable that these deformed Hoedkop peridotites contain a higher modal abundance of clinopyroxene (3.9% - 4.5%) than the granular peridotites from the same locality (0.7% - 3.5%), which was not remarked upon by Janney et al. (2010).

In terms of textures, a majority of peridotites used in the study are classified as granular and are very similar to one another in that most are coarse grained,

with typical textural equilibrium features such as 120° grain intersections. Peridotite suites studied do differ in terms of the diverse range of reaction textures they display and the extent to which these textures have developed. These textures may reflect gradual changes in pressure or temperature conditions, or exposure to (and reaction with) metasomatic agents in the mantle, or en route to the surface.

The relationship between texture and temperature in peridotites has been explored by several workers. Peridotites from Gibeon studied by Mitchell (1984), Franz et al. (1996a; 1996b) and Boyd et al. (2004) show a correlation between texture and equilibration temperatures, in that deformed peridotites appear to have equilibrated at higher temperatures than granular peridotites. This correlation was noted previously by MacGregor (1975) in peridotites from the same locality. Peridotites from Hoedkop show a similar relationship, where all the deformed peridotites have higher temperatures (1230 °C-1266 °C), than the granular peridotites (822 °C-993 °C). This association of deformation textures and high temperatures however does not apply to all peridotite suites, as peridotites with deformed textures but relatively low equilibration temperatures have been documented in Gibeon (Hanaus) by Mitchell (1984), in Kimberley by Dawson et al. (1975) and Boyd and Nixon (1978), and also in Wangqing located in NE China by Xu et al. (1998). It is therefore clear that deformed textures cannot be explained as a simple outcome of high temperature and lithostatic pressures, but rather require significant shear stress as well, considering that some high temperature deformed peridotites exhibit relatively low equilibration pressures (Nicolas et al., 1973). One hypothesis is that rising mantle plumes and diapirs provide heat to the surrounding rocks at shallow levels in the mantle, resulting in high temperatures and low equilibration pressures (Franz et al., 1996a; Xu et al., 1998). Melts from these rising plumes or diapirs, in combination with the high temperatures, would aid plastic deformation of the mantle rocks and hence resulting in deformed peridotites with high temperatures relative to their pressures of equilibration.

Such melts or fluids could have also played a significant role in creating some textures observed in the samples. Kelyphite rims around garnet grains are present in samples from both Hoedkop and Louwrensia and are a result of metasomatic reaction. The extent of kelyphite replacement differs greatly between xenolith suites. For example, kelyphite replacement is much greater in Hoedkop than in Louwrensia garnets. The fact that xenoliths from different kimberlites display markedly different extents of kelyphitisation and other forms of garnet breakdown suggests that it cannot entirely occur during kimberlite entrainment. The near- to complete replacement of primary peridotite minerals by metasomatic assemblages, such as clinopyroxene by phlogopite (as seen in several Louwrensia samples) or garnet by phlogopite, spinel and clinopyroxene (as seen in some Hoedkop samples) is a strong indication of metasomatic reactions involving hydrous fluids.

A small number of peridotite xenoliths display textures reflecting exsolution apparently caused by changes in equilibration temperature and/or pressure in these areas (decompression and cooling or some combination of the two). For example, Rietfontein sample RIET-2 contains clinopyroxene with exsolved garnet and orthopyroxene, while in RIET-1, spinel forms fingerprint symplectite intergrowths with clinopyroxene and orthopyroxene. The exsolution of garnet and/or spinel from pyroxene occurs because pyroxenes are able to include a substantial amount of aluminium in their crystal structure through substitution of Ca, Mg, Fe and Si, thus decreasing the temperature or pressure decreases the solubility of aluminium in the pyroxene. Consequently, as portions of the mantle cool or move upward, these changes can result in the unmixing of pyroxenes and the exsolution of garnet and spinel (e.g., Ringwood, 1967; Exley, 1982; Gasparik, 2000; Faryad et al., 2009; Spengler et al., 2012). Other symplectitic intergrowths such as between diopside + spinel + garnet (e.g. Figure 4.1a) are understood to form from more complex processes that can involve exsolution during isobaric cooling or continued reaction between minerals through isothermal progressive dynamic metamorphism of the lithosphere (Field and Haggerty, 1994).

Other mineralogical reactions in the peridotites, such as conversion of olivine to serpentine, more likely occurred during near-surface alteration after kimberlite emplacement. Serpentinisation occurs when relatively low-temperature aqueous fluids are introduced in the lherzolite, allowing it to react with ferromagnesian minerals such as olivine to form secondary serpentine. The degree of serpentinisation therefore depends on the degrees of fracturing of the minerals, as well as the amount and temperature of fluid flow which the xenoliths have experienced. For example, samples RIET-1 and RIET-3 from Rietfontein are more serpentinized than any of the samples from Louwrensia or Hoedkop, while those from Pofadder show the highest degrees of serpentinisation overall.

In general, the investigated peridotite xenoliths from beneath the north-western Namaqua-Natal Province and the Rehoboth Province display very similar mineralogies and textures, with a majority of samples displaying coarse granular textures and the rest showing evidence of incipient deformation. Reaction textures, such as those caused by exsolution and metasomatism, are common in peridotites from both regions and all suites display varying degrees of serpentinisation. Overall, there is no distinctive clear indication of significant systematic petrographic difference between the mantle beneath the NW Namaqua-Natal and the Rehoboth provinces.

5. SAMPLE PREPARATION AND ANALYTICAL METHODS

5.1. SAMPLE PREPARATION

All Louwrensia and Hoedkop xenoliths, as well as some xenoliths from Rietfontein vary in size between 3 and 10 cm in maximum dimension, and were therefore large enough to have thin sections prepared, whereas all xenoliths from Pofadder and most from Rietfontein were too small (< 2 cm in maximum dimension) and fragile due to their state of alteration to do this, so for this reason their minerals were prepared as grain mounts.

Thin sections for Louwrensia samples were prepared as 100 μm thick, standard 45 x 25 mm polished sections that were used for both petrography and for in-situ trace element analysis. For xenoliths from Hoedkop and the larger ones from Rietfontein, normal 30 μm-thick polished thin sections were prepared that were used for petrography and major element mineral chemistry analysis, while the polished slabs left over from thin section preparation were used for in-situ trace element analysis. Peridotites from Pofadder and most from Rietfontein, which were quite small (<2cm in maximum dimension) were crushed to liberate individual mineral grains. The resulting material was sieved and washed with distilled water to separate the denser primary minerals from the more buoyant alteration phases. In each sample, the primary minerals was then carefully hand-picked under a binocular microscope to select fresh, clean individual mineral grains. The grains selected were free of visible inclusions and cracks in order to minimise the possibility of contamination by kimberlite or secondary minerals. Most grains selected were 1 to 2 mm in size. The individual mineral grains were mounted in 25 mm diameter epoxy discs which were subsequently polished.

5.2. ANALYTICAL METHODS

5.2.1. Electron Probe Micro-analyser

Bulk-rock and mineral major element data have previously been presented for the Louwrensia and Hoedkop samples (Boyd et al., 2004; Janney et al., 2010), but peridotite xenoliths from Rietfontein and Pofadder are largely (Rietfontein) or entirely (Pofadder) undescribed previously in the published literature. Therefore, major element mineral data for garnet, clinopyroxene, orthopyroxene and olivine were obtained for these latter samples in the Department of Geological Sciences at UCT. Polished epoxy discs and thin sections were carbon coated and major element compositions of garnet, clinopyroxene, orthopyroxene and olivine were determined using a JEOL JXA-8100 Electron Probe Micro-analyser (data found in appendix). This instrument is equipped with four wavelength dispersive spectrometers and a range of analysing crystals (LDE1, LDE2, PETJ, PETH, TAP, LIF, and LIFH).

For the purpose of analysis, the beam current of the equipment was set to 40nA and an accelerating voltage of 15kV was used. The electron probe was calibrated using mineral in-house standards of known composition, which were also run after every 10 analyses to monitor instrumental drift. If the measured composition of a mineral standard drifted outside of normal analytical uncertainty for a particular element, the problematic element would be recalibrated. Table 5.1 depicts the values from standards run during the analysis sessions. In each sample, at least 5 grains of each of the minerals were analysed, with two spot measurements conducted on each grain.

Table 5.1 *Average major elements values for minerals analysed by electron probe micro-analysis*

	SiO_2	TiO_2	Al_2O_3	Cr_2O_3	FeO	MnO	MgO	CaO	Na_2O	K_2O	Total
(a) In-house garnet											
Average	41.78	0.25	23.48	1.07	8.10	0.38	20.32	4.62	0.47	0.95	99.91
Relative std. Dev.	0.01	0.12	0.00	0.02	0.01	0.08	0.01	0.01	0.03	0.01	0.00
Accepted values	41.79	0.37	23.49	1.09	8.11	0.45	20.33	4.62	0.50	0.96	99.91
(b) In-house clinopyroxene											
Average	54.32	0.26	3.09	0.76	1.67	0.24	16.69	21.36	1.60	1.01	99.82
Relative std. Dev.	0.00	0.13	0.01	0.05	0.06	0.07	0.01	0.02	0.03	0.08	0.00
Accepted values	54.32	0.38	3.11	0.81	1.74	0.32	16.70	21.38	1.63	1.19	99.83
(c) In-house orthopyroxene											
Average	57.30	0.18	1.27	0.25	4.96	0.16	35.65	0.22	0.35	n.a.	99.90
Relative std. Dev.	0.01	0.09	0.03	0.08	0.02	0.12	0.01	0.05	0.05	n.a.	0.00
Accepted values	57.31	0.27	1.30	0.33	4.99	0.28	35.65	0.27	0.39	n.a.	99.90
(d) In-house olivine											
Average	40.01	0.61	0.78	0.80	13.66	0.19	45.62	0.12	0.32	n.a.	99.92
Relative std. Dev.	0.01	0.01	0.04	0.02	0.02	0.15	0.01	0.07	0.11	n.a.	0.00
Accepted values	40.02	0.64	0.82	0.82	13.67	0.34	45.63	0.19	0.42	n.a.	99.92

Averages represent the means of 15 analyses of garnet, 15 analyses of clinopyroxene, 15 analyses of orthopyroxene and five analyses of olivine standards, analysed as unknowns during the electron probe analysis sessions. Relative standard deviations represent the 1σ standard deviation of these replicate data for each oxide expressed as a percentage of the average value obtained. Note that "n.a." is an abbreviation for "not analysed".

5.2.2 Laser Ablation Inductively Coupled Plasma-Mass Spectrometry

Trace element data for peridotite xenoliths from Rietfontein, Hoedkop and Pofadder have never been described previously in the published literature, however limited trace element data for Louwrensia peridotites do exist in the literature (Mitchell, 1984; Boyd et al., 2004). However, only a small number of samples were analysed in these studies and these data were obtained using a different analytical technique (secondary ion mass spectrometry) than used here. Further, a smaller number of elements were measured. A wide range of trace elements were measured in garnet and clinopyroxene grains from the 44 peridotite xenoliths from the four localities investigated here. These two minerals contain well over 90% of all incompatible trace elements in peridotites.

All trace element analyses employed a Thermo-Fisher X-series 2 quadrupole ICP-MS coupled with a New Wave Research UP 213 nm solid-state ultraviolet laser ablation system in the Department of Geological Sciences at UCT. A 100 μm diameter laser spot, with an energy density of 2 Jcm^{-1} and a frequency of 10 Hz was used in the analysis of all mineral grains. Instrumental calibration was accomplished using synthetic glass standards NIST 610 and 612 that were also run after every 20 measurements, while the well-characterised mineral standards (Monastery garnet and JJG1424 CPX) were also run after every 10 measurements during the analytical session to monitor the accuracy of the data and the analytical precision of the method. Five to ten grains of each mineral in each sample were analysed. Each mineral grain analysed was characterised by two to four measurements, depending on its size. Measurements were validated to check for any errors and a mean was calculated to give an average composition for each mineral type in a given sample. Table 5.2 shows the average values from standards run during the analysis sessions. The CaO and SiO_2 values from microprobe analysis were used as internal standard to normalise results from each clinopyroxene and garnet analysis, respectively.

Table 5.2 Trace element values for Monastery garnet and JJG 1424 clinopyroxene analysed in this study

	(a) Monastery garnet			(b) JJG1424 Clinopyroxene		
	Average	Relative std. Dev.	Accepted values	Average	Relative std. Dev.	Accepted values
Sc	62.37	0.13	62.50	30.35	0.09	30.44
V	221.95	0.09	222.04	536.30	0.07	536.37
Cr	1559.28	1.09	1560.37	6287.72	0.09	6287.81
Ni	62.42	0.35	62.77	226.40	0.04	226.44
Rb	1.00	0.06	1.06	0.96	0.06	1.02
Sr	0.41	0.20	0.62	302.72	0.07	302.79
Y	27.86	0.14	27.99	2.33	0.11	2.44
Zr	87.23	0.16	87.39	42.31	0.13	42.44
Nb	0.15	0.12	0.27	2.23	0.02	2.25
Ba	0.61	0.04	0.65	3.43	0.73	4.16
La	0.28	0.03	0.31	21.93	0.12	22.06
Ce	0.35	0.13	0.48	61.68	0.09	61.77
Pr	0.15	0.12	0.27	7.06	0.07	7.13
Nd	1.36	0.12	1.48	27.18	0.08	27.26
Sm	1.21	0.11	1.31	3.79	0.07	3.86
Eu	0.68	0.10	0.78	1.04	0.06	1.10
Tb	0.60	0.11	0.72	0.21	0.13	0.35
Gd	2.76	0.14	2.89	2.12	0.08	2.20
Dy	4.93	0.12	5.05	0.84	0.09	0.93
Ho	1.14	0.13	1.26	0.16	0.10	0.26
Er	3.46	0.11	3.57	0.17	0.14	0.30
Tm	0.49	0.16	0.65	0.36	0.01	0.37
Yb	3.79	0.12	3.91	0.21	0.08	0.29
Lu	0.52	0.12	0.64	0.34	0.01	0.35
Hf	2.23	0.14	2.37	2.03	0.11	2.14
Ta	0.39	0.01	0.40	0.98	0.00	0.98
Pb	1.52	0.05	1.57	0.75	0.42	1.17
Th	0.58	0.01	0.59	1.35	0.12	1.47
U	0.33	0.01	0.34	0.24	0.07	0.31

The average values shown are means of 22 Monastery garnet and 24 JJG 1424 clinopyroxene standard analyses obtained during laser ablation analysis in the course of this study. Relative standard deviations represent the 1σ standard deviation of these replicate data for each element expressed as a percentage of the average value obtained.

6. GEOCHEMICAL RESULTS

6.1. MAJOR ELEMENT GEOCHEMISTRY

Major element mineral data were obtained by electron probe microanalysis for garnet, clinopyroxene, orthopyroxene and, where present, olivine in peridotite xenoliths from Pofadder and Rietfontein, and these new data are combined with previously published mineral major element data for Hoedkop, Louwrensia and Rietfontein, and are presented in the appendix as a single data set. There were no significant compositional differences observed between cores and rims of the grains tested, and therefore it is appropriate to report average values for each mineral in the peridotite samples. The calculated average major element compositions of garnet, clinopyroxene, orthopyroxene and olivine for each sample from the four populations studied are reported in Table 6.1, Table 6.2, Table 6.3 and Table 6.4 respectively.

In the following figures in this section, the mineral compositions of the samples investigated are compared to those from granular and deformed lherzolites from the Hanaus, Gibeon Townlands and Anis Khubub kimberlites of the Gibeon cluster in the Rehoboth Province, peridotites (all coarse granular) from the Uintjiesberg, Hebron and Melton Wold kimberlites that are located in the western Namaqua-Natal Province southwest of the Kaapvaal Craton and finally, they are compared with coarse granular garnet lherzolites from the Kimberley kimberlites located on the Kaapvaal Craton. This suite of cratonic peridotites was selected for comparison because the Kimberley lherzolites exhibit a similar range of equilibration pressures to the samples studied and, like the xenoliths in this study, they were also exhumed by group 1 kimberlites

Table 6.1 *Average major element data for garnets obtained by Electron Probe analysis*

		oxides (wt. %)											
location	**sample name**	**SiO_2**	**TiO_2**	**Al_2O_3**	**Cr_2O_3**	**FeO**	**MnO**	**MgO**	**CaO**	**Na_2O**	**K_2O**	**Total**	**Mg no.**
Louwrensia	FRB 1180	42.15	0.11	19.54	5.79	6.57	0.38	21.00	6.16	0.02	0.00	101.73	85.10
Louwrensia	FRB 1183	41.22	0.04	21.97	2.59	8.12	0.48	20.51	5.53	0.02	0.00	100.48	81.83
Louwrensia	FRB 1652	41.96	0.04	20.88	4.28	7.67	0.47	20.12	5.88	0.02	0.00	101.33	82.40
Louwrensia	FRB 1683	41.06	0.84	16.70	8.23	6.69	0.36	20.00	6.94	0.07	0.00	100.90	84.20
Louwrensia	FRB 1684	42.15	0.03	21.75	3.30	7.50	0.39	20.70	5.29	0.01	0.00	101.13	83.10
Louwrensia	FRB 1686	42.07	0.38	19.85	5.20	6.66	0.37	21.13	5.69	0.05	0.00	101.40	85.00
Louwrensia	JJG 2513	42.02	0.01	21.44	3.41	7.74	0.41	20.81	5.50	0.00	0.00	101.35	82.70
Louwrensia	JJG 2514	42.19	0.03	21.52	3.38	7.66	0.39	21.15	5.31	0.02	0.00	101.66	83.11
Louwrensia	PHN 5316	42.37	0.03	21.78	3.17	7.62	0.38	21.01	5.24	0.02	0.00	101.62	83.10
Louwrensia	PHN 5364	42.19	0.01	21.49	3.55	7.72	0.45	20.56	5.66	0.03	0.00	101.66	82.60
Louwrensia	PHN 5365	42.27	0.04	19.83	2.56	7.41	0.47	20.20	7.20	0.08	0.00	100.07	82.90
Rietfontein	RIET-2	42.05	0.01	22.26	0.88	8.83	0.50	19.81	5.24	0.01	0.01	99.61	80.00
Rietfontein	RIET-3	41.05	0.15	20.93	4.02	8.20	0.50	19.08	5.25	0.05	0.00	99.22	80.58
Rietfontein	RIET-4	41.35	0.09	22.90	1.18	11.29	0.49	16.95	5.21	0.02	0.00	99.48	72.81
Rietfontein	RIET-5	41.64	0.16	22.13	2.77	8.07	0.43	19.00	5.38	0.03	0.00	99.60	80.75
Rietfontein	RIET-6	41.35	0.16	20.93	4.38	7.74	0.50	18.96	5.55	0.03	0.00	99.58	81.38
Rietfontein	RTFN 30-1	41.46	0.13	23.49	0.69	8.80	0.42	19.90	4.32	0.06	0.01	99.27	80.12
Rietfontein	RTFN 30-2	41.52	0.11	23.76	0.62	8.91	0.41	20.04	4.14	0.04	0.01	99.54	80.05
Rietfontein	RTFN 30-4	41.12	0.07	22.76	1.76	9.08	0.50	19.24	4.65	0.04	0.01	99.23	79.07
Rietfontein	RTFN 30-5	41.23	0.08	22.55	1.79	9.41	0.50	19.16	4.56	0.02	0.02	99.32	78.40

Table 6.1 *Continued*

Rietfontein	RTFN 30-7	41.58	0.14	20.33	4.23	7.92	0.50	19.16	5.16	0.04	0.01	99.07	81.18
Rietfontein	RTFN 30-8	40.76	0.05	23.44	0.31	13.82	0.34	17.56	3.32	0.05	0.01	99.65	69.36
Rietfontein	RTFN 30-13	40.90	0.13	23.33	0.85	11.53	0.39	18.39	4.42	0.01	0.03	99.98	73.97
Rietfontein	RTFN 30-14	41.55	0.12	23.54	0.65	8.76	0.44	19.97	4.26	0.03	0.01	99.33	80.25
Rietfontein	RTFN 31-5	41.30	0.11	21.00	4.04	7.64	0.48	19.72	4.89	0.05	0.01	99.22	82.16
Hoedkop	HOD-1	41.96	0.04	20.29	1.67	7.49	0.46	20.12	6.75	0.01	0.01	98.80	82.72
Hoedkop	HOD-2	41.68	0.26	20.69	2.57	6.32	0.26	21.69	5.21	0.03	0.01	98.98	85.95
Hoedkop	HOD-3	42.38	0.29	20.28	1.28	6.48	0.42	21.72	5.61	0.03	0.01	98.50	85.66
Hoedkop	HOD-4	41.62	0.30	19.63	5.30	6.37	0.27	21.04	5.58	0.03	0.01	100.16	85.48
Hoedkop	HOD-5	41.44	0.04	20.68	4.92	7.30	0.43	19.53	6.31	0.02	0.02	100.68	82.67
Hoedkop	HOD-11	42.28	0.03	21.44	1.47	7.49	0.44	19.85	6.22	0.01	0.01	99.23	82.53
Pofadder	JJG 2499-4	41.40	0.03	22.57	2.25	8.80	0.49	19.31	5.01	0.05	0.00	99.89	79.64
Pofadder	JJG 2499-6	41.46	0.05	22.45	2.32	8.64	0.53	19.17	5.00	0.05	0.01	99.69	79.82
Pofadder	JJG 2499-7	41.61	0.04	22.43	2.49	8.75	0.51	19.30	5.11	0.03	0.01	100.27	79.73
Pofadder	JJG 2499-12	41.35	0.03	22.07	2.69	8.78	0.48	19.19	5.13	0.03	0.01	99.75	79.58
Pofadder	JJG 2499-14	41.32	0.02	22.43	2.30	8.64	0.48	19.33	5.03	0.01	0.01	99.57	79.95
Pofadder	JJG 2499-15	41.78	0.02	22.18	2.51	8.74	0.48	19.28	5.20	0.01	0.01	100.21	79.73
Pofadder	JJG 2499-16	41.68	0.10	23.64	0.69	8.79	0.43	20.09	4.28	0.05	0.02	99.77	80.29

All data reported as weight percent oxide. Data for Louwrensia peridotites are from Boyd et al. (2004) and that for all Hoedkop peridotites, as well as sample RIET-2, are from Janney et. al. (2010). Mg number assumes that all Fe is present as FeO.

Table 6.2 *Average major element data for clinopyroxenes obtained by Electron Probe analysis*

		oxides (wt. %)											
Location	**Sample name**	**SiO_2**	**TiO_2**	**Al_2O_3**	**Cr_2O_3**	**FeO**	**MnO**	**MgO**	**CaO**	**Na_2O**	**K_2O**	**Total**	**Mg No.**
Louwrensia	FRB 1180	54.64	0.08	1.78	1.90	2.38	0.09	18.08	20.11	1.41	0.00	100.53	93.12
Louwrensia	FRB 1183	54.38	0.05	2.14	1.76	2.33	0.09	16.95	20.68	1.65	0.00	100.08	87.91
Louwrensia	FRB 1652	54.78	0.03	2.23	1.60	2.32	0.09	16.84	20.69	1.75	0.00	100.38	92.83
Louwrensia	FRB 1683	54.57	0.52	2.71	2.13	3.18	0.11	18.98	17.25	1.64	0.00	101.15	91.41
Louwrensia	FRB 1684	53.65	0.05	2.19	1.30	2.31	0.07	16.91	20.40	1.51	0.00	98.43	92.88
Louwrensia	FRB 1686	54.75	0.02	1.77	1.11	2.20	0.07	17.36	21.60	1.30	0.00	100.21	93.40
Louwrensia	JJG 2513	54.63	0.02	1.97	1.26	2.33	0.08	17.44	21.25	1.34	0.00	100.38	93.03
Louwrensia	JJG 2514	54.46	0.11	1.47	1.18	2.20	0.08	17.51	22.52	1.00	0.00	100.58	93.42
Louwrensia	PHN 5316	54.96	0.05	2.26	1.35	2.50	0.08	17.19	20.40	1.58	0.00	100.42	92.46
Louwrensia	PHN 5364	54.50	0.15	2.36	2.01	2.41	0.06	16.77	19.79	1.96	0.00	100.06	92.54
Louwrensia	PHN 5365	54.23	0.07	1.95	1.15	1.81	0.07	17.05	22.28	1.22	0.00	99.87	94.38
Rietfontein	RIET-1	54.07	0.08	2.63	1.13	1.45	0.07	16.36	22.04	1.94	0.04	99.81	95.26
Rietfontein	RIET-2	54.85	0.05	2.16	0.46	1.33	0.05	16.72	23.33	1.44	0.03	100.44	95.73
Rietfontein	RIET-3	54.12	0.24	3.14	2.37	2.14	0.10	15.51	20.00	2.38	0.01	100.00	92.83
Rietfontein	RIET-4	55.24	0.10	1.60	0.48	2.83	0.09	17.03	21.22	0.92	0.01	99.52	91.47
Rietfontein	RIET-5	55.07	0.16	2.61	1.55	2.08	0.09	16.10	19.99	1.69	0.01	99.36	93.23
Rietfontein	RIET-6	54.92	0.21	2.90	2.31	2.10	0.10	15.51	18.99	2.23	0.01	99.28	92.93
Rietfontein	RTFN 30-1	55.02	0.23	3.14	0.51	1.82	0.09	16.60	20.98	1.82	0.00	100.20	94.21
Rietfontein	RTFN 30-2	54.51	0.26	3.04	0.43	2.22	0.12	16.59	20.72	1.86	0.01	99.77	93.02
Rietfontein	RTFN 30-4	54.48	0.21	2.43	0.40	3.03	0.12	16.52	20.97	1.66	0.01	99.83	90.66
Rietfontein	RTFN 30-5	54.22	0.18	2.78	1.13	2.08	0.10	16.31	20.87	1.81	0.01	99.50	93.32

Table 6.2 *Continued*

Rietfontein	RTFN 30-7	54.24	0.20	3.01	2.34	1.97	0.11	15.56	19.69	2.41	0.00	99.53	93.37
Rietfontein	RTFN 30-8	55.00	0.18	7.12	0.48	2.96	0.08	13.27	16.15	4.21	0.00	99.46	88.89
Rietfontein	RTFN 30-13	54.42	0.22	2.90	0.45	3.17	0.09	16.17	20.56	2.00	0.02	99.99	90.09
Rietfontein	RTFN 30-14	54.37	0.26	3.16	0.41	1.89	0.08	16.48	20.94	1.80	0.01	99.40	93.96
Rietfontein	RTFN 31-5	54.03	0.28	3.27	2.32	1.87	0.15	15.34	19.35	2.43	0.00	99.04	93.60
Hoedkop	HOD-1	54.73	0.16	1.70	0.60	2.04	0.07	17.57	22.69	1.12	0.04	100.73	93.88
Hoedkop	HOD-2	54.84	0.12	2.48	0.96	2.90	0.09	18.71	18.05	1.60	0.07	99.83	92.00
Hoedkop	HOD-3	54.75	0.13	2.49	0.51	2.89	0.10	18.77	18.15	1.62	0.06	99.47	92.05
Hoedkop	HOD-4	54.89	0.13	2.51	1.02	2.83	0.09	18.76	17.99	1.59	0.07	99.88	92.20
Hoedkop	HOD-5	54.27	0.30	1.79	0.83	2.64	0.10	17.47	21.30	1.20	0.06	99.95	92.18
Hoedkop	HOD-6	53.40	0.02	1.83	0.65	1.44	0.05	17.35	23.78	0.67	0.06	99.27	95.55
Hoedkop	HOD-7	53.90	0.51	0.47	1.82	4.64	0.16	18.46	17.95	1.94	0.02	99.87	87.64
Hoedkop	HOD-8	53.78	0.01	1.51	0.69	1.48	0.05	17.66	23.65	0.38	0.04	99.26	95.51
Hoedkop	HOD-9	53.63	0.07	2.25	1.54	1.61	0.03	16.44	22.63	1.27	0.03	99.49	94.79
Hoedkop	HOD-10	55.11	0.00	1.98	0.67	1.53	0.06	17.16	23.73	0.69	0.05	100.98	95.24
Hoedkop	HOD-11	54.84	0.46	1.33	0.43	1.96	0.07	17.52	23.45	0.99	0.01	101.07	94.09
Pofadder	JJG 2499-4	54.45	0.03	2.43	1.48	2.17	0.11	16.85	20.58	1.43	0.01	99.54	93.26
Pofadder	JJG 2499-6	54.30	0.04	2.39	1.37	2.15	0.10	16.72	21.25	1.43	0.00	99.76	93.27
Pofadder	JJG 2499-7	54.09	0.04	2.41	1.43	2.18	0.09	16.73	21.16	1.43	0.01	99.58	93.18
Pofadder	JJG 2499-12	54.12	0.05	2.38	1.41	2.13	0.06	16.79	21.10	1.40	0.01	99.44	93.37
Pofadder	JJG 2499-14	54.33	0.04	2.36	1.45	2.14	0.10	16.83	21.26	1.50	0.01	100.03	93.33
Pofadder	JJG 2499-15	54.27	0.03	2.38	1.42	2.13	0.10	16.85	21.14	1.39	0.00	99.73	93.39
Pofadder	JJG 2499-16	54.34	0.03	2.46	1.49	2.12	0.10	16.80	21.13	1.45	0.00	99.92	93.38

All data reported as weight percent oxide. Data for Louwrensia peridotites are from Boyd et al. (2004) and that for all Hoedkop peridotites, as well as sample RIET-1 and RIET-2, are from Janney et. al. (2010). Mg number assumes that all Fe is present as FeO.

Table 6.3 *Average major element data for orthopyroxene obtained by electron probe analysis*

		oxides (wt. %)										
location	**sample name**	**SiO_2**	**TiO_2**	**Al_2O_3**	**Cr_2O_3**	**FeO**	**MnO**	**MgO**	**CaO**	**Na_2O**	**Total**	**Mg no.**
Louwrensia	FRB 1180	57.50	0.05	1.21	0.60	4.95	0.12	35.28	0.71	0.07	100.62	92.70
Louwrensia	FRB 1183	57.53	0.02	0.95	0.36	4.97	0.12	35.98	0.37	0.04	100.44	92.81
Louwrensia	FRB 1652	57.78	0.01	0.95	0.31	5.08	0.11	35.67	0.34	0.08	100.44	92.60
Louwrensia	FRB 1683	56.40	0.29	1.82	0.89	5.39	0.12	33.95	1.22	0.22	100.42	91.82
Louwrensia	FRB 1684	57.65	0.02	0.96	0.30	5.10	0.11	35.72	0.42	0.07	100.47	92.58
Louwrensia	FRB 1686	57.42	0.20	1.24	0.54	4.80	0.11	35.68	0.62	0.13	100.84	92.98
Louwrensia	JJG 2513	57.64	0.00	1.04	0.29	5.24	0.10	35.59	0.42	0.02	100.45	92.37
Louwrensia	JJG 2514	57.77	0.01	0.91	0.31	5.10	0.11	36.02	0.32	0.03	100.58	92.64
Louwrensia	PHN 5316	57.84	0.02	1.03	0.29	5.31	0.11	35.60	0.43	0.08	100.81	92.28
Louwrensia	PHN 5364	57.75	0.06	0.60	0.38	4.71	0.08	35.91	0.37	0.03	99.89	93.20
Louwrensia	PHN 5365	57.46	0.03	1.10	0.30	5.03	0.12	36.00	0.25	0.02	100.39	92.73
Rietfontein	RIET-1	56.44	0.03	1.57	0.35	4.90	0.13	35.94	0.25	0.04	99.72	92.89
Rietfontein	RIET-2	57.41	0.01	0.96	0.10	5.23	0.11	36.09	0.21	0.03	100.23	92.48
Rietfontein	RIET-3	58.08	0.08	0.88	0.31	4.89	0.15	34.98	0.22	0.07	99.64	92.73
Rietfontein	RIET-4	57.34	0.06	0.75	0.11	7.91	0.14	33.67	0.23	0.03	100.23	88.36
Rietfontein	RIET-5	57.92	0.07	0.90	0.32	5.49	0.15	34.73	0.20	0.04	99.82	91.85
Rietfontein	RIET-6	58.22	0.09	0.86	0.30	5.05	0.14	34.91	0.23	0.07	99.88	92.50
Rietfontein	RTFN 30-1	57.66	0.07	0.72	0.04	5.35	0.05	35.68	0.23	0.12	99.92	92.24
Rietfontein	RTFN 30-2	57.21	0.00	1.23	0.27	5.61	0.03	34.94	0.26	0.16	99.71	91.74
Rietfontein	RTFN 30-4	56.97	0.10	0.71	0.06	7.37	0.04	34.15	0.28	0.10	99.77	89.20
Rietfontein	RTFN 30-5	57.46	0.07	0.82	0.21	5.49	0.07	35.10	0.20	0.16	99.57	91.94

Table 6.3 *Continued*

Rietfontein	RTFN 30-7	58.35	0.04	0.68	0.07	4.39	0.03	35.94	0.23	0.11	99.83	93.59
Rietfontein	RTFN 30-8	57.03	0.08	2.91	0.20	7.17	1.39	25.77	5.21	0.10	99.84	86.50
Rietfontein	RTFN 30-13	57.69	0.11	0.71	0.06	7.37	0.07	33.98	0.27	0.12	100.39	89.16
Rietfontein	RTFN 30-14	57.95	0.08	0.75	0.06	5.35	0.06	35.60	0.24	0.11	100.20	92.22
Rietfontein	RTFN 31-5	58.16	0.06	0.87	0.30	4.74	0.08	35.80	0.24	0.16	100.40	93.09
Hoedkop	HOD-1	57.56	0.02	1.22	0.18	5.08	0.13	36.04	0.43	0.06	100.82	92.67
Hoedkop	HOD-2	56.62	0.06	1.47	0.45	4.87	0.10	35.01	1.03	0.21	99.94	92.76
Hoedkop	HOD-3	57.42	0.08	1.46	0.18	4.96	0.11	35.22	1.04	0.21	100.80	92.68
Hoedkop	HOD-4	56.74	0.07	1.43	0.47	4.79	0.11	34.44	1.03	0.19	99.40	92.76
Hoedkop	HOD-5	56.99	0.02	1.39	0.24	5.05	0.13	35.27	0.44	0.06	99.68	92.56
Hoedkop	HOD-6	56.45	0.01	2.06	0.38	5.12	0.13	35.21	0.35	0.02	100.05	92.46
Hoedkop	HOD-7	54.89	0.11	0.81	0.44	7.43	0.18	34.46	0.49	0.21	99.09	89.21
Hoedkop	HOD-8	56.44	0.01	1.86	0.48	5.04	0.11	35.15	0.58	0.01	99.79	92.56
Hoedkop	HOD-9	57.10	0.00	1.48	0.49	4.92	0.11	35.13	0.70	0.02	100.04	92.72
Hoedkop	HOD-10	57.13	0.01	2.12	0.35	5.23	0.11	34.93	0.27	0.01	100.22	92.25
Hoedkop	HOD-11	57.45	0.02	1.69	0.18	4.96	0.12	36.08	0.39	0.03	101.01	92.84
Pofadder	JJG 2499-4	56.39	0.02	1.25	0.34	5.69	0.03	35.65	0.30	0.16	99.84	91.78
Pofadder	JJG 2499-6	56.69	0.05	1.33	0.35	5.59	0.08	34.80	0.28	0.15	99.33	91.73
Pofadder	JJG 2499-7	57.88	0.03	1.18	0.32	5.79	0.14	35.77	0.26	0.04	101.42	91.68
Pofadder	JJG 2499-12	57.54	0.02	1.24	0.36	5.58	0.12	35.16	0.28	0.04	100.34	91.82
Pofadder	JJG 2499-14	57.44	0.00	1.24	0.33	5.40	0.09	34.62	0.26	0.00	99.38	91.95
Pofadder	JJG 2499-15	56.76	0.03	1.23	0.32	5.63	0.04	35.69	0.28	0.15	100.12	91.88
Pofadder	JJG 2499-16	56.29	0.00	1.26	0.35	5.69	0.06	35.82	0.31	0.11	99.89	91.82

All data given in weight percent oxide. Data for Louwrensia peridotites are from Boyd et al. (2004) and that for all Hoedkop peridotites, as well as samples RIET-1 and RIET-2, are from Janney et. al. (2010). Mg number calculation assumes that all Fe is present as FeO.

Table 6.4 *Average major element data for olivines obtained by electron probe analysis*

	oxides (wt. %)										
location	sample name	SiO_2	TiO_2	Al_2O_3	Cr_2O_3	FeO	MnO	MgO	CaO	NiO	Total	Mg no.
Louwrensia	FRB 1180	40.69	0.01	0.01	0.05	8.01	0.09	49.86	0.05	0.39	99.16	91.73
Louwrensia	FRB 1183	40.78	0.01	0.00	0.02	8.28	0.08	50.41	0.03	0.39	100.00	91.56
Louwrensia	FRB 1652	40.48	0.01	0.00	0.02	8.17	0.10	50.08	0.02	0.44	99.27	91.62
Louwrensia	FRB 1683	40.41	0.02	0.03	0.09	8.77	0.10	49.38	0.09	0.37	99.26	90.94
Louwrensia	FRB 1684	40.35	0.01	0.00	0.02	8.25	0.09	50.41	0.02	0.42	99.56	91.59
Louwrensia	FRB 1686	40.84	0.02	0.01	0.03	7.67	0.09	50.66	0.04	0.35	99.74	92.17
Louwrensia	JJG 2513	40.54	0.00	0.00	0.01	8.46	0.07	49.65	0.03	0.42	99.18	91.28
Louwrensia	JJG 2514	40.65	0.01	0.00	0.01	8.35	0.10	50.34	0.02	0.41	99.89	91.49
Louwrensia	PHN 5316	40.26	0.00	0.01	0.02	8.58	0.09	49.43	0.03	0.44	98.82	91.13
Louwrensia	PHN 5365	40.96	0.01	0.00	0.01	8.26	0.10	50.57	0.02	0.43	100.33	91.61
Louwrensia	PHN 5364	40.36	0.01	0.00	0.03	8.59	0.08	49.95	0.02	0.42	99.44	91.20
Rietfontein	RIET-1	40.64	0.00	0.08	0.01	7.82	0.11	50.66	0.01	0.36	99.68	92.03
Rietfontein	RIET-2	40.60	0.04	0.00	0.01	8.32	0.09	50.77	0.01	0.41	100.25	91.58
Rietfontein	RIET-3	41.12	0.01	0.25	0.01	7.59	0.11	50.23	0.01	0.35	99.67	92.19

Table 6.4 *Continued*

Hoedkop	HOD-1	40.65	0.03	0.01	0.02	8.34	0.12	51.01	0.03	0.39	100.60	91.60
Hoedkop	HOD-2	40.71	0.01	0.03	0.05	8.05	0.10	51.11	0.08	0.42	100.55	91.88
Hoedkop	HOD-3	40.68	0.02	0.03	0.03	7.99	0.10	51.12	0.07	0.34	100.36	91.94
Hoedkop	HOD-4	40.78	0.01	0.02	0.03	7.76	0.10	50.72	0.07	0.39	99.88	92.10
Hoedkop	HOD-5	40.61	0.01	0.01	0.01	8.32	0.11	51.14	0.03	0.39	100.63	91.64
Hoedkop	HOD-6	41.02	0.00	0.00	0.00	8.18	0.10	49.97	0.01	0.49	99.78	91.59
Hoedkop	HOD-7	39.87	0.01	0.01	0.01	12.55	0.14	47.18	0.02	0.33	100.13	87.02
Hoedkop	HOD-8	40.75	0.00	0.00	0.00	7.91	0.10	50.64	0.01	0.48	99.89	91.94
Hoedkop	HOD-9	40.52	0.00	0.00	0.00	7.94	0.10	50.88	0.01	0.48	99.92	91.95
Hoedkop	HOD-10	40.52	0.00	0.00	0.00	8.45	0.11	50.29	0.01	0.49	99.88	91.39
Hoedkop	HOD-11	40.76	0.04	0.01	0.01	7.84	0.10	51.07	0.02	0.38	100.24	92.07

All data given in weight percent oxide. Data for Louwrensia peridotites are from Boyd et al. (2004) and that for all Hoedkop peridotites, as well as samples RIET-1 and RIET-2, are from Janney et. al. (2010). Mg number calculation assumes that all Fe is present as FeO.

6.1.1 Garnet

All garnets investigated in this study are classified as pyrope and fall within the calcic-lherzolite (G9) classification as defined by Gurney (1985) in comparison to Kimberley garnets which are more evenly split between the calcic-lherzolitic and subcalcic-harzburgitic (G10) types (Figure 6.1). There is a strong correlation between CaO and Cr_2O_3 in all garnets from the four localities resulting in compositional variation that is in a direction parallel to the G9/G10 boundary. This is also true of garnets from the other Gibeon kimberlites, peridotitic concentrate garnets from Rietfontein and garnets in peridotites from other southern African off-craton localities such as the "Eastern Namaqualand" kimberlites of Uintjiesberg, Hebron, Melton Wold and Gansfontein. One sample from Louwrensia (PHN 5365), two from Rietfontein (RIET-2, RIET-4) and three from Hoedkop (HOD-1, HOD-3, HOD-5) are significantly displaced from the general trend, and fall at fairly high CaO for given Cr_2O_3 values, in addition to falling well outside the range of the Kimberley data. Pofadder peridotites have garnets that display very limited variation in CaO and Cr_2O_3 contents.

Overall, garnets from the four localities span a wide range of Mg number values (i.e., 100*[atomic Mg/ [Mg+Fe]) from 69.3 to 86.0. Pofadder and Rietfontein peridotitic garnets have the lowest Mg numbers, on average, with means of 79.8 ± 0.4 and 78.6 ± 2.6 (2σ, i.e., 2 standard deviations), respectively, which tend to be lower than those in garnets from Kimberley peridotites. Garnets from Gibeon and Hoedkop are comparable in that they both display higher Mg numbers with average values of 83.6 ± 4.2 and 84.2 ± 2.0 respectively. These garnets show more variation in Mg number than those from Pofadder and less than Rietfontein, and overlap significantly with garnets from Kimberley.

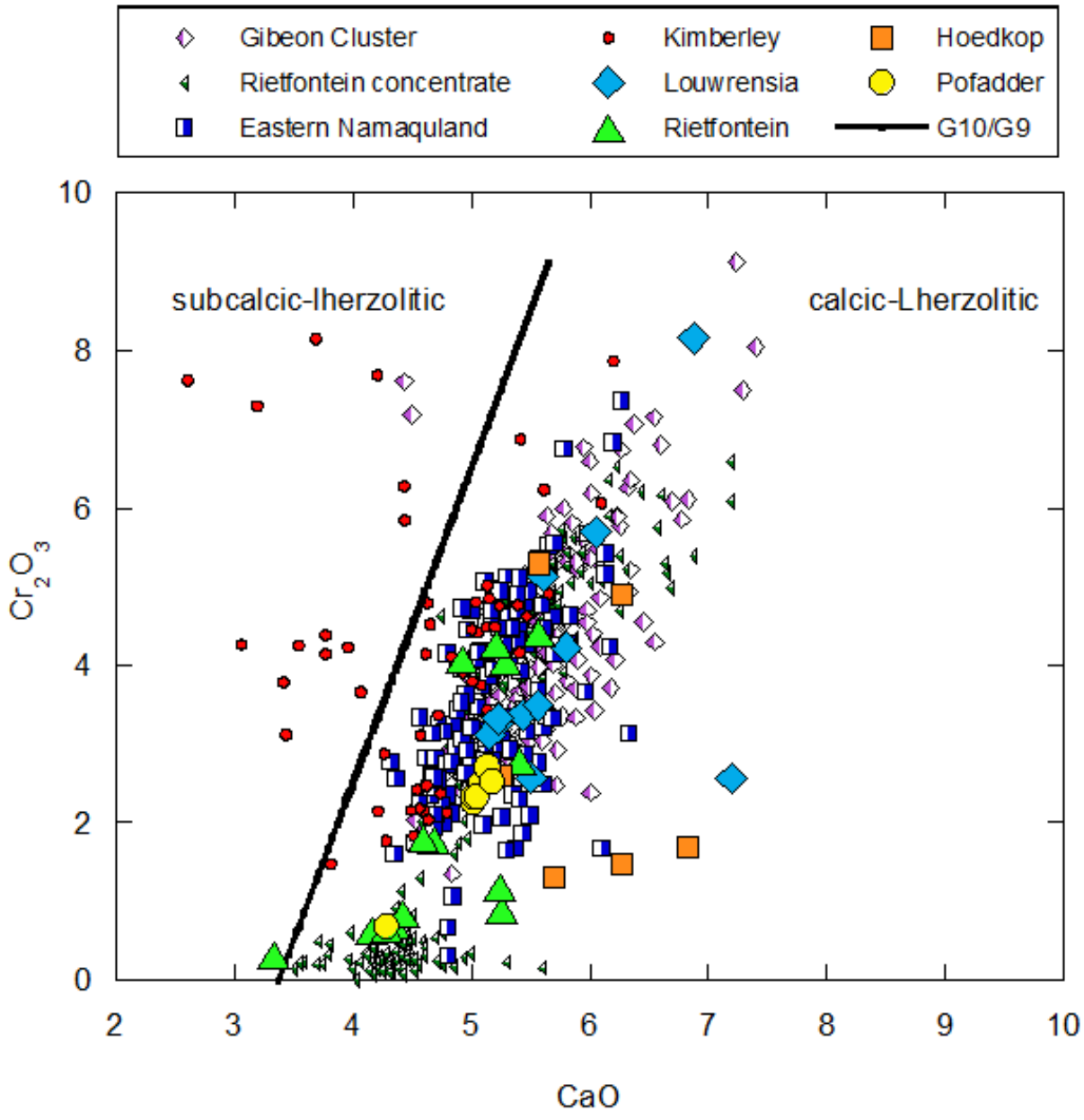

Figure 6.1 plot of wt. % CaO vs. wt. % Cr_2O_3 for garnets from off-craton peridotites from the Rehoboth Province, the western Namaqua-Natal Province and also cratonic peridotites from the Kimberley area. Data for Gibeon cluster peridotites other than those from Louwrensia studied, are from Mitchell (1984) and Franz et al., (1996a; 1996b) and Boyd et al. (2004). Data for Rietfontein concentrate garnets are from De Bruin (1999). Data for Eastern Namaqualand kimberlites is from Janney et al. (2010) and data for Kimberly peridotites is from Lawless (1978), Schulze (1995), Boyd & Nixon (1978), Cox et al (1978), and Boyd et al (1993).

Peridotitic garnets from the four investigated localities display a strong correlation between Mg number and Cr_2O_3 content with most samples lying within the main trend of data defined by peridotitic garnets from Kimberley (Figure 6.2). Garnets from Rietfontein display a wide range of Mg number and Cr_2O_3 content in a reverse L-shape distribution on Figure 6.2 (i.e., at Mg number values below about 80, all Rietfontein garnets have values below about 2 wt. % Cr_2O_3, whereas higher Cr_2O_3 values are dominant at higher Mg numbers). This appears to be a general feature in Rietfontein as the same pattern is also shown by Rietfontein concentrate garnets (De Bruin, 1999). Pofadder garnets have relatively low and uniform Cr_2O_3 concentration with most samples having 2.4 wt.% and one sample (JJG 2499-16) falling at an even lower Cr_2O_3 value of about 0.7 wt.%. Garnets from Louwrensia form a positive correlation between Mg number and Cr_2O_3 content that overlap with that of garnets from other localities within the Gibeon cluster, while those from Hoedkop shows similar Mg number vs. Cr_2O_3 relationship to those from Eastern Namaqualand off-craton peridotites.

The concentration of MnO in the studied garnets (0.3-0.5 wt. %) falls within the range displayed by other garnets in southern African off-craton peridotites from Uintjiesberg, the Gibeon cluster as well as cratonic garnets from Kimberley (Figure 6.3). For Gibeon and Hoedkop peridotites, the MnO content of garnet shows a negative correlation with Mg number, while Rietfontein displays a weak positive correlation. Pofadder garnets span a very narrow range in MnO concentration at a constant Mg number. Both the Rietfontein and Pofadder garnets are richer in MnO and lower in Mg number than most southern African (on- or off-craton) peridotitic garnets. The range of TiO_2 contents in the garnets studied is limited, with the vast majority having TiO_2 contents of $\leq$ 0.16 wt. %. The few deformed samples in the study (1 from Louwrensia and 3 from Hoedkop) all have markedly higher TiO_2 contents (> 0.25 ppm) than the granular samples (Figure 6.4).

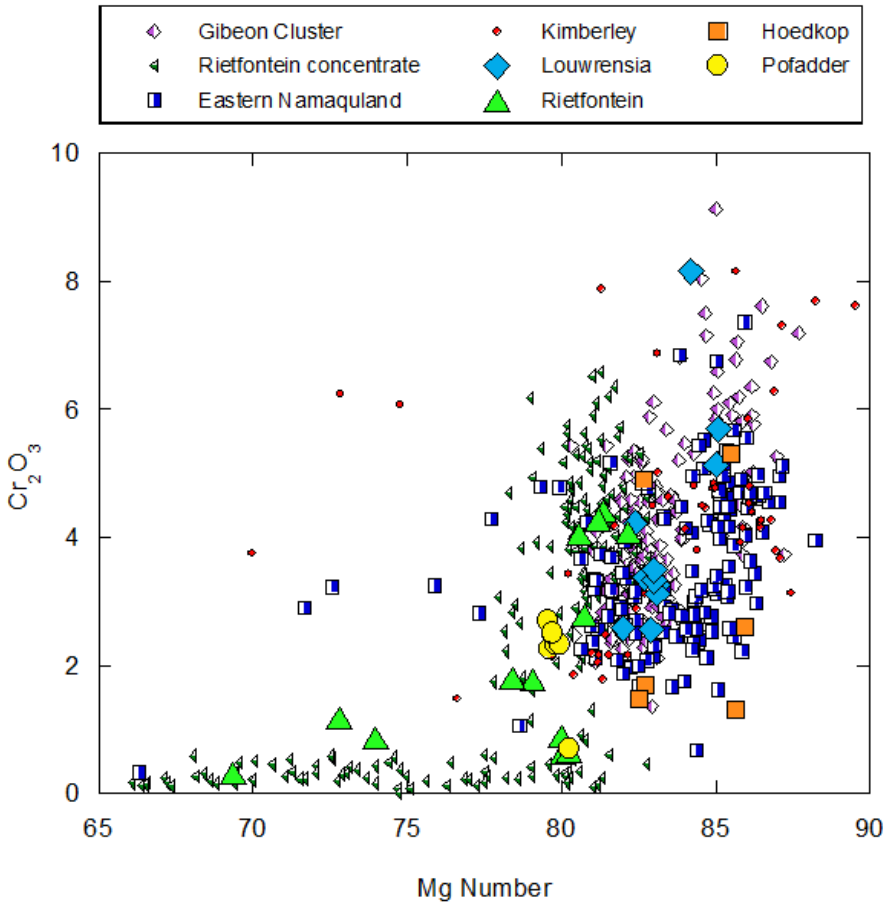

Figure 6.2 . Plot of Mg-number vs. Cr_2O_3 wt. % for garnets from southern African off-craton peridotite populations and Kimberley (cratonic) garnet. Literature data source are as listed in Figure 6.1

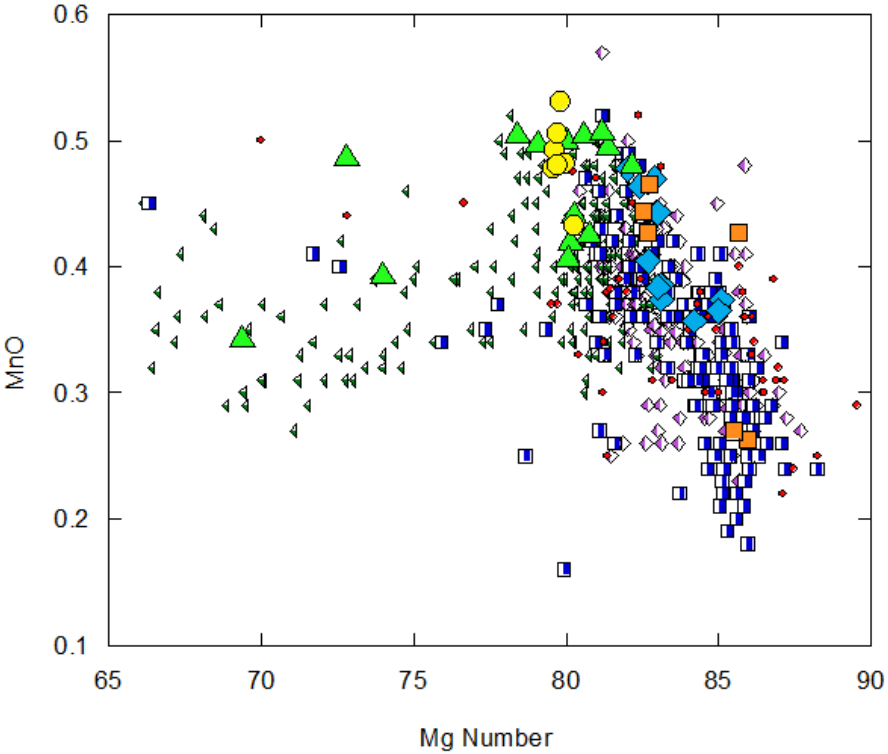

Figure 6.3. Plot of Mg-number vs. MnO wt. % for garnets from southern African off-craton peridotite populations and Kimberley (cratonic) garnets. Literature data source are as listed in Figure 6.1

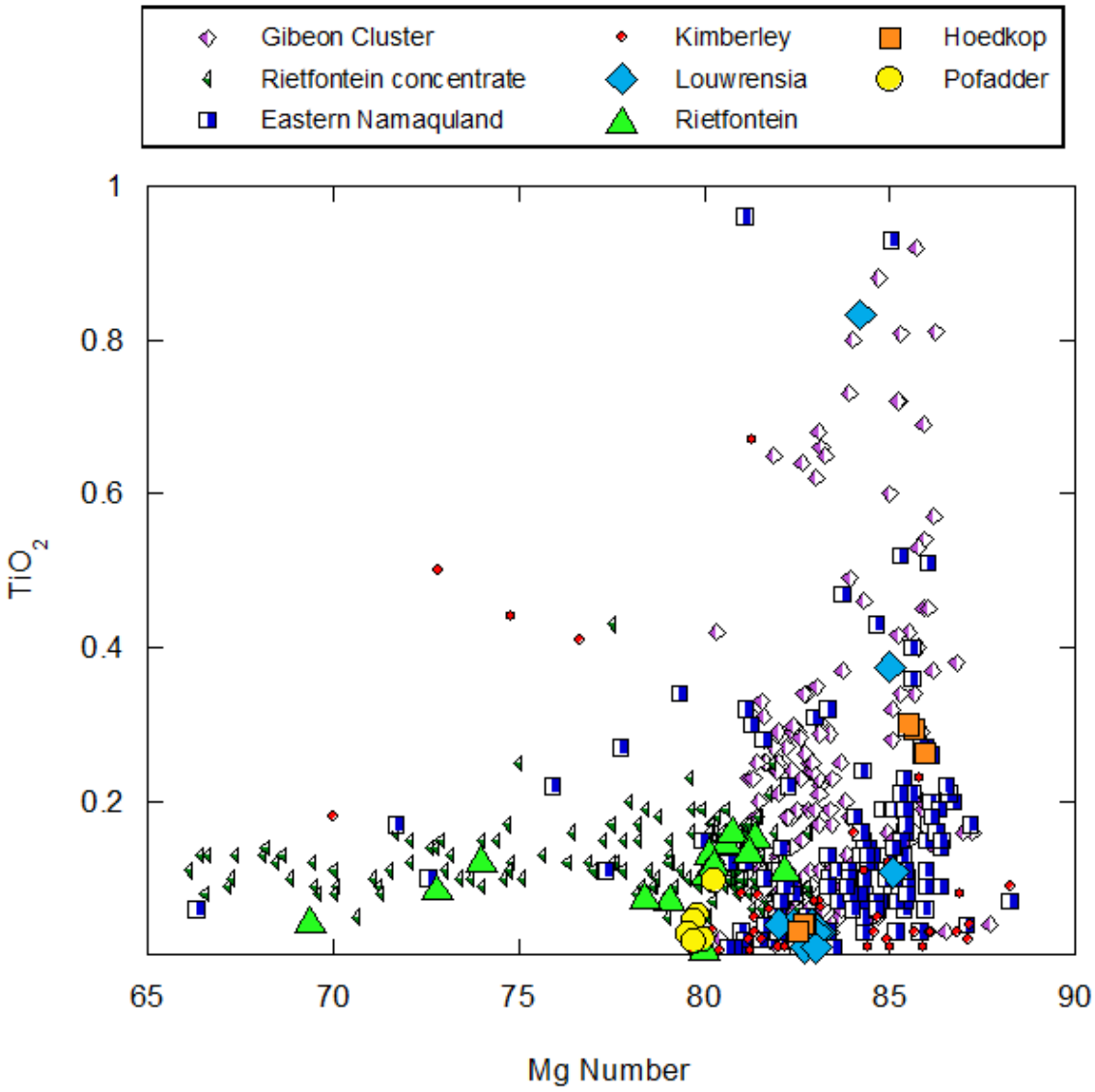

Figure 6.4. Plot of Mg-number vs. TiO_2 wt. % for garnets from southern African off-craton peridotite populations and Kimberley (cratonic) garnet. Literature data source are as listed in Figure 6.1

6.1.2 Clinopyroxene

All clinopyroxene in the studied samples is classified as Cr-diopside, and displays a wide range of compositions, with Mg numbers ranging between 87.6 and 95.7. This range overlaps with peridotitic clinopyroxene from Kimberley and southern African off-craton localities. Hoedkop clinopyroxene has an average Mg number value of 93.2 ± 4.5 (2σ) and show the largest variation in Mg number due to one unusually Fe-rich sample (HOD-7) that has very low Mg numbers for all ferromagnesian minerals. In contrast, clinopyroxene from Pofadder display a very narrow range of 93.3 ± 0.1. Clinopyroxene from Gibeon and Rietfontein have Mg numbers with moderate variations, of 92.9 ±1.5 and 92.8 ± 3.6, respectively.

The Ca number values [100*atomic Ca/ (Ca+Mg)] for clinopyroxene from the four studied localities range from 39.5 to 50.1. Amongst the populations studied, Louwrensia and Hoedkop clinopyroxenes have the lowest average Ca numbers (45.8 ± 5.0 and 46.6 ± 7.8, respectively) while Pofadder and Rietfontein have the highest (47.4 ±0.6 and 47.8 ±1.7 respectively). This mainly reflects the prevalence of high-temperature deformed peridotites at Louwrensia and Hoedkop, and their absence at Rietfontein and Pofadder, as Ca number of clinopyroxene is largely a function of temperature (e.g., Lindsley, 1983). All clinopyroxene from the xenolith suites studied display Ca numbers falling within the range spanned by peridotitic clinopyroxene from Rietfontein heavy mineral concentrate, xenoliths from Eastern Namaqualand and pipes within the Gibeon cluster, and Kimberley peridotites which span a narrower range of Ca numbers than the former (Figure 6.5). The Mg number of the analysed clinopyroxenes show a strong positive correlation with the Ca number (Figure 6.5).

On average, clinopyroxenes studied have moderate Cr numbers [100*atomic Cr/(Cr+Al)], with Louwrensia clinopyroxene having a mean value of 32.8 ±8.1 (Boyd et al., 2004), while Pofadder, Hoedkop and Rietfontein have lower mean values of 28.6 ±0.9, 25.4 ± 30.9 and 19.1 ± 21.4 respectfully. The large 2 sigma standard deviations for most of these values indicates that they are all essentially indistinguishable within errors. Cr number values of clinopyroxene from the samples studied overlap with Kimberley peridotite clinopyroxene, but extend to lower values (Figure 6.6).

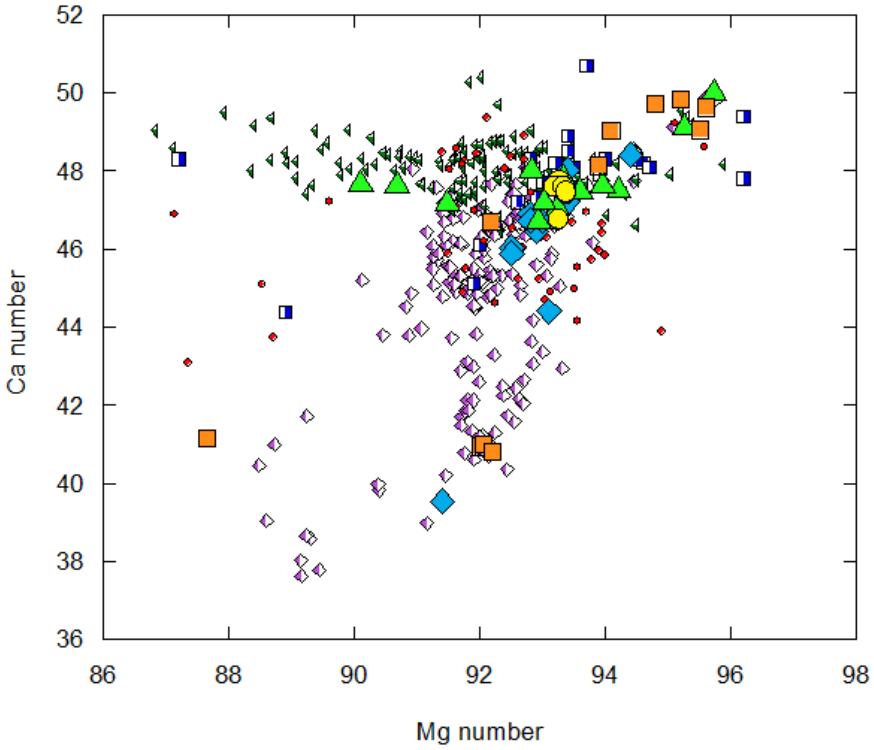

Figure 6.5. Plot of Mg-number vs. Ca-number for clinopyroxenes from southern African off-craton peridotite populations and Kimberley (cratonic). Literature data source are listed in Figure 6.1

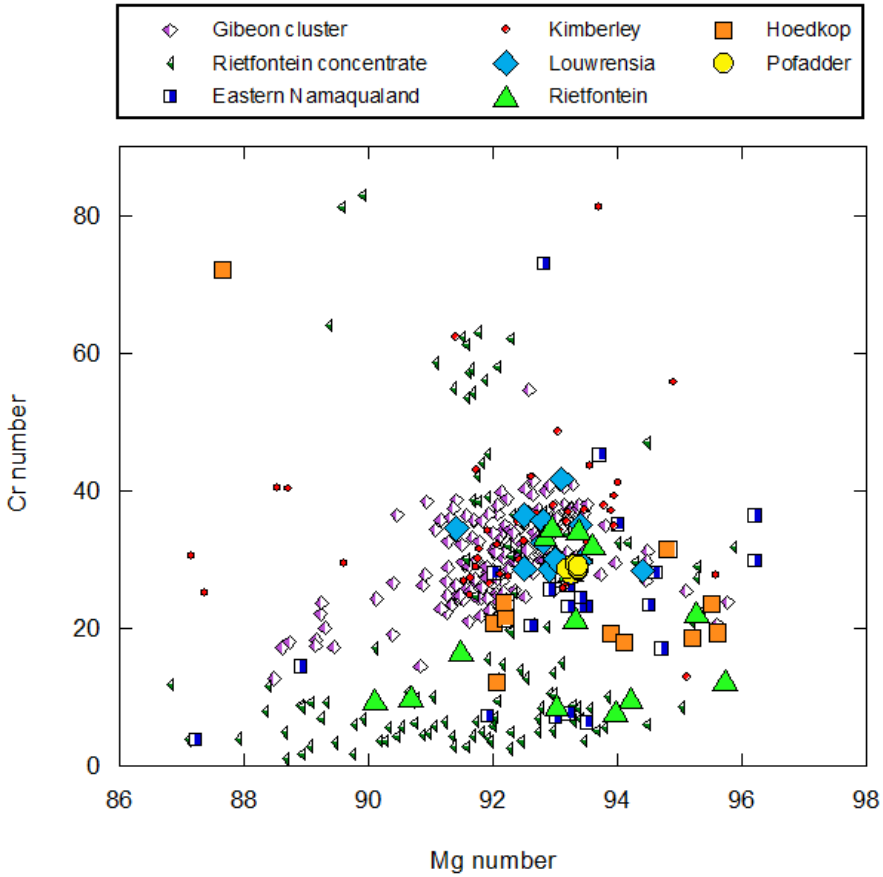

Figure 6.6. Plot of Mg-number vs. Cr-number for clinopyroxenes from southern African off-craton peridotite populations and Kimberley (cratonic). Literature data source are listed in Figure 6.1

The concentration of major oxides such as TiO_2, MgO, CaO and Cr_2O_3 in clinopyroxene from the studied samples are fairly similar and display a large degree of overlap with data for peridotitic clinopyroxene from other southern African off-craton localities and from Kimberley. It is also notable that Pofadder clinopyroxenes display nearly uniform compositions of the various oxides. Clinopyroxenes from the four localities studied have moderate amounts of Al_2O_3 ranging between 1.4 wt. % and 3.3 wt. % (Figure 6.7). Rietfontein clinopyroxenes show the highest variation in Al_2O_3 and Cr_2O_3 content, while Pofadder clinopyroxenes have a nearly uniform content of both oxides of about 2.4. % and 1.4 wt. % respectively. All clinopyroxenes from Louwrensia, Pofadder and a majority from Hoedkop fall within the 'garnet peridotite' field of the Al_2O_3 vs. Cr_2O_3 plot defined by Nimis (1998), while half of the clinopyroxenes from Rietfontein and two from Hoedkop fall on the border between the 'garnet peridotite' field and the 'eclogite, megacrysts and cognate' field (Figure 6.7).

The Na_2O contents of clinopyroxenes studied fall between 0.4 -and 2.5 wt. %. Hoedkop and Rietfontein show the largest variations (0.4 to 1.9 wt. % and 0.9 to 2.5 wt. %, respectively) and also extend to lower concentrations than those displayed by other localities studied and by Kimberley clinopyroxenes. Louwrensia and Hoedkop clinopyroxenes display a negative correlation between Na_2O content and Mg number (Figure 6.8).

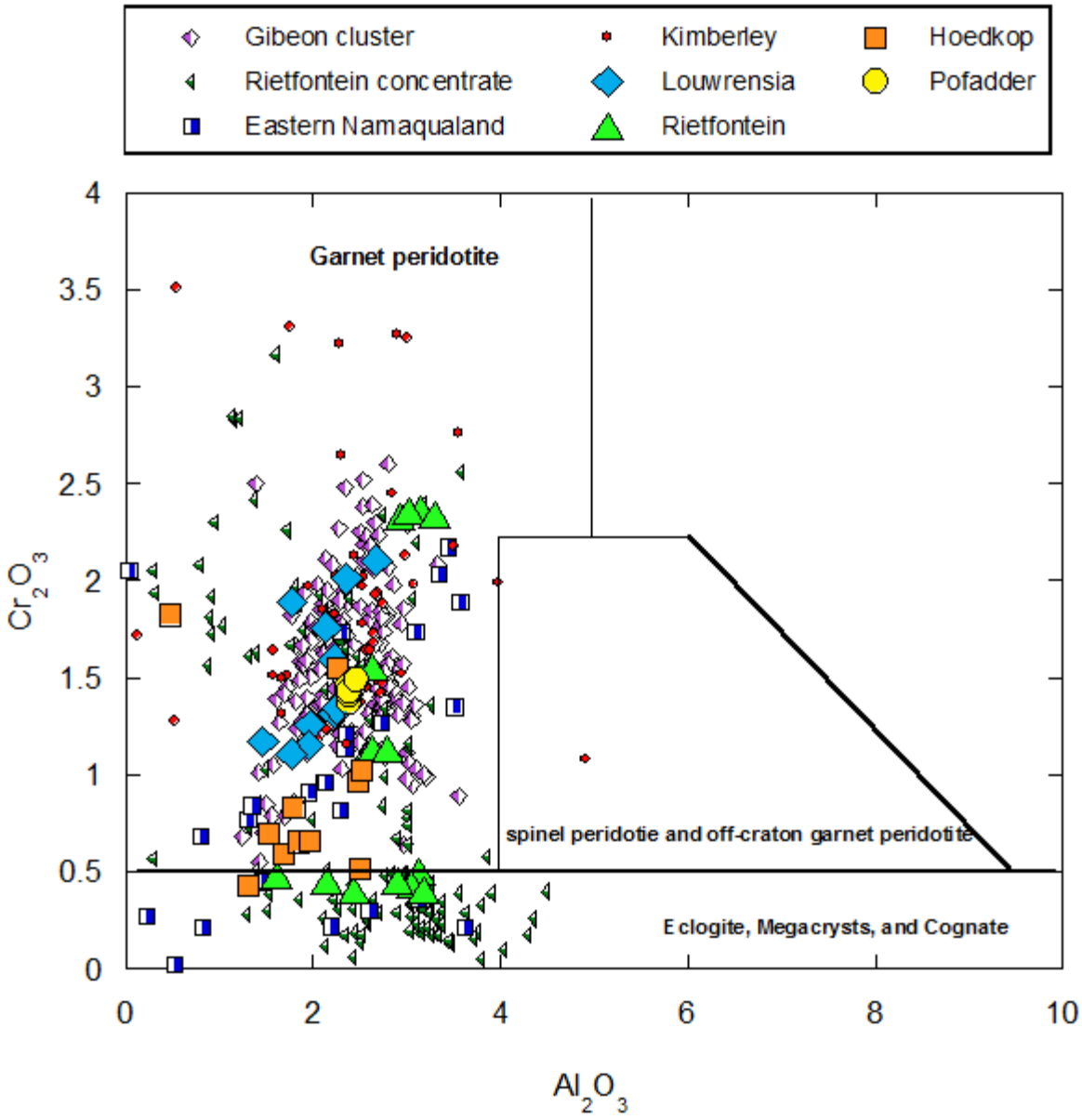

Figure 6.7. Plot of Al_2O_3 vs. Cr_2O_3 w.t. % for clinopyroxenes from southern African off-craton peridotite populations and Kimberley (cratonic). Literature data source are listed in Figure 6.1

The concentration of the minor element TiO_2 falls between 0 to 0.5 wt. %, with sample HOD-7, HOD-11 from Hoedkop and the deformed sample FRB 1683 from Louwrensia having some of the highest TiO_2 contents (around 0.5 wt. %), although clinopyroxenes from the Gibeon cluster extend to much higher TiO_2 values (Figure 6.9).

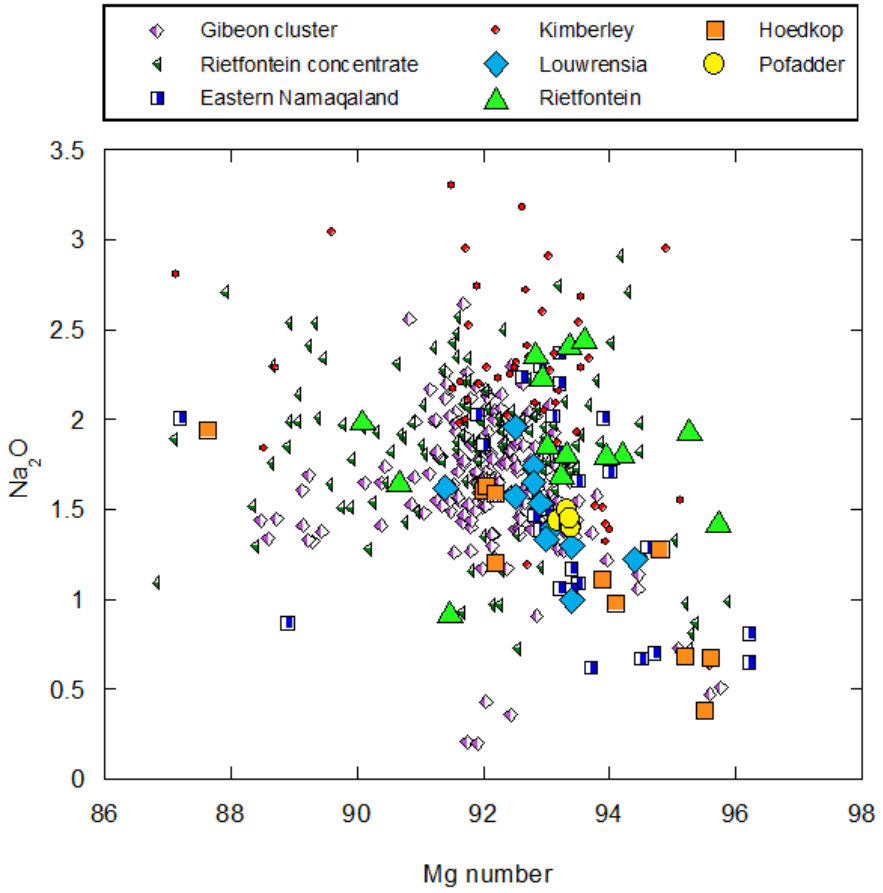

Figure 6.8. Plot of Mg-number vs. Na_2O wt. % for clinopyroxenes from southern African off-craton peridotite populations and Kimberley (cratonic). Literature data source are as listed in Figure 6.1

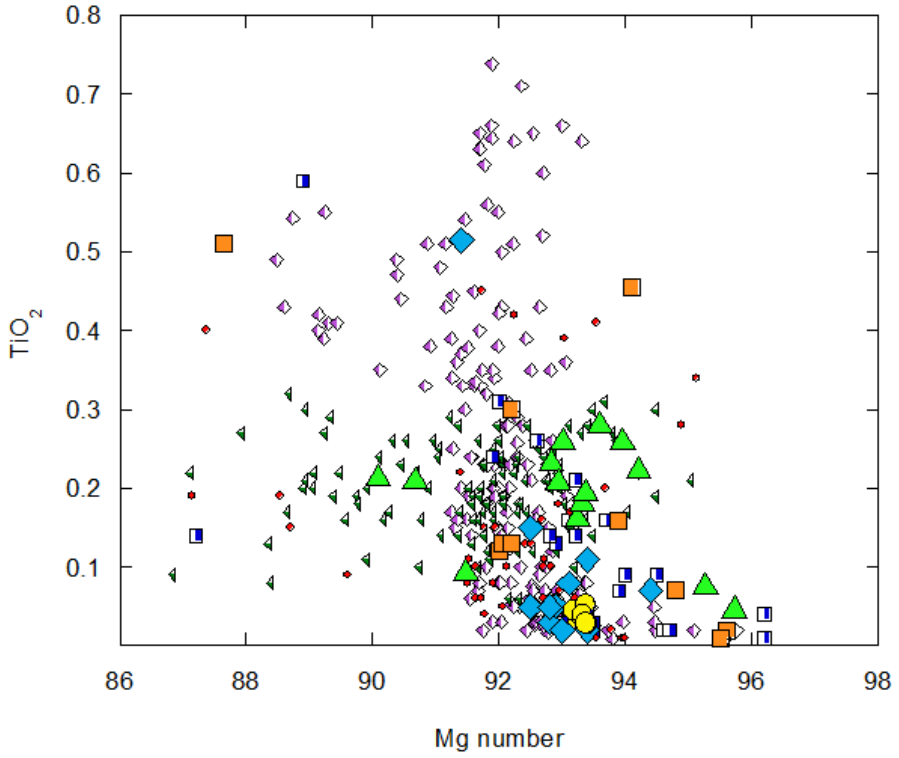

Figure 6.9. Plot of Mg-number vs. TiO_2 wt. % for clinopyroxenes from southern African off-craton peridotite populations and Kimberley (cratonic). Literature data source are as listed in Figure 6.1

6.1.3 Orthopyroxene

The Mg number of orthopyroxenes from lherzolite populations studied range between 88.4 and 93.6. The mean Mg# values for the four localities all lie within a much narrower range of 91.4 to 93.0. Similar to the clinopyroxenes, Cr numbers in the orthopyroxenes increase in the same order, with Louwrensia having a much higher average Cr number of 19.4 ± 3.4, in comparison to those from Pofadder (15.5 ± 0.5) Hoedkop (13.6 ± 5.7) and Rietfontein (10.8 ± 5.9).

Within each suite, there is a significant concentration range of Cr_2O_3 values in orthopyroxene, with the single exception of Pofadder, which has compositionally uniform orthopyroxene. Orthopyroxene from the deformed sample FRB 1683 from Louwrensia is richest in Cr_2O_3 of all samples investigated, and is significantly higher than orthopyroxenes from Eastern Namaqualand or Kimberley and is near the upper end of the range for all Gibeon orthopyroxenes (Figure 6.10a). As with clinopyroxene, the CaO content in orthopyroxene is also related to temperature (Hafner and Virgo, 1970). Orthopyroxenes from Rietfontein and Pofadder have low and nearly uniform amounts of CaO (0.20 % to 0.27 wt. %) as both localities have no high-temperature, deformed peridotites and therefore lack orthopyroxenes with high CaO values. On the other hand, orthopyroxenes from Gibeon and Hoedkop show higher and more variable CaO values (0.3 -1.2 wt. % and 0.3-1.0 wt. %, respectively) as these suites do have high-temperature deformed peridotites. Samples from Louwrensia, and from the Gibeon cluster as a whole, are the only ones that show a significant positive correlation between Cr_2O_3 and CaO in orthopyroxene (Figure 6.10a). Orthopyroxenes in the peridotites investigated all have Al_2O_3 contents greater than about 0.7 wt. %, with Hoedkop samples having the highest and most variable Al_2O_3. Rietfontein and Kimberley orthopyroxenes both cluster around 0.7 wt. % Al_2O_3 (Figure 6.10b).

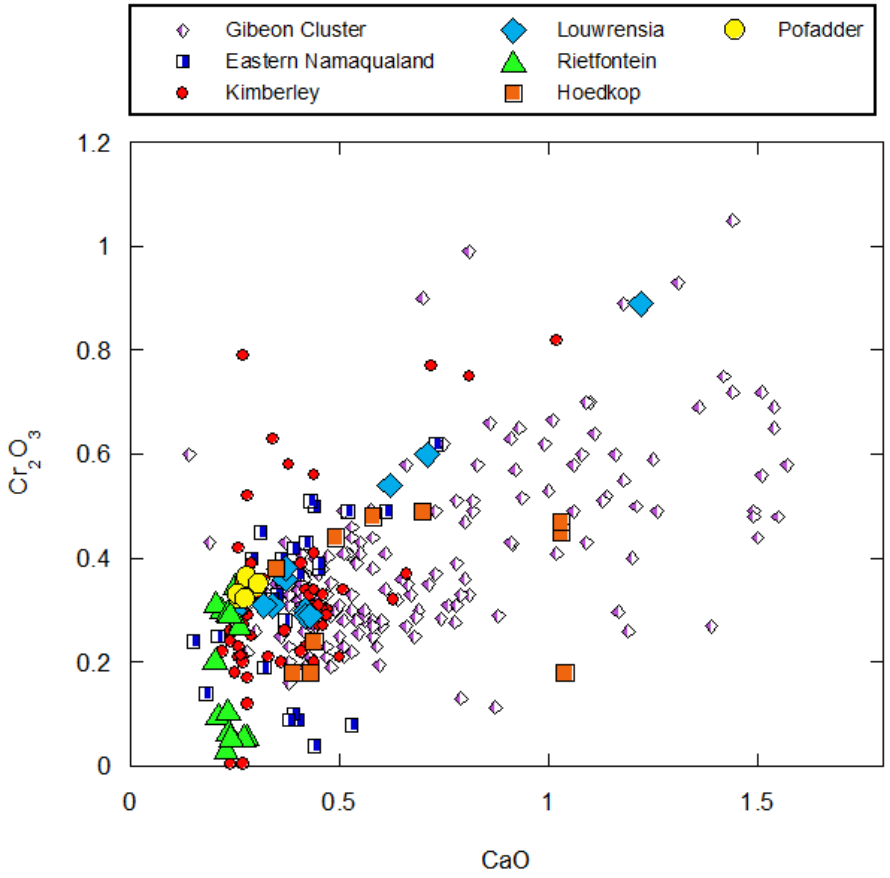

Figure 6.10. Plot of Mg-number vs. Cr_2O_3 wt. % for orthopyroxenes from southern African off-craton peridotite populations and Kimberley (cratonic). Literature data source are as listed in Figure 6.1

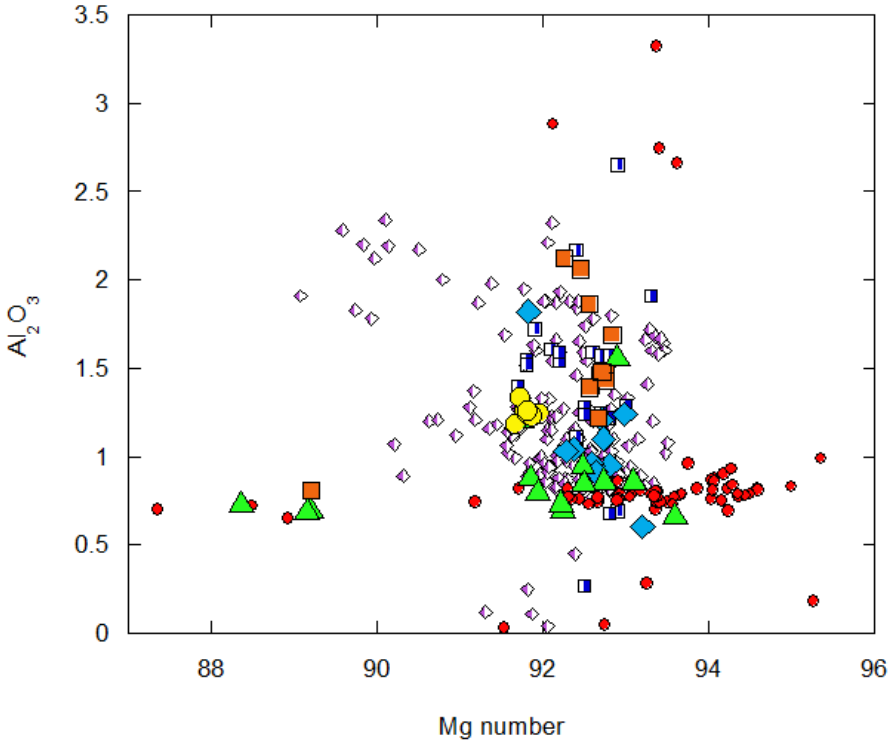

Figure 6.11. Plot of Mg-number vs. Cr_2O_3 wt. % for orthopyroxenes from southern African off-craton peridotite populations and Kimberley (cratonic). Literature data source are as listed in Figure 6.1

6.1.4 Olivine

In general, olivines from the Rehoboth Province localities (Louwrensia, Anis Kubub, Gibeon Townsland, Hanaus and Rietfontein) have average Mg numbers that are very comparable to those from the Namaqua-Natal Province (Hoedkop, Uintjiesberg, Hebron and Gansfontein) of 91.4 ± 1.6 (2σ) and 91.6 ± 1.7, respectively. Most olivines from both off-craton provinces have Mg numbers between 91 and 92, while olivines from cratonic peridotites most commonly have Mg numbers between 92 and 93 (Figure 6.12a).

Within the xenoliths investigated, Louwrensia and Rietfontein have average olivine Mg numbers of 91.5 ± 1.3 and 91.9 ± 0.5 respectively, while Hoedkop has an average of 91.4 ± 2.8 (Figure 6.12b). No olivines have been analysed from Pofadder because these small, altered xenoliths do not contain fresh olivine. The low average Mg number for Hoedkop olivine is due to the unusually Fe-rich sample HOD-7 (olivine Mg number = 87.1). If this sample is excluded, the mean value for Hoedkop olivine becomes 91.8 ± 0.5.

The olivines from the localities studied have similar, overlapping NiO contents (varying from 0.3 wt. % to 0.5 wt. %) that are also similar to those of olivines from cratonic peridotites, but with distinctly lower Mg numbers (Figure 6.13).

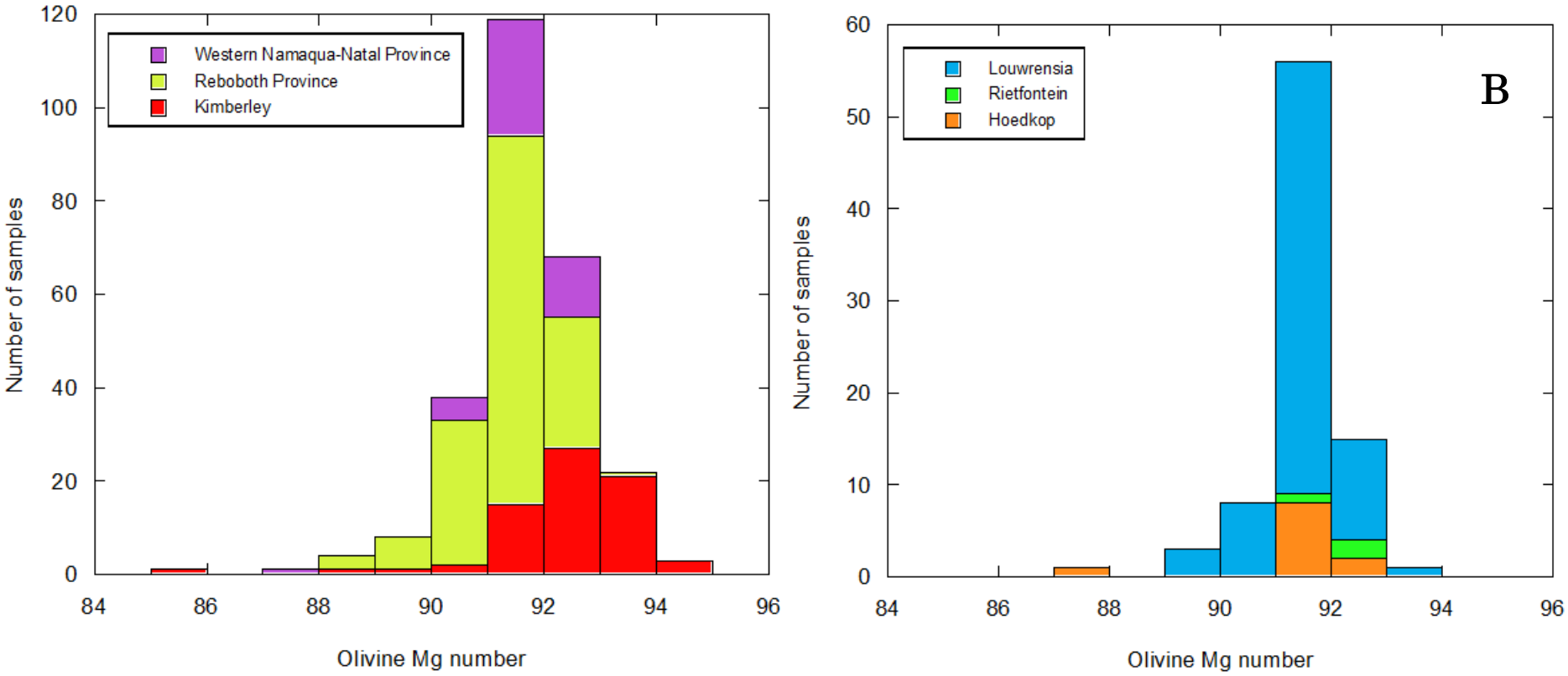

Figure 6.12. Histogram of Mg-number [100 Mg/ (Mg + Fe)] for southern African olivines from. (**A**) Kimberley (cratonic) peridotites and peridotite xenoliths from the Rehoboth and western Namaqua-Natal provinces (including samples from this study); **B**: Xenoliths from localities investigated in this study. Literature data source are as listed in Figure 6.1

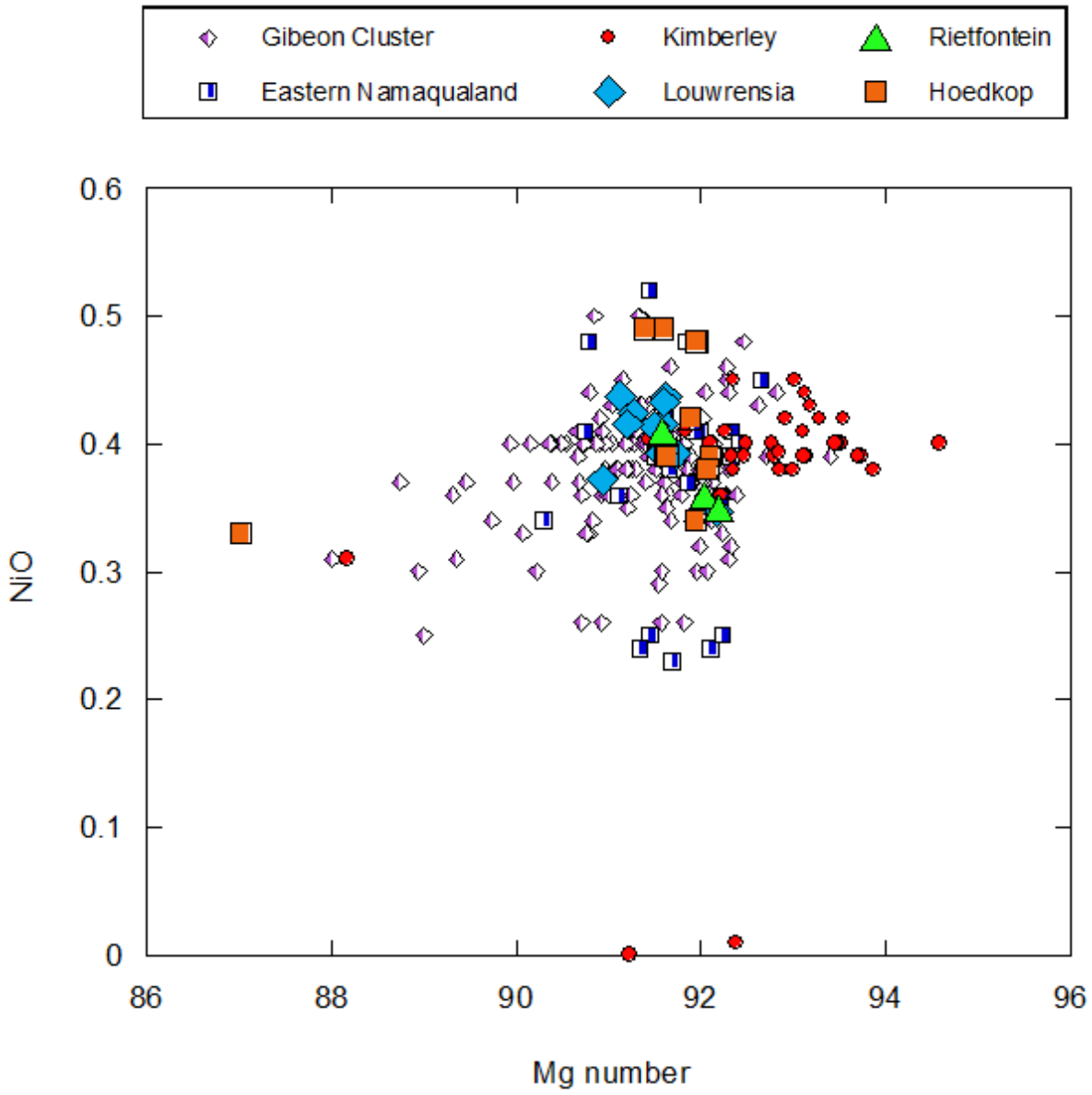

Figure 6.13. Plot of Mg-number vs. NiO wt. % for olivines from southern African off-craton peridotite populations and Kimberley (cratonic). Literature data source are listed in Figure 6.1

6.2. TRACE ELEMENT GEOCHEMISTRY

6.2.1 Introduction

Elements present in a rock or mineral at a concentration of less than 1000 parts per million by weight (0.1 wt. %) are regarded as trace elements and commonly substitute for major elements in the rock-forming minerals. Trace elements are grouped according to similar chemical properties, such as their position on the periodic table and their valence state and ionic radii and, as a consequence, they are usually studied in groups. The deviation of an element from the groups' behaviour or the systematic changes within the group are used as an indicator of fractionation by petrological processes (Rollinson, 1993). The abundances of trace elements in primary phases of peridotitic partial melting residues in the upper mantle can be measured and provide important information on the compositional variations of the mantle and provide understanding on a great variety of mantle processes such as the depth and degree of melting, and the nature and extent of metasomatic alteration related to fluid or melt percolation (Aldanmaz, 2012).

In this section, the trace elements are studied in four main groups, namely the rare earth elements (REE), large-ion lithophile elements (LILE), the high field strength elements (HFSE) and the first series transition metals. The REE refer to the lanthanide series of elements (La through Lu) that are all characterised by a +3 valence state. Ce and Eu also have second valence states of +4 and +2 respectively, the stability of which is dependent on the local oxygen fugacity. LILE are described as those elements with a low ratios of charge to ionic radius (K, Rb, Cs, Sr and Ba). These elements have ionic radii larger than the main elements constituting minerals in mafic and ultramafic rocks. Their substitution, therefore, strongly distorts the mineral lattice, resulting in their incompatibility in mantle minerals. LILE are known to be fluid-mobile and thus their concentrations are sensitive to metasomatic processes in rocks involving both

melts and fluids. The HFSE refer to elements with small ionic radii and high charges (Hf, Zr, Nb, Ta as well as Ti). These elements also distort the lattice structure of the minerals in which they substitute for major elements (e.g. Fe, Mg and Ca, usually requiring coupled substitutions to maintain charge balance), also making them incompatible in mantle minerals. However, unlike the LILE, the HFSE are not fluid-mobile and, thus, they are generally only affected by metasomatic processes involving melts. The first series transition metals are chalcophile (Zn, Cu and to some extent Ni), siderophile (Co, Ni) or lithophile (Ti, V, Sc, Cr, Mn). They range from moderately incompatible (e.g., Sc, Ti) to highly compatible (e.g., Cr, Ni), but their behaviour is generally a strong function of their individual ionic radius and charge characteristics. Additionally, there are trace elements such as Pb, Th and U which are not officially members of any of these groups, but may have chemical affinities with one or more of them (e.g., Pb with the LILE and Th with the HFSE) (Rollinson, 1993).

The REE are a special class of elements because they all have the same nominal valence state and vary smoothly in ionic radius from largest (La) to smallest (Lu). Normalizing REE concentrations in samples to their abundances in chondrite meteorites removes the saw tooth pattern (given by the Oddo-Harkins law) of abundance differences in elements of even vs. odd atomic number elements caused by nucleosynthesis. Thus normalised, the REE patterns of mantle minerals and rocks reveal smooth variations in elemental abundances with atomic number caused by different extents and depths of partial melting (resulting in incompatible element depletion) and melt percolation and metasomatism (resulting in incompatible element enrichment).

This thesis only reports trace element data for garnet and clinopyroxene, but these two minerals contain the vast majority of the inventory of incompatible element in peridotite xenoliths. Significant variations between core and rim trace element composition were not observed in the analysed minerals and therefore, the data provided are simply the average of all spot analyses of the garnet grains in each sample (typically [number] analyses measured in [number] grains). Trace element concentrations are given in ppm and shown as chondrite-

normalised or primitive mantle-normalised values on some figures, using the chondrite values of Evensen et al. (1978) and primitive mantle values of McDonough and Sun (1995). The calculated average trace element compositions of garnet and clinopyroxenes for each sample from the four populations studied are reported in Table 6.5 and Table 6.6 respectively.

6.2.2 Garnet

Louwrensia - Garnets from Louwrensia are characterised by highly variable chondrite normalised REE patterns (Figure 6.14a), but three groups of REE patterns can be distinguished from the data. Most garnets belong to the "normal/N-type" group as defined by Luchs et al. (2013). These garnets are highly depleted in the lightest REE such as La (0.06-0.76 times chondrite) and Ce (0.37-0.57 times chondrite) and have smooth increasing trends from La to Eu. These garnets are also characterised by an enrichment in the middle and heavy REE of about 10 times chondrite, which results in relatively flat trends from the MREE towards the HREE. The second group of garnets are similarly characterised by a depletion of the lightest REE, but, in addition, have steep positively sloping MREE-HREE patterns (Figure 6.14a). The third group consists of two samples (FRB-1180 and FRB-1183) with garnets having "sinusoidal/sigma" shaped REE patterns and showing strong depletion in the LREE, maximum enrichment in the MREE (Sm-Eu) as well as significant depletion in the HREE relative to the MREE (Figure 6.14a). The large variation in composition within the population can also be seen in the primitive normalised trace element patterns (Figure 6.14b). Louwrensia garnets display large negative anomalies in Ba, La, Sr, Hf and Ti, as well as significant positive anomalies in U. Moreover, it is noted that the trace element data for JJG 2513 garnet obtained in this study is very similar to the data for this sample published by Boyd et al. (2004).

Rietfontein - Garnets from the majority of Rietfontein peridotites investigated have "normal" REE patterns. They are characterised by either flat or mildly positively sloping patterns from the middle to the heavy REE, ($(Gd/Yb)_N$ = 0.23 to 1.1) as seen in Figure 6.15a. Most of the grains are strongly depleted in the LREE (from La to Eu) with $(La/Sm)_N$ ranging between 0.009 and 0.082, with the exception of anomalous, LREE-enriched sample RIET-2. Most grains in this population (about 70%) have MREE and HREE concentrations greater than 10 times chondrite. Garnets in RIET-2 are unusual in that they are remarkably enriched in LREE, with a high $(La/Sm)_N$ value of 3.9 and also display significantly lower concentration of MREE in the population (≈2.5x chondrite rather than the average of ≈12x). As with Louwrensia garnets, garnets from Rietfontein peridotites show strong negative Ba, Sr, Hf and Ti anomalies in addition to positive U and (unlike Louwrensia) positive Pb anomalies (Figure 6.15b). Again, with the exception of RIET-2, primitive mantle-normalised trace element patterns of the garnets closely resemble those from the Gibeon kimberlite field reported by Luchs et al. (2013; Figure 6.15b).

Hoedkop - All garnets from Hoedkop peridotites are mildly to moderately depleted in the LREE relative to the MREE ($(La/Sm)_N$ = 0.027 to 0.90) as illustrated in Figure 6.16a. Garnets from four of the six garnet bearing peridotites have strongly LREE-depleted patterns, with flat patterns in the MREE to HREE that have an average concentration of about 10 times chondrite. Garnets from two samples are distinct. Those from HOD-4 have relatively flat chondrite-normalised LREE and MREE (≈ 9 times chondrite) with a $(La/Sm)_N$ value of 0.90, in addition to having slightly negatively sloping patterns from the middle to the heavy REE, ($(Gd/Yb)_N$ = 1.14). Garnets in sample HOD-11 display a subtle sinusoidal trend with only mild LREE depletion ($(La/Sm)_N$ = 0.34) and low MREE contents of ≈2.5x chondrite, and a positive slope in the HREE (Ho to

Lu). Overall, primitive normalised trace element patterns of Hoedkop garnets show strong enrichments in Rb and U, and lack the strong negative Sr anomalies that characterise peridotitic garnets from the other localities. The garnets also have relatively flat and uniform trace element patterns from the moderately to mildly incompatible elements except for prominent negative Ti anomalies in some samples, with the exception of HOD 11 due to its fractionation of the MREE and HREE.

Pofadder - Peridotitic garnets from the Pofadder kimberlites have nearly uniform patterns in the REE and primitive mantle-normalised incompatible element diagrams (Figure 6.17a & b). The grains have nearly linear, positively sloping REE patterns from the LREE to HREE (Figure 6.17a). They have very low LREE contents (e.g., La = 0.08 to 0.2 and Ce = 0.2 to 0.4 times chondrite) and are enriched in the HREE (e.g., Er = 9.4 to 13 and Yb = 13.4 to 19.7 times chondrite) with $(Gd/Yb)_N$ value ranging from 0.16 to 0.24. In the primitive mantle normalised trace element plot, the garnets display a large positive anomalies in U as well as large negative anomalies in Ba Sr, Hf and (for most samples) Ti (Figure 6.17b). The patterns displayed by the garnets are well within the range of garnets from Uintjiesberg and Hebron (Eastern Namaqualand) in the western Namaqua-Natal Province.

Table 6.5 *Average major elements values of garnet from Laser Ablation ICPMS analysis. b.d. = below detection limit*

	Sc	Ti	V	Cr	Ni	Rb	Sr	Y	Zr	Nb	Ba	La	Ce	Pr	Nd	Sm	Eu	Tb	Gd	Dy	Ho	Er	Tm	Yb	Lu	Hf	Ta	Pb	Th	U
Louwrensia																														
FRB 1180	199	266	211	50152	54.70	0.08	0.33	7.72	67.99	0.21	0.04	0.02	0.27	0.14	1.96	2.59	1.22	0.44	3.33	1.92	0.30	0.68	0.09	0.74	0.12	1.03	0.01	0.03	0.01	0.04
FRB 1183	143	132	175	35825	44.53	0.06	0.92	12.08	76.30	0.39	0.39	0.12	0.65	0.21	2.45	2.17	1.06	0.59	3.48	3.05	0.48	1.05	0.12	0.87	0.13	0.81	0.01	0.03	0.04	0.02
FRB 1652	156	271	181	36337	32.50	0.19	1.66	8.51	21.68	0.45	1.25	0.32	0.86	0.17	1.29	0.80	0.40	0.24	1.25	1.66	0.33	0.85	0.12	1.04	0.19	0.23	0.02	0.02	0.05	0.05
FRB 1683	138	159	299	64738	105.60	0.08	0.99	27.39	81.56	0.36	0.35	0.18	0.90	0.26	2.51	1.91	0.97	0.78	3.54	5.42	1.12	3.05	0.41	2.89	0.39	1.90	0.02	0.01	0.02	0.03
FRB 1684	103	528	191	26290	36.78	0.07	0.86	4.03	7.78	0.63	0.72	0.13	0.51	0.11	0.85	0.31	0.12	0.07	0.30	0.48	0.14	0.52	0.10	0.93	0.16	0.04	0.02	0.04	0.04	0.09
FRB 1686	111	109	264	44449	52.77	0.06	0.22	35.11	54.77	0.08	0.05	0.01	0.23	0.11	1.30	1.42	0.66	0.57	2.28	5.24	1.37	4.18	0.61	4.28	0.59	1.03	0.01	0.02	0.00	0.02
JJG 2513	105	89	200	26235	37.13	0.05	0.08	3.69	4.15	0.18	0.03	0.02	0.11	0.03	0.22	0.10	0.05	0.04	0.16	0.42	0.12	0.50	0.08	0.90	0.16	0.03	0.01	0.02	0.03	0.01
PHN 5316	99	213	182	24467	37.93	0.06	0.03	5.58	7.94	0.24	0.06	0.01	0.12	0.03	0.27	0.14	0.07	0.08	0.25	0.66	0.20	0.69	0.14	1.15	0.20	0.09	0.01	0.01	0.02	0.04
PHN 5365	154	418	110	22460	21.97	0.04	0.20	16.85	32.52	0.17	0.07	0.04	0.35	0.12	1.36	1.20	0.58	0.48	2.29	3.30	0.67	1.62	0.20	1.32	0.20	0.37	0.01	0.02	0.01	0.07
Rietfontein																														
RIET 2	93	892	176	31867	46.17	1.27	16.34	4.69	6.87	2.09	12.88	2.18	3.99	0.35	1.55	0.35	0.13	0.09	0.51	0.67	0.15	0.58	0.10	0.89	0.14	0.10	0.05	0.31	0.24	0.15
RIET 3	63	198	138	25344	20.20	0.02	0.15	8.41	9.78	0.03	0.14	0.02	0.12	0.03	0.49	0.51	0.26	0.21	1.43	1.55	0.35	1.09	0.16	1.26	0.20	0.19	b.d.	0.02	0.01	0.03
RIET 4	90	42	198	7566	27.30	0.01	0.03	10.31	5.58	0.01	b.d.	b.d.	0.02	0.01	0.12	0.19	0.13	0.21	0.78	1.81	0.45	1.29	0.18	1.34	0.19	0.10	b.d.	0.01	b.d.	0.01
RIET 5	74	147	149	17058	20.87	0.01	0.07	11.40	9.46	0.03	0.01	0.01	0.10	0.04	0.48	0.44	0.25	0.24	1.49	1.94	0.48	1.42	0.22	1.82	0.28	0.23	b.d.	0.01	b.d.	0.02
RIET 6	77	73	159	27023	20.57	0.01	0.12	10.96	38.23	0.01	0.00	0.01	0.17	0.06	0.76	0.72	0.36	0.28	2.04	2.08	0.46	1.37	0.20	1.54	0.22	0.64	b.d.	0.01	0.01	0.01
RTFN30-1	117	94			39.05	1.39	0.09	39.78	28.67	0.08	0.32	0.02	0.06		0.60	0.80	0.43		1.87	5.01		5.00		6.51		0.46		0.02	0.01	0.02
RTFN30-2	131	70			28.07	0.17	0.10	44.08	31.24	0.01	0.37	0.02	0.07		0.54	0.82	0.53		2.47	6.13		5.29		6.753		0.36		0.03	0.01	0.01
RTFN30-4	118	82			38.94	0.03	0.08	17.79	20.59	0.02	b.d.	0.01	0.10		0.55	0.75	0.41		1.88	3.10		1.95		2.129		0.22		0.03	0.00	0.01
RTFN30-5	180	169			35.66	0.14	1.17	34.01	36.64	0.15	0.56	0.15	0.37		0.96	1.15	0.61		2.57	5.16		4.03		5.085		0.40		0.03	0.03	0.03
RTFN30-7	138	216			35.86	0.02	0.10	18.33	42.68	0.04	b.d.	0.02	0.18		1.01	1.08	0.66		2.34	3.33		2.33		2.853		0.55		0.01	0.01	0.04
RTFN30-8	79	64			61.68	0.14	0.67	14.54	1.64	0.02	0.23	0.02	0.11		0.47	0.62	0.39		1.38	2.26		1.52		1.928		0.03		0.04	0.01	0.01
RTFN30-13	132	187			82.65	0.06	0.28	26.43	21.45	0.04	0.50	0.02	0.11		0.65	0.98	0.58		2.30	4.26		3.13		3.513		0.37		0.10	0.01	0.03
RTFN30-14	114	553			33.67	0.07	0.11	38.03	29.36	0.02	0.06	0.01	0.07		0.51	0.69	0.45		1.95	5.12		5.19		6.639		0.41		0.02	0.01	0.09
RTFN31-5	194	64			34.78	0.17	0.40	18.31	29.84	0.07	0.64	0.05	0.40		1.81	1.50	0.76		2.48	3.38		1.94		2.066		0.36		0.04	0.03	0.01
Hoedkop																														
HOD 1	291	518	174	41852	37.35	9.55	6.23	12.53	27.04	0.41	5.78	0.06	0.61	0.17	1.95	1.41	0.67	0.34	2.06	2.23	0.49	1.47	0.21	1.99	0.30	0.27	0.02	0.04	0.02	0.09
HOD 2	131	3739	393	49226	117.74	304.33	30.00	15.18	34.70	0.42	94.91	0.17	0.73	0.18	1.75	1.24	0.55	0.35	1.98	2.63	0.55	1.67	0.23	1.96	0.27	0.89	0.02	0.68	0.02	0.62
HOD 3	106	249	332	45112	94.16	134.76	44.22	12.44	26.04	0.65	78.87	0.09	0.60	0.16	1.64	1.11	0.42	0.31	1.79	2.29	0.46	1.33	0.17	1.44	0.22	0.66	0.01	0.14	0.01	0.04
HOD 4	96	526	586	45508	165.13	225.04	102.76	10.94	26.13	5.40	117.89	1.90	5.28	0.76	4.18	1.33	0.56	0.27	1.65	2.06	0.38	1.15	0.13	1.18	0.14	0.75	0.13	0.20	0.25	0.09
HOD 5	424	2326	406	57134	203.77	343.39	53.99	13.45	74.20	2.02	95.08	0.12	0.67	0.18	1.73	1.33	0.59	0.36	2.01	2.46	0.56	1.80	0.33	2.84	0.50	0.67	0.04	0.49	0.08	0.39
HOD 11	261	2162	318	35575	107.04	74.30	25.39	3.93	15.39	0.84	47.39	0.22	0.71	0.13	1.04	0.41	0.18	0.08	0.56	0.62	0.12	0.47	0.09	1.06	0.18	0.25	0.02	0.53	0.04	0.36
Pofadder																														
JJG 2499-4	168	294			30.61	0.12	0.06	17.82	2.16	0.25	b.d.	0.03	0.14	0.23	0.37	0.26	0.16		0.74	2.13		2.22		3.29		0.03		0.05	0.02	0.05
JJG 2499-6	172	403			30.97	0.14	0.06	18.54	1.21	0.27	0.07	0.03	0.18	0.25	0.35	0.26	0.14		0.75	2.19		2.27		3.28		0.03		0.03	0.04	0.07
JJG 2499-7	146	502			32.90	0.09	0.04	14.22	2.81	0.18	0.04	0.02	0.12	0.19	0.30	0.24	0.13		0.66	1.85		1.87		2.69		0.03		0.02	0.02	0.08
JJG 2499-12	136	580			35.85	0.05	0.05	12.68	1.01	0.15	0.65	0.03	0.13	0.20	0.31	0.21	0.12		0.64	1.63		1.71		2.39		0.02		0.02	0.01	0.10
JJG 2499-14	125	536			29.29	0.05	0.04	11.48	0.87	0.13	b.d.	0.02	0.12	0.17	0.24	0.18	0.10		0.45	1.40		1.52		2.25		0.01		0.02	0.01	0.09
JJG 2499-15	135	755			32.12	0.07	0.06	12.27	2.43	0.15	0.04	0.02	0.17	0.24	0.34	0.26	0.13		0.67	1.56		1.56		2.22		0.02		0.02	0.02	0.13
JJG 2499-16	200	1567			46.03	0.09	0.05	17.75	3.60	0.26	b.d.	0.05	0.27	0.37	0.52	0.36	0.21		0.92	2.28		2.16		3.26		0.02		0.03	0.03	0.26

Table 6.6 *Average major elements values of clinopyroxene from Laser Ablation ICPMS analysis. b.d. = below detection limit*

	Sc	Ti	V	Cr	Ni	Rb	Sr	Y	Zr	Nb	Ba	La	Ce	Pr	Nd	Sm	Eu	Tb	Gd	Dy	Ho	Er	Tm	Yb	Lu	Hf	Ta	Pb	Th	U
Louwrensia																														
FRB 1180	32	325	218	14862	441	0.10	134	0.97	19.82	0.33	0.38	0.96	4.27	0.89	5.65	1.91	0.58	0.11	1.20	0.39	0.05	0.06	b.d.	0.04	0.01	0.94	0.02	0.14	0.02	b.d.
FRB 1183	35	599	318	15072	355	0.03	291	0.89	43.29	0.55	0.05	5.53	22.92	3.98	21.61	4.08	0.96	0.15	1.82	0.44	0.04	0.05	b.d.	0.03	b.d.	1.41	0.05	0.42	0.06	0.01
FRB 1652	30	180	314	12329	343	0.09	204	1.13	34.46	2.26	15.92	8.75	27.79	4.01	18.37	3.18	0.87	0.14	1.60	0.45	0.05	0.06	0.01	0.03	b.d.	0.71	0.11	0.38	0.27	0.08
FRB 1684	19	300	266	10471	381	0.51	199	2.83	63.01	2.42	27.75	7.74	22.83	3.35	16.42	3.28	0.95	0.23	2.08	1.00	0.12	0.23	0.02	0.12	0.01	2.15	0.11	0.38	0.33	0.08
JJG 2513	16	120	257	9845	396	0.11	179	1.45	32.83	0.71	3.96	7.07	22.85	3.09	13.86	2.20	0.60	0.12	1.22	0.48	0.06	0.11	0.01	0.05	b.d.	0.75	0.06	0.41	0.10	0.03
JJG 2514	12	659	203	9000	340	0.37	221	2.33	29.12	3.07	75.04	13.09	36.67	4.69	19.60	2.88	0.77	0.16	1.54	0.70	0.09	0.19	0.02	0.09	0.01	0.44	0.15	0.47	0.98	0.17
PHN 5316	17	300	278	9967	382	0.06	106	2.04	41.75	0.46	0.68	4.16	13.00	1.94	9.11	1.80	0.53	0.15	1.19	0.64	0.09	0.16	0.02	0.09	0.01	1.05	0.03	0.29	0.07	0.02
PHN 5365	39	899	222	9176	310	0.13	265	1.45	23.97	0.97	1.43	16.55	42.22	5.05	21.04	3.10	0.76	0.16	1.56	0.55	0.06	0.10	0.01	0.05	b.d.	1.06	0.08	0.96	0.70	0.15
PHN 5364	28	420	302	15823	359	1.07	188	3.01	92.21	1.39	15.35	4.62	16.15	2.64	13.63	3.04	0.90	0.24	1.96	0.95	0.15	0.26	0.03	0.17	0.01	4.14	0.09	0.28	0.15	0.04
Rietfontein																														
RIET 1	98	479	179	8642	391	0.28	268	4.08	44.70	2.95	27.23	24.99	56.85	5.72	26.51	4.25	1.16	0.22	2.48	1.18	0.14	0.34	0.03	0.30	0.04	0.90	0.11	0.99	0.72	1.53
RIET 2	30	300	295	11600	252	1.04	52	1.03	4.37	1.26	10.63	5.94	10.02	0.95	3.35	0.48	0.13	0.04	0.28	0.20	0.04	0.11	0.01	0.13	0.02	0.11	0.03	0.43	0.46	0.15
RIET 3	25	1418	436	15174	244	0.02	173	1.77	21.19	0.63	3.29	8.43	21.09	2.70	12.75	2.37	0.62	0.14	1.24	0.59	0.08	0.20	0.02	0.10	0.01	0.97	0.05	0.58	0.58	0.13
RIET 4	27	576	417	3739	495	0.02	42	0.85	4.51	0.05	0.31	1.74	4.03	0.54	2.67	0.65	0.20	0.07	0.62	0.32	0.04	0.07	0.01	0.03	b.d.	0.25	b.d.	0.13	0.09	0.02
RIET 5	23	985	314	10671	283	0.01	117	1.00	13.29	0.62	2.81	6.42	15.69	1.89	8.31	1.47	0.39	0.09	0.88	0.35	0.05	0.09	0.01	0.04	b.d.	0.65	0.03	0.52	0.29	0.07
RIET 6	28	1257	449	15955	268	0.04	209	1.09	58.99	0.30	1.62	9.33	23.15	2.90	13.43	2.23	0.52	0.11	1.09	0.43	0.05	0.11	0.01	0.05	0.01	2.70	0.02	0.74	0.53	0.05
RTFN30-1	20	1354			248	0.01	122	2.21	27.21	0.21	1.38	2.18	7.79		7.81	1.94	0.54		1.16	0.64		0.18		0.10		1.37		0.22	0.10	0.06
RTFN30-2	23	1569			198	0.02	144	2.56	26.34	0.84	2.88	3.79	10.90		9.23	2.19	0.69		1.58	0.83		0.21		0.11		1.17		0.40	0.46	0.08
RTFN30-4	25	1274			307	0.02	159	1.81	31.51	0.49	1.93	5.44	13.88		9.35	2.11	0.66		1.36	0.61		0.13		0.07		1.05		0.43	0.27	0.08
RTFN30-5	28	1107			305	0.06	132	1.57	25.99	0.35	1.01	3.85	13.08		10.59	2.07	0.58		1.17	0.51		0.11		0.06		0.93		0.34	0.19	0.06
RTFN30-7	33	1178			332	0.01	216	1.45	45.02	0.58	3.75	7.52	21.73		13.54	2.39	0.70		1.37	0.48		0.10		0.06		1.58		0.66	0.46	0.11
RTFN30-8	16	1065			448	0.06	336	0.96	4.09	0.64	1.05	5.04	11.12		6.58	1.42	0.48		0.84	0.33		0.07		0.04		0.19		0.43	0.30	0.11
RTFN30-13	23	1305			430	0.04	178	2.34	21.12	0.86	1.69	6.79	17.88		12.04	2.55	0.75		1.57	0.73		0.18		0.10		0.72		0.50	0.31	0.08
RTFN30-14	28	1561			332	0.11	179	3.30	38.65	1.12	6.50	4.50	13.35		12.16	2.85	0.82		1.73	0.97		0.28		0.15		1.93		0.46	0.33	0.26
RTFN31-5	40	1688			266	0.10	288	1.12	31.90	1.32	4.55	11.87	33.73		19.74	3.15	0.75		1.34	0.43		0.08		0.04		1.56		0.87	0.95	0.09
Hoedkop																														
HOD 1	22	959	449	15955	358	0.05	272	1.03	31.54	0.47	1.34	7.18	17.14	2.90	10.01	1.82	0.50	0.11	0.97	0.38	0.05	0.09	0.01	0.04	0.01	1.45	0.02	0.59	0.41	0.08
HOD 2	17	719	234	13251	492	1.55	236	1.50	5.39	0.26	1.41	2.11	7.03	1.11	6.13	1.32	0.37	0.09	0.82	0.42	0.06	0.12	0.01	0.07	0.01	0.29	0.01	2.40	0.03	0.65
HOD 3	16	779	240	10946	415	7.97	461	3.86	40.04	4.65	55.18	6.12	13.91	1.73	8.36	1.74	0.52	0.15	1.27	0.84	0.13	0.37	0.04	0.29	0.04	0.95	0.16	1.06	0.63	0.20
HOD 4	16	779	228	12683	480	0.10	221	1.46	4.83	0.08	0.38	2.08	7.21	1.08	6.02	1.25	0.36	0.08	0.82	0.41	0.05	0.11	0.01	0.07	0.01	0.29	0.01	1.19	0.02	0.01
HOD 5	59	1798	186	7991	353	0.45	306	2.82	41.39	0.61	0.90	18.62	51.09	6.57	29.67	4.84	1.31	0.28	2.74	1.09	0.14	0.22	0.02	0.11	0.01	1.50	0.05	0.85	0.41	0.13
HOD 6	83	120	176	5176	287	0.11	246	3.42	4.22	3.09	0.17	54.45	124.57	12.63	38.32	1.99	0.42	0.12	0.82	0.68	0.14	0.39	0.06	0.41	0.06	0.07	0.06	0.52	0.51	0.27
HOD 10	88	b.d.	189	4804	294	0.11	65	0.44	0.07	0.15	0.07	11.22	10.40	0.41	0.44	0.02	0.01	0.01	0.03	0.04	0.01	0.07	0.02	0.18	0.03	0.00	0.00	0.29	0.46	0.18
HOD 11	36	2757	150	7270	313	0.14	92	0.21	8.45	0.34	0.12	11.78	24.49	2.52	8.89	0.75	0.17	0.03	0.28	0.07	0.01	0.02	0.00	0.01	0.00	0.34	0.04	0.65	0.64	0.23
Pofadder																														
JJG 2499-4	25	203			317	0.01	210	0.67	6.73	0.61	0.07	14.01	24.83		8.30	0.95	0.25		0.47	0.20		0.05		0.03		0.09		1.20	2.54	0.51
JJG 2499-6	33	229			389	0.02	295	0.97	9.55	0.79	0.15	19.88	33.08		11.72	1.35	0.33		0.71	0.27		0.07		0.04		0.14		1.57	3.56	0.65
JJG 2499-7	19	267			328	0.05	185	0.52	5.20	0.58	0.09	11.19	20.04		6.70	0.72	0.20		0.37	0.18		0.04		0.02		0.09		1.13	2.04	0.59
JJG 2499-12	24	311			296	0.51	228	0.86	9.04	0.56	0.11	14.43	20.94		8.87	1.10	0.32		0.54	0.22		0.06		0.03		0.17		1.14	1.39	0.35
JJG 2499-14	27	230			428	0.04	276	0.71	8.43	0.62	0.19	16.26	29.14		10.20	1.27	0.34		0.67	0.27		0.07		0.03		0.13		1.51	3.04	0.86
JJG 2499-15	32	167			367	0.03	292	0.80	8.45	0.79	0.18	18.63	27.88		10.54	1.20	0.32		0.62	0.25		0.06		0.03		0.11		1.53	1.96	0.44
JJG 2499-16	32	174			360	0.11	270	0.93	7.93	0.77	0.12	18.16	26.70		10.32	1.14	0.30		0.60	0.24		0.06		0.03		0.15		1.44	2.02	0.54

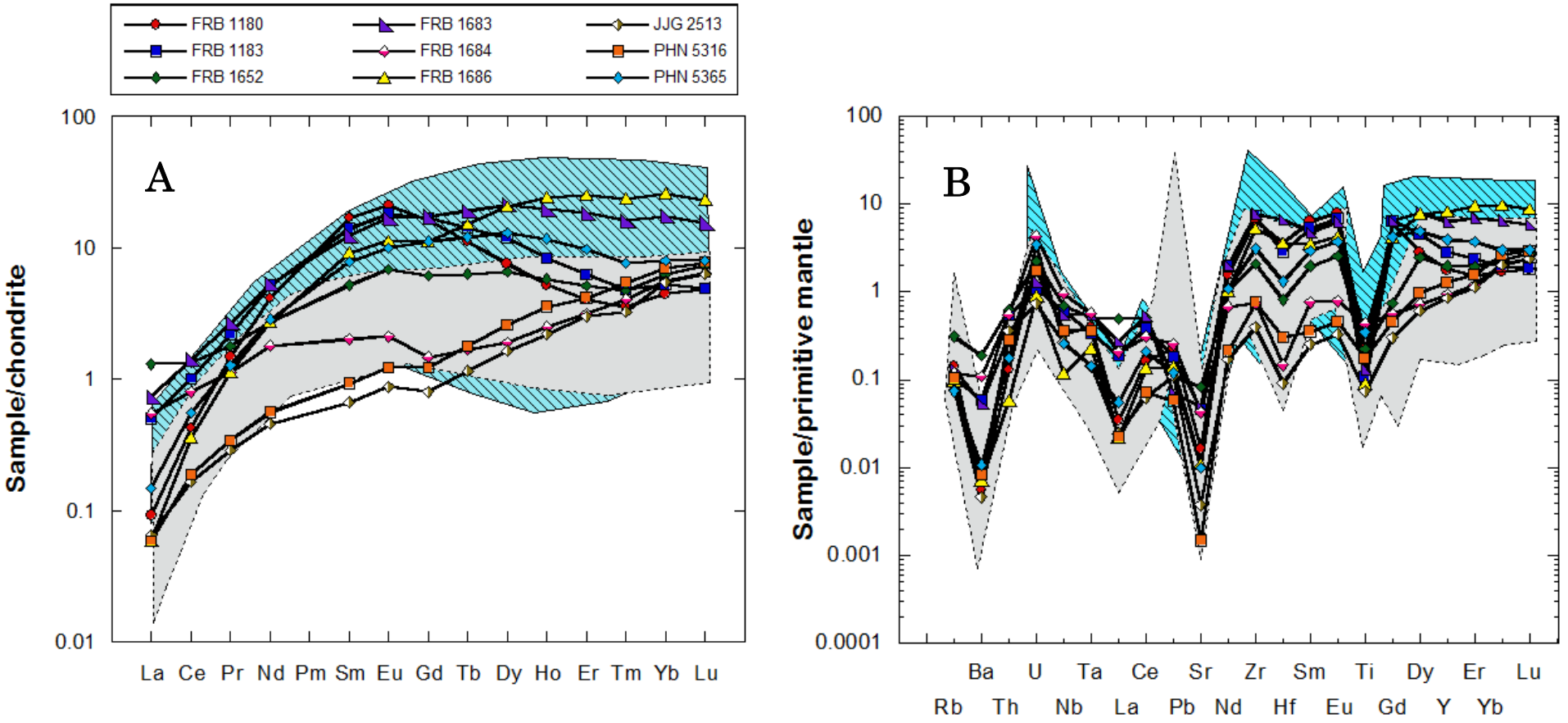

Figure 6.14. **A:** Chondrite normalised REE diagram and **B:** Primitive mantle normalised trace element diagram for garnets from Louwrensia. The compositional range of garnets from Kimberley is indicated by the blue zone (Gregoire et al., 2003), while that of Gibeon garnets is indicated by the grey zone (Luchs et al., 2013).

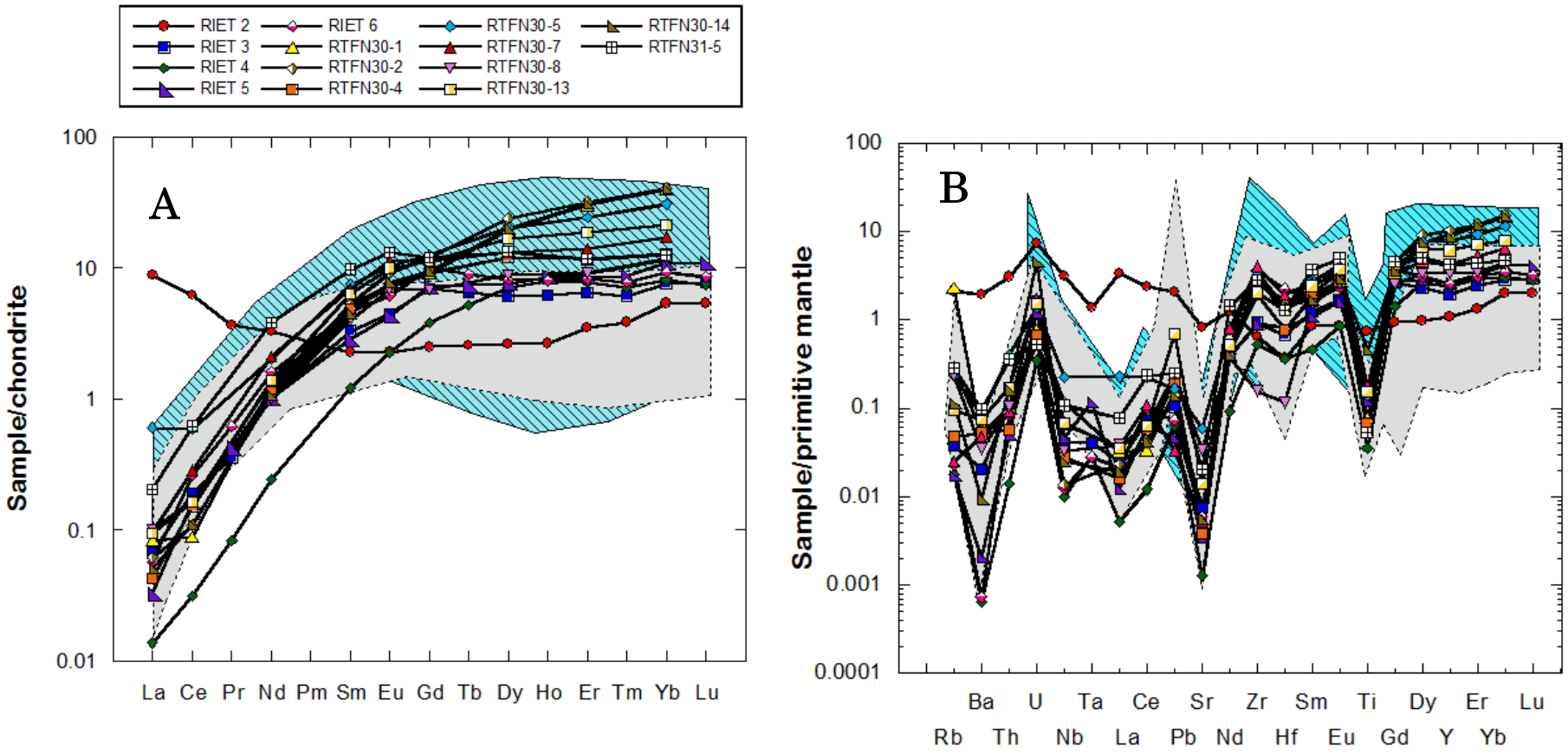

Figure 6.15. **A:** Chondrite normalised REE diagram and **B:** Primitive mantle normalised trace element diagram for garnets from Rietfontein. The compositional range of garnets from Kimberley is indicated by the blue zone (Gregoire et al., 2003), while that of Gibeon garnets is indicated by the grey zone (Luchs et al., 2013).

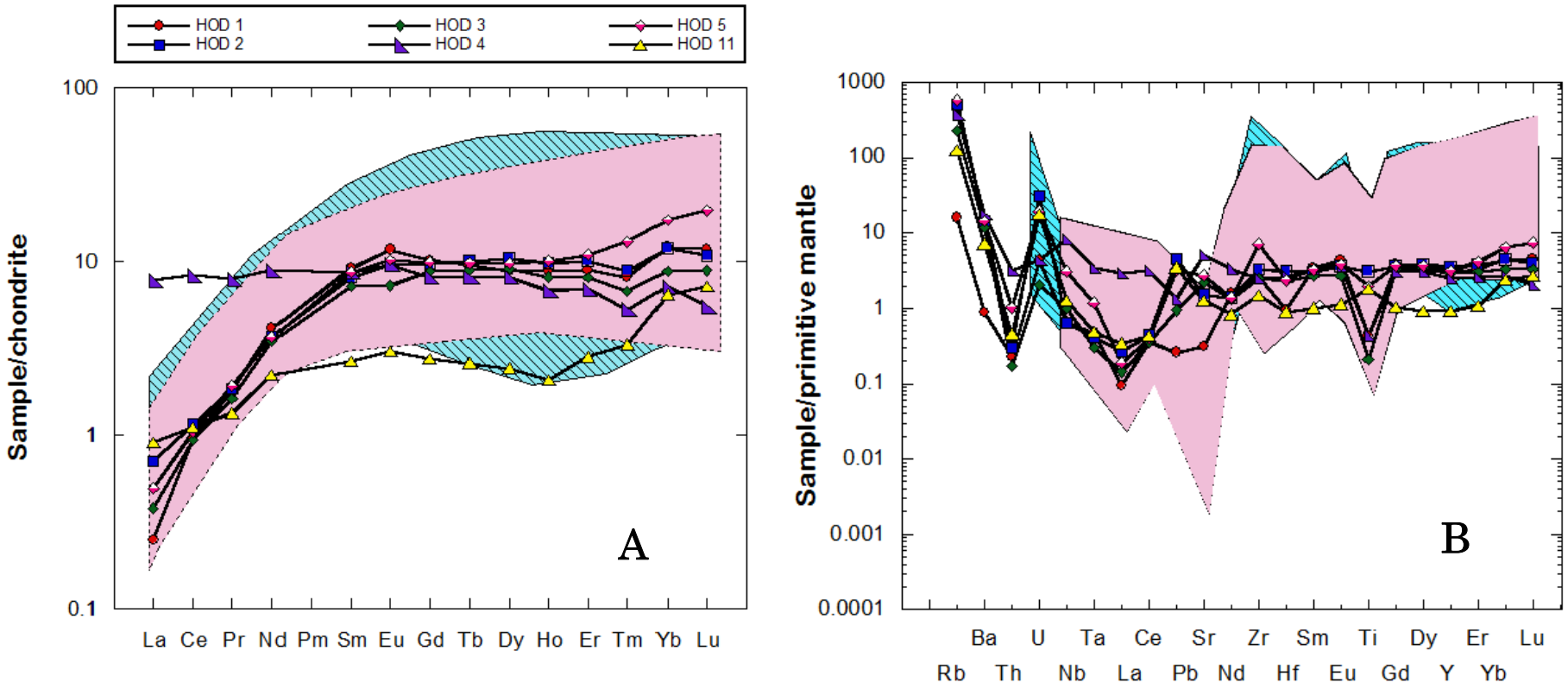

Figure 6.16. **A:** Chondrite normalised REE diagram and **B:** Primitive mantle normalised trace element diagram for garnets from Hoedkop. The compositional range of garnets from Kimberley is indicated by the blue zone (Gregoire et al., 2003), while that of Uintjiesberg and Hebron garnets (Eastern Namaqualand) is indicated by the pink zone (Kobussen et al., 2008; 2009).

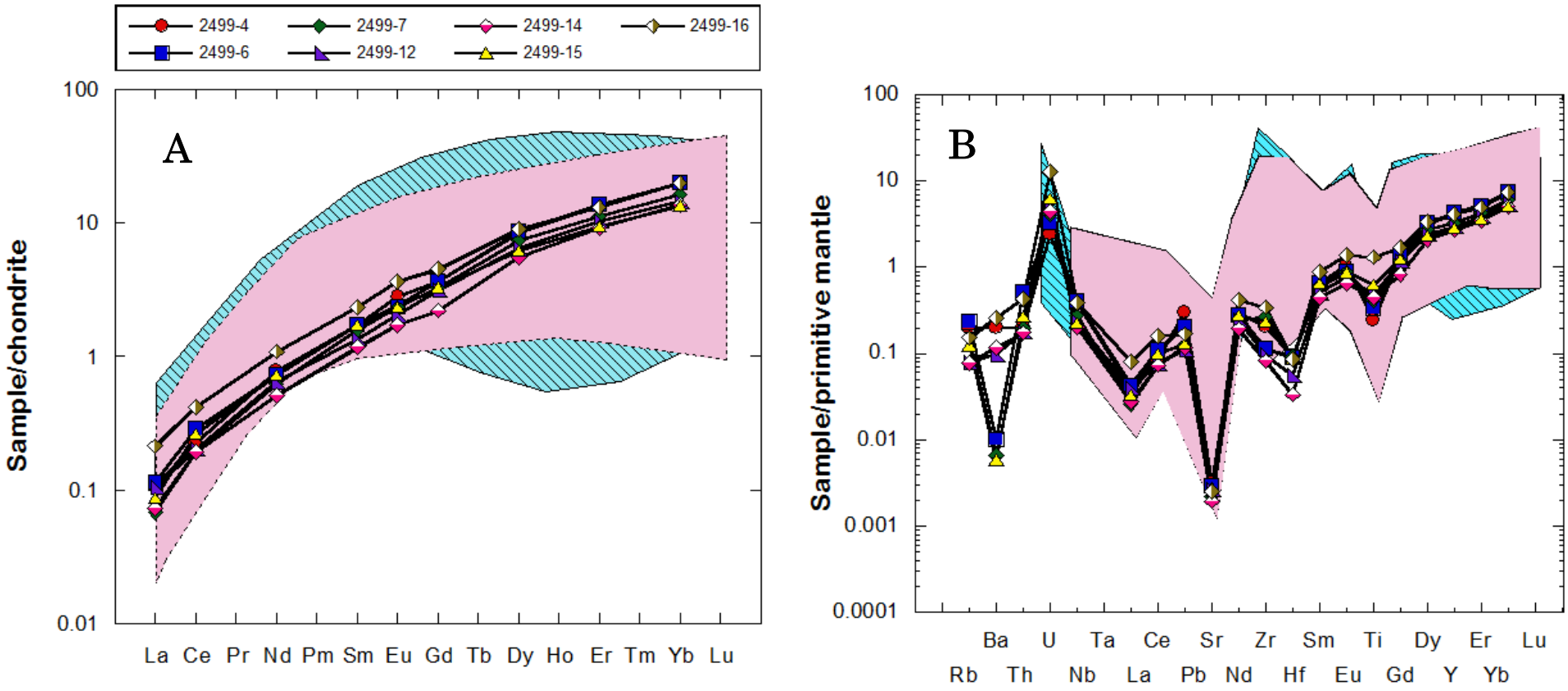

Figure 6.17. **A:** Chondrite normalised REE diagram and **B:** Primitive mantle normalised trace element diagram for garnets from Pofadder. The compositional range of garnets from Kimberley is indicated by the blue zone (Gregoire et al., 2003), while that of Uintjiesberg and Hebron garnets (eastern Namaqualand) is indicated by the pink zone (Kobussen et al., 2008; 2009).

Trace element Relations and Abundances - Overall, peridotite garnets from all four locations exhibit a very rough positive relationship between the MREE/HREE ratio and their Mg-number. Figure 6.18 illustrates that garnets from Louwrensia and Hoedkop that display normal (non-sigma) REE patterns have roughly, even MREE and HREE concentrations resulting in flat MREE-HREE patterns with $(Sm/Yb)_N$ ranging between 1.5 and 0.5, while garnets from Rietfontein and Pofadder with normal REE patterns are more enriched in the HREE relative to the MREE ($(Sm/Yb)_N < 0.5$). Garnets from two Louwrensia samples (FRB 1180 and FRB 1183) have sinusoidal (i.e., sigma-type) REE patterns that are enriched in the MREE relative to the HREE, with $(Sm/Yb)_N > 1$ and are also characterised by high Mg-numbers (85 and 82 respectively). These samples plot in the same field as sinusoidal garnets studied by Luchs et al., (2013) from the same kimberlite field (Figure 6.18).

The concentration of LILE in garnets from Hoedkop is higher and much more variable than in garnets from other suites studied (Figure 6.19). For example the Rb and Ba contents in Hoedkop garnet range from 10 ppm to 343 ppm and 6 ppm to 118 ppm respectively, whereas the concentration of both elements in other populations is <1.4 ppm and <13 ppm respectively, and show similar concentrations with garnets from Gibeon studied by Luchs et al., (2013). The concentration of most HFSE is typically low and uniform in garnets from Pofadder in contrast to the higher concentration and variability observed in garnets from Louwrensia and Hoedkop. These concentrations are well within the range recorded by garnets from the Kaapvaal craton localities such as Kimberley and off-craton localities such as Uintjiesberg, Hebron and Gibeon. Three samples, HOD-4 and HOD-5 from Hoedkop and RIET-2 from Rietfontein generally have much higher Nb contents of 5.4 ppm, 2.0 ppm and 2.1 ppm, respectively (and correspondingly higher Ta contents) relative to the bulk of southern African peridotite garnets which have Nb concentrations below 1 ppm. A strong correlation also exists between Zr and Hf in all grains studied. The Y content increases at constant Zr value for garnets from Pofadder, while those from Rietfontein, Hoedkop and Louwrensia exhibit a moderate to strong correlation between the two elements. In particular, garnets with sinusoidal

REE patterns (especially FRB 1180, FRB 1183 and HOD-5) are located off the main trend, with high Zr values at relatively low Y contents compared to the rest of the population (Figure 6.20).

The concentration of first series transition metals is higher and more variable in garnets from Hoedkop than in garnets from other populations studied. In particular two samples HOD-4 and HOD-5 display much higher concentrations in Ni (165 ppm and 204 ppm respectively) than the bulk of southern Africa garnets (which only reach up to 125 ppm) (Figure 6.21), while HOD-5 is also highly enriched in Sc with concentration of 424 ppm. In general, garnets from the Namaqua-Natal Province are more enriched in Ti with an average of 872 ppm, than garnets from the Rehoboth province, which have an average Ti 633 ppm (Figure 6.21).

Between localities there is significant variability in the concentration of other incompatible elements (e.g., U, Pb, and Sr). In particular, Hoedkop and Pofadder garnets extend to significantly higher U concentrations than garnets from the Rehoboth Province localities or from the Kaapvaal craton.

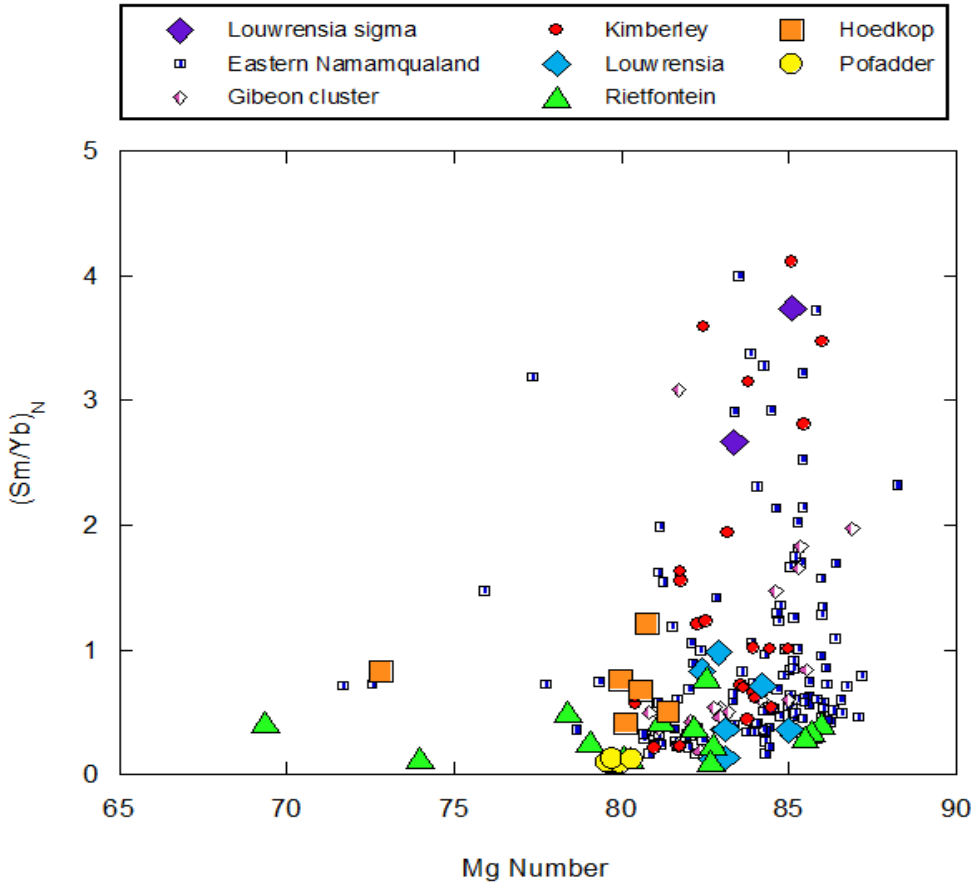

Figure 6.18 Mg-number vs. chondrite normalised Sm/Yb ratio of garnets investigated. Data for Gibeon garnets is from (Luchs et al., (2013), while that of Uintjiesberg and Hebron garnets (eastern Namaqualand) is from Kobussen et al., (2008) and Kobussen et al., (2009).

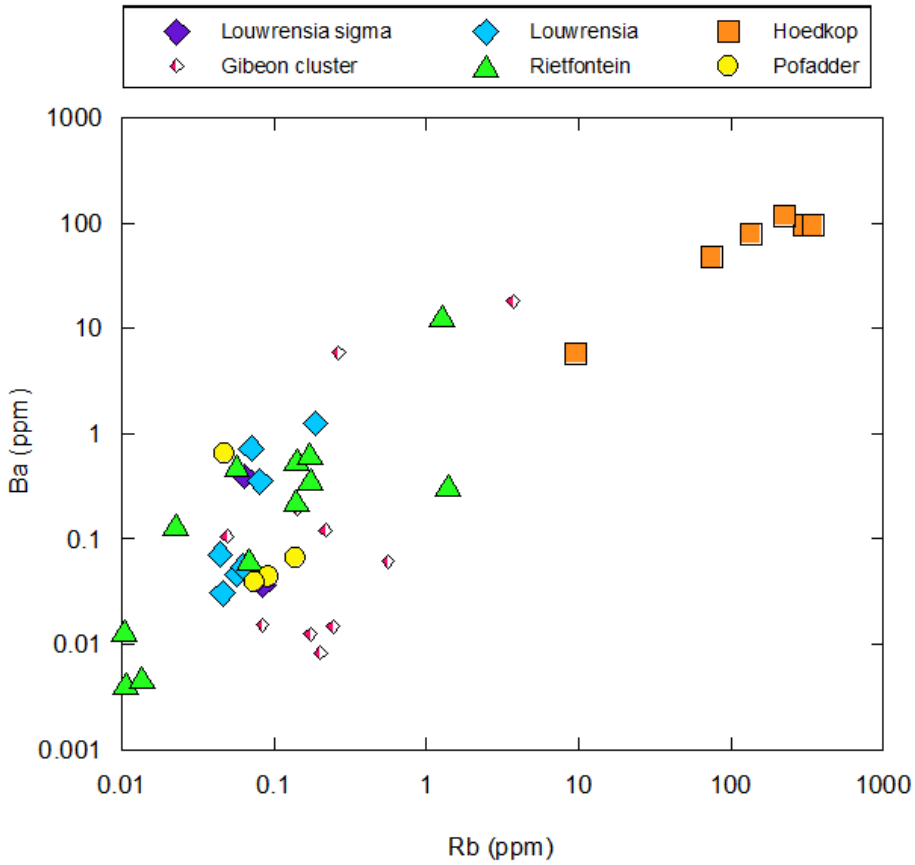

Figure 6.19. Plot of Rb vs. Ba ppm of garnets investigated. Sources of data from the literature are listed in Figure 6.18

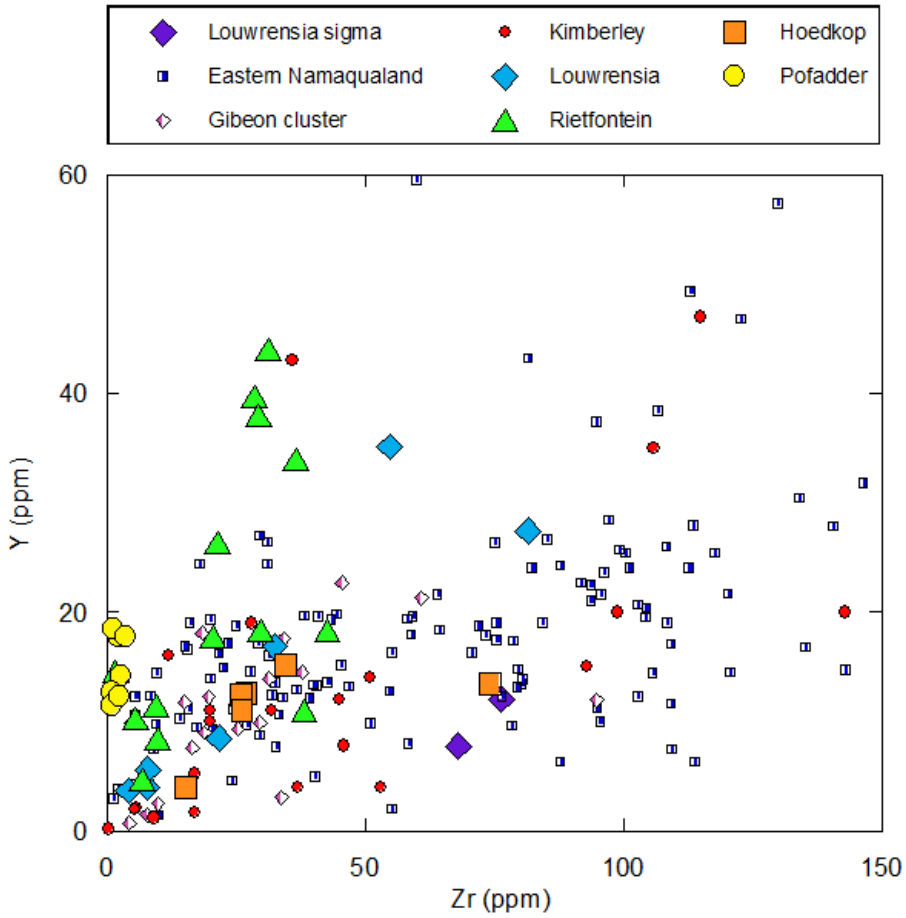

Figure 6.20. Plot of Zr vs. Y ppm of garnets investigated. Sources of data are the same as in Figure 6.18

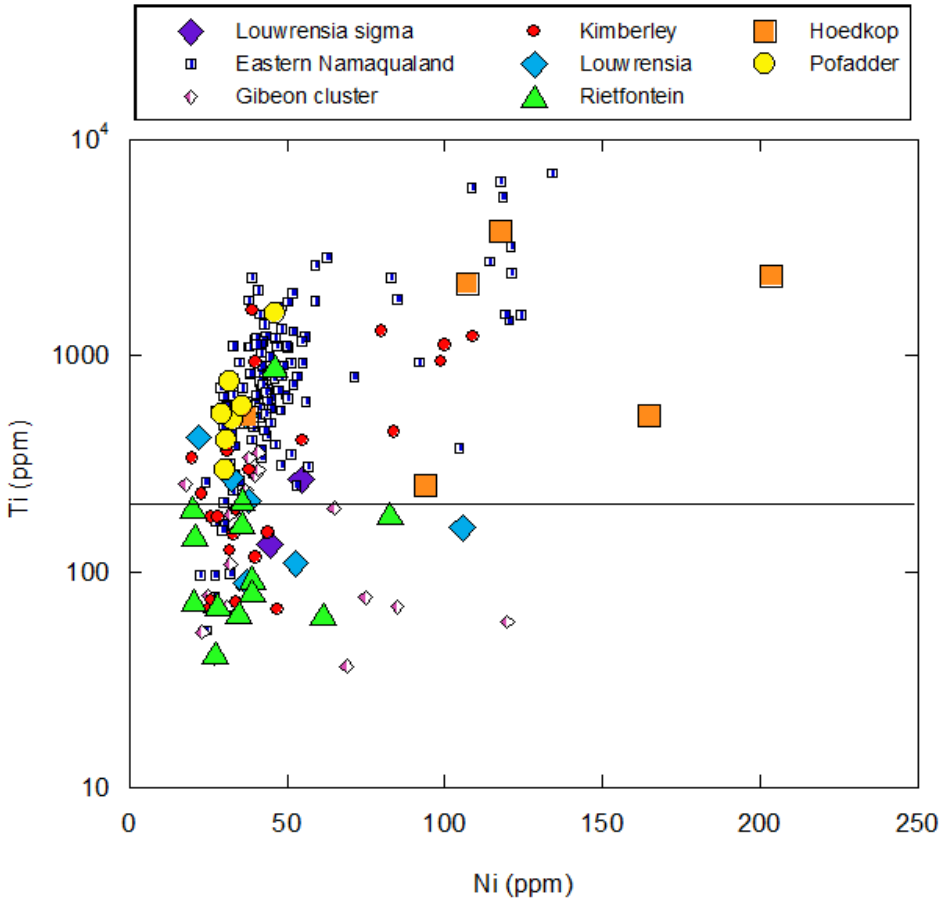

Figure 6.21. Plot of Ni vs. Ti ppm of garnets investigated. Sources of data from the literature are the same as in Figure 6.18

6.2.3 Clinopyroxene

Louwrensia - Clinopyroxenes from Louwrensia peridotites have LREE-enriched REE patterns with $(Sm/Yb)_N$ values ranging from 18.9 to 149.4 and most grains show the slight depletion in the lightest REE (e.g. La and, in some cases, Ce and Nd as well), which is typical of mantle clinopyroxene. Otherwise, they have relatively linear, negatively sloping patterns although the patterns fan out slightly in the HREE (Figure 6.22a). Two samples, FRB 1183 and FRB 1652 have clinopyroxene grains with steeper slopes in the MREE to HREE and are characterised by unusually high $(Sm/Yb)_N$ ratios of 149.4 and 109.3 respectively which are higher than the $(Sm/Yb)_N$ ratio exhibited by the rest of the population (with a mean of 59.7±42). The primitive mantle-normalised trace element diagram Figure 6.22b further demonstrates the enrichment of the LREE and the depletion of the HREE in most clinopyroxenes from Louwrensia. All clinopyroxenes shows negative Pb and Ti anomalies, and highly variable Rb, Ba, Th, U, Nb and Ta concentrations.

Rietfontein - The REE and primitive mantle-normalised trace element patterns of clinopyroxenes from Rietfontein fall into two main groups (Figure 6.23a), although all show significant enrichments of the LREE relative to the HREE, with $(Sm/Yb)_N$ values ranging from 4.0 to 80.4. The main group has REE patterns similar to Louwrensia, though with less depletion in the lightest REE. The "anomalous" group consists of samples RIET-2 and RIET-4, which have maximum enrichments in La and either concave upward REE patterns with relatively low MREE contents (RIET-2) or relatively low LREE concentrations of less than 10x chondrite, a strong change in slope (from mildly negative to strongly negative) at Gd and strong depletions in the heaviest REE.

Most clinopyroxenes from Rietfontein peridotites show negative anomalies in high field strength elements (Figure 6.23b), most notably showing strong negative anomalies in Nb, Zr, Hf (somewhat less depleted) and Ti.

Hoedkop - Clinopyroxenes from Hoedkop display both concave-downward (e.g. HOD-4) and concave-upward (e.g. HOD-6), negative sloping REE patterns with $(Sm/Yb)_N$ values ranging from 0.10 to 54.7. Clinopyroxenes from spinel peridotite HOD-10 display a "sinusoidal/sigma" shape and are characterised by strong enrichment in the LREE, depletion in the MREE as well as mild enrichment in the HREE, resulting in a deep, 'bow-shaped' pattern (Figure 6.24a). Clinopyroxenes from this locality are enriched in the LREE with those from HOD-2 and HOD-4 showing a maximum enrichment in Nd, whereas the rest of the samples have maximum LREE enrichment in the lightest REE such as La or Ce (Figure 5.24a). They vary in terms of their HREE depletion, with most samples having negative slopes from Er to Lu, others being flat over this interval (e.g., HOD-6 and HOD-11) and the anomalous HOD-10 showing a strong positive slope. Hoedkop clinopyroxenes have a strong negative anomalies in the HFSE (Nb, Ta, Zr, Hf and Ti), with grains from HOD-2 also featuring a large positive anomaly in U (Figure 6.24b).

Pofadder - The trace element compositions of clinopyroxenes from Pofadder peridotites are all very similar (Table 6.6), which has resulted in the very uniform and parallel chondrite normalised REE patterns observed in Figure 6.25a. Pofadder clinopyroxenes are highly enriched in LREE with $(Sm/Yb)_N$ ratio ranging from 33.6 to 49.6. They show very linear, steep negatively sloping REE patterns with maximum enrichment in La, rather than showing the flattening of the patterns from Nd to La, which is more typical of peridotitic clinopyroxene (e.g., Louwrensia, Rietfontein and Hoedkop; Gregoire et al., 2003). In addition, they are all strongly depleted in the HREE. The primitive mantle-normalised plot (Figure 6.25b) reveals that Pofadder clinopyroxenes have strong negative anomalies in the HFSE (Nb, Zr, Hf and Ti) relative to elements of similar incompatibility (e.g., the REE, Th and U), along with unusually high Th and U concentrations.

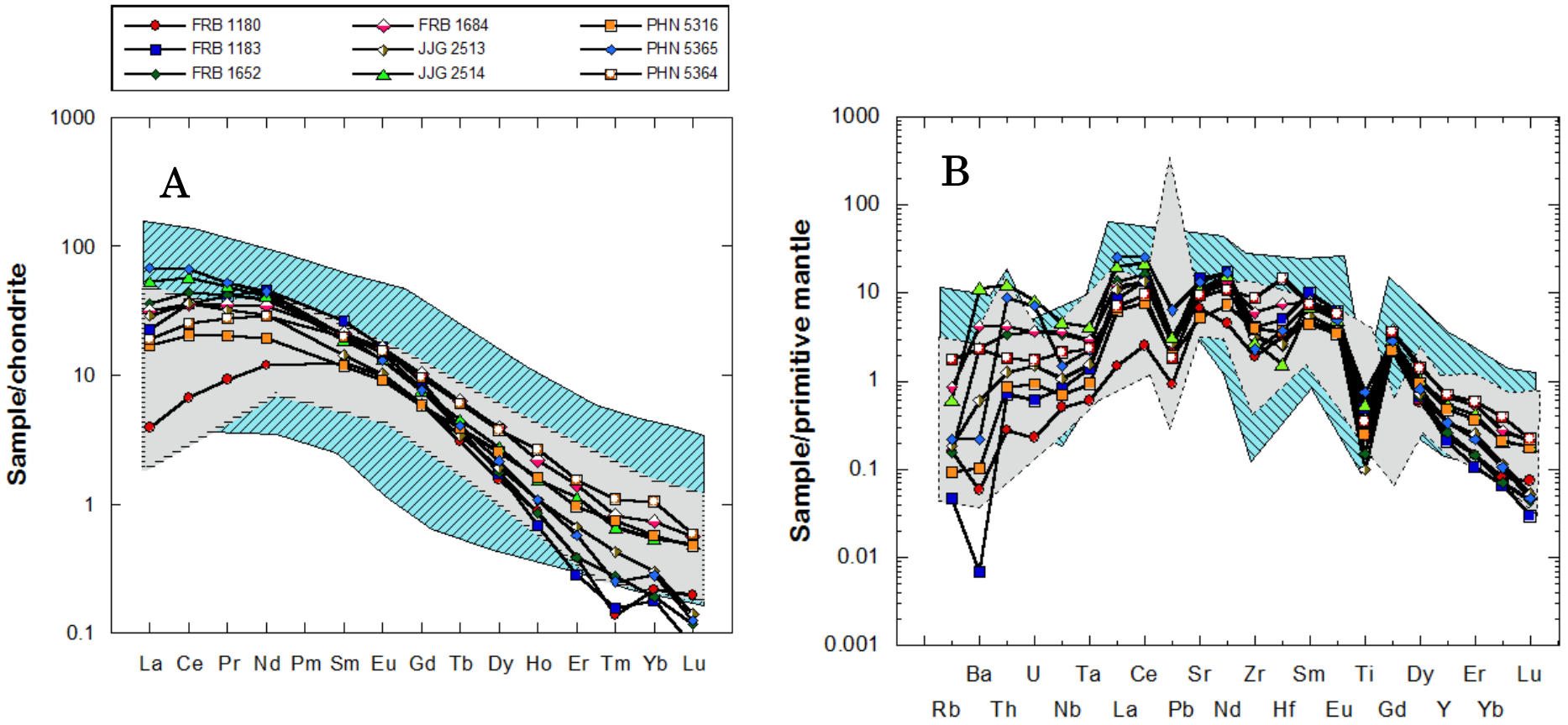

Figure 6.22. **A:** Chondrite normalised REE diagram and **B:** Primitive mantle normalised trace element diagram for clinopyroxene from Louwrensia. The compositional range of clinopyroxenes from Kimberley is indicated by the blue zone (Gregoire et al., 2003), while that of Gibeon clinopyroxenes is indicated by the grey zone (Luchs et al., 2013).

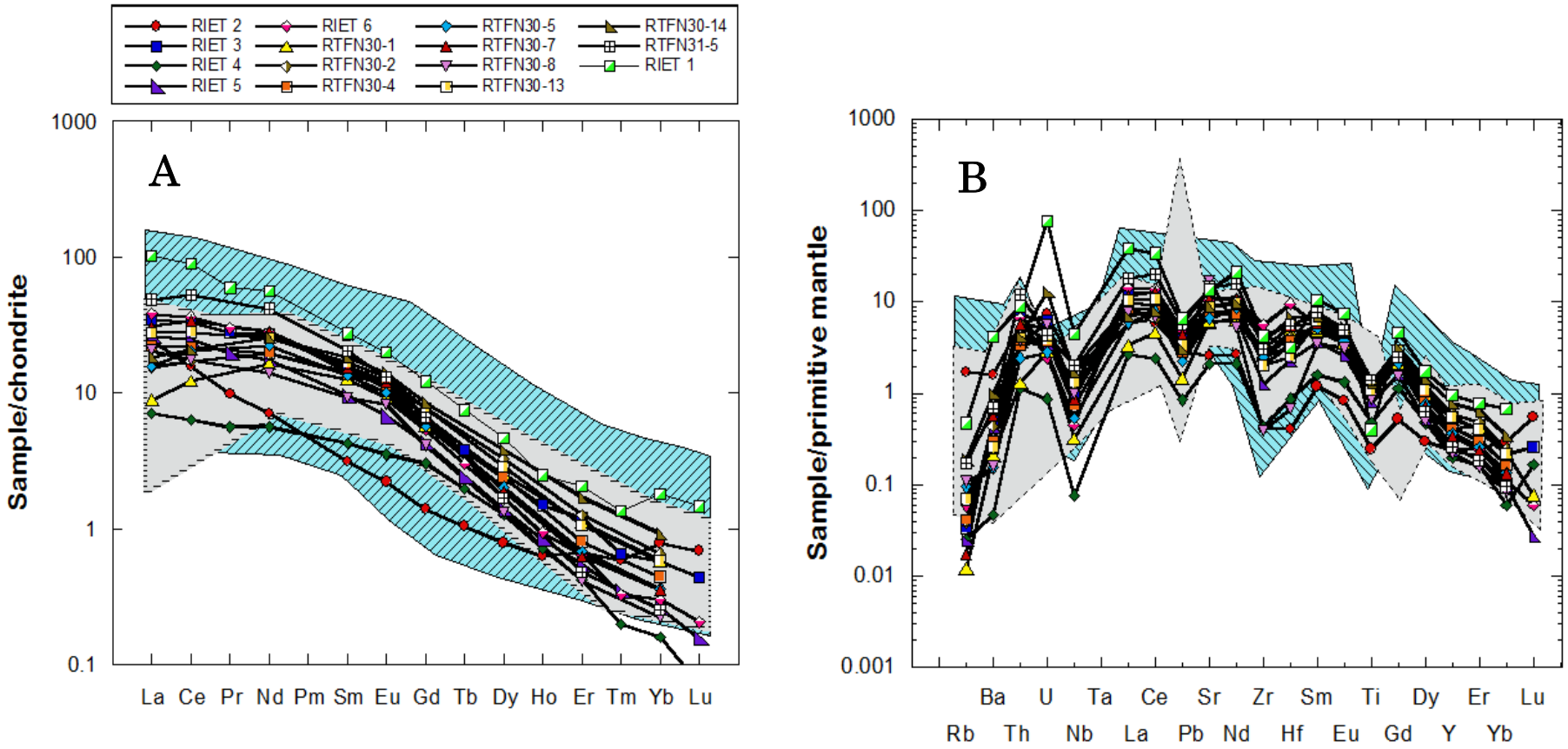

Figure 6.23. **A:** Chondrite normalised REE diagram and **B:** Primitive mantle normalised trace element diagram for clinopyroxene from Rietfontein. The compositional range of clinopyroxenes from Kimberley is indicated by the blue zone (Gregoire et al., 2003), while that of Gibeon clinopyroxenes is indicated by the grey zone (Luchs et al., 2013).

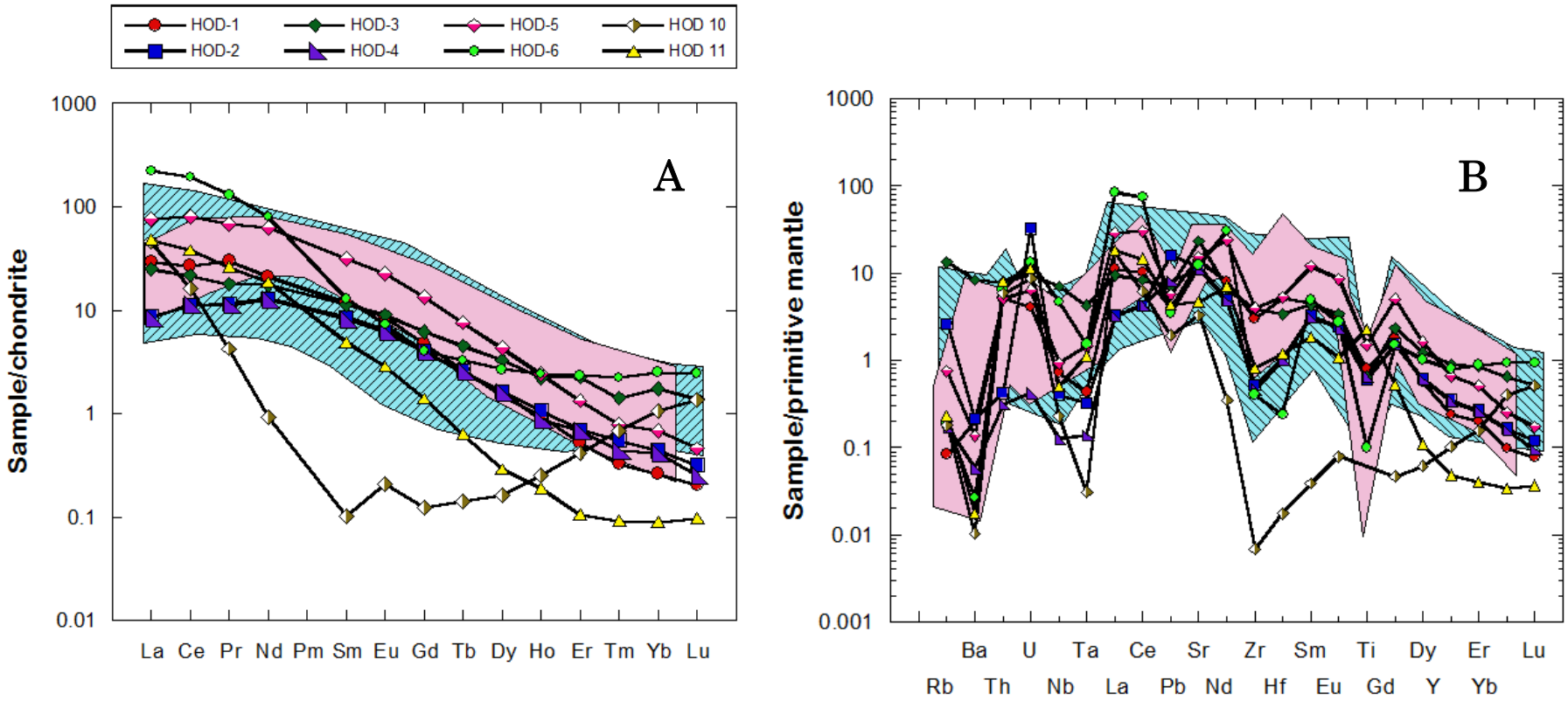

Figure 6.24. **A:** Chondrite normalised REE diagram and **B:** Primitive mantle normalised trace element diagram for clinopyroxene from Hoedkop. The compositional range of clinopyroxene from Kimberley is indicated by the blue zone (Gregoire et al., 2003), while that of Uintjiesberg and Hebron clinopyroxenes (eastern Namaqualand) is indicated by the pink zone (Kobussen et al., 2008; Kobussen et al., 2009).

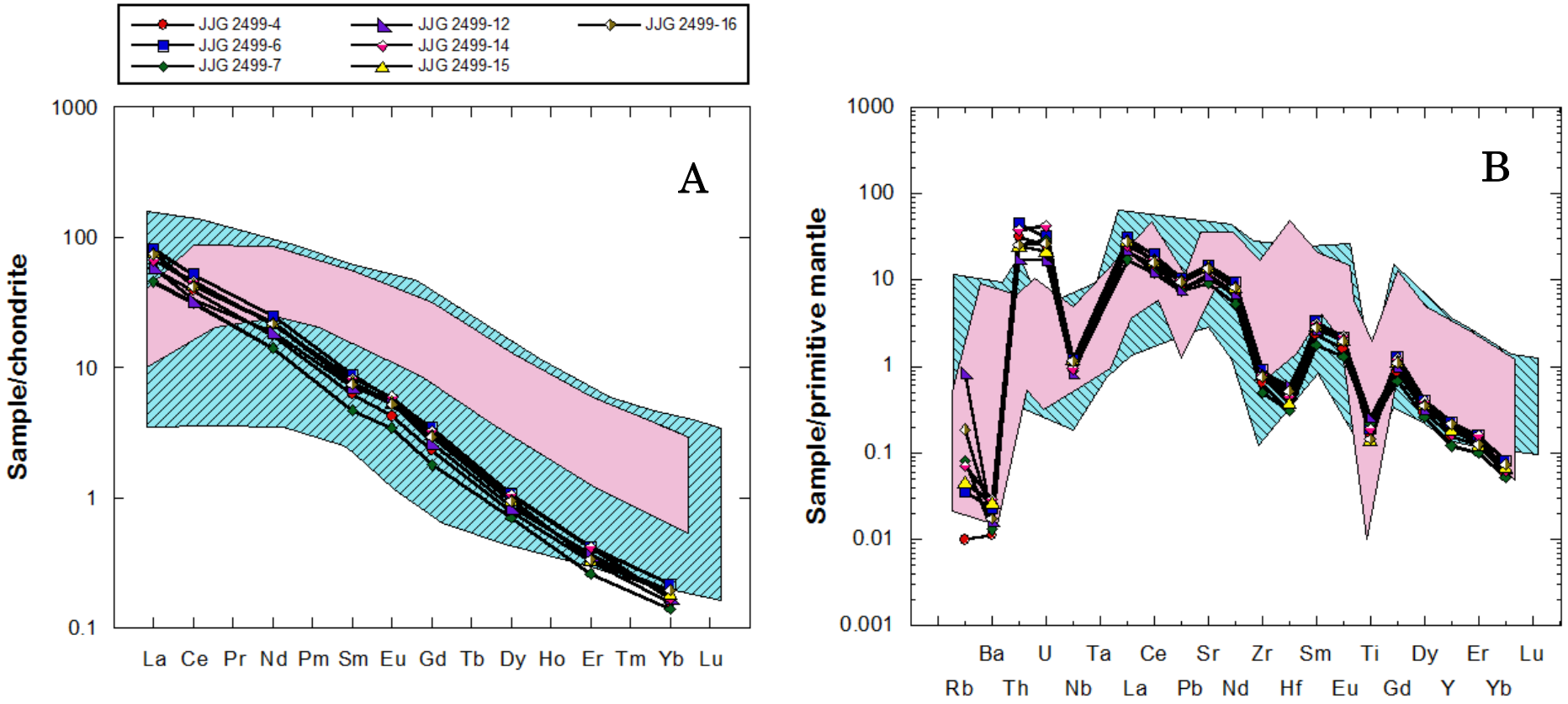

Figure 6.25. **A:** Chondrite normalised REE diagram and **B:** Primitive mantle normalised trace element diagram for clinopyroxene from Pofadder. The compositional range of clinopyroxene from Kimberley is indicated by the blue zone (Gregoire et al., 2003), while that of Uintjiesberg and Hebron clinopyroxenes (eastern Namaqualand) is indicated by the pink zone (Kobussen et al., 2008; Kobussen et al., 2009).

Trace element Relations and Abundances - Clinopyroxenes are known to be the mineral hosting the greatest concentrations of the incompatible elements in mantle peridotite, and therefore they exert the main control on the budget of these elements, especially the LREE (Rampone et al., 1991; Xu, 2000).

In terms of REE abundances, clinopyroxenes from Pofadder peridotites have characteristics that are fairly distinct from those of the other localities studied. Although there is a general positive correlation between $(Sm/Yb)_N$ and $(Ce/Yb)_N$ ratios of clinopyroxene for all localities studied, those from Pofadder fall slightly to the right of the main trend defined by the other localities due to their high $(Ce/Yb)_N$ ratios at moderate and nearly constant Sm/Yb ratios (Figure 6.26). Additionally, the Louwrensia (FRB 1183 and FRB 1652) and Hoedkop (HOD-6 and HOD-10) suites each have two samples that fall well above and below this trend, respectively.

The concentration of LILE such as Rb and Ba is highly variable, with Ba values extending from below detection to 55 ppm. Louwrensia clinopyroxenes have a higher average Ba content of 15.5 ± 23 (1σ) ppm, while those from Rietfontein. Hoedkop and Pofadder have Ba contents of 4.7 ± 6.5 ppm, 7.4 ± 18 ppm and 0.13 ± 0.04 ppm respectively. As with the garnets, Rb contents of Hoedkop clinopyroxenes (1.31 ± 2.6 ppm) are much higher than those from Louwrensia (0.27 ±0.32 ppm), Rietfontein (0.12 ±0.25 ppm) or Pofadder (0.11 ±0.17 ppm; Figure 6.27).

The clinopyroxenes investigated exhibit a wide range of HFSE concentrations, but do not extend to values as high as some of those for clinopyroxenes in cratonic peridotites. For example the maximum concentration of Zr and Hf recorded from the off-craton localities studied are 92 and 4.1 ppm respectively, while cratonic clinopyroxenes from Kimberley (Gregoire et al., 2003) extend up to 256 ppm and 6.9 ppm for these same elements. Unsurprisingly given their

similar geochemical behaviour, a strong positive correlation also exists between Zr and Hf in clinopyroxene for all localities studied (Figure 6.28). Ti behaves more variably with respect to Eu, a middle REE with similar magmatic incompatibility. Clinopyroxenes from Louwrensia and Pofadder cluster at low Ti/Eu ratios respectively, while those from Rietfontein and Hoedkop tend to exhibit higher ratios. (Figure 6.29).

The average concentrations of transition metals such as Ni and Sc are very similar amongst the clinopyroxenes studied. Grains from Louwrensia have Ni and Sc contents of 367 ± 36 (1σ) ppm and 25.2 ± 8.8 ppm respectfully, while those from Rietfontein, Hoedkop and Pofadder have average Ni contents of 320 ± 83 ppm, 374 ± 75 ppm, 355 ± 42 ppm and Sc contents of 31 ± 96 ppm, 42 ± 29 ppm and 27 ± 5 ppm respectfully.

Between the localities investigated, there is significant variability in the concentration of other incompatible elements (e.g., Th, U and Pb). A strong positive correlation exists between Th and U concentrations in clinopyroxene from all four localities (with one sample each from Rietfontein and Hoedkop falling off the main trend) that is identical to the trend formed by the Gibeon clinopyroxene data of Luchs et al. (2013; Figure 6.30). The clinopyroxene from Pofadder display the highest average Th and U contents by far. It is also important to note that the clinopyroxenes exhibit a general positive correlation between primitive mantle normalised Th/Nb and La/Nb ratios but Pofadder clinopyroxenes have extremely high Th/Nb values at a moderate La/Nb ratios, falling well above the main trend defined by the other localities (Figure 6.31).

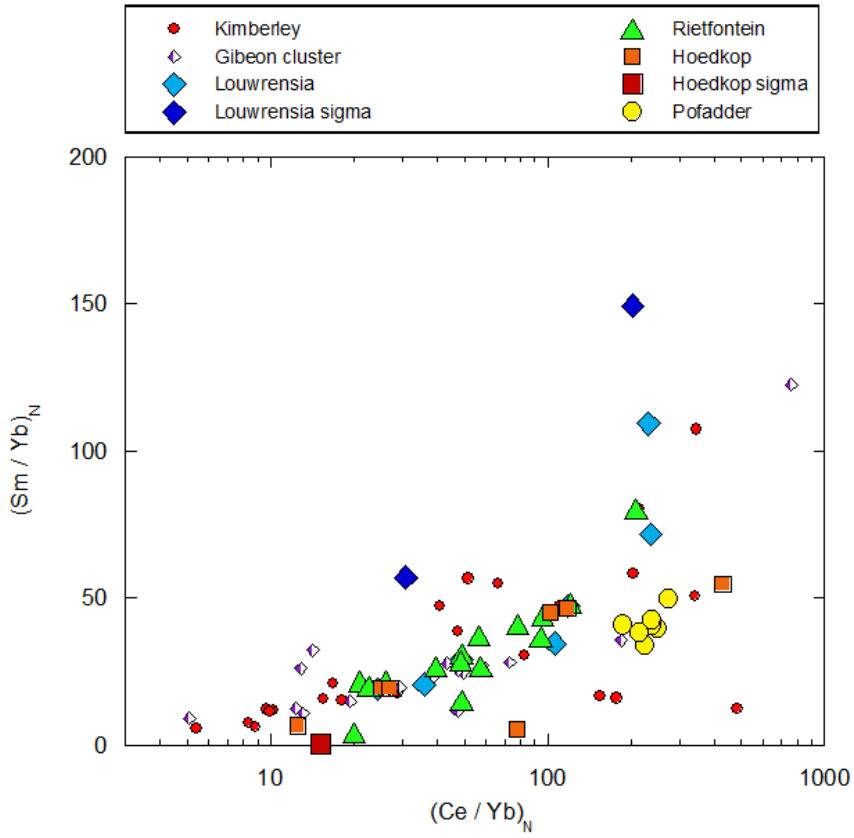

Figure 6.26. Plot of chondrite normalised Ce/Yb vs. Sm/Yb (i.e., $(Ce/Yb)_N$ and $(Sm/Yb)_N$) ratios in clinopyroxenes investigated. Data for Gibeon clinopyroxene is from Luchs et al., (2013), while that of Kimberley is from Gregoire et al., (2003)

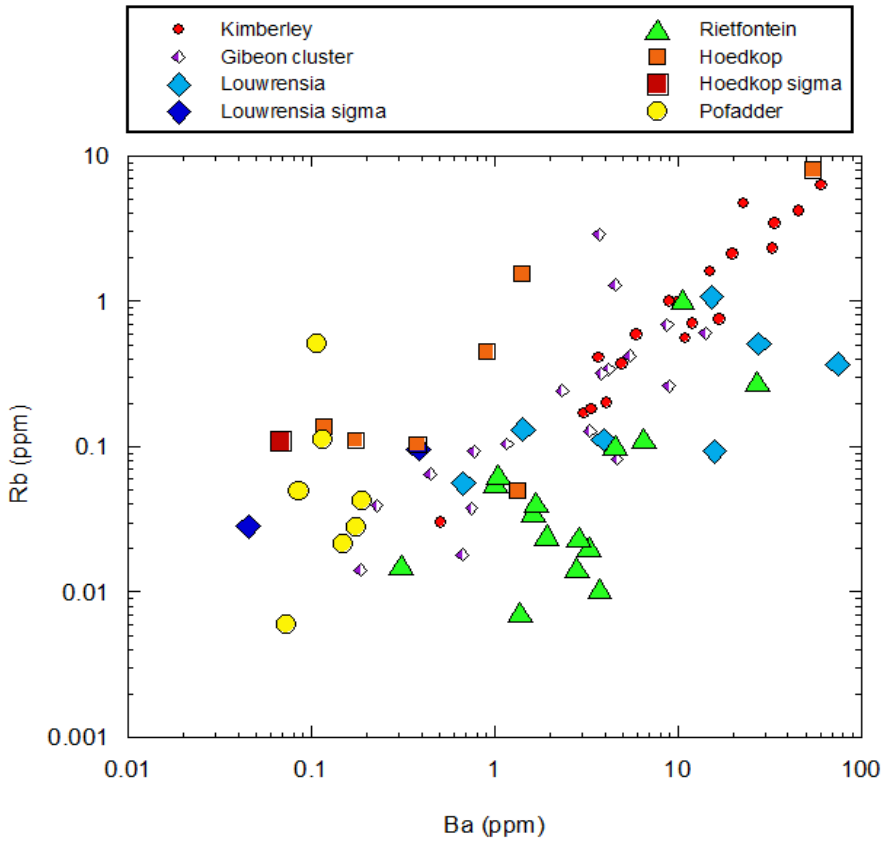

Figure 6.27. Plot of Ba vs. Rb contents in clinopyroxenes investigated. The source of data from the literature is listed in Figure 6.26).

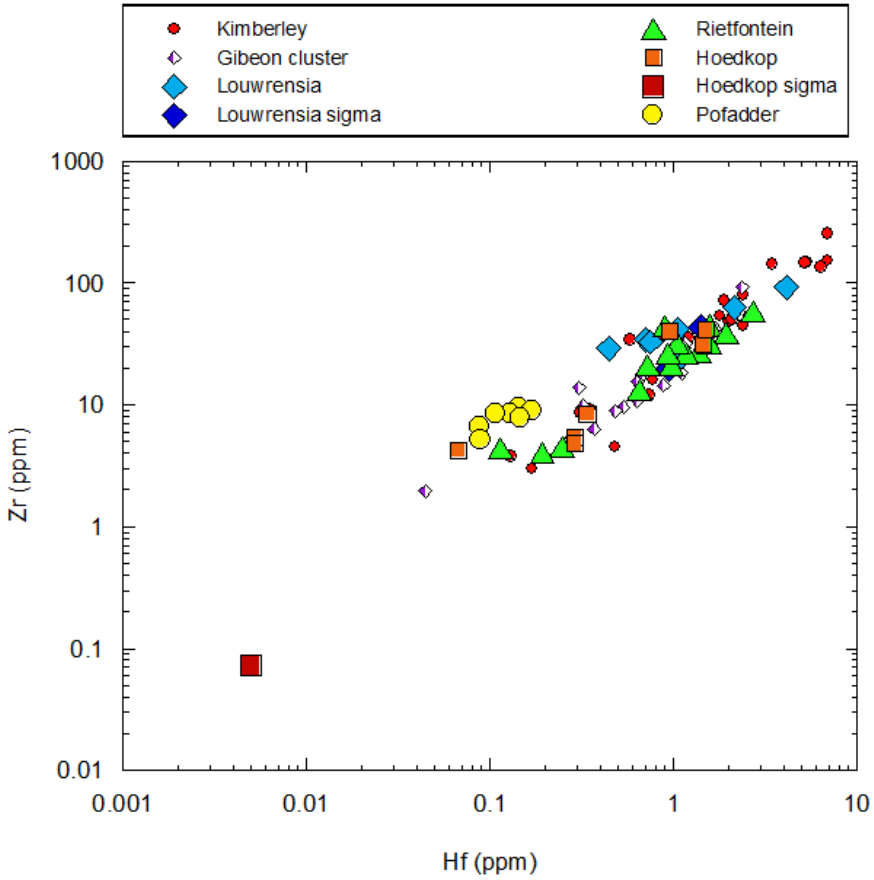

Figure 6.28. Plot of Hf vs. Zr contents in clinopyroxenes investigated. The source of data from the literature is listed in Figure 6.26).

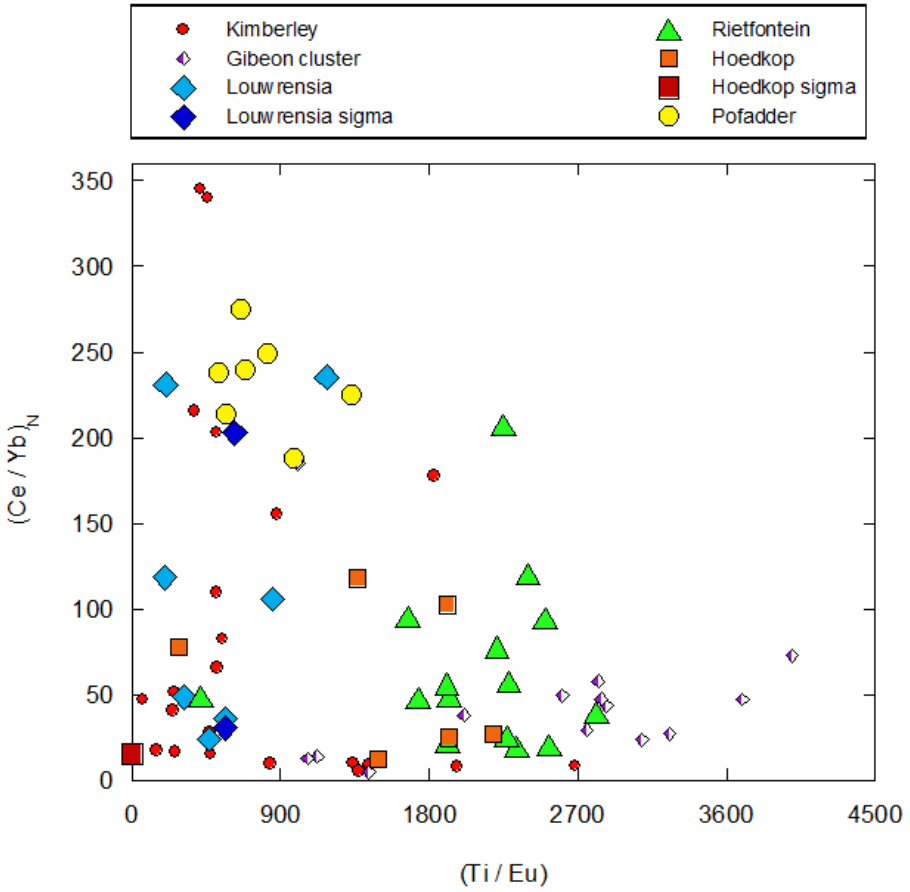

Figure 6.29. Plot of Ti/ Eu ratio vs. chondrite normalised (Ce/Yb) N ratio in clinopyroxenes investigated. The source of data from the literature is listed in Figure 6.26).

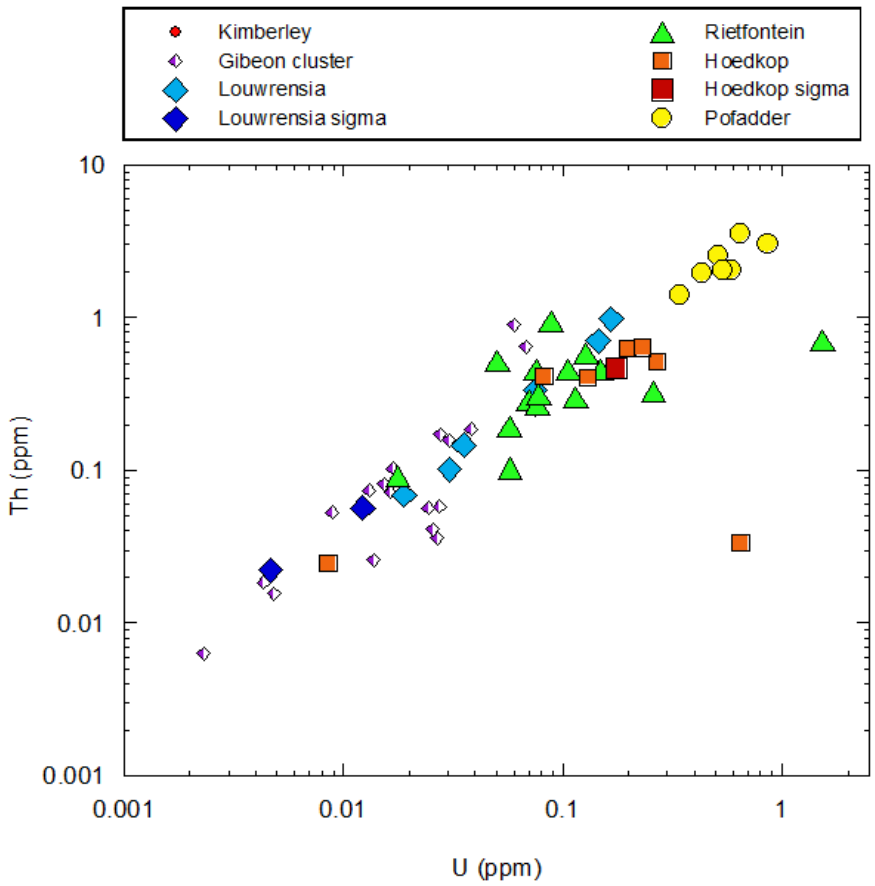

Figure 6.30. Plot of U vs. Th contents in clinopyroxenes investigated. The source of data from the literature is listed in Figure 6.26).

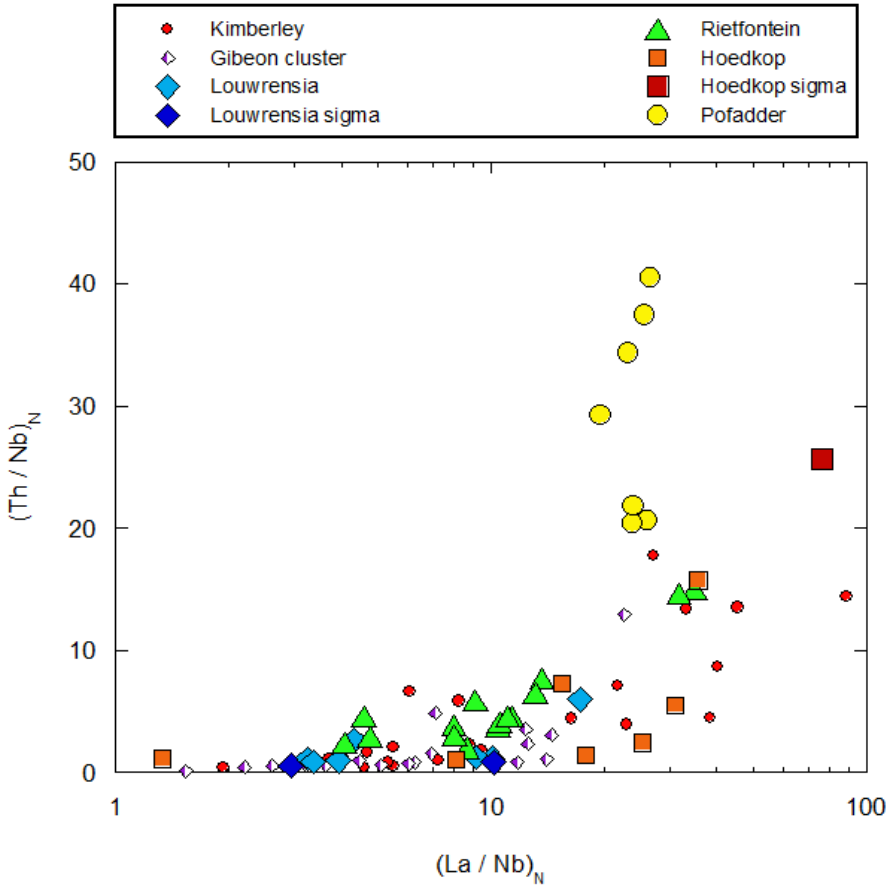

Figure 6.31. Plot of primitive mantle normalised (Th/Nb) N vs. (La/Nb) N ratios in clinopyroxenes investigated. The source of data from the literature is listed in Figure 6.26). Note the high Th/Nb values at a moderate La/Nb values for clinopyroxenes from Pofadder. The source of data from the literature is listed in Figure 6.26)

7. THERMOBAROMETRY

7.1. INTRODUCTION

In order to understand the thermal structure of the lithospheric mantle beneath the Rehoboth Province and the adjacent north-western Namaqua-Natal Province, along with any differences between these two terranes, it is crucial to determine the pressures and temperatures at which the investigated xenoliths last equilibrated. This is made possible by the fact that minerals undergo elemental exchanges that are sensitive to pressure and temperature (e.g. Boyd, 1973). The partitioning of elements between coexisting mineral pairs at different P-T conditions, which are determined experimentally, has been used to calibrate a variety of geothermometers and geobarometers (Finnerty and Boyd, 1987; Nikitina, 2000; Simakov, 2008). These are then applied to natural rock samples using the measured major element (or in some cases, trace element) compositions of coexisting minerals in xenoliths by establishing the partition between elements that are both sensitive to pressure and temperature and then applying the experimentally determined thermometers and barometers in an iterative fashion (Brey and Köhler, 1990; Glebovitsky et al., 2004). In peridotites, the accuracy of thermobarometric results are limited due to the very few univariant mineral reactions that are usable as absolute references, and also due to limited continuous mineral reactions which allow the use of changing mineral compositions in determining pressure-temperature conditions (Finnerty and Boyd, 1987). Uncertainties in geothermobarometry can emerge as a result of analytical inaccuracies, as well as poor assumptions in applying temperature and pressure calibrations from simple experimental systems to complex natural samples. For example, in thermometers that are based on the partitioning of

$Fe^{2+}$and Mg between minerals, uncertainties can result because some Fe^{3+} is present in the natural samples were none was present in the experimental system. Similarly, errors may arise from differences in the coordination of Al ions in pyroxenes between natural and experimental samples (Smith, 1999). Significant errors may also rise from the extrapolation of calibrations beyond experimental conditions, from a lack of thermodynamic data or the use of the data in the absence of correct thermodynamic expressions. Even with these potential problems, geothermobarometry provides the most robust and direct means of estimating the thermal state of the lithospheric mantle.

Data from thermobarometry can define a P-T array that allows the construction of a local geotherm for that particular area during the time of kimberlite emplacement. Pioneering work by Boyd (1973) involved using mineral data to compute pressures and temperatures for peridotites from the northern Lesotho kimberlites using an Al-in-orthopyroxene barometer and a two pyroxene thermometer. He noted two distinct groupings of the data. The first group consisted of granular, low temperature peridotites that record temperatures ranging from 900 ^{o}C - 1050^{o}C and pressure ranging from 3.5 Gpa - 5.2 Gpa, while the second group largely consisted of sheared, high temperature peridotites that record temperatures, ranging from 1150 ^{o}C -1450 ^{o}C, and much greater pressures of 55 Gpa - 6.5 GPa. The granular (undeformed), low temperature peridotites defined a geotherm similar to that of the shield as defined by Clarke and Ringwood (1964), while the high temperature deformed cluster lay at higher temperatures and defined a steeper geotherm (greater temperature change for a given pressure change) and is therefore "inflected" from the geotherm defined by granular samples. Such distinct data groupings and geotherms have subsequently been noted from numerous localities, including off-craton regions such as the Gibeon kimberlite field in the Rehoboth Province (Mitchell, 1984; Franz et al., 1996a; Franz et al., 1996b) and in East Griqualand in the Namaqua-Natal Province (Bell et al., 2003; Janney et al., 2010).

The temperature and pressure data from off-craton peridotites in southern Africa indicate a complex thermal history (Bell et al., 2003; Janney et al., 2010). It is

characterised by a relatively early regional thermal disturbance in the eastern NNP (East Griqualand, 200-150 Ma), and a later regional thermal disturbance in the western NNP. Peridotites from the oldest kimberlite in the western NNP (Melton Wold, ≈150 Ma) lie on the Kaapvaal geotherm, but younger Namaqua-Natal localities southwest of the Craton (Uintjiesberg, Hebron and Gansfontein 101-74 Ma) lie at temperatures 100-150°C higher than the Kaapvaal geotherm at low to moderate pressures. In contrast, there is little to no regional disturbance in the Rehoboth Province and most data for granular Gibeon peridotites, as well as orthopyroxene-bearing eclogites from Rietfontein, fall on the Kaapvaal geotherm (e.g., Mitchell, 1984; Franz et al., 1996a; Franz et al., 1996b; Appleyard et al., 2007), however there is some evidence for local heating (e.g., as shown by the deformed Gibeon peridotites; Boyd et al., 2004) .

The origin of the differences in the geotherms defined by granular samples are controversial. Originally, the intersection of the regular and inflected geotherms resulted in "kinked" geotherms, with the kink interpreted by Nixon et al. (1973), Boyd (1973b) and MacGregor & Basu (1974) as representing the lithosphere/ asthenosphere boundary, but this was inconsistent with estimates of lithospheric thickness from seismology (e.g., Jordan, 1975). Later, these kinked geotherms were explained as artefacts of the thermobarometry calibrations and the particular thermobarometers chosen (Carswell and Gibb, 1987).

The appearance of the inflection between geotherms defined by granular and deformed samples in numerous xenolith suites, as well as the application of new, well calibrated thermobarometers based on the mineral chemistry data of such peridotite suites (e.g., the T_{BKN} - P_{BKN} thermobarometer of Brey and Köhler (1990)), has led to the hypothesis that these high temperature deformed peridotites are in most cases a result of the local interaction between the lithospheric mantle and upward percolating melts. These melts have been proposed to originate from rising diapirs (Mitchell, 1984) and/or rising mantle plumes that induce kimberlite magmatism and caused deformation of the lower part of the lithosphere, (Franz et al., 1996a; Franz et al., 1996b).

Heat flow measurements have also been used to constrain lithospheric geotherms. In particular, Pollack and Chapman (1977) constructed geotherms for both continental and oceanic lithosphere, in which surface heat flow is the principal independent variable. A global analysis of heat flow in various Precambrian terranes by Nyblade and Pollack (1993) further improved understanding of the relationship between heat flow and lithosphere thickness and age. Their study concluded that Archean cratons (composed of the oldest, thickest lithosphere) are characterised by a much lower heat flow than younger, thinner, Proterozoic terranes. The present day heat flow of the off-craton sublithospheric mantle in the Namaqua-Natal Province is about 61 ± 10mWm^{-2}, while that in the Rehoboth province is about 45 mWm^{-2} (Muller et al., 2009). These values are higher than the 41 mWm^{-2} and 44 mWm^{-2} recorded from eastern and western Kimberley blocks, respectively, of the neighbouring Archean Kaapvaal craton, which could indicate thinner lithosphere in the off-craton regions, although this is complicated by variations in the thickness and composition of continental crust in the region (e.g., Nguuri et al., 2001). This relationship between heat flow and lithospheric age has been reported in other parts of the world (Ballard et al., 1987; Nyblade and Pollack, 1993; Muller et al., 2009). However, the xenolith-derived P-T array suggest paleo-heat flow of 41-42 mWm^{-2} in the Rehoboth province (Bell et al., 2003; Boyd et al., 2004; Appleyard et al., 2007). This heat flow is indistinguishable from the 40-42 mWm^{-2} heat flow that corresponds to the average cratonic pressure-temperature (P-T) array.

Rudnick and Nyblade (1999) constructed a mean cratonic paleogeotherm for southern Africa based on both high and low temperature peridotite data calculated using the T_{BKN}-P_{BKN} thermobarometer combination for a set of xenoliths from Lesotho, Kimberley and Letlhakane. This was accomplished by applying a best-fit curve to the mantle P-T array produced by data from over 100 xenoliths. This "Kalahari" geotherm has been widely used to represent the thermal state of the Archean core of the southern African lithospheric mantle. It is also preferred over the traditional 40 mWm^{-2} cratonic geotherm of Pollack and Chapman (1977). This is because the latter is only useful above pressure of 3.5 GPa, below which it yields

higher temperatures that are in conflict with the data for cratonic granular peridotites (Boyd et al., 2004).

In this study, I apply a variety of thermometers and barometers to mineral data for peridotite xenoliths from the four locations studied in order to constrain the pressure and temperature conditions in the lithospheric mantle of the Rehoboth Province and the north-western Namaqua-Natal Province. The results are used to identify any systematic differences and similarities in the thermal structure of these two lithospheric terranes. The thermobarometry data are also compared with that of the "Kalahari" geotherm for the Kaapvaal-Zimbabwe cratons and data from other off-craton coarse granular suites from southern Africa.

7.2. SUMMARY OF THE GEOTHERMOMETERS AND GEOBAROMETERS USED

The 'TP99' thermobarometry program of Doug Smith (1999) was used to generate temperatures and pressures from five thermometers and three barometers using the major element compositions of coexisting garnets, clinopyroxenes, orthopyroxenes and olivines from the four xenolith localities studied. The various geothermobarometers used (Table 7.1) are briefly reviewed, followed by a discussion of the results obtained once applied to the data.

Table 7.1 *Geothermometers and geobarometers used in this study.*

Geothermomemter	Reference	Method
T_{FB-86}	Finnerty and Boyd (1987)	Pyroxene solvus
T_{BKN}	Brey and Köhler (1990)	Pyroxene solvus
T_{Brey}	Brey and Köhler (1990)	Na partitioning between two-pyroxene
$T_{BKCa-opx}$	Brey and Köhler (1990)	Ca-in-orthopyroxene
T_{Kr}	Krogh (1988)	Fe-Mg exchange between garnet and clinopyronexe
Geobarometer		
PM74	MacGregor (1974)	Al-in-orthopyroxene
P_{BKN}	Brey and Köhler (1990)	Al-in-orthopyroxene
$P_{Nickel\&Green}$	Nickel and Green (1985)	Cr-Al exchange between garnet and orthopyroxene

7.2.1. Geothermometers

Two-pyroxene thermometers: These thermometers are based on the solvus between clinopyroxene and coexisting orthopyroxene. Since the two minerals have similar crystal structures, they exhibit continuous solid solutions at high temperatures, but as temperatures decrease a miscibility gap grows between them. As the gap is strongly temperature dependent, it can be used as a geothermometer. The shape of the solvus has an impact on the geothermometers, as small changes in mineral composition correspond to large temperature differences along the steep limbs but correspond to only moderate temperature differences near the crest of the solvus. Therefore, the shape of the solvus compels the geothermometers to become increasingly more sensitive indicators with increasing temperature (Bucher and Frey, 1994).

The T_{FB-86} thermometer was developed by Finnerty and Boyd (1987) and it is based on this diopside-enstatite miscibility gap, from reversed experiments in the simple CaO-MgO-SiO_2 (CMS) system. Brey and Köhler (1990) developed two thermometers T_{Brey} and T_{BKN}, which are principally based on pyroxene experimental data of Brey et al. (1990). The T_{BKN} geothermometer is also based on

the pyroxene miscibility gap and calibrated using experimental data, while T_{Brey} is based on the partitioning of Na between clinopyroxene and orthopyroxene and is calibrated using data from natural rocks. The only problem with using pyroxene solvus geothermometers is that they are less sensitive at temperatures below 900 ^{o}C, hence are less reliable in estimating equilibration conditions of low temperature peridotites. Additionally, the effects of Fe^{2+} on the solvus may also lead to some uncertainties (Griffin and O'Reilly, 1987).

Ca-in-orthopyroxene thermometer: This method uses only the calcium content of orthopyroxene co-existing with clinopyroxene to estimate equilibration temperatures of the xenoliths. Brey and Köhler (1990) fitted reversed experiments in the CaO-MgO-SiO_2 (CMS) system as a function of pressure and reciprocal temperature to estimate equilibration temperatures, $T_{BKCa\text{-}opx}$. They did note, however, that the $T_{BKCa\text{-}opx}$ thermometer yields temperatures for natural mineral compositions from granular and deformed peridotites that are slightly higher and lower, respectively, than their two-pyroxene geothermometers.

Fe-Mg exchange thermometers: These thermometers are based on the temperature-sensitive exchange of Fe^{2+} and Mg between two coexisting minerals in a rock. Fe^{2+} and Mg^{2+} have similar charge and ionic radius, and their exchange therefore leads to small volume changes and large entropy changes. Such an exchange can occur between garnet and olivine, garnet and clinopyroxene, and garnet and orthopyroxene. Krogh (1988) used existing experimental data on the partitioning of Fe^{2+} and Mg between garnet and clinopyroxene to revise and construct the thermometer T_{Kr}. This thermometer is widely used and tends to generate fairly reliable results when applied to low temperature peridotites and eclogites but has been criticised due to its larger uncertainties compared to thermometers such as T_{BKN}.

7.2.2.Geobarometers

Al-in-orthopyroxene barometers: Two barometers used in this study are based on the sensitivity of Al content to pressure in orthopyroxene co-existing with garnet.

The first barometer to use this relationship, P_{M74}, was calibrated by MacGregor (1974), who developed it by studying the solubility of Al within the MgO-Al_2O_3-SiO_2 system between temperature conditions of 900 ^oC -1600 ^oC at 0.5-4 GPa. However, the barometer is known to be strongly temperature-sensitive, therefore overestimation of input temperatures will result in greater overestimation of equilibration pressure as noted in the Louwrensia suite of Mitchell (1984). The second geobarometers is the P_{BKN} of Brey and Köhler (1990) that has become one of the most widely used barometers. In their formulation, the workers treated orthopyroxene as a two-site solid solution, with ideal mixing at the M2 site. They also assumed statistical distribution of Fe and Mg between M1 and M2 with no cross-site interactions and treat the M1 site as a ternary regular solution in the combined CaO-FeO-MgO-Al_2O_3-SiO_2 (CFMAS) and SiO_2-MgO-Al_2O_3-CaO-Cr_2O_3 (SMACCr) systems to reproduce equilibration pressure results in the natural system.

Cr-Al exchange barometer: A second barometer was developed by Nickel and Green (1985; $P_{Nickel\&Green}$) based on Cr-Al exchange between orthopyroxene and garnet. They formulated their barometer by refining existing Al-in-orthopyroxene barometers and by studying the substitution of Cr for Al as a function of pressure and temperature in both the CaO-MgO-Al_2O_3-SiO_2 (CMAS) and SiO_2-MgO-Al_2O_3-CaO-Cr_2O_3 (SMACCr) systems between the temperatures of 1000 ^oC and 1400 ^oC at 1.0 to 3.5 GPa. However, it is noted by Nickel and Green (1985) that the barometer should be used with caution as elements, such as Ni and Ti, can also substitute for Al in the M1 sites of orthopyroxene crystal structure.

7.3. EVALUATING THE AGREEMENT BETWEEN GEOTHERMOBAROMETERS

The agreement between thermometers and barometers employed is evaluated by calculating the difference between the output values of the various thermometers and barometers and that of the T_{BKN} and P_{BKN} values that are used as a reference. The comparisons are shown in detail in Figure 7.3 and Figure 7.4 where the differences are plotted against the T_{BKN} temperature from Brey and Köhler (1990).

7.3.1. Evaluation of Geothermometers

There is mostly good agreement between temperature estimates of T_{Brey} and T_{BKN}, with increasingly negative values for $[T_{Brey} - T_{BKN}]$ occurring above T_{BKN} values of about 1100 ^{o}C and higher, but temperature estimates from the two thermometers are all within 100 ^{o}C of each other (Figure 7.1a). All peridotites have negative values for $[T_{FB\text{-}86} - T_{BKN}]$, suggesting a systematic underestimation of temperatures when using $T_{FB\text{-}86}$. Nonetheless, 97% of temperature estimates from $T_{FB\text{-}86}$ thermometer fall within 100 ^{o}C of those estimated using T_{BKN} (Figure 7.1b). Only two samples show good agreement between $T_{BKCa\text{-}opx}$ and T_{BKN} thermometers. A majority of $T_{BKCa\text{-}opx}$ temperature estimates plot to negative deviations, indicative of temperature underestimation, while another set of two samples plot to positive deviations (Figure 7.1c). Peridotites produce equally positive and negative deviations for the comparison between T_{Kr} and $T_{BKN,}$ resulting in temperature overestimation of most peridotites from Hoedkop and a systematic temperature underestimation for Rietfontein and Pofadder peridotites (Figure 7.1d).

Overall, all temperature estimates from the various thermometers applied to the peridotites studied are all within 200 ^{o}C of those estimated using T_{BKN}. Further, the discrepancies between thermometers for the new data are of comparable or lesser magnitude than for the published data.

7.3.2. Evaluation of Geobarometers

The $P_{Nickel\&Green}$ barometer yields estimates that are in good agreement with those assessed using $P_{BKN,}$ with slight underestimation of pressure occurring in the deformed Hoedkop sample HOD-3 (Figure 7.2a). In a comparison between P_{MC74} and P_{BKN} most peridotites plot to positive deviations, although there is good agreement in a few samples.

In general there appears to be a reasonable agreement between pressure estimates from the various barometers employed with those estimated using P_{BKN} as the results are all within 1 GPa of each other (Figure 7.2b).

7.4. ESTIMATED EQUILIBRATION PRESSURES AND TEMPERATURES

In the following sections, new thermobarometry results from Rietfontein and Pofadder are added to the existing data base for the Louwrensia and Hoedkop peridotite suites from the published literature. In order to efficiently compare and contrast the thermal state in the four locations, it is necessary to employ a single thermometer and barometer set. The combined T_{BKN}-P_{BKN} thermometer-barometer set has been selected because it is the most widely used in the literature for estimating equilibration temperature and pressure from garnet peridotite data. It is unlikely that this will result in any significant bias or inaccuracy, since there is generally reasonable agreement between this pair and other thermometers and barometers used.

In the Rehoboth province, 80% of granular peridotites from Louwrensia investigated lie between 850 °C and 1150°C and between 3.0 and 4.5 GPa, while Rietfontein peridotites show very similar and overlapping equilibration conditions of 685 °C - 1079 °C at 2.1 GPa - 4.6 GPa, with both peridotite populations lying between the 40mWm^{-2} and 45mWm^{-2} conductive geotherms of Pollack and Chapman (1977; Figure 7.3). Further, both Louwrensia and Rietfontein peridotite suites lie on the Kalahari geotherm as do granular peridotites from Kimberley on the Kaapvaal craton, peridotites from other Gibeon localities (Gibeon Townlands, Anis Kubub, and the vast majority of peridotites from Hanaus), and orthopyroxene-bearing eclogites from Rietfontein (Figure 7.4). Two granular garnet peridotites from Louwrensia, PHN 5301 and PHN 5364 record much higher temperatures than the other granular peridotites, of 1226 °C and 1278 °C, both at 4.1 GPa respectively. These samples lie above both the Kalahari geotherm and the 50 mWm^{-2} conductive geotherm and hence coincide with the P and T values for deformed peridotites from the same pipe and with the approximately 30% of granular peridotites from Hanaus that give anomalously high temperatures (Figure 7.4).

In the Namaqua-Natal Province, all peridotites from Pofadder show similar equilibration conditions, resulting in a tight cluster between 933 °C and 964°C at 2.9 GPa to 3.2 GPa. At a given pressure, these peridotites record temperatures 100-150°C warmer than the Kalahari geotherm and also lie between the 45 mWm^{-2} and 50 mWm^{-2} conductive geotherm. Peridotites from Hoedkop record a much wider range of pressures and temperatures. The three granular samples have equilibrated to T and P conditions similar to those of Pofadder, between 822 °C and 993°C at 2.5 GPa - 3.1 GPa, whereas three incipiently deformed peridotites record much higher temperature and pressure values between 1230 °C and 1266°C at 4.5 GPa – 5.0 GPa (Figure 7.3). At a given pressure, the Hoedkop peridotites fall at higher temperatures than the Gibeon or Kimberley peridotites, and lie about 100-200°C warmer than the Kalahari geotherm. Four out of six Hoedkop xenoliths lie between the 45 mWm^{-2} and 50 mWm^{-2} conductive geotherms of Pollack and Chapman (1977) of Pollack and Chapman (1977) and the remaining two fall above the 50 mWm^{-2} conductive geotherm. In general, both Pofadder and Hoedkop granular peridotites display P-T ranges similar to other off-craton granular peridotites from the western Namaqua-Natal Province such as Uintjiesberg, Hebron and Gansfontein (Bell et al., 2003; Janney et al., 2010) (all grouped under E. Namaqualand young in Figure 7.4). On the other hand, the deformed peridotites data for Hoedkop fall within the range of high temperature deformed peridotites from the Gibeon cluster including those from Louwrensia, as well as granular peridotites from the ≈150 Ma Melton Wold kimberlite in the western Namaqua-Natal province (indicated as E. Namaqualand old in Figure 7.4).

It is also important to note that the pressure and temperatures recorded by all xenoliths studied fall within the stability field of graphite or on the graphite-diamond univariant curve of Kennedy and Kennedy (1976).

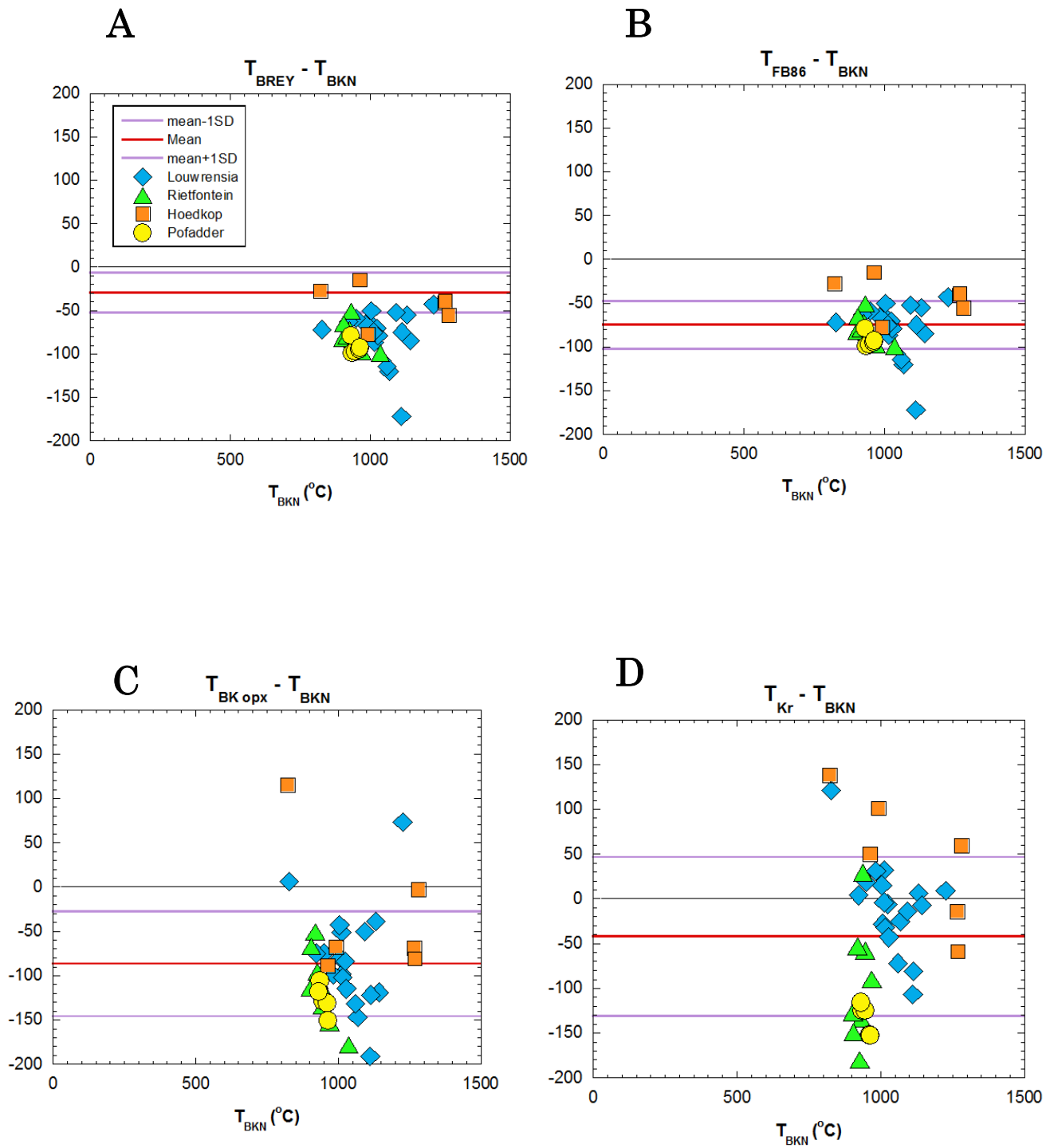

Figure 7.1 T_{BKN} versus ΔT (both in °C) diagrams for primary mineral assemblages of granular peridotites from the Rehoboth and Namaqua-Natal province. Information on the various geothermobarometers is summarised in Table 7.1

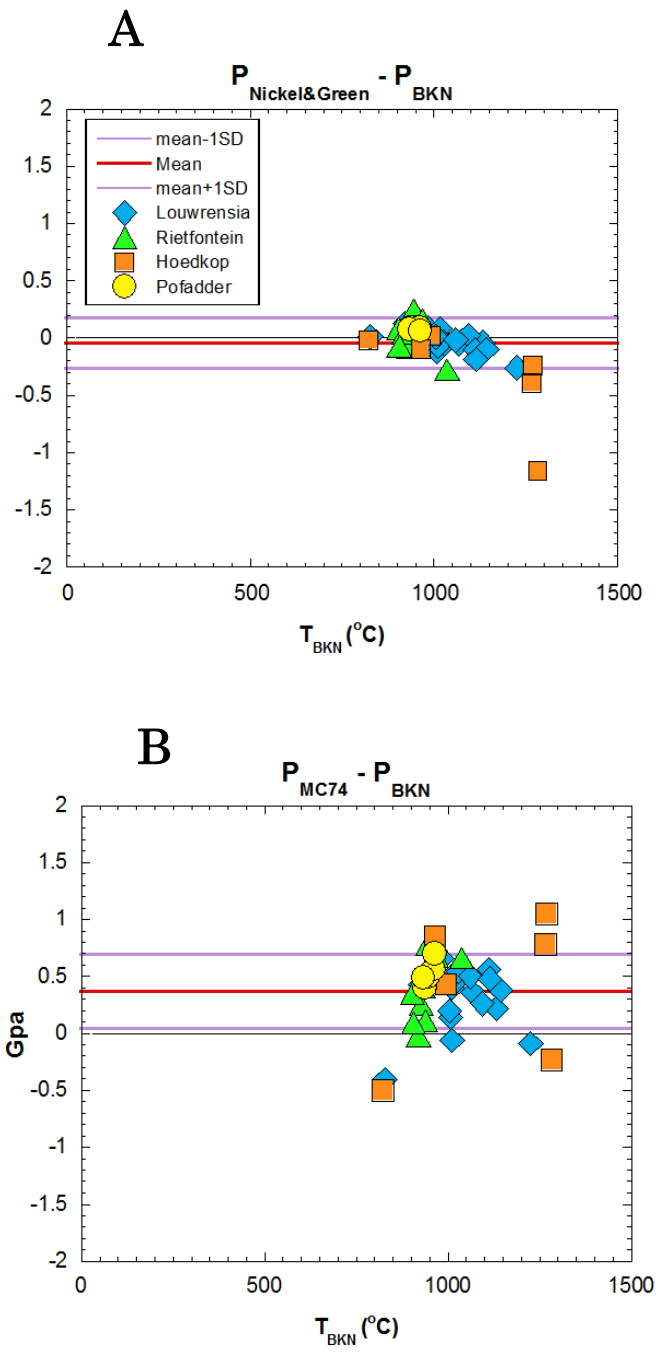

Figure 7.2 T_{BKN} (°C) versus ΔP diagrams for primary mineral assemblages of granular peridotites from the Rehoboth and Namaqua-Natal province. Information on the various geothermobarometers is summarised in Table 7.1

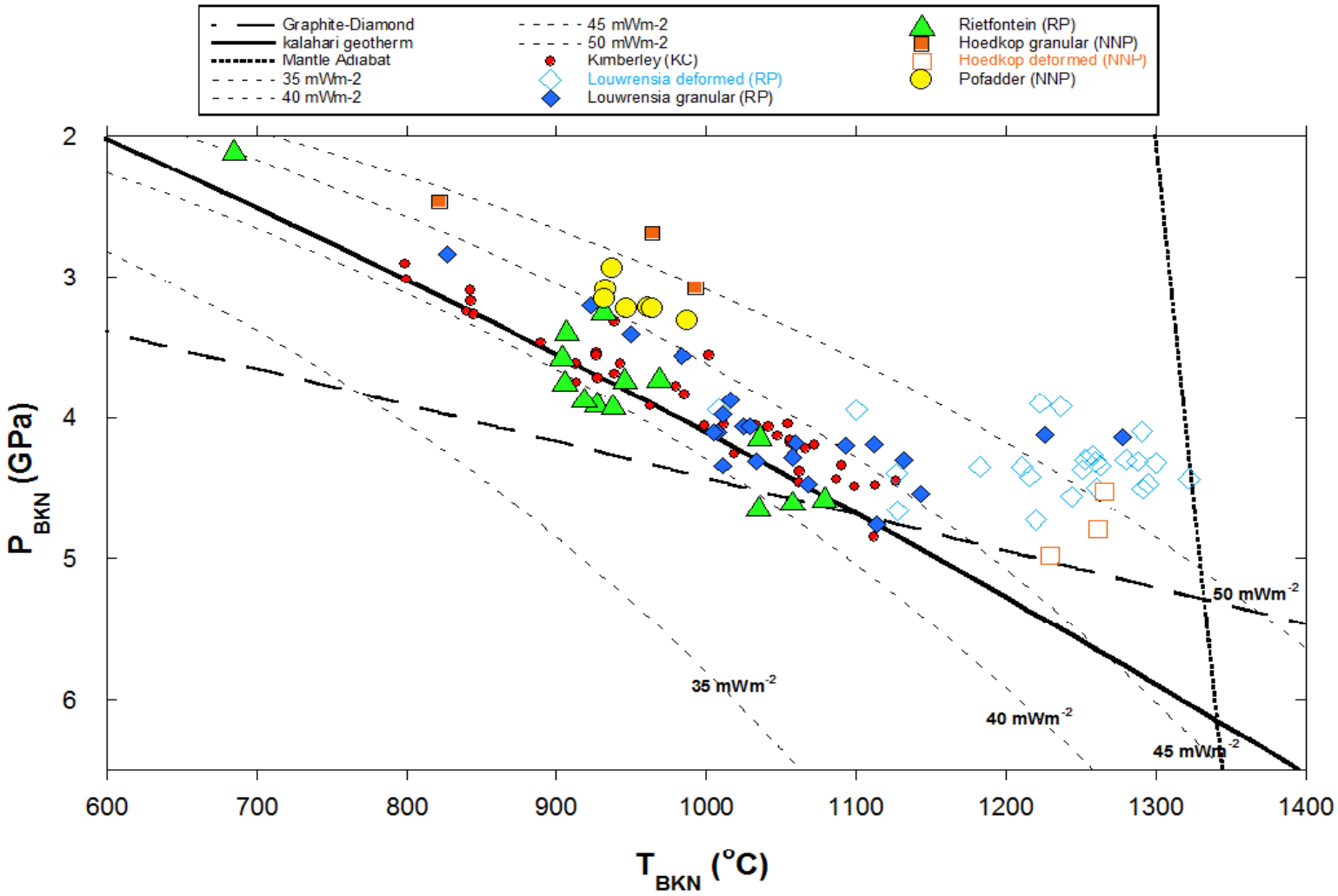

Figure 7.3. P-T arrays with estimates calculated with the TBKN - PBKN thermobarometer combination for peridotites from the studied localities and Kimberley (Kaapvaal). The diamond-graphite transition is after Kennedy and Kennedy (1976), while geothermal gradients are after Pollack and Chapman, (1977) that cross the mantle adiabat with potential temperature of ≈ 1300 oC. The bold continuous curve represents the 'Kalahari' geotherm of Rudnick and Nyblade, (1999).

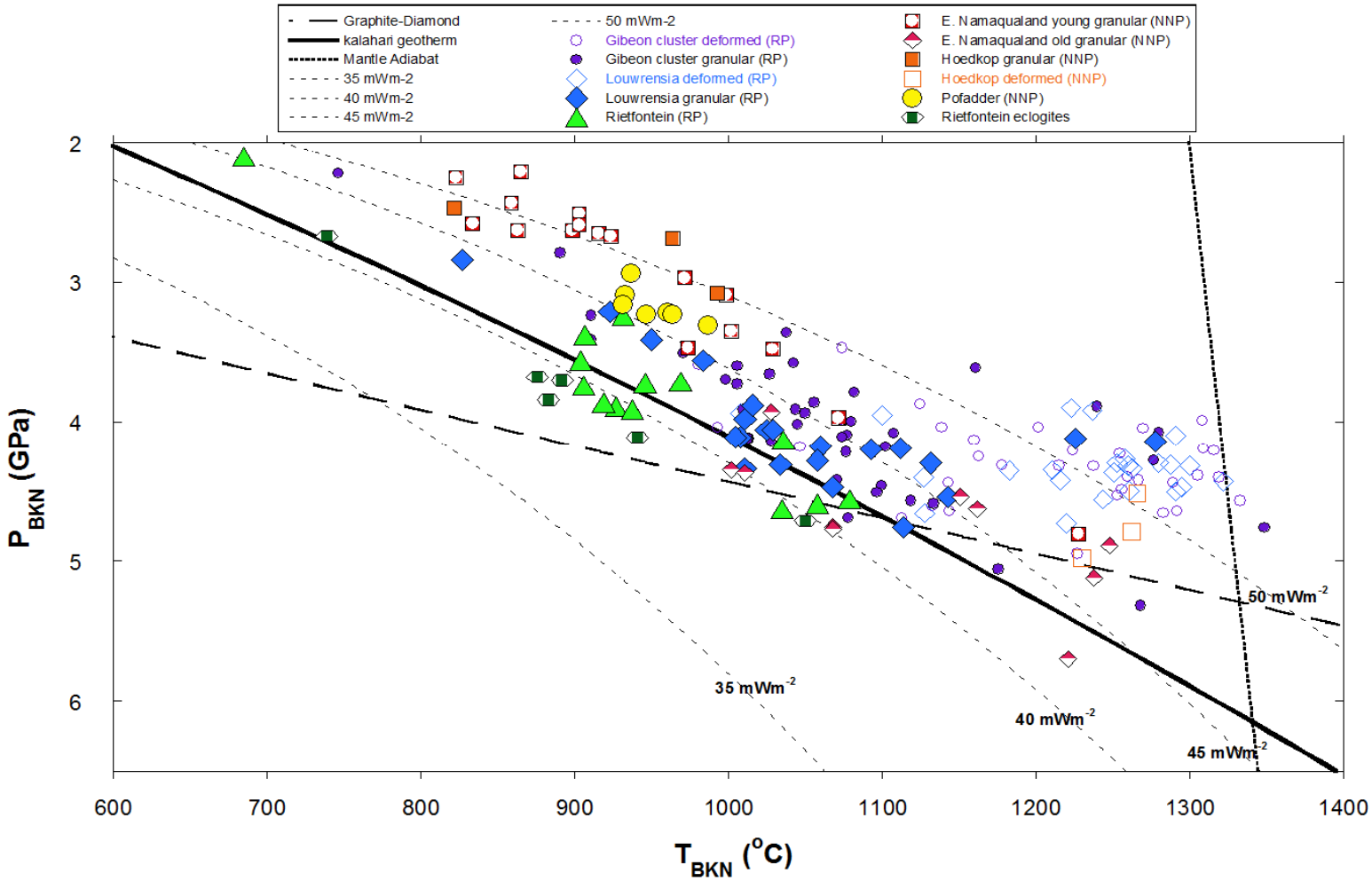

Figure 7.4. P-T arrays with estimates calculated with the TBKN - PBKN thermobarometer combination for peridotites localities studied, from other off-craton localities and from Kimberley. The diamond-graphite transition is after Kennedy and Kennedy (1976), while geothermal gradients are after Pollack and Chapman, (1977) that cross the mantle adiabat with potential temperature of ≈ 1300 °C. The bold continuous curve represents the 'Kalahari' geotherm of Rudnick and Nyblade, (1999). Data for Gibeon peridotites is sourced from Mitchell, (1984); Franz et al., (1996a); Franz et al., (1996b); Boyd et al., (2004), while data for eastern Namaqualand young (i.e. Uintjiesberg, Hebron and Gansfontein, all 74-100 Ma) and eastern Namaqualand peridotites (i.e. Melton world 150 Ma) is from Janney et al., (2010) and that of Rietfontein eclogites is from Appleyard et al., (2007).

8. DISCUSSION

In the following chapter, topics related to the formation, structure and history of southern African off-craton lithosphere are addressed in order to understand and characterise the off-craton mantle located to the west of the Kaapvaal Craton. The first section attempts to characterise the extent of melt depletion in the four localities studied by using evidence from major and trace element data. The second section addresses the thermal state and structure of the mantle in Rehoboth and western Namaqua-Natal provinces by examining the results from mineral thermobarometry. The third section aims to characterise metasomatic enrichments in the peridotites studied using both major and incompatible trace element abundances and partitioning and in fourth section, trace element melt modelling is used in determining the possible metasomatic agent(s) that led to incompatible element enrichment in garnet and clinopyroxenes studied. Issues regarding the timing of melt depletion or metasomatism in the two southern Africa off-craton provinces are outside the scope of this study, but have been addressed previously in the literature (Hoal et al., 1995; Carlson et al., 1999; Janney et al., 2010; Luchs et al., 2013; Aulbach et al., 2014; Pearson, 2014).

8.1. MELT DEPLETION

In order to constrain the extent of melt extraction of the off-craton mantle in the four localities studied, it is necessary to review the Mg-numbers of olivines and pyroxenes of the xenoliths. The olivine Mg-number correlates with the extent of melt depletion and/or the subsequent enrichment in iron due to melt-rock interaction (Pearson et al., 2014). Assuming that all peridotite xenoliths are

residues of partial melting at or below pressures of 3 GPa (Canil, 2004), then pressure variations will not have a significant impact on Mg-numbers, but rather will be a function only of varying degrees of melt extraction (Boyd et al., 2004; Pearson et al., 2014). However, it must be acknowledged that the pressure of melt extraction for cratonic peridotites (i.e., whether primarily forming by melt extraction at pressures of less or greater than 3 GPa) remains vigorously debated (e.g., Pearson and Wittig, 2008; Griffin et al., 2009; Aulbach, 2012).

The Mg-number of orthopyroxene is slightly greater than that of coexisting olivine, as a result of the P-T independent partition coefficient (K_D) between Fe and Mg in these two minerals is slightly greater than 1 (von Seckendorff and Neill, 1993) while the Mg-number of clinopyroxene is typically significantly higher than that of coexisting olivine, because of a Fe-Mg K_D value significantly greater than 1 (Pearson et al., 2014).

A global analysis of olivine data shows that the vast majority of cratonic peridotite xenoliths have olivine Mg-number values between 91and 94, with a mean at 92.6 (Boyd, 1996; Pearson and Wittig, 2008). This mean value can therefore regarded as that associated with the typical extent of melt depletion of southern African cratonic lithosphere generated during the Archean (e.g., Pearson and Wittig, 2008). In contrast, abyssal peridotites contain olivines with a lower average Mg-number of 90.8 reflecting the lower average level of melt depletion occurring at modern day mid-ocean ridges (Dick et al., 1984; Boyd, 1989). Olivine from Louwrensia has an average Mg-number of 91.5 ± 0.3 (1σ), while olivines from Rietfontein and Hoedkop have average Mg-number values of 91.9 ± 0.3 and 91.4 ± 1.4 respectively. These values are lower than those of cratonic olivines from Kimberley (with an average Mg-number of 92.4), demonstrating the more iron-depleted characteristic of the latter, but are higher than for olivines from abyssal peridotites.

Although it has been documented that the infiltration and reaction of melt with peridotite can alter the composition of olivines, and hence their Mg numbers, theoretical models have shown that melt infiltration, which typically either

consumes or produces olivine, is expected to generate significant mineralogical changes in the affected mantle (Pearson, 2014). The high variation in the proportion of modal olivine in cratonic peridotites (Bernstein et al., 2007; Boyd, 1989; Pearson and Wittig, 2008) at a near constant Mg-number similarly demonstrates that melt extraction and not melt-rock reaction is the main cause of variation in olivine Mg numbers (Pearson, 2014). However, olivines obviously affected by metasomatic processes have been noted in various on and off-craton localities, but are usually distinguishable by their unusually low Mg numbers. For example, sample HOD-7 from Hoedkop has olivine with a low Mg-number of 87, and appears to have experienced metasomatic enrichment of Fe. It is not unusually fertile in terms of clinopyroxene content and it contain aggregates of phlogopite with spinel and minor clinopyroxene that are clearly reaction products after garnet and, therefore, has textural evidence of metasomatism-induced garnet breakdown. However, there are a number of olivines characterised by low Mg numbers (86–88) from cratonic peridotites from Greenland (Sand et al., 2009) that appear to have been metasomatically added, and consequently altered the bulk composition of the peridotite from that generated by early melt depletion (Pearson, 2014).

In order to assess the extent of melt depletion that peridotite xenoliths have experienced, one should only consider peridotite samples with olivines having plausible mantle compositions (i.e., with Mg-number > 88) and those in which the olivines and pyroxenes appear to be in chemical equilibrium. Based on data for peridotites that follow these two rules, empirical average values for Fe-Mg partitioning relationships between clinopyroxene and olivine, and between orthopyroxene and olivine, were calculated based on a large dataset of coexisting mantle minerals in southern African peridotites. The main dataset from which these values were calculated are from Cox et al. (1973), Carswell et al. (1979), Danchin (1979), Moore (1986), Winterburn (1987), Hill (1989) and Steifenhofer (1993). The relationships for the Mg-number value of olivine in equilibrium with

clinopyroxene is: Mg# olivine $_{IN\ EQ\ WITH\ CPX}$ = Mg #$_{CPX}$ ÷ 1.025. For olivine in equilibrium with orthopyroxene is: Mg# olivine $_{IN\ EQ\ WITH\ OPX}$ = Mg #$_{OPX}$ ÷1.01.

In order to use olivine Mg number to evaluate and compare melt extraction in the four locations hypothetical average olivine Mg numbers (Mg#$_{OL}$) were determined for Rietfontein and Pofadder samples that lack fresh olivine and therefore have no measured olivine compositions. This average olivine Mg number (Mg#$_{OL}$) was calculated from Mg#$_{CPX}$ and Mg#$_{OPX}$ values assuming equilibrium with clinopyroxene and orthopyroxene (i.e. Mg#$_{OL}$ = mean [Mg# olivine $_{IN\ EQ\ WITH\ CPX}$ + Mg# olivine $_{EQ\ WITH\ OPX}$]). This allows the Pofadder peridotites to be included in the discussion despite the lack of measured olivine compositions, and it also eliminates uncertainties in the average measured Mg number of olivine from Rietfontein caused by the relatively small number of samples (3 out of 15) with fresh olivine compared to Louwrensia and Hoedkop.

The Mg-numbers of olivine from the four localities are as follows, Louwrensia, 91.5 ± 0.3 (1σ), Hoedkop, 91.4 ±1.4, Rietfontein, 90.8 ±1.4 (mean from both measured and calculated Mg#$_{OL}$) and Pofadder, 91.0 ±0.1 (calculated Mg#$_{OL}$). These off-craton olivines therefore all have similar olivine Mg-numbers. Taking into consideration that olivines from the fertile mantle have Mg-numbers usually ranging between 88 to 90 (Ionov et al., 2005), while that of olivine from the depleted Archean mantle is generally greater than 92, this suggests that peridotites from Louwrensia, Rietfontein, Hoedkop and Pofadder have experienced relatively mild melt depletion, implying lower degrees of melt extraction in the off-craton lithosphere of southern Africa in comparison to cratonic lithosphere.

Garnet compositions are also useful to examine the extent of melt depletion. To a first order, the Cr_2O_3 content of peridotitic garnet is controlled by the level of melt depletion, as evident from the good negative correlation with bulk rock Al_2O_3 (Griffin et al., 1999a). Sobolev (1977) showed that cratonic harzburgitic garnets from Yakutia are characterised by broad compositional variations at low CaO and Al_2O_3 content, reflecting that the depletion of Ca in garnet, as well as Al, is caused by extreme melt extraction. Garnets from lherzolites tend to

produce positive correlations between CaO and Cr_2O_3 at relatively high CaO contents of garnet, referred to as the 'lherzolite' trend. . This relationship is largely controlled by crystal chemistry (i.e., the larger space required for the Cr ion makes it easier for Ca to fit in the structure as well) and harzburgitic garnets do not display this trend (Gurney and Switzer, 1973; Sobolev, 1977; Gurney, 1984). Abundances of the HREE and Y can also be used as measures of melt depletion. Garnet is the only phase in which the HREE are compatible in peridotites and their abundance is mostly dictated by the amount of garnet remaining in the peridotite following partial melt extraction. Since most likely metasomatising agents, such as low-degree silicate or carbonate melts, have very low HREE concentrations, we can assume that the HREE content of garnet reflects the unmodified compositions of the garnet remaining subsequent to the last partial melting event (e.g., Canil, 2004). Therefore, the concentrations in garnet of HREE and chemically similar elements, such as Y, can be used to quantify melt depletion in the residual peridotite (Luchs et al., 2013). Generally, most calcium-poor garnets, such as those that occur as inclusions in diamonds, display Y concentrations of less than 10 ppm, while calcium-rich garnets from fertile or strongly metasomatised peridotites have Y contents of greater than 20 ppm (Griffin et al., 1999b; Griffin et al., 2003; Kobussen et al., 2008; Kobussen et al., 2009).

Garnets from the four peridotite populations studied all plot in the calcic-lherzolitic field on a CaO versus Cr_2O_3 diagram (Figure 6.1). This implies that, as a group, the xenoliths studied have not experienced high degrees of melt extraction. It should be noted that there is significant overlap between the Kimberley garnet data and that for the xenoliths studied here, but the Kimberley population garnets generally contain less CaO at a given Cr_2O_3 content and also extend well into the harzburgitic/subcalcic field.

In the discussion below, the heavy rare earth element Er is chosen as a proxy for the HREE rather than Yb or Lu because it behaves more systematically and

avoids variability due to anomalous enrichments in the heaviest REE seen in some suites, particularly Hoedkop. Garnets from Rietfontein peridotites are characterised by high chondrite normalised HREE contents with an average Er content of 15.6 ± 9.9 (1σ) times chondrite. In particular, the roughly one third of Rietfontein samples that are distinguished by positive sloping patterns from Ho to Yb (that are therefore least likely to have equilibrated with metasomatic melts) have higher HREE contents than the rest and also have lower Cr_2O_3/ Al_2O_3 ratios compared to the rest of the population, reflecting the less depleted nature of these peridotites. Anomalous garnet REE and trace element patterns, such as those form from RIET-2 (LREE and HREE enriched) are rare, and are likely related to the unusual origin of this garnet by exsolution from clinopyroxene (as shown in Figure 4.1b). Peridotitic garnets from Rietfontein have a high average Y content of 21 ±12 ppm, which is similar to the 20 ppm displayed by garnets from fertile peridotite (e.g., Kobussen et al., 2008; Kobussen et al., 2009)). About 39% of garnet grains have sufficiently high Y contents at low to moderate Zr contents that they plot in the "undepleted zone" in the Zr vs. Y plot of Griffin et al. (1999b; Figure 8.1). In general, these garnet REE systematics and Y contents are compatible with those expected from garnets in mantle melting residues less depleted than cratonic mantle as well as undepleted fertile peridotites (Figure 8.1).

Pofadder garnets have uniform, positively sloping normal REE patterns, showing moderate HREE concentrations with an average Er content of 11.6 ± 2.0 (1σ). These garnets, which all have positive sloping MREE-HREE patterns, are either melt-undepleted or they have experienced re-fertilisation that has restored their HREE contents. However, the Pofadder garnets are also characterised by a moderate average Y content of 15 ±3 ppm suggesting mild melt extraction. Pofadder garnets have very uniform compositions and lie as a tight group along a single line in CaO vs. Cr_2O_3 space that is more or less parallel to the subcalcic-calcic divide (dark black line) on Figure 6.1, signifying that these samples are all the product of virtually identical extents of melt extraction.

Garnets from Hoedkop have normal REE patterns, mainly characterised by flat MREE-HREE with variable increase at the heaviest REE, and have an average Er content of 8.0± 2.9 (1σ) times chondrite. The flat MREE-HREE garnet patterns suggest that the peridotites have experienced moderate melt extraction (to lower HREE) followed by metasomatism (to supply MREE). The grains also have a low average Y content of 11 ± 4 ppm which is consistent with compositions that are slightly more fertile than cratonic peridotites, which are characterised by a mean Y content of less than 10 ppm.

The four garnets from Louwrensia that have normal REE patterns characterised by flat trends from the MREE to HREE and have a high average Er content of 14.6 ± 7.7 (1σ) times chondrite. The REE patterns of the Louwrensia garnets suggest that most experienced significant melt extraction, followed by variable extents of metasomatism that increased MREE contents to a greater or lesser extent. These grains are also characterised by a high average Y content of 22 ±10 (1σ) ppm. The three garnets from Louwrensia that are characterised by positively sloping patterns from Gd to Lu show lower chondrite normalised HREE contents, with an average chondrite normalised Er content of 3.4± 0.5. It seems more likely that these N-type garnets with low HREEs experienced high degrees of melt extraction without later MREE enrichment. These three unusually depleted garnets yielded Y contents of 3.6 to 5.6 ppm, causing them to fall in the "depleted zone" in Figure 8.1. Two samples (FRB 1180 and FRB 1183) have garnets with sinusoidal REE patterns with an average chondrite normalised Er content of 5.2± 1.1 (1σ). These patterns are most easily explained as the result of a two-step process: first a depletion in all REE including the HREE due to extreme melt extraction, and second by introduction of the MREE and LREE due to metasomatism (Burgess and Harte, 2004). These sinusoidal garnet REE patterns are typically found in peridotites from the craton than in off-craton lithosphere, presumably because of the greater average degrees of melting that have affected the former and also display a low Y content of 10± 2 ppm similar to cratonic garnets. Overall, Louwrensia samples represent garnets from highly depleted melt residues possibly equivalent to cratonic peridotites. They all experienced strong REE depletion, but they have also

experienced variable metasomatism subsequent to melt extraction that variably increased the MREE and LREE. Sample PHN 5316 represents perhaps the most REE depleted sample that has not experienced subsequent metasomatism, sample FRB 1684 has experience moderate metasomatism and FRB 1180 experienced the greatest subsequent metasomatism.

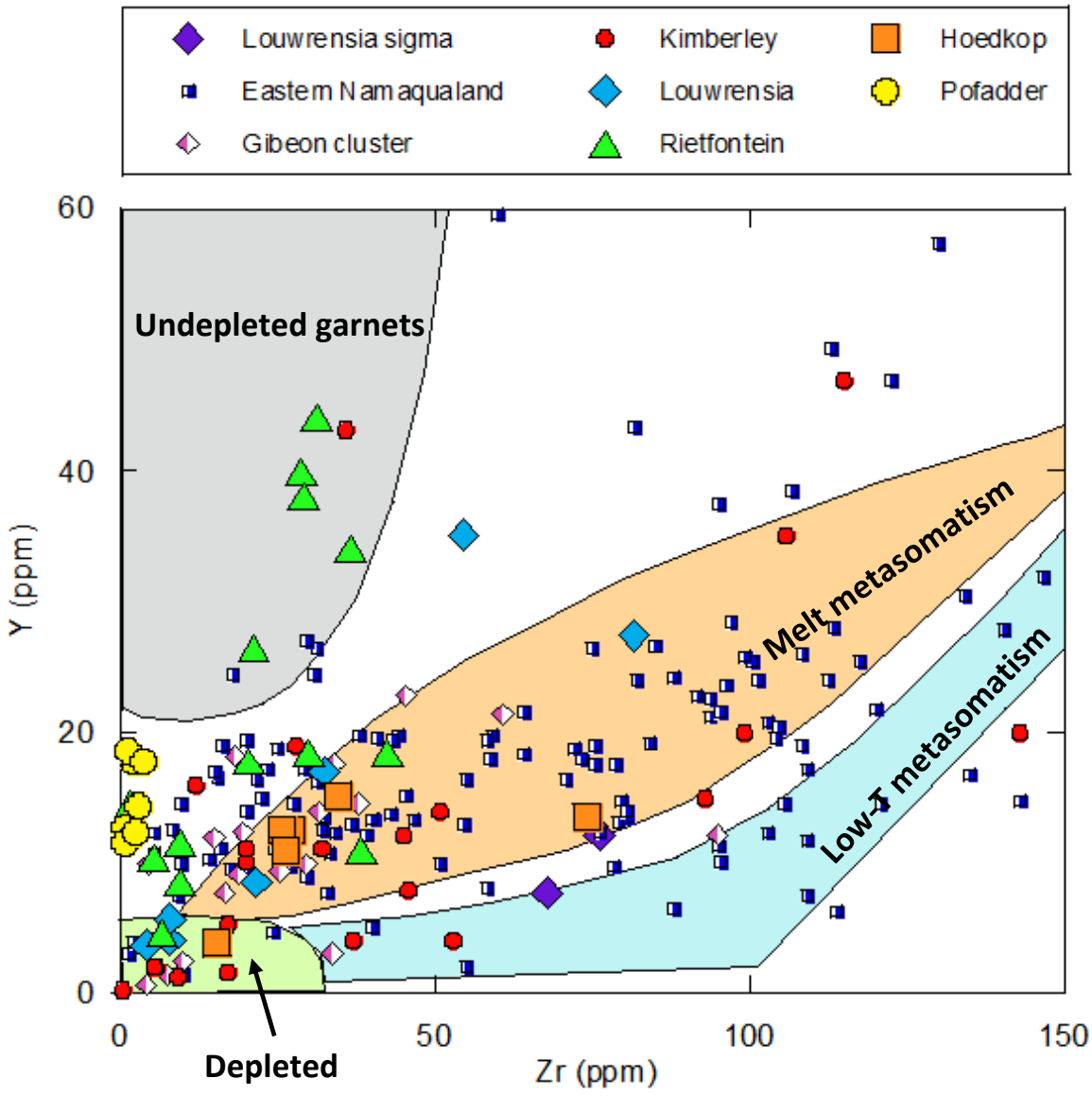

Figure 8.1. Plot of Zr vs. Y in garnets from peridotite xenoliths studied. The coloured fields are from Griffin et al. (1999b), which represent the Zr-Y signature of depleted garnets and of those affected by two kinds of metasomatism: high temperature interaction with basaltic melts and low temperature interaction with fluids (resulting in phlogopite precipitation). Data for Gibeon garnets is from (Luchs et al., (2013), while that of Uintjiesberg and Hebron garnets (eastern Namaqualand) is from Kobussen et al., (2008) and Kobussen et al., (2009).

8.2. THERMAL STRUCTURE OF THE OFF-CRATON LITHOSPHERE BENEATH THE REHOBOTH AND WESTERN NAMAQUA-NATAL PROVINCES

Aside from the deformed peridotites and a few anomalous high-temperature granular peridotites from Louwrensia and Hanaus, peridotite xenoliths from the Rehoboth Province (Gibeon and Rietfontein, both roughly 72 Ma) generally display moderate equilibration conditions that overlap with granular peridotites from Kimberley on the Kaapvaal Craton. Like cratonic peridotites, these granular off-craton peridotites lie between the 40mWm^{-2} and 45mWm^{-2} conductive geotherms of Pollack and Chapman (1977) and also fall along the Kalahari paleogeotherm of Rudnick and Nyblade (1999). This appears to be a distinctive regional feature of the Rehoboth Province, which is also consistent with thermobarometry results for orthopyroxene-bearing eclogites from the Rietfontein kimberlite pipe (Appleyard et al., 2007). The available evidence therefore suggests that the thermal state of the lithospheric mantle in the Rehoboth Province during the Late Cretaceous was similar to cratonic, with no evidence for significant thermal disturbances since the Namaqua orogeny (1.3-1.0 Ga), the last major geological event to modify the lithosphere in this region (Bell et al., 2003; Jacobs et al., 2008; Janney et al., 2010). However, a geothermal gradient that is virtually identical to that of the Kaapvaal craton defined by off-craton peridotite xenoliths could only be maintained by a lithospheric mantle that is considerably thicker than what is currently inferred from seismic studies (140-180 km Priestley et al., 2006; Chevrot and Zhao, 2007) as presented in Figure 8.2. Therefore the similarity in geothermal gradients between the Rehoboth province and the older, thicker Kaapvaal craton suggests a similar thermal structure and, therefore, a similar thickness (180-210 km, with only a few parts of the craton extending to greater depth, Priestley et al., 2006; Priestley and McKenzie, 2006; Chevrot and Zhao, 2007) of the two lithospheres at the time of kimberlite eruption (Bell et al., 2003; Boyd et al., 2004; Janney et al., 2010). Subsequently, the Rehoboth Province lithosphere must have been thinned

by ≈25% to achieve its current thickness. This interpretation, however, is complicated by the fact that peridotite xenoliths originating from pressures in excess of 5 GPa (≈150 km), which are not uncommon in Kaapvaal and Zimbabwe craton kimberlites (e.g., Shee et al., 1982) have never been documented in kimberlites from the Rehoboth Province.

The small number of anomalous granular peridotites from Louwrensia and Hanaus with temperatures greater than 1150°C plot above the Kaapvaal geotherm in the same T-P space occupied by the highest temperature deformed peridotites from the Gibeon cluster, which all fall on or near a plausible mantle adiabat (MacGregor, 1975; Mitchell, 1984; Franz et al., 1996a; Franz et al., 1996b) and are thought to have experienced warming during a local heating event prior to kimberlite magmatism (Boyd et al., 2004). Therefore, Louwrensia high temperature granular peridotites show strong evidence of localized heating possibly due to melt infiltration.

In contrast to most peridotites from the Rehoboth province, granular peridotites from Hoedkop and Pofadder, as well as from all other xenolith-bearing kimberlites younger than about 100 Ma in the Namaqua-Natal Province, generally display higher temperatures at a given pressure than peridotites from either the Rehoboth province or the Kaapvaal craton. As a result, they fall between the 45mWm^{-2} (and in many cases above the 50 mWm^{-2}) conductive geotherms of Nyblade and Pollack (1993) and lie at temperatures 100°-200°C warmer than the Kalahari geotherm for a given pressure. If the Kalahari geotherm represents the average long-term undisturbed thermal state of southern African lithosphere (Rudnick and Nyblade, 1999) then this suggests that the lithospheric mantle beneath Hoedkop, Pofadder and the rest of the western Namaqua-Natal Province has experienced a similar degree of thermal disturbance (Bell et al., 2003; Janney et al., 2010). The thermal disturbance is somewhat less pronounced in samples plotting at temperatures greater than about 1100°C and at pressures greater than 4.5 GPa. Peridotites from the older, 140-150 Ma Melton Wold kimberlite appear undisturbed and form an elongate grouping centred on the Kalahari geotherm (Figure 7.2). This evidence for an earlier, cooler state of the western Namaqua-Natal lithosphere suggests

that warming immediately preceded, or was concurrent with, Late Cretaceous Group 1 kimberlite magmatism, as suggested previously (Bell et al., 2003; Kobussen et al., 2008; Janney et al., 2010).

Although only the Namaqua-Natal Province has peridotites that show evidence for significant regional lithospheric heating, both it and the Rehoboth Province have yielded peridotites that show a variety of textures reflecting near-isothermal decompression that is linked to lithosphere thinning. For example in Rietfontein, sample RIET-2 contains clinopyroxene with exsolved garnet, while in samples RIET-1 (Rietfontein), PHN 5365 (Louwrensia) and HOD-8 (Hoedkop), spinel forms large fingerprint symplectite intergrowths with pyroxene. The exsolution of garnet and/or spinel from pyroxene results from the ability of pyroxenes to include a substantial amount of aluminium in their crystal structure by substituting Ca, Mg, Fe and Si for Al. The solubility of aluminium decreases with decreasing pressure in the pyroxene, resulting in unmixing and exsolution as the peridotites ascend during a transient event, with the excess aluminium (and chromium) being lost from the pyroxene through exsolution of garnet or spinel (Ringwood, 1967; Exley, 1982; Gasparik, 2000; Faryad et al., 2009; Spengler et al., 2012).

Overall, the new thermobarometry data support a regional difference in thermal state between the Namaqua-Natal and Rehoboth provinces of southern Africa. This may indicate pervasive thermal disturbance of the lithospheric mantle in the Namaqua-Natal Province concurrent with Cretaceous continental breakup or kimberlite magmatism, whereas the Rehoboth province appears to have largely escaped this, except for local infiltration of the lithosphere at depth, by silicate melts. This notion is plausible considering the position of the two provinces. The Namaqua-Natal Province is outboard of the Rehoboth Province i.e., closer to the western coast of southern Africa, which may possibly indicate its greater exposure to the heating effects of mantle upwelling and thinning associated with the breakup of supercontinent Gondwana and Karoo flood basalt magmatism (Bell et al., 2003; Kobussen et al., 2008; Janney et al., 2010).

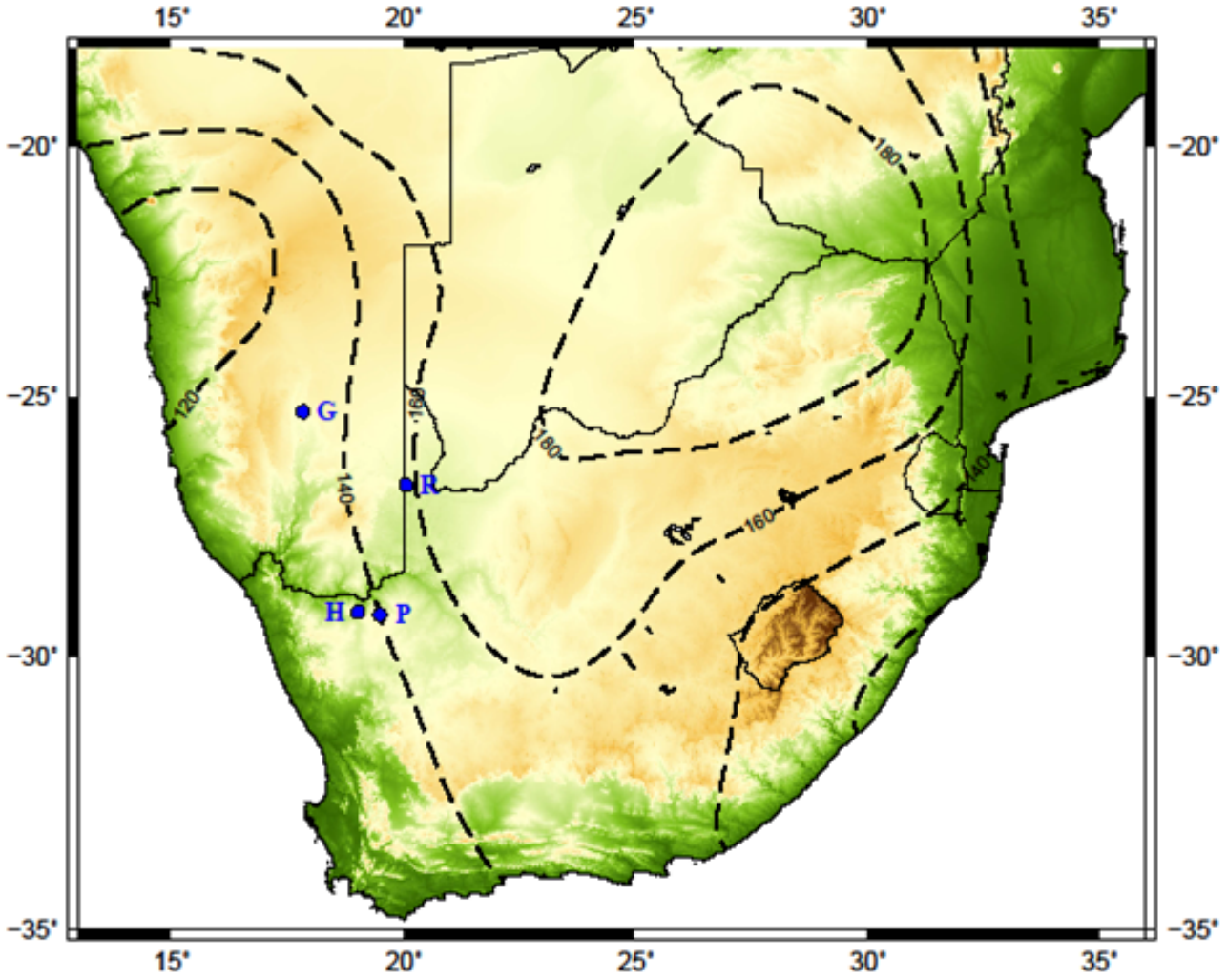

Figure 8.2. Map showing estimated present day lithospheric thickness in southern Africa, derived from Priestley and McKenzie (2006). Their approach uses both shear velocity structure and pressure and temperature data from kimberlite borne mantle xenoliths to estimate thickness. Abbreviations: G = Gibeon (Louwrensia), R = Rietfontein, H = Hoedkop and P = Pofadder.

8.3. CONSTRAINTS ON METASOMATIC ENRICHMENT AND TRACE ELEMENT EQUILIBRATION

Peridotites from the four localities investigated mostly show good textural equilibrium between minerals. However some xenoliths show evidence for the introduction of hydrous minerals, primarily phlogopite, as well as mineral reactions, particularly of garnet to phlogopite + spinel ± clinopyroxene, which was likely enabled by metasomatic addition of hydrous fluids. In addition, the minerals in many peridotite samples show high concentrations of incompatible elements, which would be expected to be present at low concentration in peridotitic residues of partial melting. This strongly suggests that many or most of the peridotites experienced equilibration with metasomatic agents such as incompatible element-enriched melts or fluids. In order to evaluate the extent of metasomatic enrichment experienced by the peridotites, the trace element composition of garnets and clinopyroxenes from the samples studied where normalised to those from the fertile peridotite sample 313-105 of Ionov et al. (2005) from the Vitim volcanic field located off-craton in central Asia. This sample is a garnet lherzolite with an equilibration pressure of 2.1 GPa at 1034 ^{o}C. It has modal mineralogy and trace element characteristics similar to, but slightly more depleted than, the primitive mantle and the garnet and clinopyroxene REE patterns correspond to those of an undepleted mantle (Ionov et al., 2005). This off-craton garnet peridotite was found hosted in a picrite tuff (olivine-rich basaltic magma). Having been entrained in basalt rather than kimberlite is important for two main reasons. Firstly, unlike kimberlites, basalts have relatively high viscosity and hence cannot infiltrate as effectively into the peridotite therefore minimizing metasomatic interaction between the xenolith and host magma. Secondly, basalts have much lower incompatible element concentrations in comparison to kimberlites. Therefore, although this sample likely experienced metasomatism/refertilisation by basaltic melts (Ionov et al., 2005), it is far less likely to have experienced non-equilibrium trace element enrichments than kimberlite-borne xenoliths. The

garnet and clinopyroxene trace element patterns from sample 313-105 are shown in Figure 8.3. The normalisation of the garnets and clinopyroxenes from this study to those from this Vitim peridotite allows changes caused by enrichments after the last partial melting event to be quantified and evaluated. In order to estimate the extent of metasomatic enrichment in garnet and clinopyroxene, a hypothetical range of incompatible element concentrations for these minerals prior to metasomatic enrichment was estimated by extrapolating from the abundances of the HREE, which are only mildly incompatible and hence among the least sensitive elements to metasomatism. In Figures 8.4 to 8.7, the coloured fields represent these hypothetical ranges, with the arrows indicating the typical extent of relative enrichment.

Clinopyroxene and garnet are, by far, the most important host minerals for incompatible elements in peridotite xenoliths (Frey, 1969; Shimizu, 1975; Stosch, 1982; McDonough et al., 1992; Xu, 2000). Therefore, it is important to know if the extent of trace element equilibration between cpx and garnet in order to know if the patterns for the REE and other trace element patterns are the result of equilibrium or disequilibrium processes. The state of trace element equilibration in peridotite can be evaluated by examining the partitioning of incompatible elements between coexisting phases. Unlike the partitioning of major elements between phases (as used in thermobarometry, for example) trace element partitioning is not dependent upon variations in mineral stoichiometry, but rather on the substitution of effectively infinitely dilute trace elements into particular mineral vacancies governed by Henry's Law behaviour (e.g., Blundy and Wood, 2003). Under normal circumstances in the mantle, mineral phases should be in trace element equilibrium and any departure from this equilibrium due to disequilibrium processes such as might be expected to be associated with metasomatic reaction with percolating volatile-rich fluids. Such disequilibrium effects should be erased by diffusion within a few tens of millions of years (e.g.,Van Orman et al., 2001; 2002), so their presence would also provide information on the timing of such disequilibrium processes.

In this study, the partitioning behaviour between garnet and clinopyroxene was evaluated by calculating concentration ratios ($D_{grt/cpx}$) of incompatible elements between clinopyroxene and garnet of samples from the four locations studied, and normalizing them to concentration ratios of the same incompatible elements between clinopyroxene and garnet from sample 313-105. This sample is believed to be well-equilibrated because it shows evidence of re-fertilization by basaltic melts (which should serve to equilibrate trace elements due to their rapid diffusion in the melt phase) and the minerals are unzoned ([need to cite Ionov ref here]). The normalised $D_{grt/cpx}$ values for trace elements from the four xenolith suites investigated are plotted in Figure 8.8.

In the Louwrensia suite, the garnets are characterised by metasomatic enrichment in LREE and LILE in addition to Nb, Ta, Th and U (Figure 8.4a). Garnets that display sinusoidal REE patterns are particularly enriched in the MREE and are more enriched in the HFSE such as Zr and Hf than the non-sinusoidal garnets. Clinopyroxenes are moderately enriched in LREE, LILE and HFSE with concentrations falling between 1 and 50 times that of sample 313-105 clinopyroxenes (Figure 8.4b). A clear, observable metasomatic consequence is the replacement of clinopyroxene by phlogopite that is very widespread in Louwrensia samples, as stated and shown in Chapter 4. Clinopyroxene-garnet trace element partitioning suggests that Louwrensia peridotites show internal mineral equilibrium for most elements since the normalised garnet/clinopyroxene ratio for most elements is close to 1, particularly for the REE, Zr, Hf and Sr, although minor disequilibrium in Rb, Ba, Ta, Th, U, Pb and Ti is observed (Figure 8.8a). Trace element equilibration as a typical characteristic of Gibeon peridotites has also been found previously by Shimizu (1975), Boyd et al. (2004) and Luchs et al. (2013).

Due to their higher overall REE concentrations, metasomatic effects are not nearly as obvious in garnets from Rietfontein compared to those from Louwrensia. However, enrichments in the LILE, LREE, Nb, Ta, Th and U (Figure 8.5a) are

notable. Clinopyroxenes also show moderate enrichment, mostly in the LREE and LILE, U and Th (Figure 8.5b). Rietfontein peridotites show good internal mineral equilibrium for most elements (Nd to Yb) as they all lie fairly close to 1. Minor disequilibrium occurs in the more highly incompatible elements such as Rb, Ta, La and Ce as well as moderate disequilibrium in Sr. Sample RIET-2, is anomalous in that incompatible elements from Ba to Nd and also Ti are significantly out of equilibrium and have mainly partitioned into garnet. This may be related to the fact that, as noted in Chapter 4, most garnets in this sample are small and have exsolved from clinopyroxene, presumably at high pressure.

Garnets from Hoedkop peridotites exhibit strong evidence for metasomatic enrichment, particularly in the LILE, LREE, Th and U, with concentrations of these elements (normalised to Vitim sample 313-105) mostly falling between 10 and 10 000 times, as well as much smaller MREE and HFSE enrichments (Figure 8.6a). Garnets from samples HOD-2, HOD-5 and HOD-11 are remarkably rich in the transitions metals Sc (> 200 ppm), Ti (> 2000 ppm), V (> 300 ppm) and Ni (> 100 ppm) which is probably related to melt infiltration. Hoedkop clinopyroxenes display evidence for strong metasomatic enrichment in incompatible elements, with enrichment mainly in the LILE, LREE, Th and U (Figure 8.6b). Hoedkop peridotites (especially deformed peridotites HOD-2 and HOD-4) are also characterised by a varying degree of disequilibrium in the most incompatible elements (Rb to Sr) which, except for Pb, have partitioned mainly into garnet, reaching $D_{grt/cpx}$ ratios up to 1000 times that of the reference sample 313-105 (Figure 8.8c). The rest of the incompatible elements appear to be well-equilibrated, resulting in the observed flat patterns in the MREE-HREE (Nd to Lu) with values approaching close to 1.

Garnets from Pofadder show evidence for moderate metasomatic enrichment predominantly in the LREE and LILE as well as in U, Th, Nb, Ta, with 313-105-normalised concentrations mostly falling between 2.5 and 100 times. These garnets also display strong negative Zr and Hf anomalies (Figure 8.7a).

Clinopyroxenes, in contrast, display evidence for extreme overall metasomatic enrichment in the LILE, LREE, Th and U, with concentrations typically falling between 1 and 100 times that of the reference sample 313-105, as significant HREE depletion (0.1 to 0.2 times the reference sample concentration; Figure 8.7b). Pofadder clinopyroxene is also characterised by extremely high LREE/HREE ratios, combined with pronounced negative Nb-Ta, Zr-Hf and Ti anomalies. The garnet/clinopyroxene partitioning at Pofadder indicates major disequilibrium between garnet and clinopyroxene, particularly for Th, U, Zr, Hf and the MREE, which partition disproportionately into clinopyroxene, and, uniquely among the suites investigated here, the HREE, which partition disproportionately into garnet. The unusually great extent of garnet-cpx disequilibrium for the Pofadder samples could indicate separate origins for the two minerals (Figure 8.8d). In particular, clinopyroxenes show some trace element similarities to Cr-rich megacrysts which are found in abundance in the Pofadder pipes (Figure 8.9; Janney and Bell, unpublished data, 2015). There is thus some evidence to suggest that clinopyroxenes may be metasomatic in origin, having formed shortly prior to xenolith entrainment by the carrier kimberlite, as suggested by Simon et al. (2007) to explain unusually young garnet-clinopyroxene

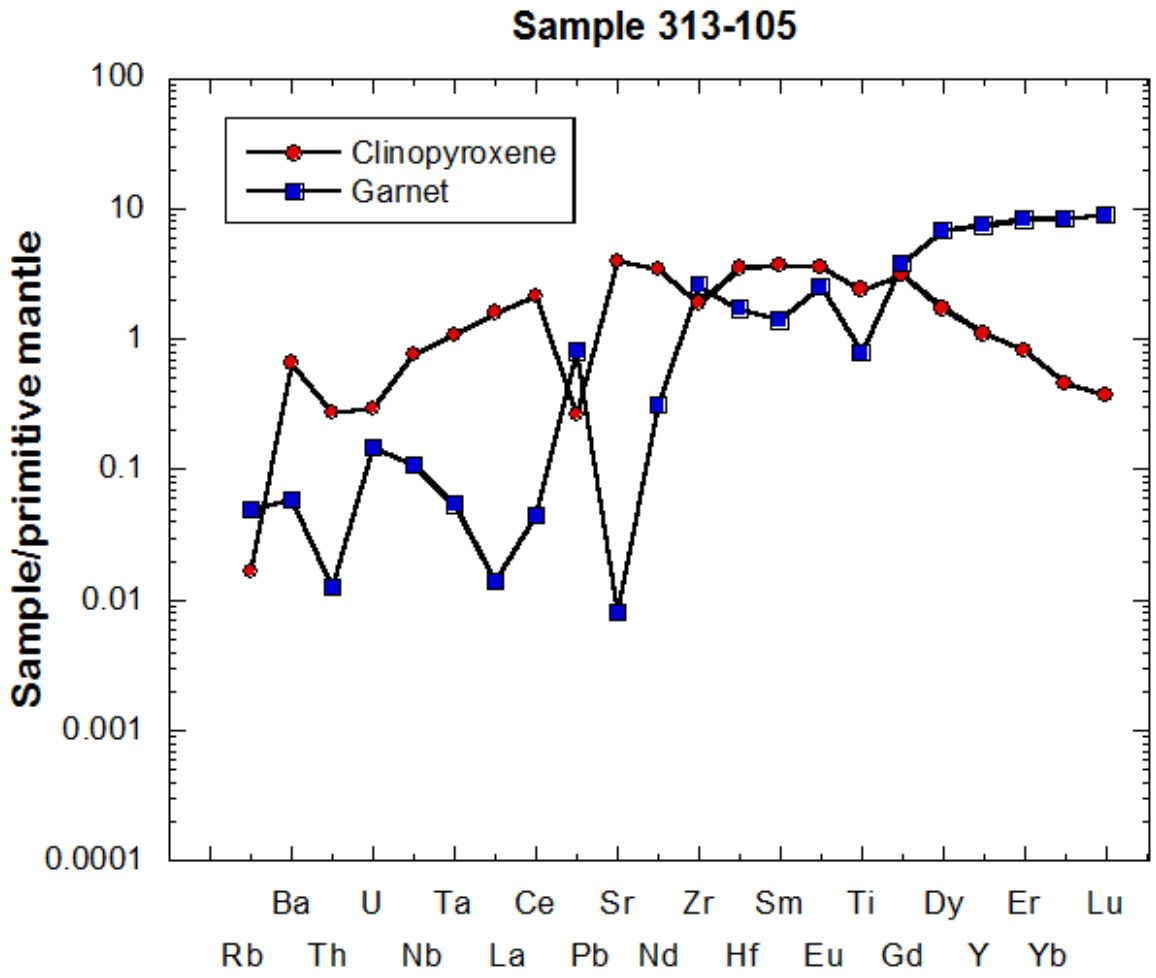

Figure 8.3. Primitive mantle normalized trace element patterns for garnet and clinopyroxene from sample 313-105 of Ionov et al. (2005)

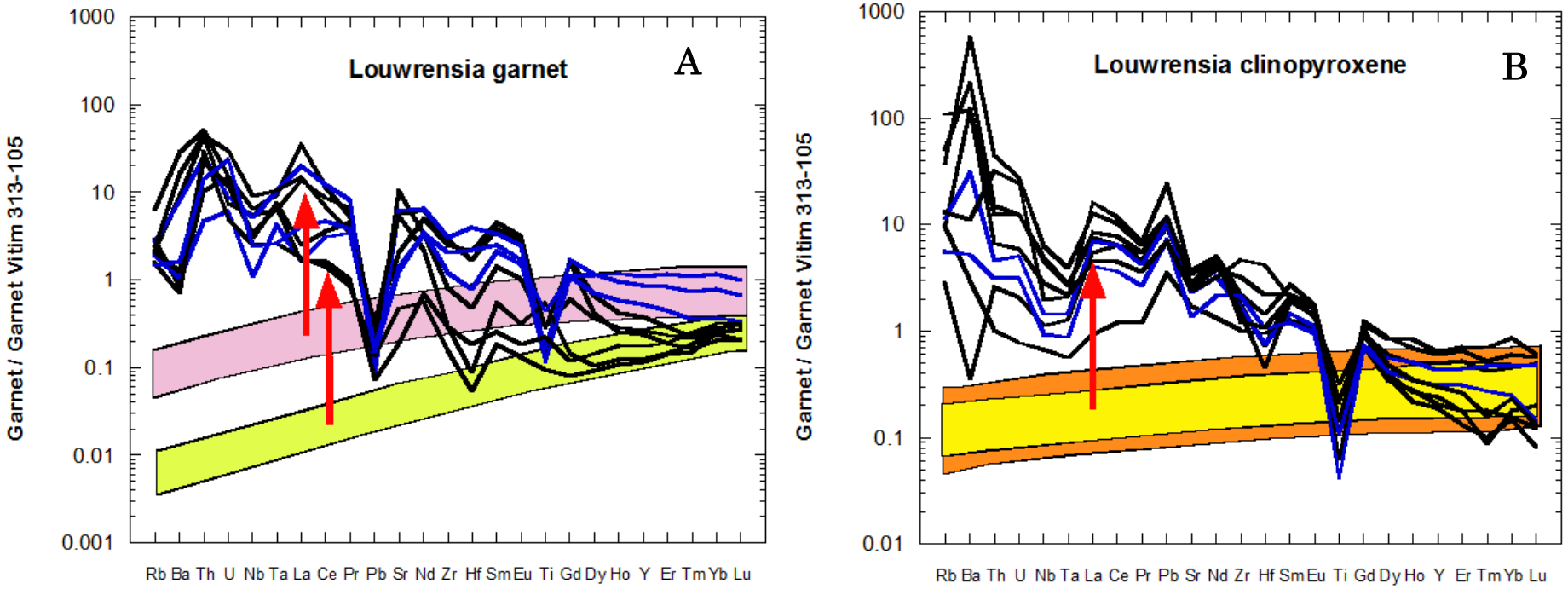

Figure 8.4. **A**: Trace element patterns of garnets from Louwrensia. The coloured bands (pink and green) represent an estimated range of incompatible trace element patterns for the garnets with higher and lower HREE contents, respectively, assuming the HREE abundances have been unaffected by metasomatism. The arrows indicating the representative enrichment. **B:** Trace element patterns of clinopyroxenes from Louwrensia. The coloured band (orange and yellow) represent an estimated range of incompatible element patterns for the clinopyroxenes studied, assuming the HREE abundances have been unaffected by metasomatism.

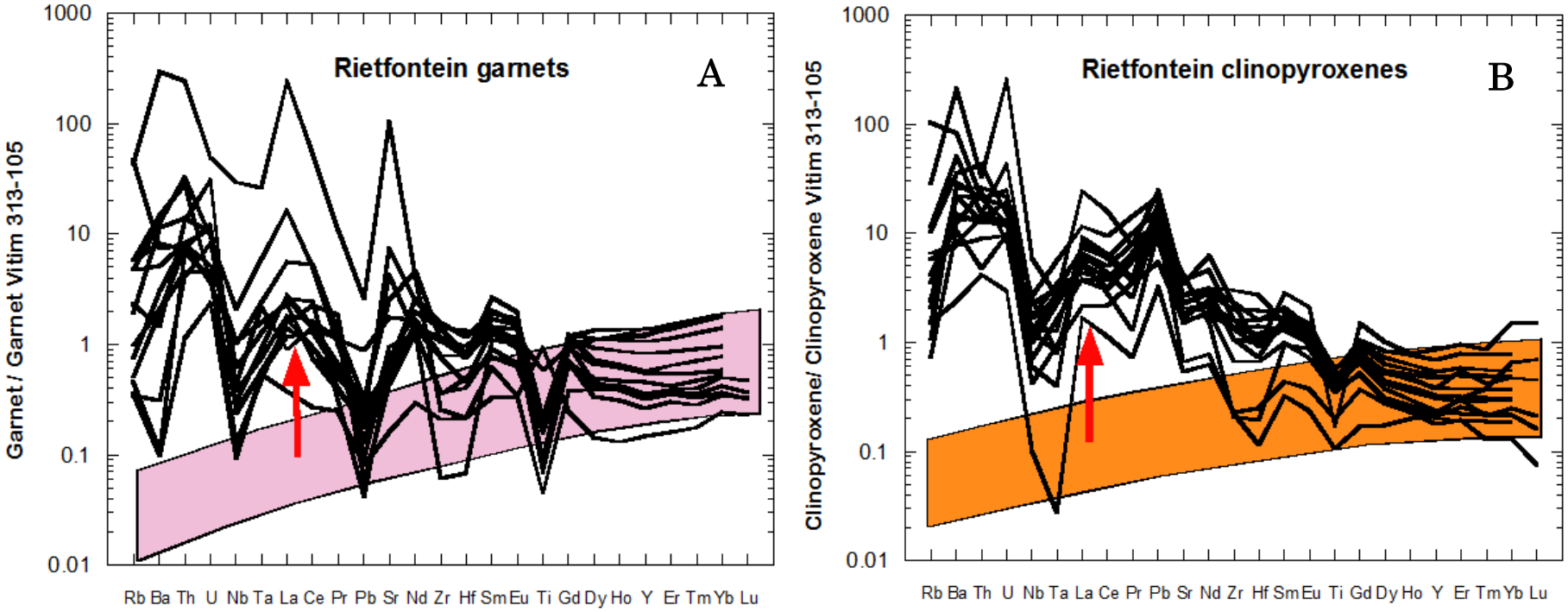

Figure 8.5. **A**: Trace element patterns of garnets from Rietfontein. The coloured band (pink) represents an estimated range of incompatible trace element patterns for the garnets with higher and lower HREE contents, respectively, assuming the HREE abundances have been unaffected by metasomatism. The arrows indicating the representative enrichment. **B:** Trace element patterns of clinopyroxenes from Rietfontein. The coloured band (orange) represent an estimated range of incompatible element patterns for the clinopyroxenes studied, assuming the HREE abundances have been unaffected by metasomatism.

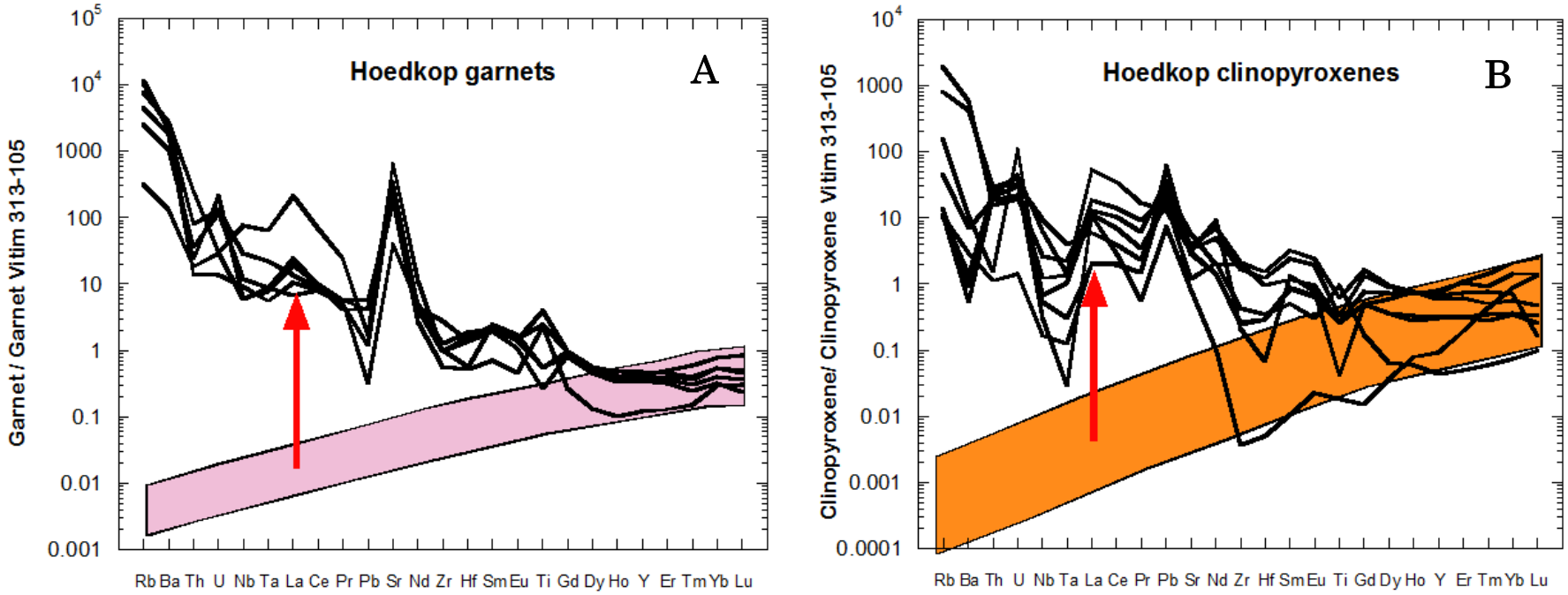

Figure 8.6. **A**: Trace element patterns of garnets from Hoedkop. The coloured band (pink) represents an estimated range of incompatible trace element patterns for the garnets with higher and lower HREE contents, respectively, assuming the HREE abundances have been unaffected by metasomatism. The arrows indicating the representative enrichment. **B:** Trace element patterns of clinopyroxenes from Hoedkop. The coloured band (orange) represent an estimated range of incompatible element patterns for the clinopyroxenes studied, assuming the HREE abundances have been unaffected by metasomatism.

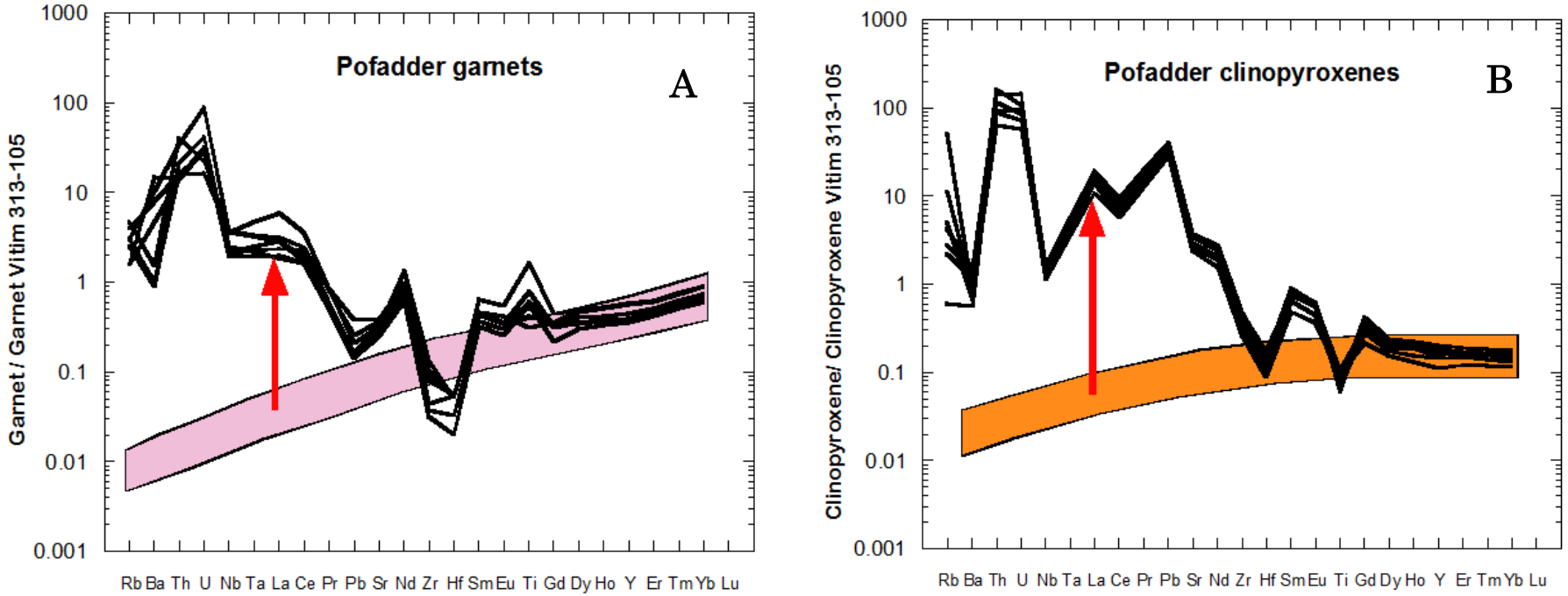

Figure 8.6. **A**: Trace element patterns of garnets from Pofadder. The coloured band (pink) represents an estimated range of incompatible trace element patterns for the garnets with higher and lower HREE contents, respectively, assuming the HREE abundances have been unaffected by metasomatism. The arrows indicating the representative enrichment. **B:** Trace element patterns of clinopyroxenes from Pofadder. The coloured band (orange) represent an estimated range of incompatible element patterns for the clinopyroxenes studied, assuming the HREE abundances have been unaffected by metasomatism.

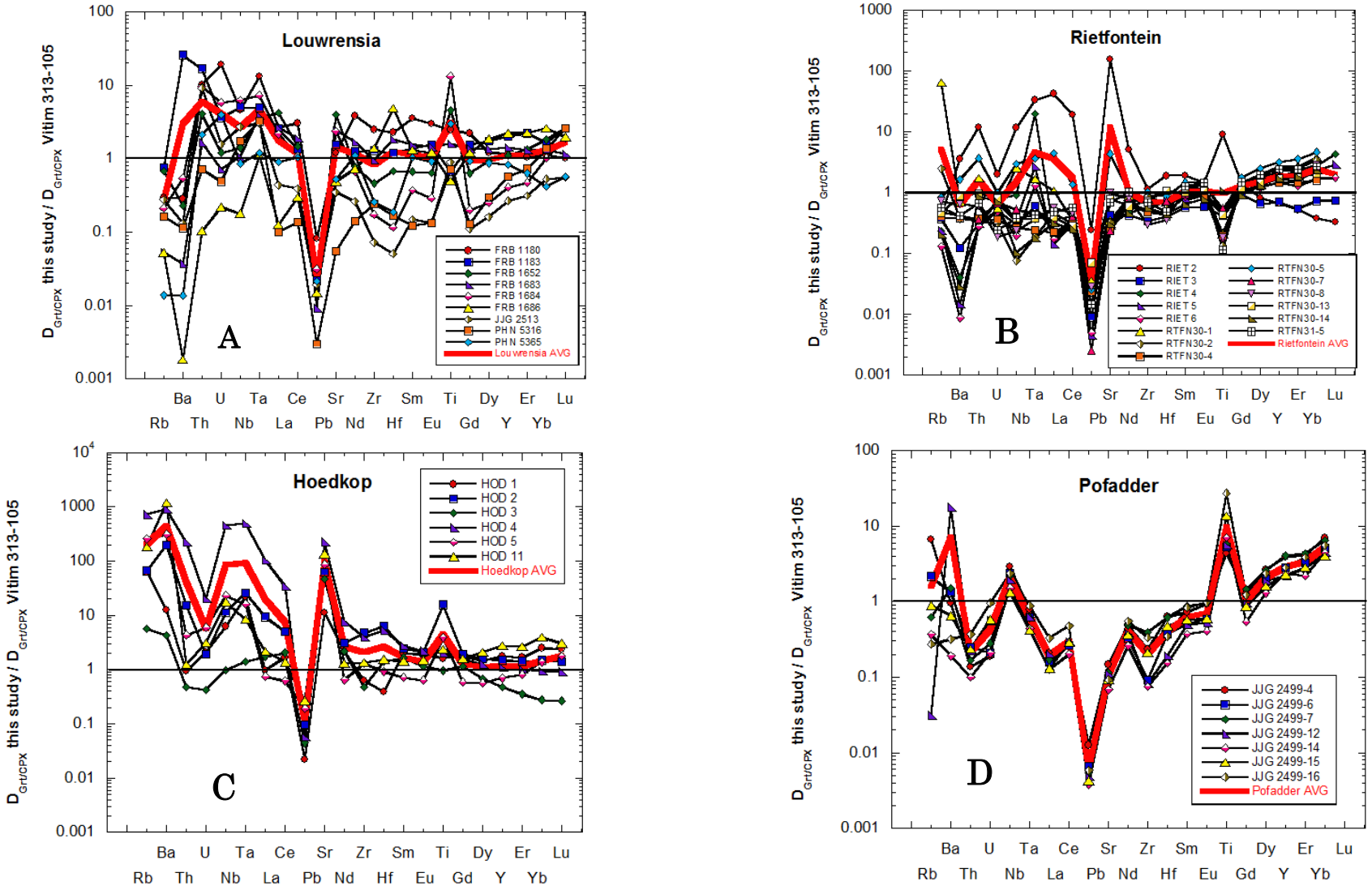

Figure 8.8: Garnet/clinopyroxene trace element ratios in samples from the four peridotite suites studied normalised to garnet/clinopyroxene trace element ratios for Vitim sample 313-105 from Ionov et al. (2005), showing the relative partitioning of elements into garnet vs. clinopyroxene. The thick red line indicates the average normalised garnet/clinopyroxene ratios for each suite. See text for discussion.

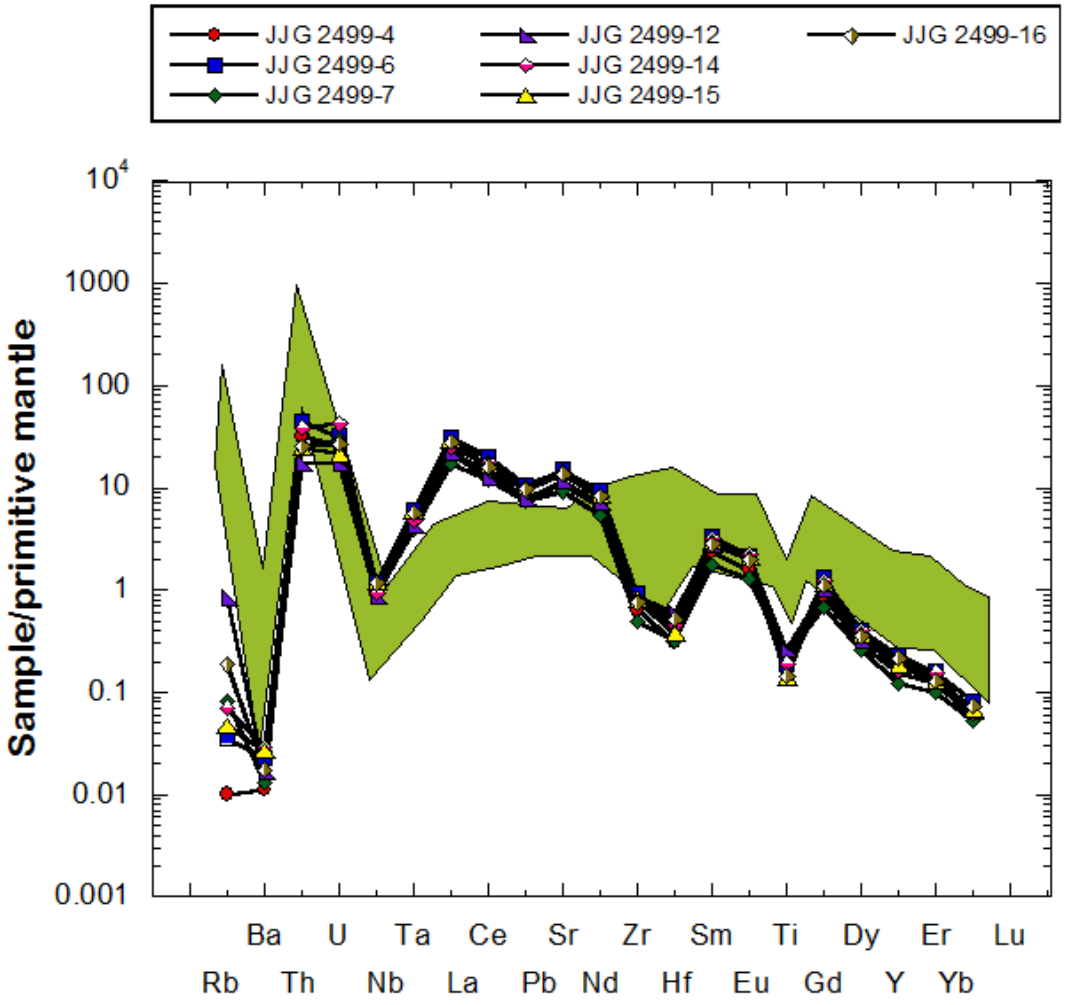

Figure 8.9. Plot highlighting the similarity between primitive mantle normalized trace elements for clinopyroxenes from Pofadder, with the trace element composition of clinopyroxene megacrysts from the same locality which is indicated by the green zone. Pofadder cpx megacryst data is from Janney (unpublished).

8.4. METASOMATIC MELT COMPOSITIONS

In order to constrain the nature of possible metasomatic agents that led to the incompatible element enrichment of garnets and clinopyroxene, the trace element compositions of hypothetical liquids in equilibrium with garnets and clinopyroxenes in the peridotites were calculated using the garnet-melt partition coefficients of trace elements from Salters and Longhi (1999) and the clinopyroxene-melt partition coefficients values from Keshav et al. (2005). This type of modelling relies only on Henry's Law assumption that the trace elements are ideally dilute, so that the ratio of the concentration in the solid to that of the coexisting melt is constant and controlled only by the partition coefficients (D values). Salters and Longhi (1999) conducted garnet–liquid partitioning experiments and obtained partition coefficients that are close to multiple saturation with an anhydrous lherzolite assemblage. Keshav et al. (2005) conducted partition coefficient experiments between clinopyroxene and CO_2 -rich kimberlitic melts in the model CaO-MgO-Al_2O_3-SiO_2 -CO_2 system. Both authors have shown that their $D_{REE\ (mineral/liquid)}$ satisfies Henry's law within a wide range of REE contents and the crystal chemical control on $D_{REE\ (mineral/liquid)}$ is much more significant than the influence of temperature, pressure, CO_2 and H_2O activity. The partition coefficients used are presented in Table 8.1. Primitive mantle normalised trace elements and chondrite normalised REE compositions of the melts in equilibrium with garnets and clinopyroxenes from this study, calculated using these partition coefficients, are plotted in Figures 8.10 to 8.13.

The liquids in equilibrium with garnets from Louwrensia display negatively sloping and sinusoidal REE patterns as well as low to moderate chondrite normalised LREE contents (e.g., La = 78 ± 81 (1σ) and Ce = 35 ± 22) that are generally lower in comparison to southern Africa group 1 kimberlite and carbonatite (Figure 8.10a). In the primitive mantle-normalised plot (Figure 8.10b) the melts are characterised by negative Sr, Hf, Ti and less pronounced, Zr anomalies. Although the calculated melt in equilibrium with Louwrensia garnets has lower primitive mantle normalised concentrations than group 1 kimberlites

for most elements, these have comparable LILE concentrations and display very similar trace element patterns. The calculated high concentrations of highly incompatible elements in these melts and similarities between their trace element patterns and those of group 1 kimberlites suggest equilibration with melts with compositions similar to kimberlites. This metasomatic agent is LREE enriched and HREE-poor. Therefore, equilibrating a highly depleted garnet with this agent produces a sinusoidal pattern in the garnet (e.g., FRB 1180 and FRB 1183) since the HREE are not significantly increased (due to low HREE concentrations in the agent) and the LREE & MREE are both significantly increased. The LREE were strongly depleted in the melt residue garnet, so that even though they are significantly increased in a relative sense, in an absolute sense they still have low LREE/MREE ratios.

The liquids in equilibrium with Louwrensia clinopyroxenes have negatively sloping REE patterns and are highly enriched in LREE with average chondrite normalised La and Ce contents of 2528 ±1490 and 3635 ±1715 respectively (Figure 8.10c). The melts also display positive Zr and Hf anomalies and strong negative Ti anomalies (Figure 8.10d). The calculated melt in equilibrium with Louwrensia clinopyroxenes has primitive mantle normalised concentrations of LILE, LREE-MREE and HFSE very similar to that of group 1 kimberlites and the two produce very similar trace element patterns. This, in combination with evidence for trace element equilibrium between clinopyroxene and garnet (Figure 8.8a), suggests clinopyroxenes have also equilibrated with melts that have compositions similar to kimberlites, which correspondingly appears responsible for metasomatism in coexisting garnets. But the calculated melts in equilibrium with clinopyroxene have much higher incompatible trace element concentrations than those calculated for coexisting garnet. A possible explanation is that both minerals interacted with kimberlitic melt, over a period of time sufficient enough to allow LILE, LREE-MREE and HFSE equilibration, especially in clinopyroxenes but not enough to allow LREE-MREE and HFSE in garnet as well as for HREE equilibration in both minerals. But this would also be expected to result in significant zoning in the garnets, which is not seen. It must also be realised that for garnet, the partitioning experiments utilised volatile-free assemblages. Given

the significant differences in D values between clinopyroxene and melt in the volatile-free experiments (Salters and Longhi, 1999; Salters et al., 2002), and between clinopyroxene and carbonated silicate melt (Keshav et al, 2005), the difference between the melts in equilibrium with garnet and with clinopyroxene are perhaps not surprising, and may only reflect experimental artefacts and not disequilibrium effects.

The liquids in equilibrium with garnets from Rietfontein are characterized by relatively flat LREE-MREE with a slight negative slope in the MREE-HREE and display moderate chondrite normalized LREE (e.g., average La= 149 ±454 and Ce= 32 ±78) (Figure 8.11a). They have positive U and Pb as well as negative Hf, Ti and to a lesser extent, Zr anomalies on the primitive mantle normalised plot (Figure 8.11b). The high content of highly incompatible elements indicate re-equilibration with an alkali basalt, with mild/moderate LREE enrichment.

Melts in equilibrium with Rietfontein clinopyroxenes are also comparable to those from Louwrensia, in that they display negatively sloping REE patterns and are enriched in LREE with an average chondrite normalised La and Ce content of 2389 ±1800 and 2867 ±1956 respectively (Figure 8.11c). Chondrite normalised REE patterns show an excellent overlap between LREE in the clinopyroxene and carbonatite melt from Marinkas Quellen, while the MREE also show an exceptional overlap with group 1 kimberlite melt. The melts show slight negative Nb and Ti anomalies in primitive mantle normalised trace element plot Figure 8.11d, and overall, an excellent overlap between the trace element content of the clinopyroxene and group 1 kimberlite melt (with the exception of the heaviest REE in most samples). The high concentration of incompatible trace elements in addition to the overlap between LILE, LREE, MREE, HFSE and some HREE with kimberlite melt suggests that peridotites from Rietfontein have been metasomatised by a hybrid carbonate-silicate melt, such as a kimberlite extremely rich in LREE.

Melts in equilibrium with garnets from Hoedkop have negatively sloping LEE-MREE and flat HREE patterns with moderate LREE enrichment (average chondrite normalised La = 350 ± 539 and Ce = 112 ± 134) (Figure 8.12a) as well as

REE patterns similar to, but with contents falling below those of group 1 kimberlites. In particular, the melts are extremely enriched in the LILE such as Rb and Ba with the rest of the trace elements (besides U, Pb and Sr) falling at concentrations below that of group 1 kimberlites. The only exception is the melt in equilibrium with HOD-4 garnets that show LREE contents comparable to group 1 kimberlite. It is also important to note that some garnets from Hoedkop are partly or completely replaced by phlogopite, clinopyroxene and spinel which occur in polygonal aggregates (reflecting the shape of the original garnet) due to reaction with metasomatic liquids. Erlank et al. (1987) showed that this reaction is not related to the garnet-spinel transition which is controlled by pressure but instead. It is produced by infiltration of a K-bearing hydrous fluid into peridotites. It is quite possible that this fluid could also be responsible for the strong spinel-phlogopite kelyphite replacement of garnets. The following reactions may well be responsible for the new metasomatic minerals observed:

2 Pyrope + Enstatite + 4 H_2O + 2 K_2O (in fluid phase) ←→ Phlogopite

Pyrope + Forsterite + H_2O + K_2O (in fluid phase) ←→ Phlogopite + Enstatite + Spinel

Pyrope + 2 Grossular + 3 Forsterite ←→ 6 Diopside + 3 Spinel

Overall, the high incompatible trace element content in addition to the replacement texture of garnets suggests Hoedkop garnets underwent enrichment by more than one metasomatic liquid: a melt that is kimberlitic in composition that is rich in LILE and a hydrous K-bearing fluid.

Melts in equilibrium with clinopyroxenes also have negatively sloping REE patterns that are LREE enriched with an average chondrite normalised La content of 4718 ±5337 and a Ce content of 5013 ±5877 (Figure 8.12c). In the primitive mantle normalised plot, these melts have negative Nb and Ta anomalies (Figure 8.12d) and display extreme enrichments in the LREE, Sr, Zr and Hf. Because these melts contain high concentrations of LREE, Sr, Zr and Hf, which are amongst the most highly enriched elements in kimberlites relative to primitive mantle (Mitchell and Brunfelt, 1975) and display REE patterns that overlap with that of

typical alkali melt compositions it can therefore be inferred metasomatism was by a melt with kimberlite composition.

In Pofadder, hypothetical melts in equilibrium with garnets have mildly negative sloping LREE-MREE and relatively flat MREE-HREE patterns. The melts have relatively very low LREE concentrations with La and Ce having an average chondrite normalised concentration of La 22 ±9 and 13 ±4 respectfully (Figure 8.13a). The melts have very strong negative Zr and Hf anomalies (Figure 8.13b). Only the primitive mantle normalised LILE content of the melts fall within typical kimberlite compositions, with the rest of the REE falling slightly below kimberlite compositions, while LILE, Ta, Pb and Ti contents fall within that of carbonatite melt from Marinkas Quellen.

In contrast, hypothetical melts in equilibrium with clinopyroxenes are characterised by positively sloping REE patterns and are extremely enriched in LREE (e.g., average chondrite normalised contents for La = 534 ±943 and Ce = 4089 ±666) (Figure 8.13c) the primitive mantle normalised trace element patterns show strong negative Nb, Hf and Ti anomalies (Figure 8.13d). The melts have primitive mantle normalised patterns that resemble carbonatite melt with the LREE contents falling within the Marinkas Quellen carbonatite composition field and above those of group 1 kimberlite. Altogether, it is evident that Pofadder minerals display a large metasomatic overabundance of incompatible elements into the melt residue (Figure 8.7a and b). This combined with the mild negative Zr and Hf anomalies in garnets (Figure 6.17b) and the pronounced negative Nb, Zr-Hf and Ti anomalies in clinopyroxenes (Figure 6.25b) in the primitive mantle-normalized incompatible element patterns indicates an input of light and middle REE into the Pofadder peridotites.

At Pofadder, the melts in equilibrium with clinopyroxene are distinctly different from those in equilibrium with garnet, indicating significant trace element disequilibrium between these two minerals. Metasomatic interaction over a short time interval, could explain the trace element disequilibrium because of different diffusion rates in cpx (faster) and garnet (slower). But this would also be expected to result in significant zoning in the garnets i.e., rims of garnet should show

significant enrichments in incompatible elements relative to cores because any interaction long enough to affect all clinopyroxenes would have to be long enough to allow some introduction of trace elements into the exterior portions of garnets. However, since this is not seen, this hypothesis can be regarded as implausible. An alternative explanation is that the clinopyroxene is the crystallization product of the metasomatic magma. This has been proposed previously for some Kaapvaal peridotites (e.g., Simon et al., 2007) on radiogenic isotopic grounds as the age of the clinopyroxene in some peridotites appears, ≈5-15 million years younger than the host kimberlite, so was likely introduced by kimberlite metasomatism prior to the kimberlite eruption. This second, hypothesis seems more plausible and it is the most likely.

The combination of strong LREE-U-Th enrichment with relatively minor enrichment in the HFSE in Pofadder minerals would be consistent with the effects of carbonatite metasomatism (e.g., Rudnick et al., 1993), However, Pofadder minerals (especially clinopyroxene) do not have extremely high Nb/Zr ratios which is characteristics of carbonatite metasomatism, as carbonatites tend to have HFSE depletion except for Nb which is present at high concentrations in carbonatites, leading to them having extremely high Nb/Zr ratios. Therefore carbonatite metasomatism seems less likely. Similarly, the depletion in Zr, Hf and Ti are not unique to carbonatites as many kimberlites and other alkaline magmas have mild to strong negative anomalies in these elements.

The striking resemblances in primitive mantle normalised trace element patterns between Pofadder clinopyroxene and Cr-rich megacrysts (Figure 8.9) that are dominantly viewed to be related to their host kimberlite magma on the basis of isotopic studies (e.g., Jones, 1987; Nowell, 2004) suggests that Pofadder garnets were metasomatised by kimberlite-like magma and their coexisting clinopyroxenes crystallized directly from this metasomatic melt. Cr-rich megacrysts are likely the product of extensive kimberlite-peridotite interaction, where assimilation of metasomatised peridotite resulted in increased Cr and Mg content in the megacryst parent magma i.e., presumably a kimberlite magma that has experienced assimilation-fractional crystallisation (Bell and Moore, 2004).

This modified kimberlite (Cr-rich megacryst parent) magma would presumably be a relatively low volume, low-flux magma that would be relatively cool (the Cr-rich Pofadder megacrysts are also dominantly calcic, meaning that they crystallized at relatively cool temperatures). The Ca-rich composition of this magma would make it possible to precipitate coarse clinopyroxene (as megacrysts) and presumably fine grained cpx as well (Boyd et al., 1984). It is important to emphasise that, in this hypothesis, the Pofadder cpx and Cr-rich megacrysts are not envisioned to be phenocrysts cognate with the host kimberlite, but rather they are the product of extensive differentiation and assimilation of precursor magmas, also likely originally kimberlitic, that did not make it to the surface but "died out" at depth leaving behind the cpx and other minerals as their trace. A later, larger pulse of kimberlite magmatism exhumed this material as xenoliths and megacrysts.

Table 8.1. *Partition coefficient values between mineral and CO_2-rich kimberlitic melt from Keshav et al. (2005) (garnet values are based on those of Salters & Longhi, 1999 and Salters et al. 2002).*

	Ba	Th	U	Nb	Ta	La	Ce	Pb	Sr	Nd	Zr	Hf	Sm	Eu	Ti	Y	Er	Yb	Lu
Clinopyroxene	0.00208	0.00195	0.0006	0.0052	0.0035	0.0123	0.01	0.013	0.05	0.031	0.016	0.035	0.082	0.1	0.15	0.15	0.182	0.18	0.18
Garnet	0.0006	0.01	0.0276	0.0171	0.017	0.005	0.0201	0.005	0.01	0.0939	0.5648	0.597	0.331	0.5	0.305	3.046	3.441	5.724	7.407

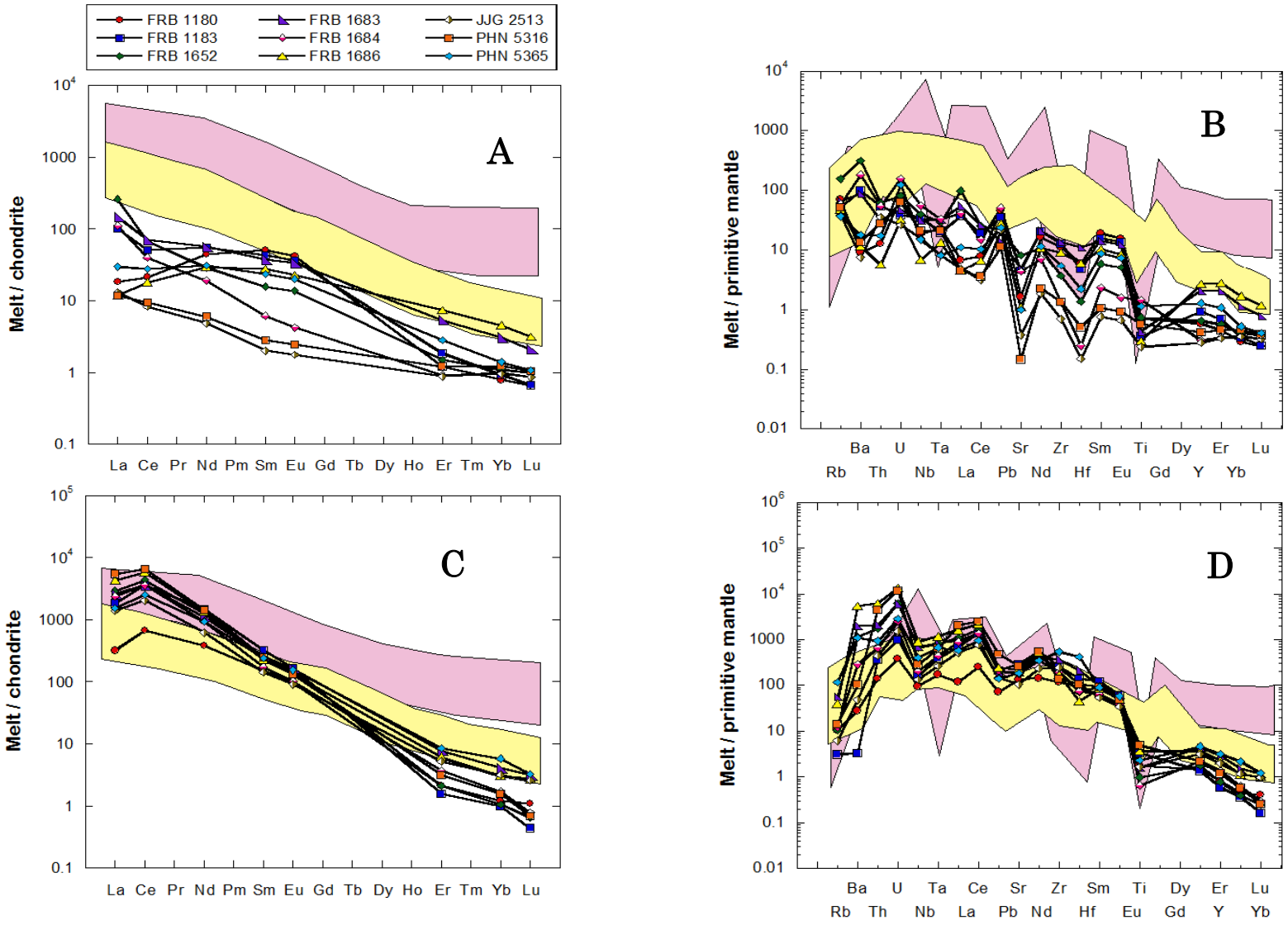

Figure 8.10: Chondrite normalised REE patterns and Primitive mantle normalised trace element patterns of melt in equilibrium with garnet **(A and B) or clinopyroxene (C and D)** from Louwrensia. The pink coloured band represents typical composition of Kaapvaal craton group 1 kimberlite (Le Roex et al. 2003) and the yellow coloured band represents carbonatite composition from Marinkas Quellen in the Namaqua-Natal province,(Ogungbuyi, unpublished data)

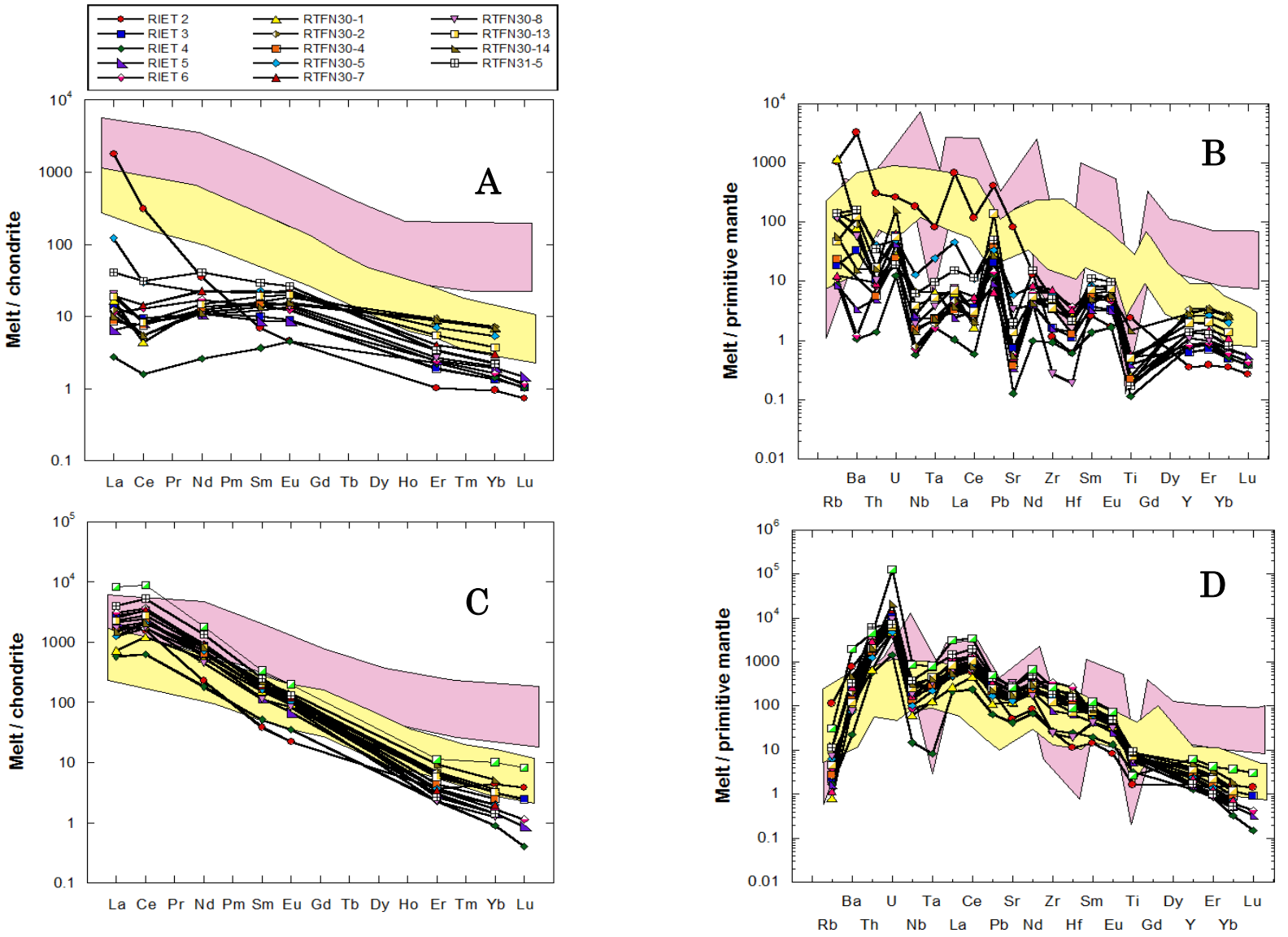

Figure 8.11: Chondrite normalised REE patterns and Primitive mantle normalised trace element patterns of melt in equilibrium with garnet **(A and B) or clinopyroxene (C and D)** from Rietfontein. The pink coloured band represents typical composition of Kaapvaal craton group 1 kimberlite (Le Roex et al. 2003) and the yellow coloured band represents carbonatite composition from Marinkas Quellen in the Namaqua-Natal province,(Ogungbuyi, unpublished data)

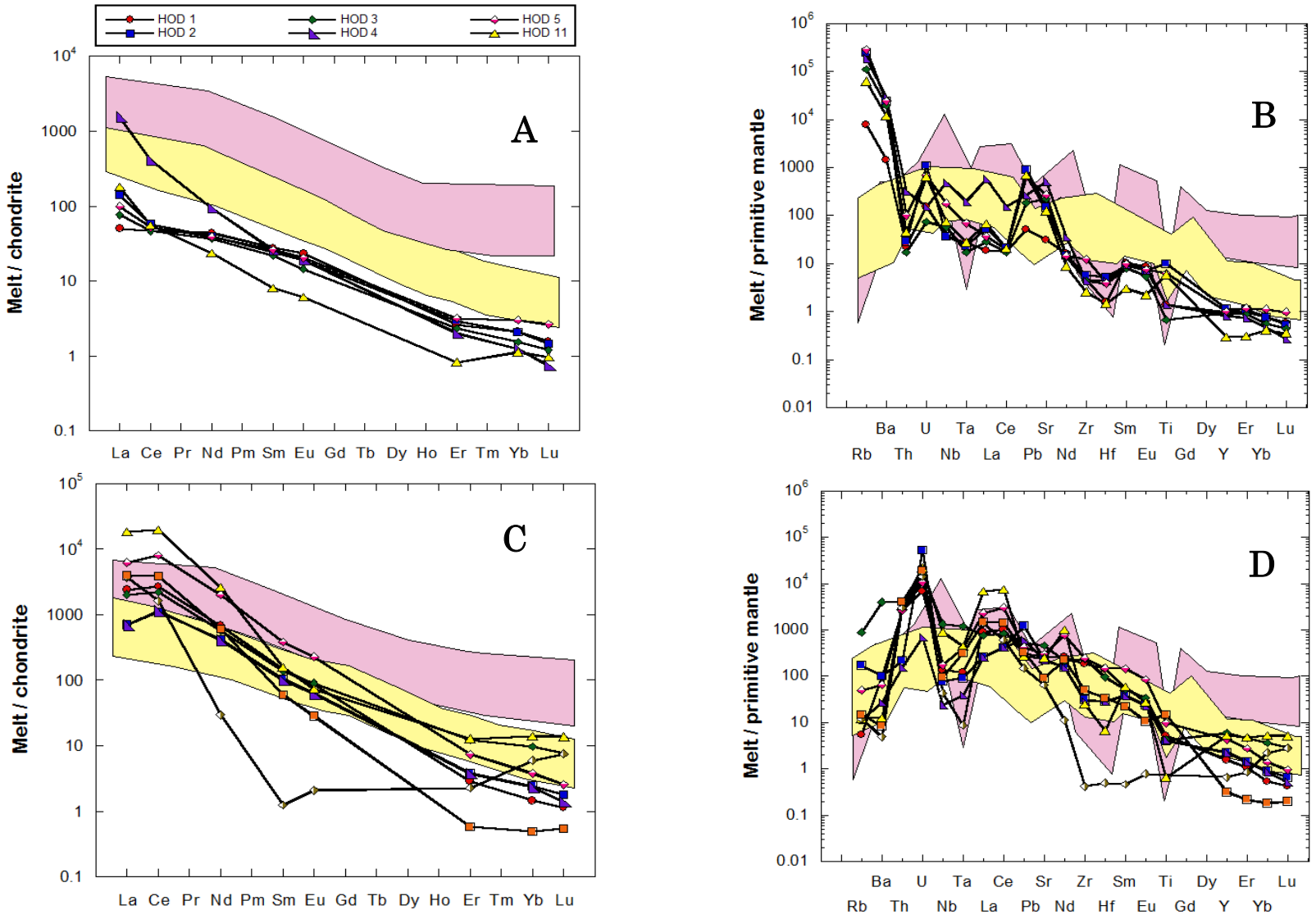

Figure 8.12: Chondrite normalised REE patterns and Primitive mantle normalised trace element patterns of melt in equilibrium with garnet **(A and B) or clinopyroxene (C and D)** from Hoedkop. The pink coloured band represents typical composition of Kaapvaal craton group 1 kimberlite (Le Roex et al. 2003) and the yellow coloured band represents carbonatite composition from Marinkas Quellen in the Namaqua-Natal province,(Ogungbuyi, unpublished data)

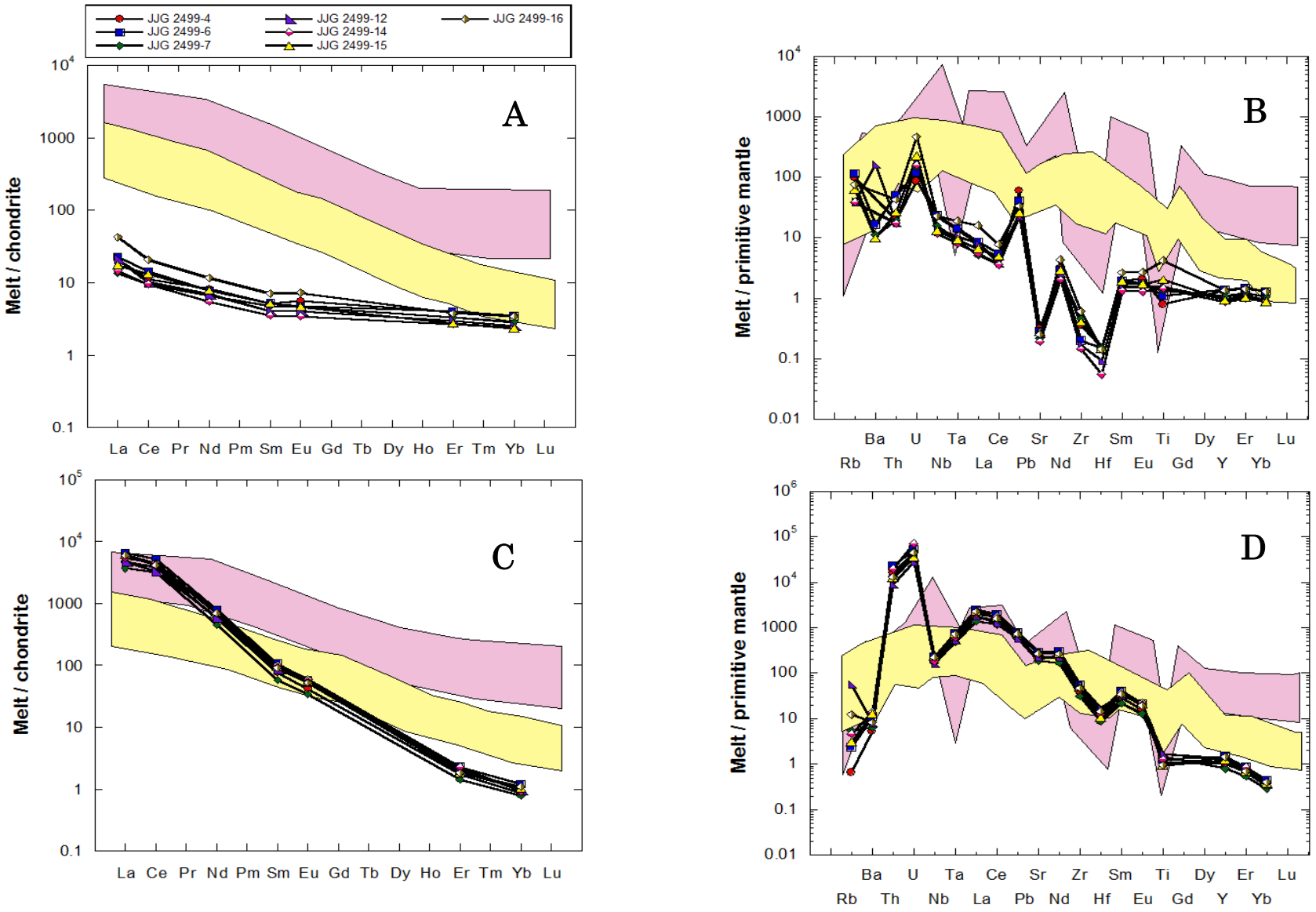

Figure 8.12: Chondrite normalised REE patterns and Primitive mantle normalised trace element patterns of melt in equilibrium with garnet (**A and B**) **or clinopyroxene** (**C and D**) from Hoedkop. The pink coloured band represents typical composition of Kaapvaal craton group 1 kimberlite (Le Roex et al. 2003) and the yellow coloured band represents carbonatite composition from Marinkas Quellen in the Namaqua-Natal province,(Ogungbuyi, unpublished data)

9. CONCLUSIONS

The detailed chemical analysis of major elements in olivine, garnet, clinopyroxene and orthopyroxene, and trace elements in garnet and clinopyroxene from four off craton localities in southern Africa allow the following main conclusions to be drawn regarding the chemical and thermal state of the off-craton lithospheric mantle in the Rehoboth and the western Namaqua-Natal Provinces of southern Africa:

- Peridotites from the Rehoboth and western Namaqua-Natal Provinces have undergone moderate degrees of melt extraction, as indicated by the relatively infertile major and trace element compositions of the minerals as compared to those expected for fertile asthenospheric mantle. Xenoliths from the Rehoboth (Louwrensia and Rietfontein) Province possibly underwent a greater average extent of melt extraction than xenoliths from the western Namaqua-Natal Province as evident from the slightly higher olivine Mg-numbers and lower Y contents in coexisting garnets. On average, the lithospheric mantle samples from these off-craton localities is more fertile than cratonic lithospheric mantle xenoliths from the Kaapvaal craton. It is widely agreed that Proterozoic mantle lithosphere stabilised (i.e., separated from the convecting mantle) as the result of relatively shallow fluid-mediated melt extraction at subduction zones, which were established in Proterozoic time. Osmium isotopes (e.g., Carlson et al., 1999; Pearson et al., 2004; Janney et al., 2010; Pearson, 2014) revealed strong evidence that the off-craton portions of southern Africa experienced multiple melt extraction events. In other words, cratonic mantle appears to have formed from melting at very high degrees that may have occurred at spreading centres (e.g., Herzberg and Rudnick, 2012), above subduction zones (e.g., Pearson & Wittig, 2008) or within deep-seated mantle

upwellings (Aulbach, 2012) to produce harzburgitic melting residues. In contrast, off-craton mantle experienced a more moderate initial phase of melt extraction and, in many cases, experienced subsequent additional melting events related to tectonism and orogeny to produce lherzolites intermediate in fertility between cratonic mantle and fertile asthenospheric mantle.

- Granular peridotite xenoliths from the Rehoboth Province lie between the 40mWm^{-2} and 45mWm^{-2} conductive geotherms of Pollack and Chapman, (1977) and also fall along the Kalahari paleogeotherm of Rudnick and Nyblade (1999) similar to Kaapvaal peridotites. This is a regional characteristic of the Rehoboth Province, as it is consistent with thermobarometry results for eclogites from the Rietfontein kimberlite pipe (Appleyard et al., 2007). The data therefore suggests that the thermal state of the lithospheric mantle in the Rehoboth Province during the Late Cretaceous was cool, with no apparent thermal disturbances since the Namaquan orogeny (1.3-1.0 Ga). Thus, similarity in geothermal gradients between the Rehoboth province and the older, thicker Kaapvaal craton suggest a similar thermal structure and, therefore, a similar thicknesses (probably 180-210 km, Chevrot and Zhao, 2007) of the two lithospheric terranes before kimberlite eruption (Bell et al., 2003; Boyd et al., 2004; Janney et al., 2010). Subsequently, the Rehoboth Province lithosphere was likely thinned by ≈25% as a result of thermal erosion to achieve its current thickness. In contrast, peridotites from the Namaqua-Natal Province, display higher temperatures at a given pressure than peridotites from either the Rehoboth province or the Kaapvaal craton. Consequently, they fall between the 45mWm^{-2} and 50 mWm^{-2} or above the 50 mWm^{-2} conductive geotherms of Nyblade and Pollack (1993) and lie at temperatures approximately 100°–200°C warmer than the Kalahari geotherm for a given pressure. This indicates that the lithospheric mantle

in Hoedkop, Pofadder and the rest of the western Namaqua-Natal Province has experienced a similar degree of thermal disturbance and lithosphere thinning due to thermal erosion (Bell et al., 2003; Janney et al., 2010). Because peridotites from the older, ≈150 Ma Melton Wold kimberlite lie on or very near the Kalahari geotherm, warming and lithosphere thinning appears to have been immediately preceded or been concurrent with Late Cretaceous group 1 kimberlite magmatism.

- The peridotites from the Rehoboth province preserve evidence for moderate to strong metasomatic enrichment in the highly incompatible trace elements, with equilibrium between garnet and clinopyroxene for most trace elements from most localities. Louwrensia peridotites in particular have garnets with sinusoidal REE patterns reflecting strong metasomatic enrichment following extreme melt depletion, in addition to the widespread replacement of clinopyroxene by phlogopite. The most likely metasomatic agent(s) in Louwrensia and Rietfontein appear to be melts similar to kimberlite in composition, possibly representing the host kimberlite magma. In the western Namaqua-Natal Province, Hoedkop peridotites shows evidence for moderate to strong metasomatic enrichment in incompatible elements derived from kimberlitic melts. The partial to full replacement of garnets by kelyphite and, phlogopite, spinel and clinopyroxene aggregates also provides strong evidence for infiltration of a K-bearing hydrous fluid into peridotites and subsequent garnet breakdown. Pofadder peridotites show evidence for intense metasomatism characterised by extreme enrichment of garnet and clinopyroxene in incompatible trace elements, but also major trace element disequilibrium between these two minerals. This appears to be due most likely to interaction with metasomatic melt(s) similar to kimberlites that resulted in the precipitation of clinopyroxene chemically similar to Cr-rich clinopyroxene megacrysts without full equilibration with garnet.

10. REFERENCES

Aldanmaz, E., 2012, Trace element geochemistry of primary mantle minerals in spinel-peridotites from polygenetic MOR-SSZ suites of SW Turkey: Constraints from an LA-ICP-MS study and implications for mantle metasomatism: Geological Journal, v. 47, no. 1, p. 59–76.

Anderson, D.L., 1989, Theory of the Earth (J. Staples & A. Alden, Eds.): Blackwell Scientific Publications.

Anderson, D.L., 1987, Thermally induced phase changes, lateral heterogeneity of the mantle, continental roots, and deep slab anomalies: Journal of Geophysical Research, v. 92, no. B13, p. 968–980.

Appleyard, C.M., Bell, D.R., and le Roex, a. P., 2007, Petrology and geochemistry of eclogite xenoliths from the Rietfontein kimberlite, Northern Cape, South Africa: Contributions to Mineralogy and Petrology, v. 154, no. 3, p. 309–333.

Aulbach, S., 2012, Craton nucleation and formation of thick lithospheric roots: Lithos, v. 149, p. 16–30.

Aulbach, S., Luchs, T., and Brey, G.P., 2014, Distribution and behaviour during metasomatism of PGE-Re and Os isotopes in off-craton mantle xenoliths from Namibia: Lithos, v. 184, p. 478–490.

Ballard, S., Pollack, H.N., and Skinner, N.J., 1987, Terrestrial heat flow in Botswana and Namibia: Journal of Geophysical Research, v. 92, p. 6291–6300.

Becker, T., Schreiber, U., Kampunzu, A.B., and Armstrong, R., 2006, Mesoproterozoic rocks of Namibia and their plate tectonic setting: Journal of African Earth Sciences, v. 46, p. 112–140.

Begg, G.C., Griffin, W.L., Natapov, L.M., O'Reilly, S.Y., Grand, S.P., O'Neill, C.J., Hronsky, J.M.A., Poudjom Djomani, Y., Swain, C.J., Deen, T., and Bowden, P., 2009, The lithospheric architecture of Africa: Seismic tomography, mantle petrology, and tectonic evolution.: Geosphere, v. 5, p. 23–50.

Bell, D.R., and Moore, R.O., 2004, Deep chemical structure of the southern African mantle from kimberlite megacrysts: South African Journal of Geology, v. 107, no. 1–2, p. 59–80.

Bell, D.R., Schmitz, M.D., and Janney, P.E., 2003, Mesozoic thermal evolution of the southern African mantle lithosphere: Lithos, v. 71, no. 2–4, p. 273–287.

Blundy, J., and Wood, B., 2003, Partitioning of trace elements between crystals and melts: Earth and Planetary Science Letters, v. 210, no. 3–4, p. 383–397.

Boullier, A.-M., and Nicolas, A., 1973, Textures and fabric of peridotite nodules from kimberlite at mothae, thaba, utsoa and kimerley, *in* Nixon, P.H. ed., lesotho kimberlites: Maseru, Leshotho National Development Corp., p. 57–66.

Boyd, F.R., 1973, A pyroxene geotherm: Geochimica et Cosmochimica Acta, v. 37, no. 12, p. 2533–2546.

Boyd, F., 1989, Compositional distinction between oceanic and cratonic lithosphere: Earth and Planetary Science Letters, v. 96, p. 15–26.

Boyd, F.R., 1996, Origins of peridotite xenoliths: major element considerations, *in* High Pressure and High Temperature Research on Lithosphere and Mantle Materials: Proceedings of the International School Earth and Planetary Sciences, University of Siena, p. 89–106.

Boyd, F.R., Dawson, J.B., and Smith, J. V., 1984, Granny Smith diopside megacrysts from the kimberlites of the Kimberley area and Jagersfontein, South Africa: Geochimica et Cosmochimica Acta, v. 48, no. 2, p. 381–384.

Boyd, F.R., Hoal, K.E.O., and Rogers, N.W., 1994, A Re-Os isotopic and petrological study of Namibian peridotites: contrasting petrogenesis and composition of on- and off-craton lithospheric mantle: Goldshmidt Conference Edinburgh, p. 703–704.

Boyd, F.R., and Meyer, H.O., 1979, The Mantle Sample: Inclusions in Kimberlites and Other Volcanics: American Geophysical Union.

Boyd, F.R., and Nixon, P.H., 1978, Boyd, F.R., and Nixon, P.H., 1978, Ultramafic nodules from the Kimberley pipes, South Africa: Geochimica et Cosmochimica Acta, v. 42, no. 9, p. 1367–1382.

Boyd, F.R., and Nixon, P.H., 1972, Ultramafic nodules from the Thaba Putsoa kimberlite pipe.: Carnegie Inst. Wash. Yearb., v. 71, p. 362–373.

Boyd, F.R., Pearson, D.G., Hoal, K.O., Hoal, B.G., Nixon, P.H., Kingston, M.J., and Mertzman, S. a., 2004, Garnet lherzolites from Louwrensia, Namibia: bulk composition and P/T relations: Lithos, v. 77, no. 1–4, p. 573–592.

Boyd, F.R., Pearson, D.G., Nixon, P.H., and Mertzman, S.A., 1993, Low-calcium garnet harzburgites from southern Africa: their relations to craton structure and diamond crystallization: Contributions to Mineralogy and Petrology, v. 113, no. 3, p. 352–366,.

Brey, G.P., and Köhler, T., 1990, Geothermobarometry in four-phase lherzolites II. New thermobarometers, and practical assessment of existing thermobarometers: Journal of Petrology, v. 31, no. 6, p. 1353–1378.

Brey, G.P., Kohler, T., and Nickel, K.G., 1990, Geothermobarometry in four phase Lherzolites I. Experimental results from 10-60 Kb: Journal of Petrology, v. 31, p. 1313–1352.

Bucher, K., and Frey, M., 1994, Petrogenesis of Metamorphic Rocks: Springer-Verlag.

Burgess, S.R., and Harte, B., 2004, Tracing Lithosphere Evolution through the Analysis of Heterogeneous G9-G10 Garnets in Peridotite Xenoliths, II: REE Chemistry: Journal of Petrology, v. 45, no. 3, p. 609–633.

Canil, D., 2004, Mildly incompatible elements in peridotites and the origins of mantle lithosphere: Lithos v. 77, no. 1, p. 375–393.

Carlson, R.W., Pearson, D.G., Boyd, F.R., Shirey, S.B., Irvine, G., Menzies, A.H., and Gurney, J.J., 1999, Re–Os systematics of lithospheric peridotites: implications for lithosphere formation and preservation.: *in* The JB Dawson Volume—Proceedings of the Seventh International Kimberlite Conference, Cape Town. Red Roof Design, Cape Town, p. 99–108.

Carswell, D. A., 1975, Primary and secondary phlogopites and clinopyroxenes in garnet lherzolite xenoliths: Physics and Chemistry of the Earth, v. 9, p. 417–429.

Carswell, D. A., Clarke, D.B., and Mitchell, R.H., 1979, The petrology and geochemistry of ultramafic nodules from Pipe 200, northern Lesotho, *in* Boyd, F.R. and Meyer, H.O. eds., The Mantle Sample: Inclusion in Kimberlites and Other Volcanics, p. 127–144.

Carswell, D.A., and Gibb, F.G.F., 1987, Evaluation of mineral thermometers and barometers applicable to garnet lherzolite assemblages: Contributions to Mineralogy and Petrology.

Chevrot, S., and Zhao, L., 2007, Multiscale finite-frequency Rayleigh wave tomography of the Kaapvaal craton: Geophysical Journal International, v. 169, no. 1, p. 201–215.

Choi, S.H., Kwon, S.T., Mukasa, S.B., and Sagong, H., 2005, Sr-Nd-Pb isotope and trace element systematics of mantle xenoliths from Late Cenozoic alkaline lavas, South Korea: Chemical Geology, v. 221, no. 1–2, p. 40–64.

Clarke, S.P., and Ringwood, A.E., 1964, Density distribution and constitution of the mantle: Reviews in Geophysics, v. 2, p. 35–88.

Cornell, D.H., Hawkesworth, C.J., Van Calsteren, P., and Scott, W.D., 1986, Sm-Nd study of Precambrian crustal development in the Prieska-Copperton region, Cape Province: Transactions of the Geological Society of South Africa, v. 89, p. 17–28.

Cornell, D.H., Kroner, A., Humphreys, H., and Griffin, G., 1990, Age of origin of the polymetamorphosed Copperton Formation, Namaqua-Natal Province, determined by single grain zircon Pb- Pb dating. South African Journal of Geology: v. 93, p. 709–716.

Cornell, D.H., Van Schijndel, V., Ingolfsson, O., Schersten, A., Karlsson, L., Wojtyla, J., and Karlsson, K., 2011, Evidence from Dwyka tillite cobbles of Archean basement beneath the Kalahari sands of southern Africa: Lithos, v. 125, p. 482–502.

Cornell, D.H.., Thomas, R.J., Moen, H.F.G., Reid, D.L., Moore, J.M., and Gibson, R.L., 2006, The Namaqua-Natal Province, *in* The Geology of South Africa, Geological Society of South Africa, Johannesburg.

Corner, B., 2008, The crustal framework of Namibia derived from an integrated interpretation of geophysical and geological data, *in* McG, R. and Miller eds., The Geology of Namibia: Archaean to Mesoproterozoic, Ministry of Mines and Energy, Geological Survey of Namibia, Windhoek, p. 1–19.

Cox, K.G., Gurney, J.J., and Harte B, 1973, Xenoliths from the Matsoku pipe, *in* Nixon P. H. ed., Lesotho kimberlites. p. 76–100. Maseru: Lesotho National Development Corporation,

Cox, K.G., Smith, M.R., and Beswetherick, S., 1978, Textural studies of garnet lherzolites: evidence of exsolution origin from high-temperature harzburgites, *in* Nixon P. H. ed., Mantle xenoliths, p. 537–550, Wiley.

Danchin, R. V, 1979, Mineral and bulk chemistry of garnet lherzolite and garnet harzburgite xenoliths from the Premier Mine, South Africa., *in* Boyd, F.R. and Meyer, H.O. eds., The Mantle Sample: Inclusion in Kimberlites and Other Volcanics, p. 104–126, American Geophysical Union, Washington, D.C

Davies, G., Spriggs, A., and Nixon, P., 2001, A non-cognate origin for the Gibeon kimberlite megacryst suite, Namibia: implications for the origin of Namibian kimberlites: Journal of Petrology, v. 42, no. 1, p. 159–172.

Davis, G.L., 1977, The ages and uranium contents of zircons from kimberlites and associated rocks: Carnegie Institution of Washington Yearbook, v. 76, p. 631–654.

Dawson, J.B., 1980, Kimberlites and their xenoliths: Springer-Verlag, Berlin.

Dawson, J.B., Gurney, J.J., and Lawless, P.J., 1975, Palaeogeothermal gradients derived from xenoliths in kimberlite: Nature, v. 257, p. 299–300.

De Bruin, D., 1999, The omposition of garnet, clinopyroxene, chromite and ilmenite from the Rietfontein kimberlite, Northern Cape Province, South Afriica: Council of Geosciences, Report number 1999-0263, p. 19.

Dick, H.J.B., Fisher, R.L., and Bryan, W.B., 1984, Mineralogic variability of the uppermost mantle along mid-ocean ridges. Earth and Planetary Science Letters, v. 69, p. 88–106.

Downes, H., 2001, Formation and Modification of the Shallow Sub-continental Lithospheric Mantle: a Review of Geochemical Evidence from Ultramafic Xenolith Suites and Tectonically Emplaced Ultramafic Massifs of Western and Central Europe: Journal of Petrology, v. 42, no. 1, p. 233–250.

Duffy, T.S., and Anderson, D.L., 1989, Seismic velocities in minerals and the minerology of the upper mantle: Journal of Geophysical Research, v. 94, no. B2, p. 1895–1912.

Eglington, B.M., 2006, Evolution of the Namaqua-Natal Belt, southern Africa – A geochronological and isotope geochemical review: Journal of African Earth Sciences, v. 46, no. 1–2, p. 93–111.

Eglington, B., and Armstrong, R.A., 2003, Geochronological and isotopic constraints on the Mesoproterozoic Namaqua-Natal Belt : Evidence from deep borehole intersections in South Africa: Precambrian Research, v. 125, p. 179–189.

Eglington, B.M., and Armstrong, R.A., 2004, The Kaapvaal Craton and adjacent orogens, southern Africa: A geochronological database and overview of the geological development of the craton: South African Journal of Geology, v. 107, no. 1–2, p. 13–32.

Erlank, A.J., Waters, F.G., Hawkesworth, C.J., Haggerty, S.E., Allsopp, H.L., Rickard, R.S., and Menzies, M.A., 1987, Evidence for mantle metasomatism in peridotite nodules from the Kimberley pipes, South Africa, *in* Menzies, M.A. and Hawkesworth, C.J. eds., In: Mantle Metasomatism, Academic Press, London, p. 221–311.

Evensen, N.M., Hamilton, P.J., and O'Nions, R.K., 1978, Rare-earth abundances in chondritic meteorites: Geochimica et Cosmochimica Acta, v. 42, no. 8, p. 1199–1212.

Exley, R. A., 1982, Cr-rich Spinel and Garnet in two peridotite xenoliths from the Frank Smith Mine South Africa: Significance of Al and Cr distribution between spinel and garnet: Mineralogical Magazine, v. 45, no. 337, p. 129–134.

Faryad, S.W., Dolejš, D., and Machek, M., 2009, Garnet exsolution in pyroxene from clinopyroxenites in the Moldanubian zone: Constraining the early pre-convergence history of ultramafic rocks in the Variscan orogen: Journal of Metamorphic Geology, v. 27, no. 9, p. 655–671.

Field, S.W., and Haggerty, S.E., 1994, Symplectites in upper mantle peridotites: Development and implications for the growth of subsolidus garnet, pyroxene and spinel: Contributions to Mineralogy and Petrology, v. 118, no. 2, p. 138–156.

Finnerty, A.A., and Boyd, F.R., 1987, Thermobarometry for garnet peridotites: basis for the determination of thermal and compositional structure of the upper mantle, *in* Nixon, P.H. ed., Mantle Xenoliths, p. 381–402. Wiley.

Franz, L., Brey, G.P., and Okrusch, M., 1996a, Reequilibration of Ultramafic Xenoliths from Namibia by Metasomatic Processes at the Mantle Boundary: The Journal of Geology, v. 104, no. 5, p. 599–615.

Franz, L., Brey, G.P., and Okrusch, M., 1996b, Steady state geotherm, thermal disturbances, and tectonic development of the lower lithosphere underneath the Gibeon Kimberlite Province, Namibia.: Contributions to Mineralogy and Petrology, v. 126, no. 1–2, p. 181–198.

Frey, F.A., 1969, Rare earth abundances in a high-temperature peridotite intrusion.: Geochimica et Cosmochimica Acta, v. 33, no. 11, p. 1429–1447.

Frick, C., 1974, Ten kimberlites from Pofadder, Namaqualand, South Africa.: Translations Geological Society of South Africa, v. 7, p. 31–36.

Gasparik, T., 2000, An Internally Consistent Thermodynamic Model for the System CaO-MgO-Al2O3-SiO2 Derived Primarily from Phase Equilibrium Data: The Journal of geology, v. 108, no. 1, p. 103–119.

Glebovitsky, V. A., Nikitina, L.P., Khiltova, V.Y., and Ovchinnikov, N.O., 2004, The thermal regimes of the upper mantle beneath Precambrian and Phanerozoic structures up to the thermobarometry data of mantle xenoliths: Lithos, v. 74, no. 1–2, p. 1–20.

Gregoire, M., Bell, D.R., and le Roex, A. P., 2003, Garnet Lherzolites from the Kaapvaal Craton (South Africa): Trace Element Evidence for a Metasomatic History: Journal of Petrology, v. 44, no. 4, p. 629–657.

Griffin, W.L., Batumike, J.M., Greau, Y., Pearson, N.J., Shee, S.R., and O'Reilly, S.Y., 2014, Emplacement ages and sources of kimberlites and related rocks in southern Africa: U-Pb ages and Sr-Nd isotopes of groundmass perovskite: Contributions to Mineralogy and Petrology, v. 168, no. 1, p. 1–13.

Griffin, W.L., Fisher, N.I., Friedman, J., Ryan, C.G., and Reilly, S.Y.O., 1999, Cr-Pyrope Garnets in the Lithospheric Mantle . I . Compositional Systematics and Relations to Tectonic Setting: Journal of Petrology, v. 40, no. 5, p. 679–704.

Griffin, W.L., and O'Reilly, S.Y., 1987, the composition of the lower crust and the nature of the continental Moho - xenolith evidence, *in* Nixon, P.H. ed., Mantle Xenoliths, Wiley & Sons, p. 413–430.

Griffin, W.L., O'Reilly, S.Y., Afonso, J.C., and Begg, G.C., 2009, The composition and evolution of lithospheric mantle: A re-evaluation and its tectonic implications: Journal of Petrology, v. 50, no. 7, p. 1185–1204.

Griffin, W.L., O'Reilly, S.Y., Afonso, J.C., and Begg, G.C., 2008, The Composition and Evolution of Lithospheric Mantle: a Re-evaluation and its Tectonic Implications: Journal of Petrology, v. 50, no. 7, p. 1185–1204.

Griffin, W., O'Reilly, S.Y., Natapov, L.M., and Ryan, C.G., 2003, The evolution of lithospheric mantle beneath the Kalahari Craton and its margins: Lithos, v. 71, no. 2–4, p. 215–241.

Griffin, W.L., and Ryan, C.G., 1995, Trace elements in indicator minerals: area selection and target evaluation in diamond exploration: Journal of Geochemical Exploration, v. 53, no. 1–3, p. 311–337.

Griffin, W.L., Shee, S.R., Ryan, C.G., Win, T.T., and Wyatt, B.A., 1999, Harzburgite to lherzolite and back again: metasomatic processes in ultramafic xenoliths from the Wesselton kimberlite, Kimberley, South Africa: Contributions to Mineralogy and Petrology, v. 134, no. 2–3, p. 232–250

Gurney, J.J., 1985, A correlation between garnets and diamond in kimberlites. In: Glover, J. E. & Harris, P. G. (eds) . Kimberlite Occurrence and Origin; a Basis for Conceptual Models in Exploration.: Perth: University ofWestern Australia, p. 143–166.

Gurney, J.J., Mathias, M., Siebert, C., and Moseley, G., 1971, Kyanite eclogites from the Rietfontein kimberlite pipe, Mier Coloured Reserve, Gordonia, Cape Province, South Africa: Contributions to Mineralogy and Petrology, v. 30, no. 1, p. 46–52.

Gurney, J., and Switzer, G.., 1973, The Discovery of Garnets Closely Related to Diamonds in the Finsch Pipe , South Africa: Contributions to Mineralogy and Petrology, v. 39, p. 103–116.

Hafner, S., and Virgo, D., 1970, Temperature-dependent cation distribution in lunar and terrestrial pyroxenes: Proceedings of the Apollo 11 Lunar Science Conference, v. 3, p. 2183–2198.

Harte, B., 1978, Kimberlite nodules, upper mantle petrology, and geotherms: Philosophical Transactions of the Royal Society of London A: Mathematical, Physical and Engineering Sciences, v. 288, no. 1355, p. 487–500.

Harte, B., 1977, Rock Nomenoclature with particular relation to deformation and recrystallisation textures in olivine-bearing xenoliths: Journal of Geology, v. 85, no. 3, p. 279–288.

Harte, B., Hunter, R., and Kinny, P., 1993, Melt geometry, movement and crystallization, in relation to mantle dykes, veins and metasomatism: Philosophical transections: Physical Science and Engineering, v. 342, no. 1663, p. 1–21.

Hartnady, C.J.., Joubert, P., and Stowe, C.W., 1985, Proterozoic crustal evolution in southwestern Africa: Episodes, v. 8, p. 236–244.

Herzberg, C. and Rudnick, R., 2012. Formation of cratonic lithosphere: an integrated thermal and petrological model. Lithos, 149, pp.4-15.

Hill, S.J., 1989, A study of the diamonds and xenoliths from the Star kimberlite, Orange Free State, South Africa: PhD Thesis, University of Cape Town.

Hoal, B.., Hoal, K.E.., Boyd, F.R., and Pearson, D.., 1995, Age constraints on crustal and mantle lithosphere beneath South African: South African Journal of Geology, v. 98, p. 112.

Hoal, K.E.O., Hoal, B.G., Erlank, A.J., and Shimizu, N., 1994, Metasomatism of the mantle lithosphere recorded by rare earth elements in garnets: Earth and Planetary Science Letters, v. 126, no. 4, p. 303–313.

Ionov, D. a., Ashchepkov, I., and Jagoutz, E., 2005, The provenance of fertile off-craton lithospheric mantle: Sr–Nd isotope and chemical composition of garnet and spinel peridotite xenoliths from Vitim, Siberia: Chemical Geology, v. 217, no. 1–2, p. 41–75.

Jacobs, J., Pisarevsky, S., Thomas, R.J., and Becker, T., 2008, The Kalahari Craton during the assembly and dispersal of Rodinia: Precambrian Research, v. 160, no. 1–2, p. 142–158.

Jacobs, J., Thomas, R.J., and Weber, K., 1993, Accretion and indentation tectonics at the southern edge of theKaapvaal craton during Kibaran (Grenville) orogeny: Geology, v. 21, p. 203–206.

Janney, P.E., Shirey, S.B., Carlson, R.W., Pearson, D.G., Bell, D.R., Le Roex, a. P., Ishikawa, a., Nixon, P.H., and Boyd, F.R., 2010, Age, Composition and Thermal Characteristics of South African Off-Craton Mantle Lithosphere: Evidence for a Multi-Stage History: Journal of Petrology, v. 51, no. 9, p. 1849–1890.

Jones, R.A., 1987, Strontium and neodymium isotopic and rare earth element evidence for the genesis of megacrysts in kimberlites of southern Africa, *in* Mantle Xenoliths, John Wiley and Sons, Chichester, UK, p. 711–724.

Jordan, T.H., 1978, Composition and development of the continental tectosphere: Nature, v. 274, no. 5671, p. 544–548.

Jordan, T.H., 1975, The continental tectosphere: Reviews of Geophysics, v. 13, no. 3, p. 1–12.

Kennedy, C.S., and Kennedy, G.C., 1976, The Equilibrium Boundary Between Graphite and Diamond: Journal of Geophysical Research, v. 81, no. 14, p. 2467–2470.

Keshav, S., Corgne, A., Gudfinnssin, G., Bizmis, M., McDonough, W.F., and Fei, Y., 2005, Kimberlite petrogenesis : Insights from clinopyroxene-melt partitioning experiments at 6 6 GPa in the CaO-MgO-Al2O3-SiO2-CO2 system. Geochimica et Cosmochimica Acta: v. 69, no. 11, p. 2829–2845.

Kobussen, A.F., Griffin, W.L., and O'Reilly, S.Y., 2009, Cretaceous thermo-chemical modification of the Kaapvaal cratonic lithosphere, South Africa: Lithos, v. 112, p. 886–895.

Kobussen, A.F., Griffin, W.L., O'Reilly, S.Y., and Shee, S.R., 2008, Ghosts of lithospheres past: Imaging an evolving lithospheric mantle in southern Africa: Geology, v. 36, no. 7, p. 515–518.

Krogh E. J., 1988, The garnet–clinopyroxene Fe–Mg geothermometer—a reinterpretation of existing experimental data: Contributions to Mineralogy and Petrology, v. 99, p. 44–48.

Kurszlaukis, S., Franz, L., and Lorenz, V., 1998, On the volcanology of the Gibeon Kimberlite Field, Namibia: Journal of Volcanology and Geothermal Research, v. 84, no. 3–4, p. 257–272.

Lawless, P.J., 1978, Some aspects of the mineral chemistry of the peridotite xenolith suite from the Bultfontein diamond mine, Kimberley, South Africa: University of Cape Town, Unpublished PhD Thesis.

le Roex, A., and Class, C., 2016, Metasomatic enrichment of Proterozoic mantle south of the Kaapvaal Craton, South Africa: origin of sinusoidal REE patterns in clinopyroxene and garnet: Contributions to Mineralogy and Petrology, v. 171, no. 2, p. 1–24.

Li, Z.X., Bogdanova, S. V., Collins, A. S., Davidson, A., De Waele, B., Ernst, R.E., Fitzsimons, I.C.W., Fuck, R. a., Gladkochub, D.P., Jacobs, J., Karlstrom, K.E., Lu, S., Natapov, L.M., Pease, V., et al., 2008, Assembly, configuration, and break-up history of Rodinia: A synthesis: Precambrian Research, v. 160, no. 1–2, p. 179–210.

Lindsley, D., 1983, Pyroxene thermometry: American Mineralogist, v. 68, p. 477–493.

Luchs, T., Brey, G.P., Gerdes, A., and Höfer, H.E., 2013, The lithospheric mantle underneath the Gibeon Kimberlite field (Namibia): A mix of old and young components—Evidence from Lu–Hf and Sm–Nd isotope systematics: Precambrian Research, v. 231, p. 263–276.

MacGregor, I.D., 1975, Petrologic and thermal structure of the upper mantle beneath South Africa in the Cretaceous, *in* Aherens, L.H., Dawson, J.B., Duncan, A.R., and Erlank, A.J. eds., Physics and Chemistry of the Earth, vol. 9, p. 455–466.

MacGregor, I.D., 1974, The system MgO-Al2O3-SiO2: Solubility of Al2O3 in enstatite for spinel and garnet peridotites compositions: American Mineralogist, v. 59, p. 110–119.

MacGregor, I.D., and Basu, A.., 1974, thermal structure of the lithosphere: A Petrologic Model: Science, v. 185, p. 1007–1011.

Mather, K. A., Pearson, D.G., McKenzie, D., Kjarsgaard, B. A., and Priestley, K., 2011, Constraints on the depth and thermal history of cratonic lithosphere from peridotite xenoliths, xenocrysts and seismology: Lithos, v. 125, no. 1–2, p. 729–742.

McCourt, S., Armstrong, R.A., Grantham, G.H., and Thomas, R.J., 2006, Geology and evolution of the Natal Belt, South Africa: Journal of African Earth Sciences, v. 46, no. 1–2, p. 71–92.

McDonough, W.F., Stosch, H.G., and Ware, N.G., 1992, Distribution of titanium and the rare earth elements between peridotitic minerals: Contributions to Mineralogy and Petrology, v. 110, no. 2–3, p. 321–328.

McDonough, W., and Sun, S., 1995, The composition of the Earth: Chemical Geology, no. 120, p. 223–253.

Mitchell, R.H., 1984, Garnet lherzolites from the Hanaus-I and Louwrensia kimberlites of Namibia.: Contributions to Mineralogy and Petrology, v. 86, no. 2, p. 178–188.

Mitchell, R.H., and Brunfelt, A.O., 1975, Rare earth element geochemistry of kimberlite: Physics and Chemistry of the Earth, v. 9, p. 671–686.

Moen, H.F.G., and Armstrong, R.A., 2008, New age constraints on the tectogenesis of the Kheis Subprovince and the evolution of the eastern Namaqua Province: South African Journal of Geology, v. 111, no. 1, p. 79–88.

Moore, R.O., 1986, A Study of the Kimberlites, Diamonds and Associated Rocks and Minerals from the Monastery Mine, South Africa: PhD Thesis, University of Cape Town,.

Moore, A.E., 1979, The Geochemistry of the olivine melilitites and related rocks of Namaqualand-Bushmanland, South Africa: University of Cape Town, Unpublished PhD Thesis.

Moore, A.E., 1973, The olivine melilitite – kimberlite association of Namaqualand, *in* The International Kimberlite Conference, extended abstracts, p. 239–242.

Moore, A.E., and Verwoerd, W.J., 1985, The olivine melilitite-"kimberlite"-carbonatite suite of Namaqualand and Bushmanland, South Africa: South African Journal of Geology, v. 88, no. 2, p. 281–294.

Muller, M.R., Jones, A. G., Evans, R.L., Grütter, H.S., Hatton, C., Garcia, X., Hamilton, M.P., Miensopust, M.P., Cole, P., Ngwisanyi, T., Hutchins, D., Fourie, C.J., Jelsma, H. A., Evans, S.F., et al., 2009, Lithospheric structure, evolution and diamond prospectivity of the Rehoboth Terrane and western Kaapvaal Craton, southern Africa: Constraints from broadband magnetotellurics: Lithos, v. 112, p. 93–105.

Nguuri, T.K., Gore, J., James, D.E., Webb, S.J., Wright, C., Zengeni, T.G., Gwavava, O., and Snoke, J.A., 2001, Crustal structure beneath southern Africa and its implications for the formation and evolution of the Kaapvaal and Zimbabwe cratons: Geophysical Research Letters, v. 28, no. 13, p. 2501–2504.

Nickel, K.G., and Green, D.H., 1985, Empirical geothermobarometry for garnet peridotites and implications for the nature of the lithosphere, kimberlites and diamonds: Earth and Planetary Science Letters, v. 73, no. 1, p. 158–170.

Nicolas, A.., Boudier, F., and Boullier, A. M., 1973, Mechanisms of flow in naturally and experimentally deformed peridotites: American Journal of Science, v. 273, no. 10, p. 853–876–876.

Nikitina, L.P., 2000, Garnet–orthopyroxene and garnet–clinopyroxene thermobarometers for mantle xenoliths, in Glebovitsky, V.A., Dech, V.I. (Eds.), Theophrastus Contributions to Advanced Studies in Geology: 3. Capricious Earth: Models and Modelling of Geologic Processes and Objects. Theophrastus, St. Petersburg, Athens, pp. 44–53.

Nimis, P., 1998, Evaluation of diamond potential from the composition of peridotitic chromian diopside: European Journal of Mineralogy, v. 10, p. 505–519.

Nixon, P.H., Boyd, F.R., and Boullier, A.M., 1973, The evidence of kimberlite and its inclusions on the constitution of the outer part of the earth, *in* Lesotho Kimberlites, p. 312–318. Maseru: Lesotho National Development Corporation.

Nixon, P.H., and Davies, G.R., 1987, Mantle xenolith prospectives, *in* Nixon, P.H. ed., Mantle Xenoliths, p. 741–756. Wiley & Sons

Nixon, P.H., Rogers, N.W., Gibson, I.L., and Grey, A., 1981, Depleted and fertile mantle xenoliths from southern African kimberlites.: Annual Review of Earth and Planetary Sciences, v. 9, p. 285–309.

Nowell, G.M., 2004, Hf Isotope Systematics of Kimberlites and their Megacrysts: New Constraints on their Source Regions: Journal of Petrology, v. 45, no. 8, p. 1583–1612.

Nyblade, A., and Pollack, H., 1993, A global analysis of heat flow from Precambrian terrains: implications for the thermal structure of Archean and Proterozoic lithosphere: Journal of Geophysical Research, v. 98, no. 12, p. 207–218.

O'Reilly, S.Y., Griffin, W.L., Djomani, Y.H.P., and Morgan, P., 2001, Are lithospheres forever? Tracking changes in subcontinental lithospheric mantle through time: GSA Today, v. 11, no. 4, p. 4–10.

Pearson, D.G., 2014, The Formation and Evolution of Cratonic Mantle Lithosphere – Evidence from Mantle Xenoliths, *in* Carlson R.W., ed., The Mantle and Core: Treatise of Geochemistry, vol. 2, p. 255-292. Elsevier Science, Amsterdam, The Netherlands.

Pearson, D.G., Canil, D., and Shirey, S.B., 2003, Mantle Samples Included in Volcanic Rocks : Xenoliths and Diamonds, *in* Carlson, R.W., ed., The Mantle and Core: Treatise of Geochemistry, v.2, p. 171–275, Elsevier Science: Amsterdam, The Netherlands.

Pearson, D.G., Carlson, R.W., Shirey, S.B., Boyd, F.R., and Nixon, P.H., 1995, Stabilisation of Archaean lithospheric mantle: A ReOs isotope study of peridotite xenoliths from the Kaapvaal craton: Earth and Planetary Science Letters, v. 134, no. 3–4, p. 341–357.

Pearson, D.., Irvine, G.., Ionov, D.., Boyd, F.., and Dreibus, G.., 2004, Re–Os isotope systematics and platinum group element fractionation during mantle melt extraction: a study of massif and xenolith peridotite suites: Chemical Geology, v. 208, no. 1–4, p. 29–59.

Pearson, D.G., and Wittig, N., 2008, Review Formation of Archaean continental lithosphere and its diamonds : the root of the problem: Journal Geological Society London, v. 165, p. 895–914.

Pettersson, A., Cornell, D.H., Moen, H.F.G., Reddy, S., and Evans, D., 2007, Ion-probe dating of 1 . 2 Ga collision and crustal architecture in the Namaqua-Natal Province of southern Africa: v. 158, p. 79–92.

Pettersson, A., Cornell, D.H., Yuhara, M., and Hirahara, Y., 2009, Sm-Nd data for granitoids across the Namaqua sector of the Namaqua-Natal Province , South Africa: in Reddy, S.M., Mazumder, R., Evans, D.A.D., Collins, A.S. eds, Paleoproterozoic Supercontinents and Global Evolution, Geological Society, London, Special Publications, v. 323, no. 1, p. 219–230.

Pollack, H.N., and Chapman, D.S., 1977, On the regional variation of heat flow, geotherms and lithospheric thickness: Tectonophysics, v. 38, p. 279–296.

Priestley, K., and McKenzie, D., 2006, The thermal structure of the lithosphere from shear wave velocities: Earth and Planetary Science Letters, v. 244, no. 1–2, p. 285–301.

Priestley, K., McKenzie, D., and Debayle, E., 2006, The state of the upper mantle beneath southern Africa: Tectonophysics, v. 416, no. 1–2, p. 101–112.

Rampone, E., Botazzi, P., and Ottolini, L., 1991, Complementary Ti and Zr anomalies in orthopyroxene and clinopyroxene from mantle peridotites: Nature, v. 354, no. 518.

Reid, D.L., 1997, Sm-Nd and REE geochemistry of Proterozoic arc- related igneous rocks in the Richtersveld subprovince, Namaqua Mobile Belt, southern Africa: Journal of African Earth Sciences, no. 24, p. 621–633.

Reid, D.L., Smith, C.B., Watkeys, M.K., Welke, H., and Betton, P.J., 1997, Whole-rock radiogenic age patterns in the Aggeneys- Gamsberg ore district, central Bushmanland, South Afric.: South AfricanJournal of Geology, no. 100, p. 11–22.

Ringwood, A.E., 1969, Composition and Evolution of the Upper Mantle, *in* The earth's crust and upper mantle, Hart, P.J. ed., American Geophysical Union, Washington, D.C.

Ringwood, A.E., 1975, Composition and Petrology of the Earth's Mantle. McGraw-Hill, New York.

Ringwood, A.., 1967, The Pyroxene-Garnet transformation in the Earth's Mantle: Earth and Planetary Science Letters, v. 2, p. 255–263.

Robb, L.J., Armstrong, R.A., and Waters, D.J., 1999, The History of Granulite-Facies Metamorphism and Crustal Growth from Single Zircon U – Pb Geochronology : Namaqualand , South Africa: Journal of Petrology, v. 40, no. 12, p. 1747–1770.

Rollinson, H.R., 1993, Using geochemical data: evaluation, presentation, interpretation.: Longman Scientific & Technical.

Rudnick, R., and Nyblade, A., 1999, The thickness and heat production of Archean lithosphere: constraints from xenolith thermobarometry and surface heat flow: Mantle petrology: Field observations and high pressure Experimentation: A Tribute to Francis R. (Joe) Boyd, , no. 6, p. 3–12.

Ryan, C., Griffin, W., and Pearson, N., 1996, Garnet geotherms: Pressure temperature data from Cr pyrope garnet xenocrysts in volcanic rocks: Journal of Geophysical Research: Solid Earth, v. 101, no. B3, p. 5611–5625.

Salters, V.J.M., and Longhi, J., 1999, Trace element partitioning during the initial stages of melting beneath mid-ocean ridges: Earth and Planetary Science Letters, v. 166, no. 1–2, p. 15–30.

Salters, V.J.M., Longhi, J.E., and Bizimis, M., 2002, Near mantle solidus trace element partitioning at pressures up to 3.4 GPa: Geochemistry, Geophysics, Geosystems, v. 3, no. 7, p. 1–23.

Sand, K.K., Waight, T.E., Pearson, D.G., Nielsen, T.F.D., Makovicky, E., and Hutchison, M.T., 2009, Lithos The lithospheric mantle below southern West Greenland : A geothermobarometric approach to diamond potential and mantle stratigraphy: Lithos, v. 112, p. 1155–1166.

Schulze, D.J., 1995, Low-Ca garnet harzburgites from Kimberley, South Africa: Abundance and bearing on the structure and evolution of the lithosphere.: Journal of Geophysical Research: Solid Earth, v. 100, no. B7, p. 12513–12526.

Shee, S.R., Gurney, J.J., and Robinson, D.N., 1982, Two diamond-bearing peridotite xenoliths from the finsch kimberlite, South Africa: Contributions to Mineralogy and Petrology, v. 81, no. 2, p. 79–87.

Shimizu, N., 1975, Rare Earth Elements in Garnets and Clinopyroxenes from Garnet Lherzolite Nodules in Kimberlites: Earth and Planetary Science Letters, v. 25, p. 26–32.

Simakov, S.K., 2008, Garnet – clinopyroxene and clinopyroxene geothermobarometry of deep mantle and crust eclogites and peridotites: Lithos, v. 106, no. 1–2, p. 125–136.

Simon, N.S.C., Carlson, R.W., Pearson, D.G., and Davies, G.R., 2007, The origin and evolution of the Kaapvaal Cratonic Lithospheric Mantle: Journal of Petrology, v.48, p. 589–625.

Simon, N.S.C., Irvine, G.J., Davies, G.R., Pearson, D.G., and Carlson, R.W., 2003, The origin of garnet and clinopyroxene in "depleted" Kaapvaal peridotites: Lithos, v. 71, p. 289–322

Skinner, E.M.W., Clement, C.R., Gurney, D.B., Apter, D.B., and Hatton, C.J., 1992, The distribution and tectonic setting of South African kimberlites: Russian Geology and Geophysics, v. 33, no. 10, p. 26–31.

Smith, C.B., 1983, Pb, Sr and Nd isotopic evidence for sources of southern African Cretaceous Kimberlites: Nature, v. 304, p. 51–54.

Smith, D., 1999, Temperature and pressure of mineral eqilibrationin peridotites xenoliths: Review, discussion and implications, *in* Fei, Y., Berkta, C., and Mysen, B. eds., Mantle Petrology: Field Observations and High Pressure Experimentation: A Tribute to Francis R. (Joe) Boyd. Special Publication Geochemical Society, vol. 6, p. 171–188

Smith, C.B., Allsop, H.L., Kramers, J.D., Hutchinson, G., and Roddick, J.C., 1985, Emplacement ages of Jurassic-Cretaceous South African kimberlites by the Rb-Sr method on phlogopite and whole-rock samples: Transactions of the Geological Society of South Africa, v. 88, no. 2, p. 249–266

Smith, C.B., Clark, T.C., Barton, E.S., and Bristow, J.W., 1994, Emplacement ages of kimberlite occurrences in the Prieska region, southwest border of the Kaapvaal Craton, South Africa.: Chemical Geology, v. 113, no. 1–2, p. 149–169.

Sobolev, N.V., 1977, Deep-seated Inclusions in Kimberlites and the Problem of Upper Mantle Composition: In Brown, D. A., transl., and Boyd, F. R., ed.: American Geophysical Union, Washington, DC, America, p. 279

Spengler, D., Obata, M., Hirajima, T., Ottolini, L., Ohfuji, H., Tamura, a., and Arai, S., 2012, Exsolution of garnet and clinopyroxene from high-al pyroxenes in Xugou peridotite, Eastern China: Journal of Petrology, v. 53, no. 7, p. 1477–1504.

Spriggs, A.J., 1988, An isotopic and geochemical study of kimberlites and associated alkaline rocks from southern Namibia: PhD dissertation University of Leeds.

Steifenhofer, J., 1993, The petrography, mineral chemistry and isotope geochemistry of a mantle xenolith suite from the Lethakane DK1 and DK2 kimberlite pipes, Botswana: PhD Thesis, Macquarie University.

Stosch, H.G., 1982, Rare earth element partitioning between minerals from anhydrous spinel peridotite xenoliths.: Geochimica et Cosmochimica Acta, v. 46, no. 5, p. 793–811.

Stowe, C.W., 1983, The Upington Geotraverse and its implications for craton margin tectonics: Special Publication Geological Society South Africa, v. 10, p. 147–171.

Streckeisen, A., 1976, To each plutonic rock its proper name: Earth-Science Reviews, v. 12, no. 1, p. 1–33.

Tankard, A., Jackson, M.P., Eriksson, K., Hobday, D., Hunter, D.R., and Minter, W.E.L., 1982, Crustal Evolution of Southern Africa: Springer-Verlag. p 522

Tappe, S., Foley, S.F., Jenner, G.A., and Kjarsgaard, B.A., 2005, Integrating Ultramafic Lamprophyres into the IUGS Classification of Igneous Rocks : Rationale and Implications: Journal of Petrology, v. 46, no. 9, p. 1893–1900.

Trompette, R., 2000, Gondwana evolution; its assembly at around 600 Ma: Comptes Rendus de l'Academie de Sciences - Serie IIa: Sciences de la Terre et des Planetes, v. 330, no. 5, p. 305–315.

Van Acken, D., Becker, H., and Walker, R.J., 2008, Refertilization of Jurassic oceanic peridotites from the Tethys Ocean - Implications for the Re-Os systematics of the upper mantle: Earth and Planetary Science Letters, v. 268, no. 1–2, p. 171–181

Van Orman, J. a., Grove, T.L., and Shimizu, N., 2001, Rare earth element diffusion in diopside: influence of temperature, pressure, and ionic radius, and an elastic model for diffusion in silicates: Contributions to Mineralogy and Petrology, v. 141, no. 6, p. 687–703.

Van Orman, J. a., Grove, T.L., Shimizu, N., and Layne, G.D., 2002, Rare earth element diffusion in a natural pyrope single crystal at 2.8 GPa: Contributions to Mineralogy and Petrology, v. 142, no. 4, p. 416–424.

Van Schijndel, V., Cornell, D.H., Frei, D., Simonsen, S.L., and Whitehouse, M.J., 2014, Crustal evolution of the Rehoboth Province from Archaean to Mesoproterozoic times: Insights from the Rehoboth Basement Inlier: Precambrian Research, v. 240, p. 22–36.

Van Schijndel, V., Cornell, D.H., Hoffmann, K.H., and Frei, D., 2011, Three episodes of crustal development in the Rehoboth Province, Namibia: Geological Society, London, Special Publications, v. 357, no. 1, p. 27–47.

Von Seckendorff, V., and Neill, H.S.C.O., 1993, An experimental study of Fe-Mg partitioning between olivine and orthopyroxene at 1173 , 1273 and 1423 K and 1 . 6 GPa: Contributions to Mineralogy and Petrology, no. 113, p. 196–207.

Williams, A.F., 1932, The Genesis of the Diamond, Vol. I, II: E. Benn & Sons, London.

Wilson, T.J., Grunow, a. M., and Hanson, R.E., 1997, Gondwana assembly: The view from Southern Africa and East Gondwana: Journal of Geodynamics, v. 23, no. 3–4, p. 263–286.

Winterburn, P.A., 1987, Geochemical Studies of Peridotite Xenoliths from Southern African Kimberlites: PhD Thesis, University of Edinburgh.

Wittig, N., Baker, J.A., and Downes, H., 2007, U-Th-Pb and Lu-Hf isotopic constraints on the evolution of sub-continental lithospheric mantle, French Massif Central: Geochimica et Cosmochimica Acta, v. 71, no. 5, p. 1290–1311.

Xu, Y., 2000, Distribution of trace elements in spinel and garnet peridotites: Science in China Series D-Earth Sciences, v. 43, no. 2, p. 166–175.

Xu, Y., Menzies, M. a, Vroon, P., Mercier, J.-C., and Lin, C., 1998, Texture-Temperature-Geochemistry Relationships in the Upper Mantle as Revealed from Spinel Peridotite Xenoliths from Wangqing, NE China: Journal of Petrology, v. 39, no. 3, p. 469–493.

Ziegler, U.R., and Stoessel, G.F., 1993, Age determinations in the Rehoboth Basement Inlier, Namibia: Memoirs of the Geological Survey of Namibia, v. 14.